UNIVERSITAT POLITÈCNICA DE CATALUNYA

Programa de Doctorat en Enginyeria Ambiental

Ph.D. Thesis

Characterization of atmospheric pollution dynamics in Spain by means of air quality modelling

Víctor Manuel Valverde Morales

Directors:
Dr José María Baldasano Recio
Dr María Teresa Pay Pérez

Barcelona, January 2016

To the memory of my grandparents, Hermelindo, Mamita Ori, Lolita, and Víctor Manuel

"Today we are faced with a challenge that calls for a shift in our thinking, so that humanity stops threatening its life-support system. We are called to assist the Earth to heal her wounds and in the process heal our own - indeed to embrace the whole of creation in all its diversity, beauty and wonder. Recognizing that sustainable development, democracy and peace are indivisible is an idea whose time has come."

Wangari Muta Maathai

Acknowledgements

It has been my privilege to work closely with my Ph.D. supervisors, Dr María Teresa Pay and Dr José María Baldasano. I have enjoyed the opportunity to learn from their knowledge and experience. I deeply acknowledge them for their guidance, commitment, and advice throughout this process. I am very proud of what we have achieved together; thank you both.

I extend my gratitude to the Barcelona Supercomputing Center-Centro Nacional de Supercomputación and the Technical University of Catalonia for their academic, technical and financial support and for giving me the opportunity to fulfil one of my childhood dreams, doing research for a better world.

I am grateful to all the colleagues of the Earth Sciences Department at BSC for their practical support, their contributions to this research, and for sharing their experiences with me.

To all my friends who have encouraged and supported me over the last few years. ¡Gracias! Moltes gràcies! Grazie! Tack! Merci!

I am truly thankful to my family in Alicante, Barcelona, Cádiz, Geneva and Guatemala for their love and for transmitting me the joy of life. I am especially indebted with my parents, *Víctor y Sandra*, for their unconditional love, care and inspiration. ¡Gracias!

And most of all thanks to my constant, the luck of my life, Cristina. Words cannot express my gratitude to you. Thanks for accompanying me on this adventure; I am already looking forward to our next one!

All the simulations were performed at the Mare Nostrum supercomputer of the Barcelona Supercomputing Center-Centro Nacional de Supercomputación. Some of the works here presented were funded by the Iberdrola Foundation (Ayudas a la Investigación en Energía y Medio Ambiente 2013).

Summary

Atmospheric pollution causes large impacts on human health and societal economic interests and it is a threat for the ecosystems and the climate of the Earth. Improving the understanding of pollution dynamics is necessary to desing efficient air quality strategies that reduce the impacts of air pollution. This Ph.D. Thesis identifies the typical atmospheric conditions at synoptic scale that affect the Iberian Peninsula (IP) and uses them to explain the dynamics of the most relevant gaseous pollutants in Spain (nitrogen dioxide NO_2, sulphur dioxide SO_2, and ozone O_3) by means of air quality modelling.

Circulation type classifications (CTC) summarise the continuum of atmospheric circulation into a discrete number of typical circulation types (CTs). For the 1983-2012 climatic period, a CTC is derived to be useful in the characterization of air quality dynamics over the IP. Sensitivity tests to classification techniques (principal components, correlation analysis, clustering) and other factors affecting the CTC (temporal and spatial resolution, domain size, etc.) are performed to objectivize the choice of the automatic set-up that maximizes its quality. The six identified CTs – described in terms of frequency, persistence, transitions, and location of pressure systems – are consistent with CTs found in the literature. The temporal stability of the CTC, evaluated following a cross-validation process that compares the results of the climatic and yearly CTs, leads to the identification of a representative year (2012). A representative day for each CT in 2012 is identified using an objective score that minimizes the differences of the daily and the average surface pressure CT grid.

The study of NO_2, SO_2, and O_3 dynamics performed on the representative day of each CT focuses on the biggest Spanish urban areas (Madrid and Barcelona) and heavy industrial/electricity-generation areas such as Asturias (northern Spain) and the Algeciras bay (southern Spain). The state-of-the-art CALIOPE Air Quality Forecast System (CALIOPE-AQFS) that provides high-resolution data on emissions, meteorology, and pollutant concentration over Spain is the main tool used in the characterisation of pollution dynamics. The modelling system is also used to quantify the contribution of specific sources of pollutants – coal-fired power plants and on-road transport – by means of a brute-force approach and an emission-based source apportionment, respectively.

The CTs control the transport patterns of $SO_2/NO_2/O_3$ in Spanish continental and Atlantic areas, whereas in Mediterranean coastal areas and over complex-terrains a combination of synoptic and mesoscale dynamics (sea-land and mountain-valley breezes) explains the pollutant concentration patterns. The power plants' contribution to surface concentration (up to 55 $\mu gSO_2\ m^{-3}$ and 32 $\mu gNO_2\ m^{-3}$) occurs mainly close to the source (< 20 km) related to vertical diffusion when the emission is injected within the planetary boundary layer. However, the SO_2/NO_2 plumes can reach distances higher than 250 km.

The daily maximum O_3 concentration attributed to the on-road transport emissions from Madrid and Barcelona contribute up to 24% and 8% to total O_3 concentration, respectively, but it is particularly significant (up to 80-100 μg m^{-3} in an hour) to the O_3 concentration peak during the central hours of the day in April-September. The long-range transport of O_3 to the IP is controlled by the CTs and its concentration is very significant in the area of influence of Madrid and Barcelona, particularly under cold CTs (70-96%).

This Ph.D. Thesis has proven that CALIOPE-AQFS (1) is useful to characterise the 3-D dynamics of primary and secondary pollutants in Spain under typical CTs; (2) is able to attribute and quantify air pollution to its sources via brute force and source apportionment; and (3) has the potential to help in the design of specific, science-based abatement strategies that minimize air pollution impacts.

Resumen

La contaminación atmosférica genera perjuicios en la salud humana, en los intereses económicos de la sociedad y constituye una amenaza para los ecosistemas y el clima de la Tierra. Avanzar en la comprensión de la dinámica de la contaminación facilita el diseño de estrategias de calidad del aire que reduzcan sus impactos. Esta Tesis Doctoral identifica objetivamente patrones típicos de circulación atmosférica (PT) que afectan a la Península Ibérica (PI) a escala sinóptica para explicar la dinámica de los principales contaminantes gaseosos en España (dióxido de nitrógeno NO_2, dióxido de azufre SO_2 y ozono O_3) mediante modelización de la calidad del aire.

Las clasificaciones sinópticas (CS) discretizan el continuo de la circulación atmosférica en un catálogo de PT. Para el período climático 1983-2012, se establece una CS útil para el estudio de la dinámica de la contaminación atmosférica en la PI. Tests de sensibilidad para técnicas automáticas de clasificación (análisis de componentes principales, de correlación y clustering) y para otros factores que afectan a la CS (resolución temporal y espacial, tamaño del dominio, etc.) objetivizan la elección de la configuración que maximiza su calidad. Los seis PT identificados - descritos en términos de frecuencia, persistencia, transiciones y ubicación de los sistemas de presión - son consistentes con la literatura. La evaluación de la estabilidad temporal de la clasificación, mediante un proceso de validación cruzada que compara los PT climáticos con PT identificados en CS anuales, permite identificar un año representativo (2012). Un día representativo de cada PT es elegido gracias a un algoritmo que minimiza las diferencias de la malla de presiones diaria respecto de la del PT promedio.

El estudio de la dinámica de NO_2, SO_2 y O_3 se realiza en el día representativo de cada PT focalizando en las principales áreas urbanas de España (Madrid y Barcelona) y en importantes áreas industriales y/o de generación eléctrica (Asturias, bahía de Algeciras). El sistema de CALIdad del aire OPeracional para España (CALIOPE) que proporciona datos de alta resolución sobre emisiones, meteorología y concentración de contaminantes es la principal herramienta utilizada en el estudio. CALIOPE permite cuantificar la contribución de determinadas fuentes de emisión, centrales térmicas de carbón y transporte rodado, mediante un enfoque de fuerza bruta y de asignación de fuentes, respectivamente.

Los PT controlan el transporte de $SO_2/NO_2/O_3$ en áreas atlánticas y continentales de España mientras que en zonas costeras mediterráneas y/o de topografía compleja, una combinación de procesos sinópticos y de mesoescala (brisas marinas y de valle) explica los patrones de contaminación. La contribución de SO_2 y NO_2 de las centrales térmicas a la concentración en superficie (hasta 55 $\mu g\ m^{-3}$ y 32 $\mu g\ m^{-3}$, respectivamente) se produce principalmente cerca de la fuente (<20 km) por difusión vertical de la emisión cuando ésta se inyecta en la capa límite planetaria. Sin embargo, los penachos de SO_2/NO_2 pueden alcanzar distancias superiores a los 250 km.

La contribución máxima diaria de O_3 atribuido a emisiones del transporte rodado de Madrid y Barcelona alcanza el 24% y el 8%, respectivamente pero es particularmente significativa (hasta 80-100 $\mu g\ m^{-3}$ en una hora) a mediodía durante el pico de concentración de O_3. El transporte a larga distancia de O_3 hacia la PI es controlado por los PT y su contribución es muy importante en el área de influencia de Madrid y Barcelona, en particular bajo los PT fríos (70-96%).

Esta Tesis Doctoral ha demostrado que CALIOPE es (1) útil para caracterizar la dinámica 3-D de contaminantes primarios y secundarios en España bajo diferentes PT; (2) capaz de atribuir y cuantificar la contaminación a sus fuentes a través de fuerza bruta y atribución de fuentes; y (3) potencialmente útil en el diseño de estrategias de mitigación específicas que minimicen los impactos de la contaminación atmosférica.

Publications

International Journals Included in the Science Citation Index (SCI)

- Valverde V, Pay, MT, Baldasano, JM. 2014. Circulation type classification derived on a climatic basis to study air quality dynamics over the Iberian Peninsula. *International Journal of Climatology* Volume 35, Issue 10, pages 2877-2897. DOI: 10.1002/joc.4179.

- Valverde V, Pay, MT, Baldasano, JM. 2015. A model-based analysis of SO_2 and NO_2 dynamics from coal-fired power plants under representative synoptic circulation types over the Iberian Peninsula. *Science of the Total Environment* Volume 541, Issue 15, pages 701-713. DOI: 10.1016/j.scitotenv.2015.09.111.

- Valverde V, Pay, MT, Baldasano, JM. 2015. Ozone attributed to Madrid and Barcelona on-road transport emissions: characterization of plume dynamics over the Iberian Peninsula. *Science of The Total Environment* Volume 543, Part A , pages 670-682. DOI: 10.1016/j.scitotenv.2015.11.070.

Proceedings of International Congresses

- Valverde V, Pay MT, Baldasano JM. 2014. Use of a climatic synoptic classification to identify and characterize NO_2 pollution patterns over the Iberian Peninsula. 16th International Conference on Harmonisation within Atmospheric Dispersion Modelling for Regulatory Purposes. Varna, Bulgaria. 8-11 September. Oral communication.
  http://www.harmo.org/conferences/Proceedings/_Varna/publishedSections/H16-108-Valverde-EA.pdf

- Pay MT, Valverde V, Baldasano JM, Kwok R, Napelenok S, Baker K. 2014. Photochemical modeling to attributing sources and source regions to ozone exceedances in Spain. 13th Annual Community Modeling & Analysis System Conference. Chapel Hill, USA. 27-29 October. Oral communication. https://www.cmascenter.org/conference/2014/agenda.cfm#1410

- Baldasano JM, Valverde V, Pay MT. 2014. Climatic synoptic classification over the Iberian Peninsula. 25th GLOREAM-EURASAP Workshop on Tropospheric Chemical Transport Modelling. Aveiro, Portugal. 6-7 November. Oral communication.

http://gloream2014.web.ua.pt/downloads/25thGLOREAM_SessionII_JMBaldasano.pdf

- Pay MT, Valverde V, Baldasano JM. 2015. Evaluating the global contribution from MACC when modelling an ozone episode over Spain. MACC-III Policy User Workshop. Vienna, Austria. 3-4 March. https://www.gmes-atmosphere.eu/services/aqac/policy_interface/second_pol_workshop/Pay_03Mar2015.pdf

- Valverde V, Pay MT, Baldasano JM. 2015 Analysis of the transport of the plumes from coal power plants under typical circulation types over the Iberian Peninsula. European Geosciences Union General Assembly 2015. Vienna, Austria. 12-17 April. Oral communication. http://meetingorganizer.copernicus.org/EGU2015/EGU2015-13499-1.pdf

- Valverde V, Pay MT, Baldasano JM. 2016 Characterisation of the ozone plume over the Iberian Peninsula due to Madrid and Barcelona cities. 10th International Conference on Air Quality – Science and Application. Milano, Italy. 14-18 March (Poster accepted).

Proceedings of National Congresses

- Valverde V, Pay MT, Baldasano JM. Characterization of atmospheric pollution dynamics in Spain by means of air quality modelling. 1st BSC Doctoral Symposium. Barcelona, Spain. 27-28 May 2014. Poster. http://upcommons.upc.edu/revistes/handle/2099/15061

- Valverde V, Pay MT, Baldasano JM. 2015. Characterization of coal power plants plume dynamics under typical synoptic conditions over the Iberian Peninsula. 2nd BSC Doctoral Symposium. Barcelona, Spain. 5-7 May. Oral communication. http://upcommons.upc.edu/handle/2099/16561

Index

List of acronyms

ABO: Aboño power plant
ACM2: Asymmetric Convective Model, version 2
AFWA: US Air Force Weather Agency
AirBase: EEA air quality monitoring database
AND: Andorra power plant
AQG: air quality guidelines
AQZ: air quality zone
ASP: As Pontes de García Rodríguez power plant
AtlHi: Atlantic high with polar maritime advection circulation type
BSC-CNS: Barcelona Supercomputing Centre-Centro Nacional de Supercomputación
BSC-DREAM8b: Barcelona Supercomputing Center Dust REgional Atmosphere Model 8 bins
CALIOPE-AQFS: CALIdad del aire OPeracional para España air quality forecast system
CAR: Carboneras power plant
CART: classification and regression tree
CH_4: methane
CKM: k-means clustering technique
CMAQ: The Community Multiscale Air Quality Model
CO: carbon monoxide
CO_2: carbon dioxide
COM: Compostilla power plant
COST733: The European Cooperation in Scientific and Technology Action 733
CT: circulation type
CTC: circulation type classification
CTM: chemical transport model
ECMWF: European Centre for Medium-Range Weather Forecasts
EEA: European Environmental Agency
EMEP: European Monitoring and Evaluation Programme
ENEadv: E/NE advection circulation type
EPA: US Environmental Protection Agency
EU12: European mother domain at 12 km x 12 km horizontal resolution
EV: explained variation
GFS: Global Forecast System
GHG: greenhouse gases
GUA: Guardo power plant
HERMES: High-Elective Resolution Modelling Emissions System
HYSPLIT: HYbrid Single-Particle Lagrangian Integrated Trajectory model
IBtl: Iberian thermal low circulation type
IP: Iberian Peninsula

IP4: Iberian Peninsula nested domain at 4 km x 4 km horizontal resolution
IPCC: Intergovernmental Panel on Climate Change
ISAM: Integrated Source Apportionment Method
LBB: Los Barrios power plant
MACC: Monitoring Atmospheric Composition and Climate model
MAGRAMA: Ministerio de Agricultura, Alimentación y Medio Ambiente
maih: meters above injection height
masl: meters above sea level
MB: mean bias
MCIP: Meteorology-Chemistry Interface Processor
MOZART4: Model for OZone And Related chemical Tracers, Version 4
NCAR: National Center for Atmospheric Research
NCEP: National Centers for Environmental Prediction
NMVOC: non-methane organic volatile compounds
NOA: North Atlantic Oscillation
NO_2: nitrogen dioxide
NWadv: North-western advection circulation type
O_3: ozone
O_3 max 8h: daily running 8-hour maximum O_3 concentration
PBL: planetary boundary layer
PBLH: planetary boundary layer height
PCA: principal component analysis
PM: particulate matter
PM10: particulate matter with a diameter smaller than 10 μm
PM2.5: particulate matter with a diameter smaller than 2.5 μm
r: correlation coefficient
RBC: remote background concentration
RedESP: Spanish air quality monitoring network
REE: Red Eléctrica de España – Spanish national electricity grid operator
RF: radiative forcing (W m^{-2})
RI: Rand Index
RMSE: root mean square error
SLP: sea-level pressure
SNAP: Selected Nomenclature for reporting of Air Pollutants
SO_2: sulphur dioxide
VOCs: volatile organic compounds
WHO: World Health Organization
WRF-ARW: Weather Research and Forecasting model - Advanced Research WRF
WSWadv: W/SW advection circulation type
Z500: 500 hPa geopotential height
ZonWadv: Western Atlantic zonal advection circulation type

List of figures

List of tables

1. Introduction

1.1 Air pollution, definition and impacts

Air pollution can be defined as a situation in which substances are present in the atmosphere at concentration sufficiently high above their normal ambient levels to produce a measurable and undesirable effect on humans, animals, vegetation, or materials (Seinfeld and Pandis, 2006). The concentrations of pollutants in the atmosphere are a measure of air quality.

The World Health Organization (WHO) estimates that exposure to ambient air pollution causes each year approximately 3.7 million premature deaths worldwide (WHO, 2013). Under a business-as-usual socioeconomic scenario, it has been stated that the contribution of outdoor air pollution to worldwide premature mortality by 2050 could double (Lelieveld *et al.*, 2014) and that air pollution will be the top environmental cause of premature mortality (OECD, 2012). Depending on the exposure, the effects of air pollution on human health range from subclinical and symptomatic events to increased morbidity and mortality (Figure 1-1) (Brunekreef and Holgate, 2002; Gurjar *et al.*, 2010; WHO, 2013). The acute and chronic exposure to air pollutants – gases and aerosols – has been positively associated with respiratory and cardiovascular sicknesses, and lung-cancer (Pope *et al.*, 2009; Shah *et al.*, 2013; Beelen *et al.*, 2014). Recently, several European studies have highlighted that there are statistically significant positive associations between nitrogen dioxide (NO_2) and sulphur dioxide (SO_2) concentrations with total, cardiovascular and respiratory mortality, particularly in urban areas (Samoli *et al.*, 2006; Cesaroni *et al.*, 2013; Bentayeb *et al.*, 2015). Long-term exposure to tropospheric ozone (O_3) and particulate matter (PM) has also been associated with increased death risk due to cardiopulmonary causes (Jerrett *et al.*, 2009). O_3 is responsible of ~17 400 premature deaths each year in the European Union (EEA, 2014a). The degradation of air also results in an increase of the burden of other related diseases, a reduction in life expectancy, and an increase in the health care public spending which convey to air pollution considerable financial and life-quality costs (Künzli *et al.*, 2010; Vedrenne *et al.*, 2015).

The United Nation Framework Convention on Climate Change states – based on the fifth Intergovernmental Panel on Climate Change Assessment Report (IPCC, 2014) – that "the anthropogenic driven warming of the climate system is unequivocal, and that climate change is on top of the humankind major challenges". Climate change and air pollution are

highly interlinked phenomena (Figure 1-2). The radiative forcing (RF) of the atmosphere – a measure of the planetary radiation balance of which climate change relies on – strongly depends on the concentration of greenhouse gases (GHG) such as carbon dioxide (CO_2) and methane (CH_4). However, RF is also sensitive to the concentration of short-lived atmospheric pollutants such as carbon monoxide (CO), non-methane organic volatile compounds (NMVOC), O_3 (which is considered both a GHG and an air pollutant), and aerosols (Jacob and Winner, 2009). Whereas CO, NMVOC, and O_3 have a positive RF that enhances climate change (Figure 1-3), the net contribution of aerosols is yet under discussion due to the complexity of the aerosol-cloud-radiation interactions that include light absorption and back scattering, and the formation of cloud condensation nuclei (Myhre *et al.*, 2013; von Schneidemesser *et al.*, 2015). It is noteworthy that the implementation of air pollution abatement plans may lead to climate impacts. For example, Baker *et al.* (2015) have recently demonstrated using three coupled climate-air quality models that a total reduction of global SO_2 emissions results in an increase of the surface temperature motivated by an asymmetric hemispheric warming, particularly in the Northern Hemisphere. On the other hand, climate change-driven processes can enhance surface pollution for example, through an increased frequency of deep stratospheric intrusions – that elevate surface O_3 – associated to modifications of the polar jet (Lin *et al.*, 2015).

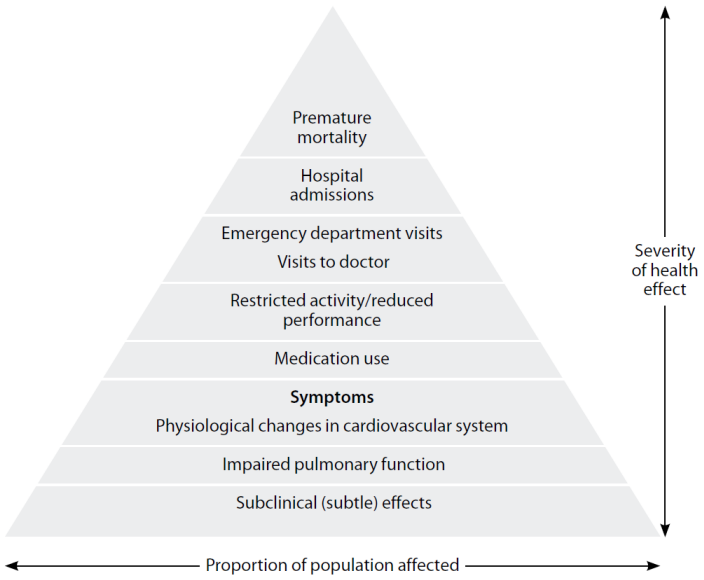

Figure 1-1. Pyramid of health effects associated with air pollution (WHO, 2006)

Air pollution is a threat for the environment affecting a wide range of ecosystems through a variety of processes including acidification, eutrophication or vegetation oxidation that can ultimately lead to a biodiversity and ecosystem services loss (Lovett *et al.*, 2009; de Vries *et al.*, 2014). As an example, trees exposed to acute or chronic high O_3 concentrations can be affected by reduced photosynthesis, damage to reproductive processes, lowered carbon transport to roots, as well as visible physiological effects on leafs that correlate with

reductions in growth in deciduous and evergreen species such as poplar and pine trees (Felzer *et al.*, 2007). As a consequence, O_3 pollution leads to a reduction on the provision of ecosystem services such as carbon sequestration – which in turn, enhances climate change (Figure 1-2).

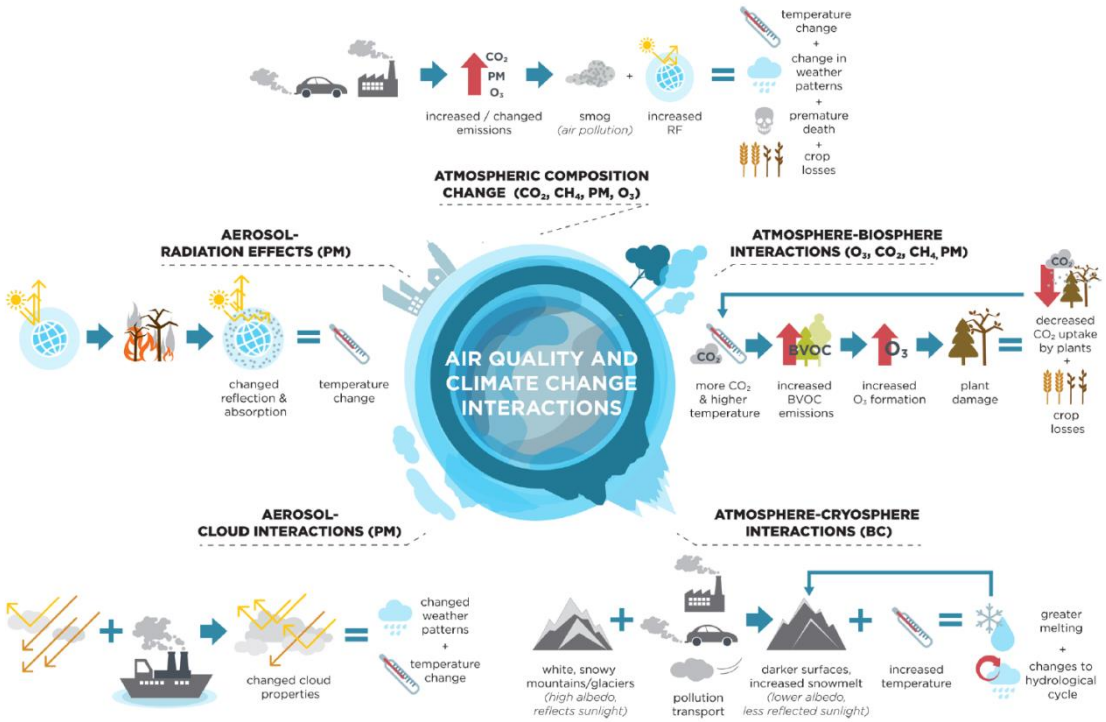

Figure 1-2. Overview of the main categories of air quality and climate change interactions and feedbacks (von Schneidemesser *et al.*, 2015)

Furthermore, high ambient concentrations of gaseous pollutants as NO_2, O_3, and SO_2 have been statistically correlated with a reduction in the productivity of several crops (wheat, mung beans, beetroot), particularly in suburban areas (Agrawal *et al.*, 2003). In the case of O_3, the typically high concentrations registered over Europe in summer causes considerable damage to crops and pastures that lead to relevant economic impacts (up to 1 billion € in 2000 in Europe according to Van Dingenen *et al.*, 2009). In the context of Climate Change, in a business-as-usual emission scenario, predicted high O_3 concentrations could lead to an increase in worldwide crop damage of up to 20% by 2050 and therefore affect the global food production (Chuwah *et al.*, 2015).

Dry and wet deposition of atmospheric pollutants can cause substantial deterioration of a diversity of materials (plaster, bricks, glass, metals, limestone, etc.) by the effect of corrosion and weathering, even in indoor environments (Kucera and Fitz, 1995). Damage caused to materials exposed in the atmosphere constitutes one of the most important direct effects of acidifying air pollutants (Chen *et al.*, 2005). It has been shown that there is a statistically significant correlation between the corrosion rate of copper by SO_2 and O_3; aluminium by NO_2 and particulate matter; and iron by SO_2 and NO_2 (Liu *et al.*, 2014). In

urban areas, where there is a high density of building structures and cultural heritage (stone façades, bronze statues, etc.), the damage can be particularly significant (Nord *et al.*, 2001). Additionally, the rubber cracking is caused by oxidative degradation of natural and synthetic rubbers due to the ozonolysis of rubber chains. This process, enhanced by air pollution leads to a deterioration of the physical and mechanical properties of rubbers such as tires and rubber seals (Li and Koenig, 2005).

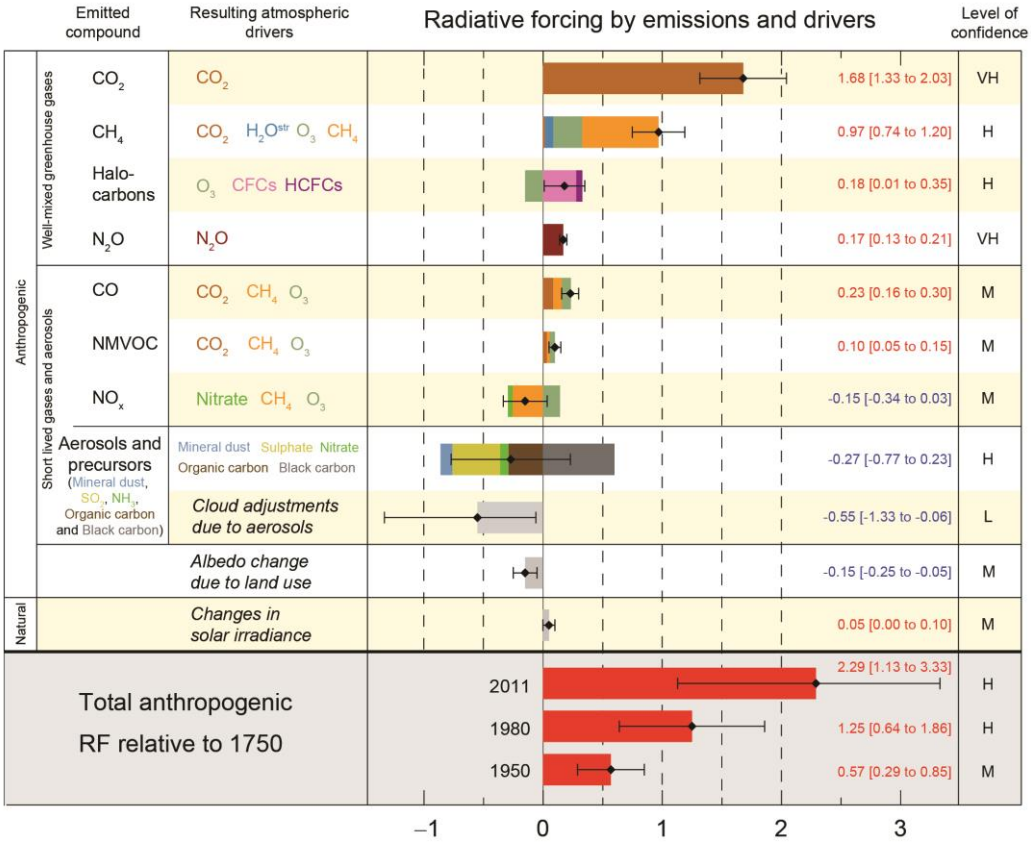

Figure 1-3. Radiative forcing (W m^{-2}) of climate change shown by emitted components and drivers relative to 1750. Horizontal bars indicate the overall uncertainty (IPCC, 2014)

The solar energy sector is also affected by air pollutants. High concentration of air pollutants reduces the sunlight radiation reaching solar cells ultimately leading to a decrease in the electricity generation efficiency (Chaturvedi and Shashank, 2015). Moreover, particulate matter (dust, sand, ashes) deposited over solar panels require permanent cleaning that increase the facilities maintenance costs (Mani and Pillai, 2010).

Visibility is another area impacted by atmospheric pollution during haze and smog events. Particles and gases in the atmosphere interact with light via scattering and absorption reducing visibility (Figure 1-4) and thence, affecting citizen's life quality and altering on-road, marine and aviation safety (Watson, 2002; Hyslop and White, 2008). It is worth mentioning that the modification of the visibility, as perceived by people, can be used as an

indicator of air quality and it is currently being tested as tool to quantify citizen's willingness-to-pay for reducing urban air pollution (Yu *et al.*, 2015).

Figure 1-4. Effect of air pollution on visibility: panorama of the city of Madrid on a clear (top) and a polluted (bottom) day. Photo credits: Jorge París (@Jorgeparis1)

1.2 Air pollution drivers

Air quality depends on emissions of air pollutants (natural and anthropogenic), meteorological fields (that govern the dispersion, deposition, and physical and chemical transformations of these pollutants in the atmosphere), and topography which modulates the circulation and transport patterns of the pollutants (Seinfeld and Pandis, 2006). This section gives an overview of these three air pollution key factors in the Spanish context.

1.2.1 Emissions

Emissions of air pollutants derive from almost all economic and societal activities as well as from natural sources. The relative contribution of different activities to the total emission depends on the considered pollutant (Figure 1-5). In 2012, the NO_x emissions accounted for ~ 850 Gg according to the Spanish National Inventory (MAGRAMA, 2015b) and the main NO_x sources were related to the energy sector (power plants, refineries, etc.) and the on-road transport sector (Figure 1-5a). The largest sources of SO_2 were related to the energy sector (power plants and refineries) accounting for 94% of the ~390 Gg emitted in 2012 (Figure 1-5b) (MAGRAMA, 2015b). However, it is important to notice that shipping

from the Atlantic, through the Strait of Gibraltar, toward the major Mediterranean harbours are also an important source of SO_2.

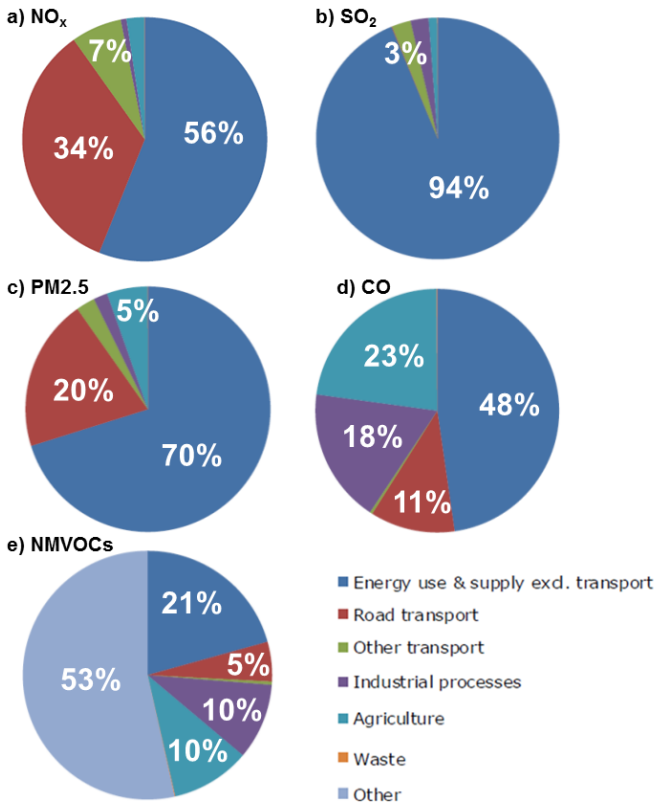

Figure 1-5. Percentage of the distribution of anthropogenic emissions by activity sectors in Spain in 2012: a)NO_x, b) SO_2, c) PM2.5, d) CO, and e) NMVOCs (EEA, 2014b)

The total estimated PM2.5 emissions in Spain were ~72 Gg. The largest emitter was the energy sector followed by on-road transport and agriculture (Figure 1-5c). Regarding CO, almost half of the ~2000 Gg emitted in 2012 in Spain correspond to the energy sector, 23% to agriculture activities, and 18% to industrial processes (Figure 1-5d). The NMVOCs emitted in Spain (~540 Gg in 2012, MAGRAMA, 2015b) have a large share of biogenic origin (Figure 1-5e). Among the anthropogenic emissions the most relevant contributing sectors are the energy industry, industrial processes (involving the use of solvents), agriculture activities, and on-road transport (associated to evaporative emissions from fuels).

Anthropogenic emissions of NO_x and PM2.5 have a similar temporal emission profile. There is a weekly cycle related to the weekday/weekend on-road traffic intensity as well as a daily profile following rush hours of on-road traffic and urban activities. Moreover, NO_x emissions tend to be higher in summer than in winter, associated to an increase in the evaporative emissions that are temperature dependent (Figure 1-6). SO_2 daily emission rate varies according to the electricity needs with maximum emissions in winter and daily peaks related with the household power demand. CO emissions are also larger in winter

associated to electricity-generation needs and in early spring due to the use of off-road machinery for agricultural practices (Guevara *et al.*, 2014a) (Figure 1-6). Biogenic NMVOC emissions depend on temperature and solar radiation and they present emission peaks during spring and summer, and on a daily basis, during midday.

Natural PM emissions can be classified between high-intensity episodic events (Saharan dust outbreaks, forest fires) or continuous events in time (sea-spray) (EEA, 2012). In the Mediterranean Basin, Saharan dust outbreaks are the major contributor to PM10 concentrations in background regions (Querol *et al.*, 2008; Pey *et al.*, 2012). Furthermore, in specific locations and for given episodes, forest fires (especially in summer), the sea-spray (in coastal areas) and dust resuspension from roads can be very important contributors to total PM emissions (Monger *et al.*, 1989; Querol *et al.*, 2004a; 2004b).

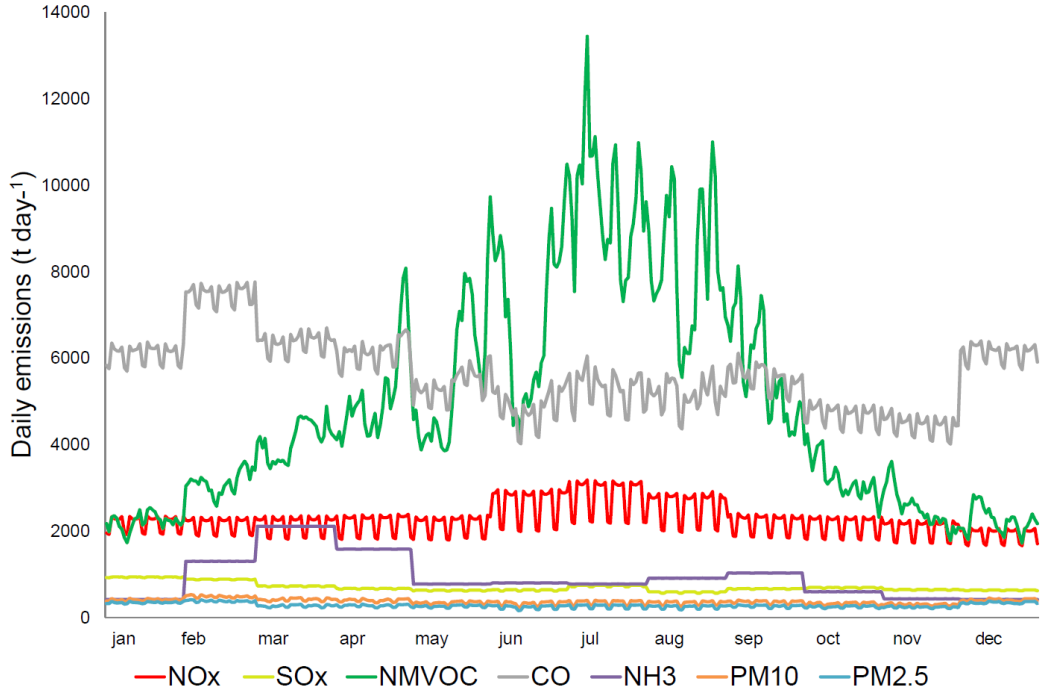

Figure 1-6. Daily emission rates (t day^{-1}) throughout the year in Spain for the main pollutants (based on Guevara *et al.*, 2013 for 2009 emissions)

As a consequence of the implementation of the National Emission Ceilings (Directive 2001/81/EC) and complimentary legislation, much progress has been made in tackling the emission of air pollutants both in the European Union and in Spain along the 21st century. The largest relative reductions of anthropogenic emissions in Europe in the 2003-2012 period have been reported for SO_2 (54%), CO (39%), NO_x (30%) and NMVOC (28%) (EEA, 2014a). In the same period, emissions in Spain decreased for SO_2 by 75%, for CO by 20%, for NO_x by 34% and for NMVOC (37%) (MAGRAMA, 2015b) (Figure 1-7). As sulphur emissions have fallen, NO_x together with ammonia have become the predominant acidifying and eutrophying air pollutants (EEA, 2014a). It is worth mentioning that in Spain, due to the dieselization of the park fleet an increase of the NO_2/NO_x ratio has been

registered (Salvador *et al.*, 2012). In relation to on-road transport emissions, the Spanish administration has recently implemented plans (e.g. the "*Plan PIMA Aire 4*", Real Decreto 989/2014) to reduce their contribution to NO_2 and CO_2 emissions through the promotion of cleaner technologies and electric vehicles.

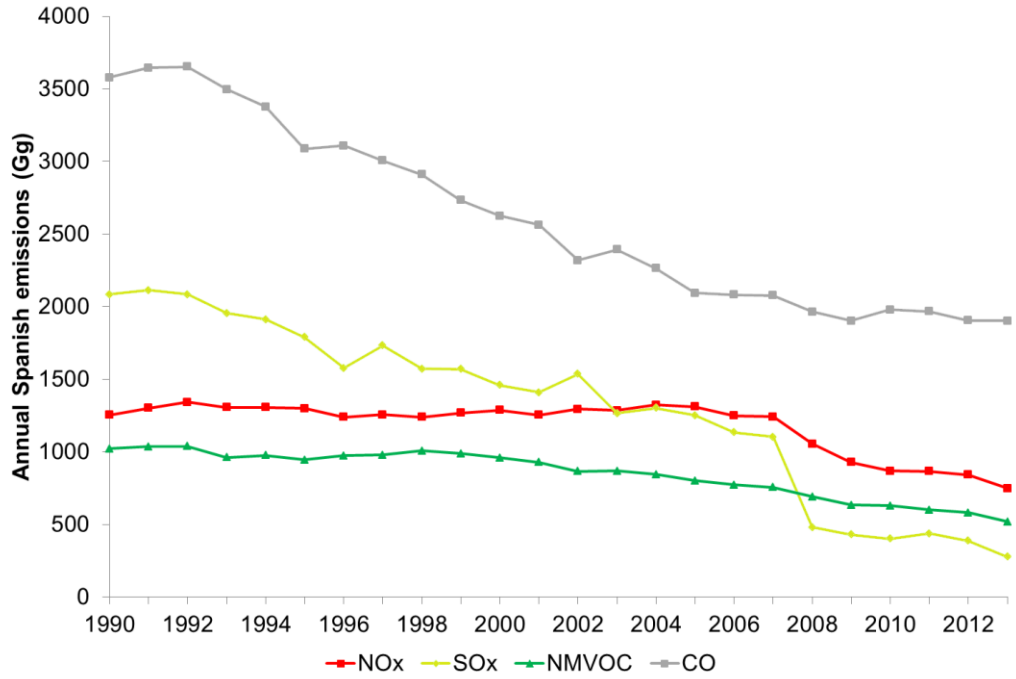

Figure 1-7. Emission trends in Spain during 2001-2013 (in Gg year^{-1}) (MAGRAMA, 2015b)

1.2.2 Topography

The Spanish Iberian Peninsula (IP) covers an area of 493,514 km^2 with an average elevation of 660 meters and a quite complex topography when compared with other European countries (Figure 1-8). The Pyrenees (3200-3400 m above sea level, masl) and the Cantabrian Mountains (2000 masl) are located in the North of Spain, arranged in a West-East direction. These mountain ranges together with the Galician Massif (2000 masl), in the NW of the IP exert a major influence on the climate of the country by preventing the arrival of wet air masses from the Atlantic Ocean towards the centre of the IP. The Ebro valley lies within the Pyrenees and the Iberian System (2000-2300 masl), which is arranged in NW-SE orientation. Wind is usually channelled in the Ebro valley towards the Mediterranean Sea or the Bay of Biscay. Another important mountain range is the Central System (2300-2500 masl) located in the centre of the IP in a SW-NE orientation (Figure 1-8) which favours the circulation of winds by the Tajo valley. The same phenomena occurs in southern Spain with the Baetic System (3200-3400 masl, SW-NE orientation), that favours wind channelling by the Guadalquivir valley towards the Gulf of Cadiz. Finally, the Catalan Pre Coastal (1500-1700 masl) and Coastal ranges (500-700 masl) run parallel to the Mediterranean coast in Catalonia, NW of Spain and they are relevant to explain the transport of pollutants over the Barcelona area.

The IP has a particular location between the European and African continents and it is under the influence of two bodies of water, a major ocean (i.e., Atlantic Ocean) and a small-warm sea (i.e. the Mediterranean Sea) linked by the Strait of Gibraltar. Furthermore, the coastline length of ~ 10 000 km is an important topographic feature in many Spanish coastal areas in relation to the sea breeze regime.

Figure 1-8. Physical map of Spain. The colour chart indicates terrain elevation

1.2.3 Meteorology

The concentration of pollutants in the atmosphere depends on several meteorological fields that occur at different spatial and temporal scales and which are all linked together (Palau *et al.*, 2005). For example, the O_3 formation, which depends on the relative concentrations of its precursors and sunlight availability, is sensitive to local meteorology such as temperature, wind speed and direction, mixing height, relative humidity, and precipitation (Ribas and Peñuelas, 2004; Jacob and Winner, 2009). On the other hand, the dispersion of O_3 through long-range transport in the troposphere is related the synoptic circulation (Cooper *et al.*, 2015). The annual PM10 concentration in European cities like Amsterdam, Paris and Barcelona, characterized by heavy loads of on-road transport emissions is alike (~80 $\mu g\ m^{-3}$) but the contribution of local emissions, and regional and long-range transport is different. This heterogeneous behaviour is explained by different atmospheric dynamics affecting each location (Querol *et al.*, 2008; Putaud *et al.*, 2010; Beekmann *et al.*, 2015). Therefore, the understanding of the relationship of the pollutants' concentration with the prevailing circulation, both at synoptic and mesoscale, is a key element to explain air pollution dynamics in a given territory (Flocas *et al.*, 2009). This

section gives an overview of the main synoptic and mesoscale atmospheric patterns affecting the IP.

1.2.3.1 Synoptic meteorology

This section summarizes the most important synoptic patterns that affect the IP according to an expert-based classification of the air masses (Martín-Vide and Olcina-Cantos, 2001). The identified air masses basically depend on the direction of the advection and the origin of the air masses (Figure 1-9).

- The arctic air masses are characterized by cold air and low humidity at the surface. **Continental arctic** air flow is a vector for transport of air pollutants from different terrestrial parts of Europe (Poland, Germany and France, among others). In turn, the **maritime arctic** air masses, originating over the Arctic Ocean, crosses the United Kingdom and France before reaching Spain by the North.
- Advection from the North Atlantic has its origin in the area comprised between Greenland, Iceland and Great Britain. The **polar maritime** air masses are also cold but in contrast to the arctic masses, they present higher humidity. The fronts of the air masses develop storms that become weaker as they move over the territory of Spain, thereby affecting mostly the northern half of the IP. Instability associated with these air masses tends to reduce air pollution concentration due to enhanced dispersion and wet deposition. The **atlantic maritime** air masses are warm and humid and are related to the Azores high pressure system. The air advected to the IP is usually clean and its flow is relatively weak. The stability of the atmosphere reduces the dispersion of emitted pollutants and promotes high local concentrations.
- **Tropical continental** air masses are advected to the IP from North Africa. It is a very dry and warm air mass and is usually related to desert dust outbreaks from the Sahara desert. A thermal high pressure system localized over North Africa is responsible for this circulation pattern. As it is temperature-related, this synoptic situation is more frequent in summer. Advection of air masses from the Mediterranean occurs mainly in summer and affects the coastal areas of Spain. This feature is essential for understanding the dynamics of coastal pollution linked to the recirculation of polluted air masses.

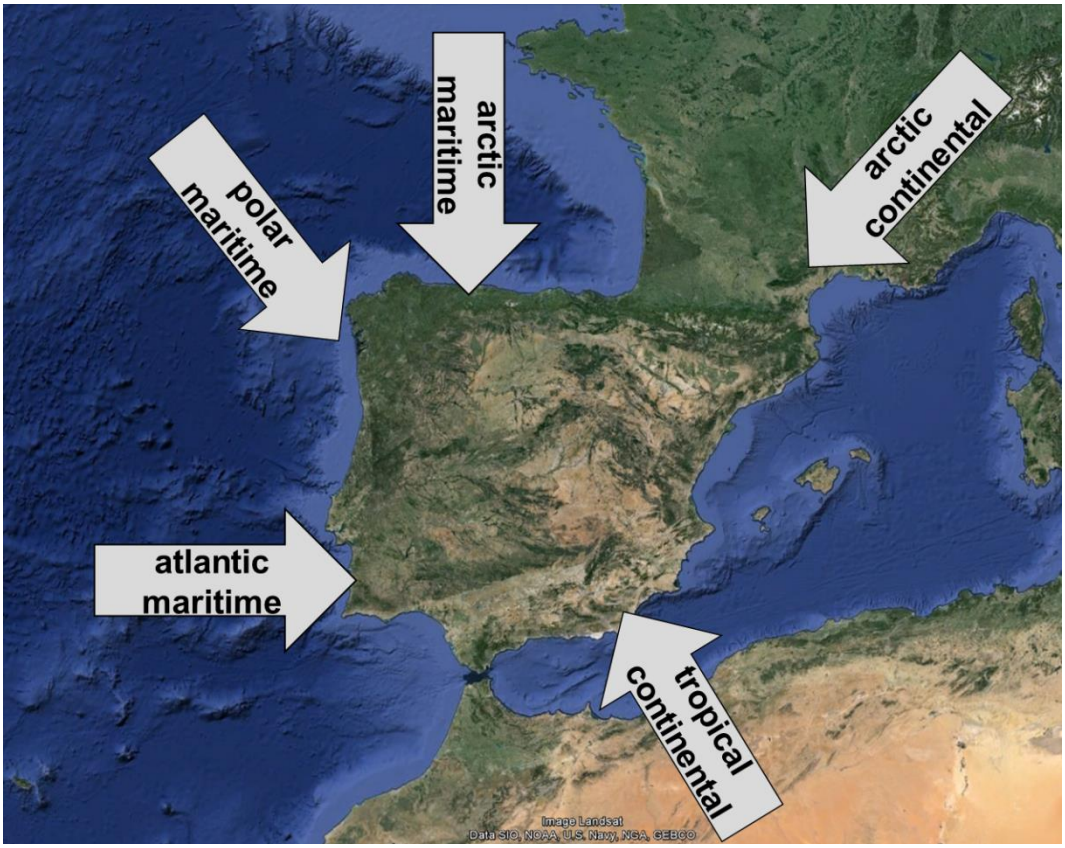

Figure 1-9. Air masses affecting the Iberian Peninsula (adapted from Martín-Vide and Olcina-Cantos, 2001)

1.2.3.2 Mesoscale meteorological patterns affecting the Iberian Peninsula

Topography and land use play an important role on synoptic pattern changes through mesoscale systems development, namely sea-land breezes, heat islands, and anabatic-katabatic winds (Stull, 1988). In Spain, superimposed to synoptic circulation, mesoscale processes conditioned by its complex topography (mountains, sea shore, types of land covers, etc.) generate meteorological conditions that are relevant to understand air pollution dynamics (e.g. influencing planetary boundary layer height, formation of inversion layers, recirculation patterns, etc.). For example, in the IP there is a frequent development of a low thermal pressure region in the centre of the Peninsula in summer, which allows mesoscale processes enhancement, especially in coastal areas (Martín *et al.*, 2001). In the presence of complex terrain near coastlines, the mesoscale phenomena of sea-breezes may be combined with mountain-valley winds creating recirculations along shore increasing the complexity of air pollutant transport in the area (Baldasano *et al.*, 1994; Millán *et al.*, 1997; Gangoiti *et al.*, 2001).

The well-documented air pollution episode of London-type smog in 1952 (Davis *et al.*, 2002) related to high-sulphur coal emissions, and the photochemical smog episodes in Los Angeles basin during the 1950s (Haagen-Smit, 1952) drew societies' attention to the

degradation of air quality, and compelled governments to act, ultimately leading to the implementation of clean air legislations. Although air pollution concentrations improved in the last decades in Europe, the situation is still far from matching the WHO air quality guidelines (AQG) (EEA, 2014a). The most serious air pollution problems in Spain are related to high levels of NO_2, O_3, PM and polycyclic aromatic hydrocarbons (Baldasano *et al.*, 2003; EEA, 2014a; Guerreiro *et al.*, 2014). In areas with elevated fossil fuels combustion sources as power plants, SO_2 is also a matter of concern (MAGRAMA, 2013a).

1.3 Air pollution in Spain

This section gives an overview of the air quality in the Spanish IP focusing in 2012 because it was the most recent year with air quality information by the time this Ph.D. Thesis started. Three complimentary approaches are used to fulfil this objective. First, the temporal trends in background concentrations over the last decade at the European Monitoring and Evaluation Programme (EMEP) stations in Spanish remote rural areas are presented. Second, monitoring data gathered from the European Environmental Agency (EEA) air quality monitoring database (AirBase) are used to discuss spatial differences in concentration levels. Third, the exceedances of the European limit and target values in the Spanish air quality zones (AQZ) are discussed. The EU air quality legislation requires the Member States to report on AQZ that are designated under the Framework Directive on ambient air quality and cover the complete territory. AQZ are defined for monitoring and management purposes by regional administrations as homogenous airsheds with similar emission patterns.

1.3.1 Temporal trends

The EMEP network provides the chemical composition of the low free troposphere at European remote rural locations. Those locations are characterised by not being directly affected by local influences (emissions, sinks, topographic features) so that the data are representative of a larger region (Tørseth *et al.*, 2012). In Spain, 9 monitoring stations have provided continuous data for NO_2, SO_2, O_3 and PM over the 2001-2013 period according to the EMEP online database (http://www.nilu.no/projects/ccc/onlinedata): ES07 - Víznar (Granada), ES08 – Niembro (Asturias), ES09 - Campisábalos (Guadalajara), ES10 – Cap de Creus (Girona), ES11 - Barcarrota (Badajoz), ES12 - Zarra (Valencia), ES13 - Peñausende (Zamora), ES14 – Els Torms (Lleida), and ES16 - O Saviñao (Lugo). This section discusses the pollution trends in Spain over the 2001-2013 period based on the averaged concentration measured at these 9 stations that are well distributed over the Spanish territory (Figure 1-10).

Figure 1-10. EMEP monitoring sites in Spain used to establish the 2001-2013 trends

The monthly NO_2 concentration ranges 3-8 μg m^{-3} with the highest values registered in winter whereas the lowest correspond to May-June. NO_2 concentrations, both maximum and minimum showed a downward trend in the 2008-2013 period (Figure 1-11a) respect the preceding period (2001-2007) with concentrations between 2.5-5 μg m^{-3}. This downward trend in the rural background concentration in Spain is consistent with other authors who have pointed out a reduction in NO_2 background concentration in Spain (Querol *et al.*, 2014) and Europe since the 1990s associated to the implementation of abatement strategies (Colette *et al.*, 2011; Tørseth *et al.*, 2012).

In Spain, the SO_2 background concentration is the highest in winter associated to an increase in the electricity demand for heating that is supplied by hydrocarbon-based power plants. In the 2001-2007 period, the monthly SO_2 concentration ranged 1-2.7 μg m^{-3}. However, since 2008 the SO_2 mean concentration in the EMEP stations in Spain was considerably reduced ranging 0.3-0.8 μg m^{-3} (Figure 1-11b). This important reduction in the background concentration affects more the EMEP stations in northern Spain where several large power plants are located (ES08, ES13, ES16) associated to emission control strategies like the use of desulphurization techniques and switching to different fuels (Querol *et al.*, 2014). It is noteworthy that the 2012 winter presents the highest SO_2 concentrations in the 2008-2013 period caused by an increase in the use of coal-fired power plants associated to a low hydropower electricity production (REE, 2013; see Chapter 5 for further discussion).

The O_3 concentration monitored at EMEP stations in Spain has been stable over the 2001-2013 period with minimum concentrations in winter (50-55 μg m^{-3}) and maximum

concentrations ~90 $\mu g\, m^{-3}$ in summer (Figure 1-11c). Despite the aforementioned reduction in the concentration of NO_2, which is an O_3 precursor, no significant reduction of background O_3 concentration was found, probably due to the long-range transport of O_3 and an insufficient decrease of the other O_3 precursors (NMVOCs) as suggested by Colette *et al.* (2011). These findings are in line with Monteiro *et al.* (2012) who did not find a clear trend of O_3 variation in Spain for the mean and maximum hourly concentrations from 2000 to 2009 using a combination of quantile regression and clustering procedures on O_3 measurements at the EMEP stations. Saavedra *et al.* (2012a) also analysed the surface O_3 concentration trend, from 2002 to 2006, in several rural monitoring stations in Galicia, NW Spain (3 from EMEP network and 5 from regional networks) and found that mean annual values where stable whereas maximal concentrations were slightly reduced. They stated that this reduction could be related to changes in the spread of Iberian precursor emissions or to the synoptic circulation over the Northern Atlantic. This is in contrast with other authors who suggest, using monitoring data from other networks, that in Spain, there has been an upward trend in the monthly mean O_3 concentration in the last decade (2001-2010) (Santurtún *et al.*, 2015). Finally, it is noteworthy that before 2007 the maximum concentration occurs in June/July whereas from 2007 there is a bimodal distribution of the maximum concentration with a maximum in April and a second maximum occurring in July-August. As a conclusion, there is not a clear trend in O_3 in Spain.

Monitoring of particulate matter in the EMEP network is done for two fractions: PM10 and PM2.5 (particles with a diameter smaller than 10 μm and 2.5 μm, respectively). The PM10 and PM2.5 background concentrations in Spain show a large inter annual variability. However, there is a shallow decrease trend in the inter- and intra-annual variability for both fractions since 2005 (Figure 1-11d). This relatively clear overall decrease in the PM concentrations during the last decade has also been observed in several European EMEP sites (Tørseth *et al.*, 2012). It is important to highlight that besides the natural variability of PM concentration, Spain has had a decrease in its economic activity since 2008 due to a still-lasting financial crisis. This reduction in the country's growth has contributed to the downward PM concentration trend (Santacatalina *et al.*, 2012; Sánchez de la Campa and de la Rosa, 2014).

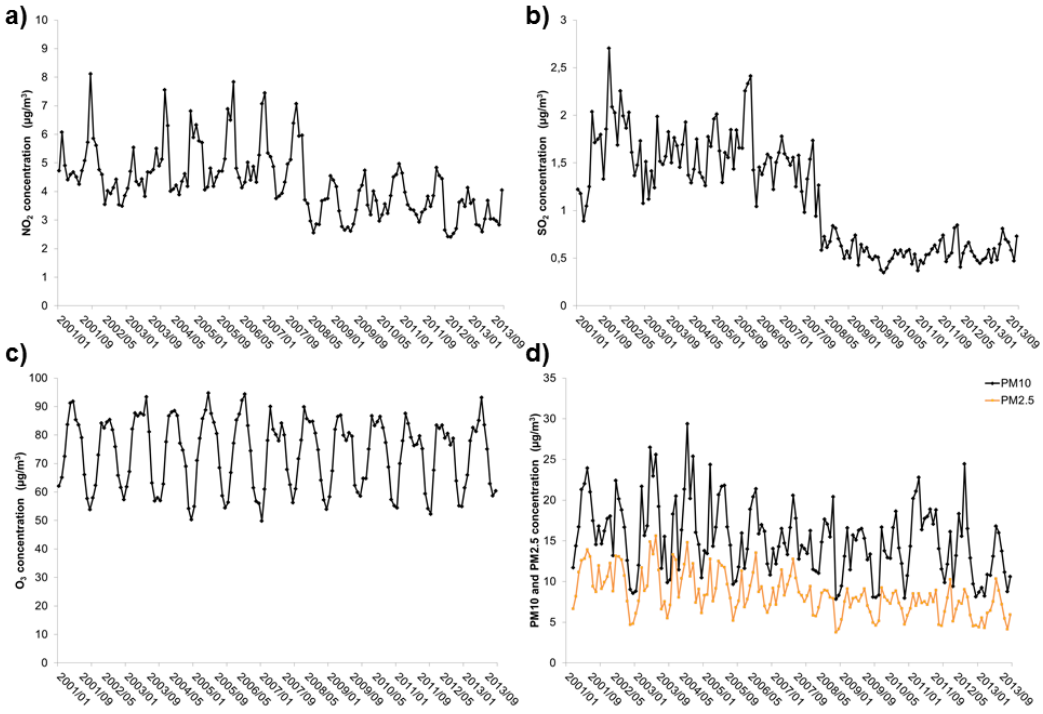

Figure 1-11. Monthly mean concentration (in µg m^{-3}) from 2001 to 2013 at the Spanish EMEP stations (Figure 1-10): a) NO_2, b) SO_2, c) O_3, and d) PM10/PM2.5

1.3.2 Spatial characteristics

This section presents a spatial characterisation of air pollution in Spain in 2012 based on the last available EEA air quality report for Europe based on AirBase database, Version 8 (EEA, 2014a). Airbase stores data monitored and reported by the Spanish government. The monitoring stations included in AirBase area categorized according to the type of area they represent (urban, suburban, and rural) and the dominant emission sources in that area (traffic, industrial, and background). To simplify the information presented here, the shortened classification used in the EEA report for Spain in 2012 (EEA, 2014b) is used – rural (background), urban (urban and suburban background), traffic (including urban, suburban and rural locations) and industrial (including urban, suburban and rural industrial sites).

The highest NO_2 concentrations are registered in traffic spots (Table 1-1) mainly in big urban areas such as Madrid and Barcelona (with annual means > 50 µg m^{-3}) but also in Sevilla, Valencia, and Murcia (annual mean 40-50 µg m^{-3}). Some locations like the Algeciras Bay, which is characterised by having heavy industry, energy facilities (a refinery and a coal-fired power plant), and one of the largest Mediterranean harbours, also presents high NO_2 concentrations in 2012 (annual mean > 50 µg m^{-3}) (Figure 1-12a). In contrast, rural stations have an annual NO_2 concentration almost 100% larger than the remote rural EMEP stations (6 and 3.5 µg m^{-3}, respectively).

Table 1-1. Annual mean concentration for NO_2, PM10 and O_3 max 8h concentration, in 2012 in Spain per station typology (EEA, 2014b)

Annual mean ($\mu g\ m^{-3}$)	NO_2	PM10	O_3 max 8h
Traffic	32	22	66
Urban	22	22	77
Rural	6	14	87
Industrial	15	21	77

Regarding SO_2, the highest annual concentrations (10-20 $\mu g\ m^{-3}$) are measured in industrial areas such as the Algeciras Bay, Puertollano, and Valle de Escombreras (Figure 1-12b). The annual SO_2 mean is also as high (10-20 $\mu g\ m^{-3}$) where the electricity-generation facilities in the coal-mining areas of Northern Spain are concentrated (Asturias, Galicia, León).

Primary PM is the result of a wide variety of emissions, both anthropogenic (industrial, power plants, transportation, off-road machinery, residential combustion, etc.) and natural (dust, sea-salt, volcanic ashes, pollen, etc.). Secondary PM results of atmospheric processing through gas-to-particle conversion and/or condensation of gaseous compounds on pre-existing aerosol particles (Monks *et al.*, 2009). Most of the secondary PM lies on within the PM2.5 fraction. Considering the complexity of PM origin it is not straightforward to explain the spatial distribution of the monitored PM concentrations and explain its causes. The PM10 annual mean concentration is in alike in urban, traffic and industrial sites ~22 $\mu g\ m^{-3}$ (Table 1-1). The PM10 maximum concentration is registered in 2012 in the urban-industrial-coastal area of Avilés (> 50 $\mu g\ m^{-3}$), followed by industrial (Puertollano, Bailén, Algeciras Bay) and traffic locations (Barcelona, Granada, Murcia) that average 30-40 $\mu g\ m^{-3}$ (Figure 1-12c). As for PM2.5, the maximum annual concentration ranges 10-20 $\mu g\ m^{-3}$ and it is monitored in a variety of locations (Madrid, Barcelona, Algeciras Bay, Atlantic coastal areas, etc.) (Figure 1-12d). The PM2.5 maximum concentration in 2012 is twice as much as the average monitored in the remote EMEP stations.

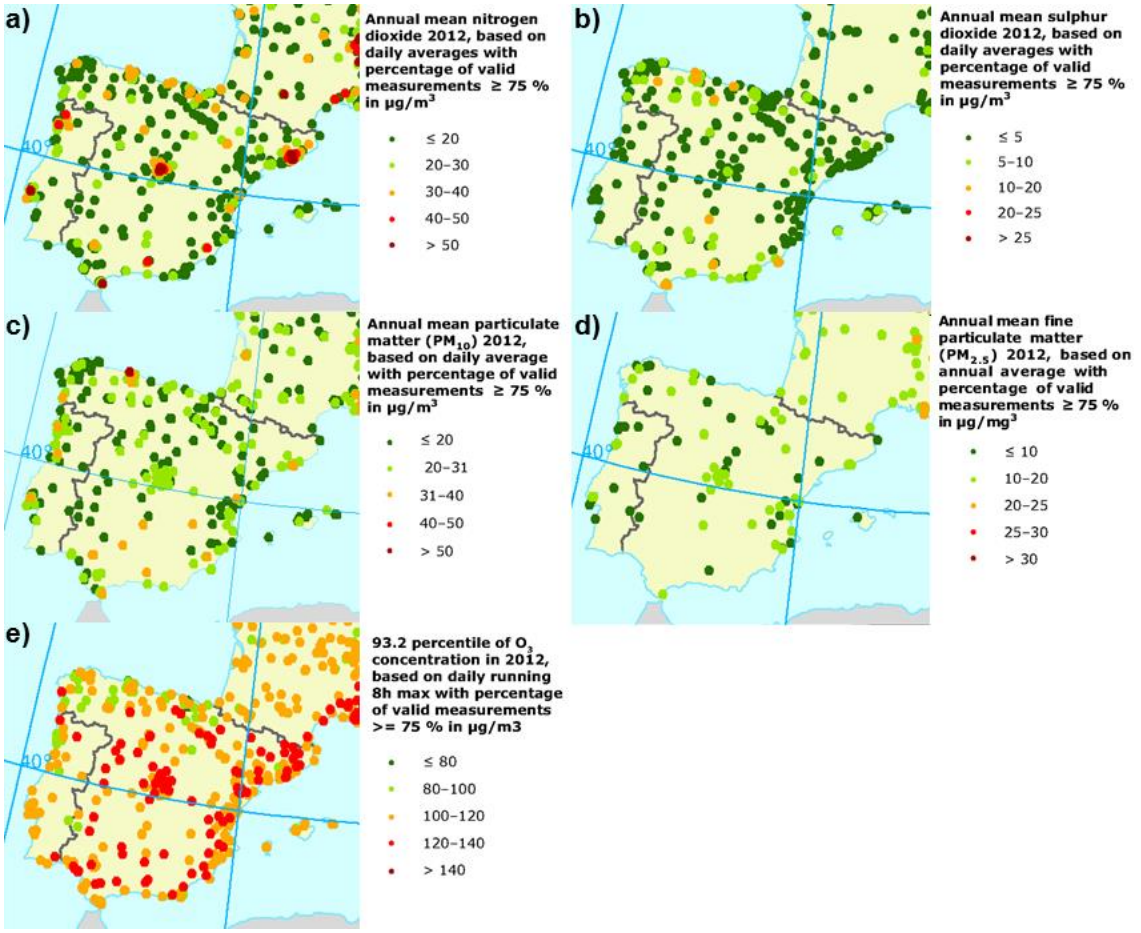

Figure 1-12. Annual mean concentration (µg m^{-3}) in 2012 at Spanish monitoring stations: a) NO_2, b) SO_2, c) PM10, d) PM2.5 and e) 93.2 percentile of O_3 max 8h (EEA, 2014a)

The O_3 formation depends on the availability of its precursors (NO_x and VOCs), the solar radiation and the temperatura (Seinfeld and Pandis, 2006). Due to large sunlight availability, Spain together with other Mediterranean countries is known for having the highest O_3 concentrations in Europe (EEA, 2014a). In Spain, a large number of monitoring stations register annual daily running 8-hour maximum (O_3 max 8h) concentrations above 120 µg m^{-3} (Figure 1-12e). Most of these stations are located in Mediterranean coastal areas as well as in the Madrid region. In contrast to other pollutants, the O_3 concentration is largest in rural areas (Table 1-1). This behaviour is explained by the fact that in traffic and urban locations, where NO_x are emitted, the formed O_3 is quickly depleted by NO_x through the titration reaction, whereas in rural areas, where the NO_x concentration is lower, the O_3 is not destroyed and it is long range transported.

1.3.3 Exceedances of normative values

The European 2008/50/EC Directive settles limit and target values for several air pollutants to protect human health and ecosystems (Table 1-2). The Directive is transposed

into the Spanish law through the "*Ley 34/2007 de calidad del aire y protección de la atmósfera*" and the "*Real Decreto 102/2011 relativo a la mejora de la calidad del aire*".

According to Ballester *et al.* (2007), who performed a review of the Spanish air quality situation based on measurements, the main problems with the compliance of the regulatory limit values in the past decade were related to i) high NO_2 and PM10 concentrations in big cities due to heavy traffic and industrialized zones such as Madrid, Barcelona or the Algeciras Bay, and ii) high O_3 concentration at rural sites in the Mediterranean area. The number of exceedances of the European limit values for the year 2012 (MAGRAMA, 2013b) and for 2014, which is the last year with official published data (MAGRAMA, 2015a), are in agreement with Ballester *et al.* (2007) (Table 1-2). Note that from a methodological point of view, the exceedance of a given limit value in a single monitoring station is enough to consider the whole AQZ it belongs to as not complying with this limit value.

In 2012, the NO_2 hourly limit value was exceeded in 2 AQZ in Madrid (downtown and in the metropolitan area, Figure 1-13a), whereas the annual limit value was exceeded in 7 zones with heavy traffic including Madrid, Barcelona, Murcia and Granada (Figure 1-13b). In contrast, the limit values of SO_2 (hourly, daily and annual) were not exceeded in any of the Spanish AQZ in 2012 and 2014 (Table 1-2).

While daily PM10 limit value was exceeded in 2012 in 9 AQZ distributed throughout the country including areas in Catalonia, Asturias, and Andalucía (Figure 1-13c), the annual limit value was exceeded only in the Asturias Central AQZ (Figure 1-13d), which is characterised by having large industrial areas and average-sized cities (Oviedo, Gijón, and Avilés: 80 000-275 000 inhabitants).

Regarding O_3, the target value for the protection of human health was exceeded in 51 AQZ (Table 1-2) including large areas of the Mediterranean coast and the centre and South of Spain (Figure 1-13e). In northern Spain (Atlantic coastal areas and in the Pyrenees) O_3 concentration was between the long term objective and the target value (at least 1 day and less than 25 with 120 $\mu g\ m^{-3}$, in orange in Figure 1-13e). The exceedances registered in 2014 are very similar in number and location as those from 2012 (Table 1-2). In 2012, the O_3 information threshold (> 180 $\mu g\ m^{-3}$ averaged during one hour between April and September) was exceeded mainly in areas downwind the cities of Madrid and Barcelona (Figure 1-13f). However, some exceedances occurred in industrial areas (Puertollano, Huelva, Vigo).

Table 1-2. Number of AQZ in Spain below and above the air quality limit values, long term objectives and target values for the protection of the human health and the vegetation, established in the 2008/50/EC Directive in 2012 (MAGRAMA, 2013b), and 2014 (MAGRAMA, 2015a). The # of AQZ depends on the pollutant

Human health

Pollutant	Temporal range, averaging period and limit value/ target value	# AQZ	Below limit/ target value		Above limit/ target value	
			2012	2014	2012	2014
NO_2	One hour (200 μg m^{-3}, not to be exceeded more than 18 times a calendar year)	134	132	133	2	1
	Annual (average of 40 μg m^{-3})	134	127	128	7	6
SO_2	One hour (350 μg m^{-3}, not to be exceeded more than 24 times a calendar year)	132	132	132	0	0
	Day (125 μg m^{-3}, not to be exceeded more than 3 times a calendar year)	132	132	132	0	0
PM10	Day (50 μg m^{-3}, not to be exceeded more than 35 times a calendar year)	135	126	132	9	3
	Annual (average of 40 μg m^{-3})	135	134	134	1	1
PM2.5	Annual (average of 25 μg m^{-3})	135	135	135	0	0
O_3	25 days of maximum daily eight-hour mean > 120 μg m^{-3}	135	84	91	51	44

Vegetation

Pollutant	Temporal range, averaging period and limit value/ target value	# AQZ	Below limit value		Above limit value	
			2012	2014	2012	2014
NO_x	Annual (average of 30 μg m^{-3})	134	134	134	0	0
SO_2	Annual (average of 20 μg m^{-3})	132	132	132	0	0
O_3	Target value: AOT40 = 18 000 μg m^{-3} h Long-term objective = 6 000 μg m^{-3} h		**Below long term objective**	**Between long term objective and target value**		**Above target value**
	2012	135	31	48		56
	2014	135	22	58		55

AOT40 (expressed in μg m^{-3} hours) it is the sum of the difference between hourly concentrations greater than 80 μg m^{-3} (= 40 parts per billion) and 80 μg m^{-3} over a given period using only the one-hour values measured between 8:00 and 20:00 Central European Time (CET) each day.

Concerning the regulations for the protection of the vegetation, O_3 was the only pollutant with exceedances on its target value both in 2012 and 2014 (MAGRAMA, 2013b). The Mediterranean Spanish zones (Andalucía, Murcia, Valencia, Catalonia, and Balearic Islands)

together with zones in the centre of the country (Madrid, Aragón and Extremadura showed exceedances of the O_3 target value).

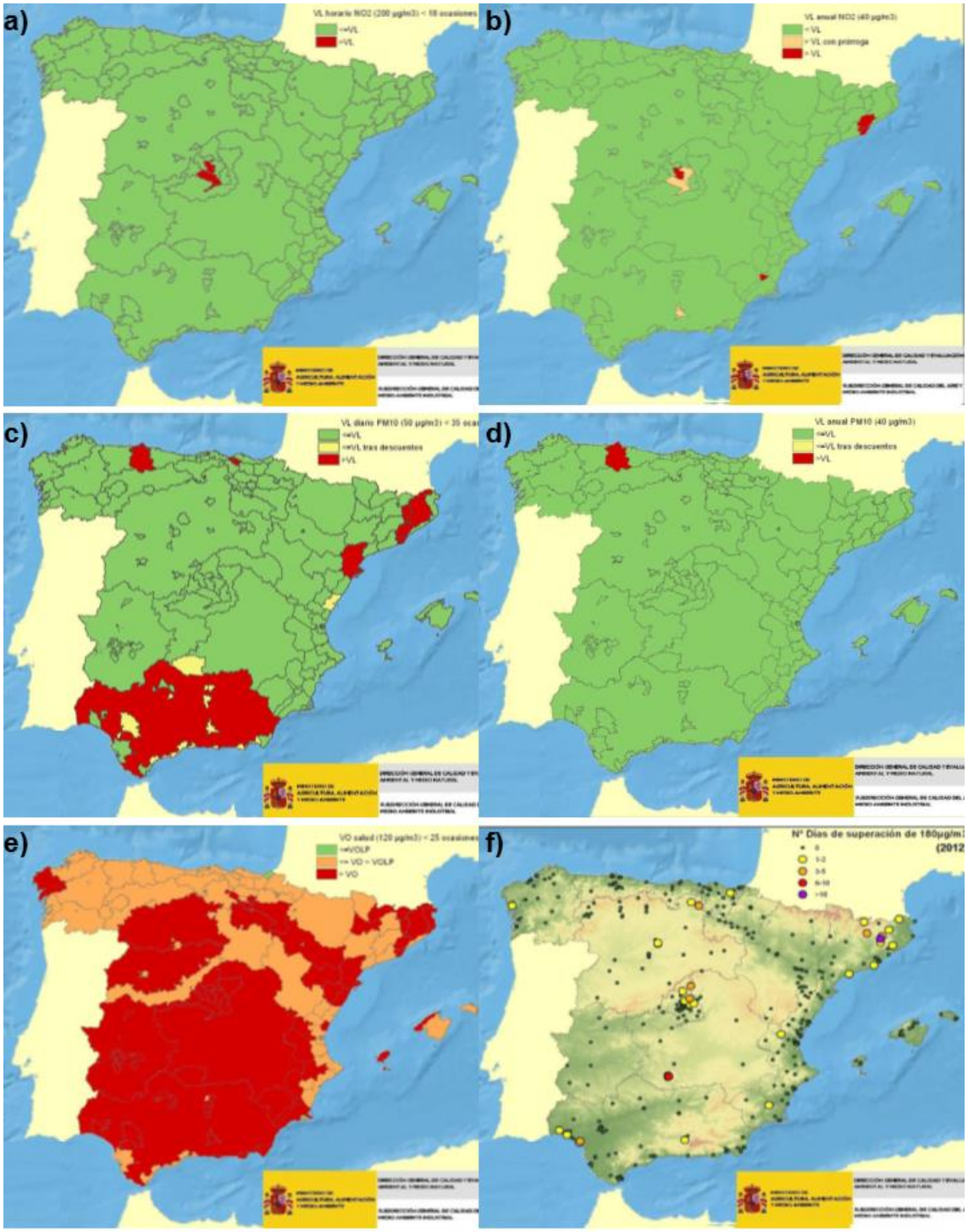

Figure 1-13. Number of exceedances of European limit and target values for the protection of human health over the Spanish AQZ in 2012: a) NO_2 hourly limit value, b) NO_2 annual limit value, c) PM10 daily limit value, d) PM10 annual limit value, e) O_3 max 8h target value, and f) O_3 max 8h information threshold (MAGRAMA, 2013b)

In 2012, the percentage of Spanish urban population exposed to exceedances of the NO_2 and PM10 limit values (annual for NO_2 and daily for PM10) and O_3 target values (O_3 max 8h) are 9.1% for NO_2, 6% for PM10,and 7.2% for O_3 (EEA, 2014b). However, the percentage of population exposed to concentrations above the target value is higher considering the more stringent WHO air quality guidelines: 17% for NO_2, 76% for PM10 and 82% for O_3 (EnAcc, 2013). In order to reduce the exceedances of the the limit values for NO_2, SO_2 , PM10, and the reduction of O_3 precursors, the Spanish Government approved in 2013, an update of the National Air Quality Plan, *Plan Aire 2013-2016* (MAGRAMA, 2013a) that sets activity-sector and transversal measures of emission abatement. Furthermore, 45 regional and 3 city scale air quality plans have been implemented since 2004 (Querol *et al.*, 2014).

1.4 Atmospheric circulation type classifications

Circulation of air masses is dynamic, and the various states of the atmosphere are not clearly separated. Synoptic climatology analyses how to classify the atmospheric circulation at synoptic scale and studies how different patterns influence a variety of surface meteorological fields (Yarnal, 1993; Dayan *et al.*, 2012). Recent examples about the analysis of how synoptic patterns influence surface meteorological fields are: the research on visibility in relation to aerosols (Dayan and Levi, 2005), desert dust outbreaks (Gkikas *et al.*, 2012), the precipitation distribution (Tveito, 2010; Casado *et al.*, 2010; Baltacı *et al.*, 2015) droughts dynamics (Fleig *et al.*, 2010), moisture flux and production of heavy rains (Müller and Kašpar, 2010), floods (Prudhomme and Genevier, 2011), wildfire occurrence (Kassomenos, 2010; Paschalidou and Kassomenos, 2016), lightning activity (Ramos *et al.*, 2011), extreme temperatures (Fernández-Montes *et al.*, 2012), the variation of North Atlantic Oscillation phases (Pastor and Casado, 2012), agricultural yields (Sepp and Saue, 2012), hospital admissions (Royé *et al.*, 2015), and air pollution (Tanner and Law, 2002; Shen *et al.*, 2015; Pope *et al.*, 2015).

The idea of analysing synoptic meteorology in relation to air quality issues started in North America as a way to forecast threatening levels of tropospheric O_3 (Wolff and Lioy, 1978). A maximum O_3 concentration fit equation was developed based on the previous day temperature and wind characteristics. Similarly, Pratt *et al.* (1983) analysed circulation variables to evaluate the origin of high O_3 concentration at rural stations in Midwestern USA. Depending on atmospheric stability and wind fields, the major contributor to local O_3 concentration was either advection of O_3 from a south-easterly suburban area or enhanced local photochemistry. Greene *et al.* (1999) stated that under different synoptic conditions, pollution patterns differed in several U.S. cities.

Therefore, in order to describe air pollution dynamics it is important to consider the characteristics of the synoptic and mesoscale patterns that affect a given territory. Flocas *et*

al. (2009) also highlight that understanding the relationship of pollutant concentrations with the prevailing synoptic patterns is a crucial matter for the analysis and forecast of air pollution.

Although atmospheric situations do not exactly repeat over time, synoptic patterns can be evaluated based on their similarities and frequency along a considered period of time. Synoptic climatologists classify the atmospheric circulation into discrete patterns or circulation types (CTs) that typify significant modes of circulation variability. Circulation type classification (CTC) techniques enable the establishment of spatial and temporal patterns of atmospheric circulation by categorizing the continuum of atmospheric circulation into a reasonable and manageable number of discrete CTs (Beck and Philipp, 2010).

The CTC techniques derive classifications from systematic analysis of one or more meteorological variables (e.g. atmospheric pressure, wind direction and vorticity). A large diversity of CTC techniques exists, especially thanks to the expansion of computer resources supporting new techniques. Nevertheless, it seems that there is not a single optimal method of classification that best fits for all purposes (Huth *et al.*, 2008). According to Yarnal (1993), the appropriate selection of a CTC technique has to be done depending on the needs of the research, the purpose of the classification and the nature of the data.

The relationship between large-scale circulation and environmental variables, including air pollutants, can be addressed in two different but complimentary approaches (Yarnal, 1993). *The circulation-to-environment approach* arranges the circulation data of interest (e.g. sea level pressure, geopotential height, etc.) according to a selected methodology and then seeks relations with the local-scale environmental variable. The circulation-to-environment approach is of interest in a predictive manner because local conditions of the studied phenomenon can be inferred from synoptic circulation. On the other hand, the *environment-to-circulation approach* structures the circulation data based on indices structuring the environmental variable (concentration levels, for example), so that composite maps of the circulation variable can be derived for a specific environmental condition. In other words, the *environment-to-circulation* approach establishes first which are the air pollution patterns and then evaluates which are the most frequent CTs within each of the studied AQ patterns. This approach provides physical insight of the large scale synoptic conditions favouring the occurrence of the studied environmental event, like high pollutant concentrations (Demuzere, *et al.*, 2011).

Within this Ph.D. Thesis, focus has been done on the circulation-to-environment approach because the aim is to characterize pollution dynamics under the typical synoptic conditions affecting the IP. An overview of recent research regarding CTC and air pollution in relation to large-scale atmospheric circulation is presented in Chapter 2.

1.5 Air quality modelling

The study of air pollution can be approached from different perspectives. Historically, ground based measurements in monitoring stations has been the most widely used technique for air pollution monitoring. The European Commission sets quality criteria to the Member States on a variety of monitoring issues (sampling methods, data validation, number and location of sampling points, etc.) through the Air Quality Directive (Directive 2008/50/EC), which has recently been amended to set more thorough criteria (Commission Directive (EU) 2015/1480). Although monitoring networks enable a spatial and temporal analysis of various air pollutants at surface level, this methodology has limitations that prevent a complete description of atmospheric pollution (discontinued data in space, insufficient temporal resolution, changes in the location of the stations that prevents long term studies, etc.).

Currently, air quality models constitute a complementary approach to monitor and characterize air pollution. Baldasano and Millán (2000) define air quality models as "computerized representations where the emissions of pollutants introduced into the atmosphere are related to the concentrations of these in the air, through the application of physical and chemical laws translated into basic thermodynamics, fluid mechanic equations, and others which are typical for chemical reactions". In other words, an air quality model is a computer-coded representation of dynamical, physical, chemical, and radiative processes in the atmosphere that aim at providing ambient concentrations of atmospheric pollutants and are useful tools to understand the transport and emissions of air pollutants from their sources, chemical reactions, physical transformation, and depositions (Jacobson, 2005).

In a model, the simulated processes are obtained by numerically solving a set of partial differential equations and parameterized equations. The basic equations considered are the equation of motion; the radiative-transfer equation; the momentum equation; the Ideal Gas equation; the thermodynamic energy equation; the continuity equation for air; the continuity equations for water in its three phases (solid, liquid, and vapour); and, the atmospheric species continuity equation (Jacobson, 2005; Seinfeld and Pandis, 2006).

Essentially, an air quality modelling system integrates three modules:

- *Meteorological model*, which describes the state and evolution of the atmosphere where the pollutants are emitted. An accurate definition of the atmospheric patterns is essential to correctly reproduce air quality, especially at urban scales and in complex terrains.
- *Emission model*, which describes the spatio-temporal distribution of both the anthropogenic and natural emissions from the emission sources. There are mainly two approaches for emission modelling: i) the top-down approach estimates total emission from national statistics combined with general emission factors and then

applies down-scaling methodologies, and ii) the bottom-up approach which estimates emissions for all the cells of the grid based on specific information. When working at high spatial resolution, especially in urban and industrial areas, the use of local information combined with bottom-up approaches is necessary in order to accurately characterise the emission sources and obtain more realistic results (Kannari *et al.*, 2007; Timmermans *et al.*, 2013). It is known that emissions are commonly the major contributor to overall uncertainty in air quality model simulations (Bieser *et al.*, 2011).

- *Chemical transport model* (CTM), which describes the physical and chemical transformation that occurs to the emitted pollutants under specific meteorological situations. The increase of the computational capacity together with advances in the knowledge of the understanding of the atmosphere processes had led to the extended use of grid-base Eulerian models in spite of Lagrangian or Gaussian plume models. Nowadays, the more advanced Eulerian models are the third generation systems which are three-dimensional non-hydrostatic online Eulerian models (Seinfeld and Pandis, 2006). The online term refers to the way in which meteorological and chemical transport models are coupled: on-line models consider the feedbacks of the simulated species on the meteorology, whereas off-line models do not (Baklanov *et al.*, 2014). The gas-phase chemical mechanism, and its aerosol module, is a central component of a CTM (Luecken *et al.*, 2008). It describes the reactions that take place in the atmosphere and interactions among chemical species that are relevant to the formation of secondary pollutants.

The main benefits of air quality models regarding the analysis of pollution dynamics are:

- They provide better spatial and temporal coverage than monitoring networks.
- They can provide information on air pollutants in remote locations, where air quality monitoring stations are unfeasible for technical/economic reasons.
- They provide information on species concentration at the surface and at several vertical levels.
- They can be used to analyse past and future events (forecast).
- They provide detailed information about emission sources, transport and deposition processes, chemical transformations, etc. with high temporal and spatial resolution.
- When used with high-resolution, they are useful to accurately assess the transport of pollutants even in regions with complex terrains like Spain.
- They can be used to track a given set of emissions (from an area of interest or a single facility) in order to analyse their contribution in terms of air pollution.
- They can be used to assess the population exposure to a given pollutant.
- They provide insight in the radiative properties of air pollution and its impact on meteorology.

- They constitute a powerful tool for air quality management and to design and implement air pollution abatement strategies.

From a regulatory point of view, when pollution is above limit values, the 2008/50/EC Directive demands a detailed diagnosis of those areas where the exceedances are found and a forecast of the evolution of ground-level concentrations. These tasks can be performed with air quality models that follow the technical guidance provided by the Air Quality Directive and its technical reference guide (EEA, 2011). Furthermore, the Forum for Air quality Modelling (FAIRMODE, http://fairmode.ew.eea.europa.eu) coordinates and gathers information from air quality modellers and users in Europe in order to develop guidance and support the harmonised use of models by EU Member States. This forum provides tools to evaluate the performance of air quality models in Europe (Thunis and Cuvelier, 2015).

Besides the list of advantages of the modelling approach aforementioned there are some important limitations that have to be considered. In first term, deterministic models that rely on solving sets of partial differential equations are computationally expensive tools and they may require large storing and computing equipment. Second, the development of emission models require extensive, reliable and updated input data which is not always easy to access and manage (Guevara *et al.*, 2013). Third, there are knowledge gaps in the physics and chemistry that governs the concentration of pollutants in the atmosphere (Luecken *et al.*, 2008). It is also a difficult task to translate the available knowledge into appropriated computer code. Therefore, there are uncertainties in the simulations provided by the models.

1.6 Motivations

Air pollution is a critic issue due to its effects on human health, climate, ecosystems and economic activities. Despite a downward trend in the emissions and in the air quality concentrations in the last years, Spain continues to exceed the legislated target and objective values to protect the human health and the environment. Currently, the main problems regarding gaseous air pollution in Spain are associated to high concentrations of NO_2 in urban areas; of SO_2 in industrial and electricity-generation sites; and high O_3 concentrations in and downwind cities associated to urban emissions of O_3 precursors (MAGRAMA, 2015a).

Due to historic reasons related to the exploitation of coal mines, in Spain, the contribution of coal-fired power plants to the electricity generation pool tends to be higher than in other European Countries. In fact, in 2012 it accounted for 19.3% of the yearly electricity production, being the second technology in electricity generation (REE, 2013). The emissions of SO_2 and NO_2 associated to the coal-fired power plants affect the air quality

close and away of the sources. However, there is not yet a comprehensive quantification of the contribution of these power plants to air quality in Spain.

Regarding on-road transport emissions, it is important to notice that over the last decades, the dieselization of the Spanish vehicle fleet has been particularly large compared with other European countries (12% Europa and 10% Spain in 1991 vs 38% and 70% in 2011, Salvador *et al.*, 2012; González *et al.*, 2014). Dieselization could explain in some extend the persisting high levels of NO_x in and downwind Spanish cities. Furthermore, several recent reports indicate that on-road vehicle NO_x emissions are far higher than those required by the requirements of the European legislation (EURO5 and EURO6) in diesel vehicles under real-world conditions (Franco *et al.*, 2014; Borken-Kleefeld, 2014; Kadijk *et al.*, 2015). The car industry not compelling the legislation has probably helped maintaining large concentrations of NO_x. Considering that the net impact on health from pollution tied with transport in Europe is greater than that associated with traffic crashes alone (Künzli *et al.*, 2010) it would be interesting to quantify the net contribution in terms of air quality concentrations of on-road transport emissions from the most congestion urban areas of Spain.

According to the European Union, there is a need of coordinated actions at international, EU, national, regional and local levels in order to properly face air pollution and minimize its impacts (EEA, 2014a). The provision of robust information on the mechanisms that explain air pollution in Spain is crucial to support national and sub-national policies and for environmental and health impact assessments. It is therefore necessary to understand the air pollution dynamics in Spain to enable the development and implementation of effective emission abatement strategies.

As it has been previously stated, it is necessary to understand the relationship of the pollutants' concentration with the prevailing circulation, both at synoptic and mesoscale to properly explain the air pollution dynamics in a given territory (Flocas *et al.*, 2009). Currently, there are still large uncertainties in the role of synoptic scale meteorology on air pollution dynamics in Spain. In order to analyse the air pollution dynamics in a multi-scale context it is first necessary to establish a discrete classification of the continuum of atmospheric circulation at synoptic scale over the IP. In Spain, there is a need of an objective and replicable circulation-type classification for air quality purposes that avoids the subjectivity of the existing synoptic classifications.

In order to go beyond the measured-based view of air quality provided by the monitoring networks, and to understand the relationship between meteorology and the air pollution dynamics associated to the key emission sources in Spain, air quality models seem to be the most suited tool since they offer a complete deterministic description of the air quality processes. However, it is necessary to verify if the models are able to properly simulate the meteorological and pollution dynamics in Spain under a variety of synoptic conditions.

Furthermore, it is interesting to check how air quality models can be used to characterise the plume dynamics and the contribution in terms of surface concentration, of a given emission source.

Currently several modelling tools are available to attribute air pollution to a specific location/emission source, namely, the brute-force approach and source-oriented apportionment techniques. The brute force approach consists on subtracting to a simulation that considers the total set of emissions a second simulation done without the emissions of interest. This approach is useful for primary pollutants but not for secondary pollutants like O_3 due to their non-linearity respect to the emissions. The study of O_3 attribution can be performed with CTMs that possess a specific source apportionment module (Cohan and Napelenok, 2011). In the Spanish context, little is known regarding the specific contribution of power plants and on-road transport emissions to SO_2/NO_2 and O_3 concentrations and dynamics, respectively. It is therefore interesting to assess how air quality models can provide insight in the understanding of the relationship between the synoptic conditions and specific plumes of SO_2/NO_2/O_3. Attributing sources to air quality concentration under typical CTs helps increasing the knowledge on the role of anthropogenic emission and synoptic patterns in the air quality dynamic in Spain, and are useful to desing efficient abatement strategies. The outcomes of the present Ph.D. Thesis will systematize differences in air quality dynamics as a function of synoptic CTs and main emission sources in urban and industrial areas (road-traffic and power plants, respectively).

1.7 Objectives

Considering the environmental and scientific contexts regarding atmospheric pollution in Spain as well as the motivations presented in the previous Sections it is possible to state the aim of the Thesis. **The main objective of the present Ph.D. Thesis is characterising air pollution dynamics in Spain under typical atmospheric circulation types at synoptic scale by means of modelling techniques, focusing on the main gaseous pollutants (NO_2, SO_2, and O_3)**.

To fulfil this main objective, it is necessary to develop the following specific objectives:

1. **Identifying the CTs affecting the IP, in a climatic basis, by means of an objective CTC and selecting representative episodes**. This objective implies trying different classification techniques and setups and evaluating the resulting classifications by means of objective evaluation metrics. Once the classification is performed, the typical CTs are characterised in terms of their spatial synoptic configuration and advective characteristics, their frequency, duration, the time of year they occur, their transitions, etc. The selection of representative episodes

is crucial because only the representative episodes are further analysed by means of air quality modelling.

2. **Characterizing the SO_2 and NO_2 dynamics over large urban areas and heavy industrial/electricity-generation areas for typical CTs.** The study of NO_2 dynamics is performed for the biggest urban and industrial Spanish areas whereas for a set of specific individual power plants the analysis is done for both SO_2 and NO_2. The pollution dynamics are characterised based on an integrated analysis of emissions, meteorology, and transport of the pollutants under each CT.
3. **Characterizing the O_3 pollution dynamics attributed to on-road transport from the biggest cities in Spain for typical CTs.** In order to fulfil this objective, it is necessary to first attribute and quantify the O_3 to the sources of interest, and second to describe how the characteristics of each CT explain the the O_3 transport dynamics.

1.8 Structure of the thesis

The present document presents the main findings and discussions of the Ph.D. Thesis entitled "Characterization of atmospheric pollution dynamics in Spain by means of air quality modelling", and it is structured as follows.

An introductory overview on air pollution impacts, the trends and current air quality levels in Spain have been provided in **Chapter 1**. Furthermore, a summary of the exceedances of the current legal framework and an introduction to the role of atmospheric circulation at synoptic scale and CTC is given. In addition, this Chapter introduces the scientific context of air quality modelling. According to all this information, the objectives to be achieved within this Ph.D. thesis have been stated.

Chapter 2 reviews the field of CTC and describes the work done to objectively establish a CTC over the IP on a climatic basis (1983-2012). This chapter also characterises each of the typical CTs identified and shows the method used to select a representative episode of each CT on a representative year.

Three dimensional modelling systems are the most advanced tools in air quality modelling and allow characterising pollution dynamics at regional scale, taking into account the emitted pollutants, the meteorological conditions, the tropospheric chemistry and topographic features that condition the final concentrations over an area. **Chapter 3** presents the air quality modelling system used in this Ph.D. Thesis and evaluates its performance on the episodes of interest.

Chapter 4 analyses the NO_2 pollution dynamics associated to the biggest urban areas in Spain (Madrid, Barcelona, and Valencia) and from industrial/energy-generation areas (Asturias and the Algeciras Bay).

Chapter 5 focusses on the SO_2 and NO_2 dynamics associated to coal-fired power plants that are a punctual cause of air quality problems. The application of a brute-force modelling approach enables to relate the power plants' emissions and the complex atmospheric dynamics that occur under the most typical CTs affecting the IP.

Chapter 6 presents the results of the study performed to characterise the O_3 dynamics attributed to on-road transport emissions from the Madrid and Barcelona metropolitan areas under the typical CTs affecting the IP. Barcelona and Madrid are the largest conurbations of Spain and they are characterised by large on-road traffic emissions. The analysis shows the differential behaviour of O_3 dynamics in a coastal and a continental environment.

A summary of the main results is given in **Chapter 7** where recommendations for future research are also discussed. Finally, all references used in the Ph.D. Thesis are compiled in **Chapter 8**.

2. Circulation type classification

This chapter is based on: Valverde V, Pay MT, Baldasano JM. 2014. Circulation-type classification derived on a climatic basis to study air quality dynamics over the Iberian Peninsula. International Journal of Climatology ***35****. DOI: 10.1002/joc.4179.*

2.1 Introduction

Air quality depends on emissions, both natural and anthropogenic, meteorology, and the topographical characteristics of the area under study (Baldasano *et al.*, 1994; Seinfeld and Pandis, 2006). At the local scale natural emissions depend on temperature and humidity. Transport relies on wind characteristics and vorticity. Photochemistry is determined by temperature, humidity, and solar radiation. Precipitation influences deposition (wet removal), and topography controls mesoscale dynamics such as land-sea breezes and mountain-valley winds. Furthermore, atmospheric circulation at the synoptic scale affects pollution transport at the regional scale (Flocas *et al.*, 2009). Therefore, in order to characterize air quality in a given territory, it is necessary to understand the role of the synoptic circulation controlling its regional and local dynamics (Elminir, 2005; Giorgi and Meleux, 2007; Demuzere *et al.*, 2009).

In recent years correlations between air quality and specific synoptic patterns or CTs have been studied. Demuzere *et al.* (2009) provides insight in regional meteorological processes that play a role in O_3 formation at four mid-latitude sites in the Netherlands. Shreshta *et al.* (2009) and Zhang *et al.* (2013) reveal that under the influence of CTs with high wind speed, low O_3 concentrations were registered in Southeast Asia, whereas with weak synoptic winds high O_3 concentrations were registered. Ganor *et al.* (2010) relates the occurrence of mineral dust outbreaks in the Eastern Mediterranean to the presence of thermal low pressure areas over Maghreb. In the IP under anticyclonic conditions mesoscale phenomena control O_3 during summer along the Spanish Mediterranean coast (Millán *et al.*, 1997; Barros *et al.*, 2003; Gonçalves *et al.*, 2009; Castell-Balaguer *et al.*, 2012). In summer under a blocking anticyclone over Central Europe, there is a net transport of O_3 and precursors towards NW Spain that increases surface O_3 concentration (Saavedra *et al.* 2012b). Exceedances of PM10 limit value have been related to the transport of mineral dust from the Sahara, especially in late spring when a deep low is centred over the Western

Portuguese coast, and in summer when a high pressure system is formed to compensate a thermal low at the surface over Algeria (Salvador *et al.* 2008, Salvador *et al.*, 2013).

Synoptic classifications enable the establishment of discrete CTs by categorizing the continuum of atmospheric circulation based on their similarities (Beck and Philipp, 2010, Philipp *et al.*, 2014). The European Cooperation in Scientific and Technology Action 733 (COST733) harmonised classification techniques over Europe (Philipp *et al.*, 2010) in three groups: subjective, automatic and hybrid. Automatic techniques based on statistical methods find patterns within the input data and assign samples (days) to the identified CTs in a systematic and objective way, although their configuration critically affects the results (Philipp *et al.*, 2014).

Several synoptic classifications have already been derived over the IP (or areas within) for different purposes. This include atmospheric transport characterization (Petisco, 2003; Rasilla, 2003; García-Valero *et al.*, 2012), wind analysis (Azorin-Molina *et al.*, 2009; Jiménez *et al.*, 2009), precipitation trend (Romero *et al.*, 1999; Casado *et al.*, 2010; Casado and Pastor, 2013), snowfall variability (Esteban *et al.*, 2005), lightning activity (Pineda *et al.*, 2010), desert dust intrusions (Alonso-Pérez *et al.*, 2011; Salvador *et al.*, 2013), and transport of pollutants (Saavedra *et al.*, 2012b; Russo *et al.*, 2014).

The present work aims to obtain an objective and automatic synoptic classification over the IP on a climatic basis (1983-2012) to enable further air quality dynamics characterization (Figure 2-1). Sensitivity analyses are first performed to several classification techniques and other factors affecting the classification to identify a reference set-up. Second, the resulting CTs are characterized. The synoptic classification is evaluated in terms of its temporal stability, which allows the identification of the most representative year during the climatic period. Kinematic back-trajectories obtained by means of the HYbrid Single-Particle Lagrangian Integrated Trajectory model (HYSPLIT, Draxler and Rolph, 2013) are used to confirm the resulting CTs.

This chapter is organized as follows. Section 2.2 gives on overview of the diversity of CTC techniques currently available. Section 2.3 describes the methods and data used to derive and evaluate the synoptic classification, and to define a representative year and representative days. Section 2.4 shows the results of the sensitivity analyses and the characteristics of the identified CTs, the temporal stability of the classification and the comparison with the back-trajectories. Finally, conclusions on the application and interpretation of the CTC over the IP are given in Section 2.5.

2.2 Circulation Type Classification Techniques

The research on classifying atmospheric patterns started long years ago (Hellmann, 1908) and has been a topic of interest, providing a wide range of classification methodologies (Yarnal *et al.*, 2001). Huth *et al.* (2008) reviewed the current tendencies and developments in both methodology and applications of CTCs. CTC are derived for a specific time and region of interest from different meteorological variables (such as sea level pressure (SLP), wind components, geopotential height for different pressures) and are used afterwards for different purposes.

In spite of the long tradition for CTC, nowadays there is not a consistent system for CTC for all Europe. Due to its interest for several environmental topics, a European Cooperation in Scientific and Technology (COST) Action (COST733) was settled to summarize all these approaches for a European and twelve national domains. The COST733 Action "*Harmonisation and Applications of Weather Type Classifications for European Regions*" was a five year activity, running from 2005 to 2010, which involved more than 60 scientists from 23 countries. The main objective of the Action was to achieve a general numerical method for assessing, comparing and classifying typical synoptic situations in the European regions scalable to any European (sub)region with time scales between 12 h and 3 days and spatial scales of ca. 200 to 2000 km, applicable for a number of issues such as AQ, meteorology, agriculture, etc. (Philipp *et al.*, 2010).

An extensive list of methods (up to 73) was identified. Most of the available CTC in Europe work on daily basis using information on SLP, geopotential height or wind fields. Nevertheless, there are few methodologies that use shorter time scale (6 to 12 hours) and/or information about cyclone trajectories or weather variables. Half of the available classifications considered by COST733 (around 40) are run in a continental scale whereas 20% have a subcontinental scale and 20% have a country scale. The rest of the CTC have a regional or local spatial scale (Huth *et al.*, 2008). After a review process, Philipp *et al.* (2010) classify CTCs methods into three main groups: subjective, automated and hybrid techniques.

When possible, methodologies were compiled into the software for classifying CTs: the *cost733class software*. The developed CTC software (hereafter, referred to as cost733class software) contains a variety of classification methods and is flexible towards choice of domain of interest, input variables, time step, number of CTs, sequencing and (weighted) target variables. It was specially developed for European domains. The availability of this automated classification schemes coupled with the generalize use of several 3D grid based reanalysis datasets has increased considerably the interest and applicability to establish links between CTs and environmental variables such as air pollutants. The cost733class software has been assessed several times and research gives confidence to the resulting

classifications (Beck and Philipp, 2010; Huth, 2010). Therefore, it is a powerful tool to assess air pollution dynamics under different atmospheric circulation patterns.

For most of the CTC methods two steps are required. First, the definition of the CT. Second, the allocation of observations (atmospheric situation of a given hour or day) to one of the CTs defined in the first step. Depending on the definition of types, the existing methods can be organized into two approaches: top-down, in which types are defined based on expert knowledge; and bottom-up, in which types are established as a result of the calculation process. According to the definition approach and how observations are assigned to a CT, five methodological families of classifications can be identified (Table 2-1).

Table 2-1. Conceptual division of CTC techniques

Top-down	1. Manual techniques	Subjective method
	2. Hybrid manual-automatic techniques	Subjective-objective method
Bottom-up	3. Automatic based on correlation techniques	Automatic and objective methods
	4. Automatic based on eigenvector techniques	
	5. Automatic based on cluster techniques	

2.2.1 Manual techniques

Manual techniques are based on the expertise of climatologists/meteorologists and integrate the perceptual experience and other unquantifiable qualities of the specialists involved. The advantage of this method is that the knowledge and experience of meteorologists is fully used in the classification. The major disadvantage is that the results are typically subjective and time consuming and cannot be reproduced. Moreover, the method can only be applied for certain geographical regions.

The criteria used by the person performing the classification, has usually been referred to features of isobars or isopleths of geopotential height. Many subjective classifications have been developed for different regions with different scales: Hess and Brezowsky (1952) for Central Europe and Lamb (1972), for the British Isles, are the more used ones. Martín-Vide (1991) established a subjective CTC for the IP.

2.2.2 Hybrid manual-automatic techniques

Hybrid manual-automatic techniques are based on manual classification systems with proven practical and scientific value but use automated-computer assisted methods to assign circulation patterns to each of the predefined CTs. Two examples of well-known classification systems that have been made hybrid are the Grosswetterlagen (James, 2007) and the Lamb systems (Jenkinson and Collison, 1977).

2.2.3 Automatic techniques

The third group of CTC is made of objective and automated techniques. It is based on the availability of computers that allow fast classification of large databases following automatized algorithms and new analytical methods and concepts. Automatic methods differ upon the way CTs are defined and on the statistical techniques used to classify individual atmospheric circulation samples among CTs. Thus, in recent years, the number of so-called objective CTC has increased rapidly (Huth *et al.* 2008) enabling the use of high spatial and temporal resolution databases. The most currently automated techniques used are those based upon multivariate statistics such as regression techniques, eigenvector techniques or clustering techniques (Esteban *et al.*, 2006).

Automatic based on correlation techniques are based on measures of similarity between observed pressure fields. Lund (1963) described this approach, and since then, very few changes have been done with this technique. Basically, the methods are based on a selection of typical grids, representing typical synoptic situations (also called leader maps). Although the method is straightforward when deciding the typical grids, doing so is critical for the results. Lund (1963) suggested selecting the synoptic situation having most occurrences with r^2 above 0.70 with all the other situations as CT. All situations having a correlation with this pattern higher than 0.70, are assigned to this CT. All these episodes are removed from the dataset, and the procedure is repeated for all remaining situations until all of them are classified. Lund (1963) chose the threshold r^2=0.70 to prevent too many unclassified days, but this threshold should be selected individually in order to establish a suitable number of circulation patterns.

The main disadvantage of this technique is their tendency to produce a huge group accompanied by many small ones (Huth *et al.*, 2010). Recent advances in correlation-based classification techniques are shown in Erpicum *et al.* (2008) and Fettweiss *et al.* (2010) which evaluate changes in mid-tropospheric circulation trends over Greenland and their relation to ice melting, using daily 500 hPa geopotential heights. These studies use a different coefficient to assess similarity among CTs obtaining improvements on CT sizes.

Automatic based on eigenvector techniques, such as Principal Component Analysis (PCA), have been used frequently in the identification of synoptic patterns (Huth *et al.*, 2008). The methods are used to decompose observed fields into few sets of orthogonal – and thereby statistical uncorrelated – fields. Their advantage is their capability to handle large datasets in an easy way, allowing an increase in the resolution (spatial, temporal or number of variables of interest) of the analysis. Redundant information is removed and relations among different variables are made evident. One of the weaknesses of the method is that it is a pure statistical technique. Therefore, there is no direct physical explanation of the results found.

Different PCA configurations are available. Kruizinga (1979) proposed an *s-mode PCA* with unseasonalysed 500 hPa geopotential height data for the evaluation of CTs over central Europe. The first CTs were related to different combinations of vorticity and zonal and meridional wind components but the results were strongly related to the size of the grid. S-mode PCA has also been used in the Catalonian domain for the assessment of daily precipitation patterns in relation to atmospheric CTs (Serra *et al.*, 1998). Using daily winter precipitation data, a PCA classification approach led to the establishment of rainfall patterns in Catalonia for the major CTs which were consistent with authors experience in forecasting in the domain.

Richman (1986) promoted the use of *t-mode PCA* with oblique rotation using mean SLP summer data. Although the first CTs obtained were clearly related to well-known circulation patterns, those CTs defined by the lower significance principal components were difficult to interpret in terms of atmospheric circulation. Romero *et al.* (1999) used a combined PCA technique followed by a cluster classification to evaluate heavy rainfalls in the Mediterranean Spain. A t-mode PCA was run using daily 500 hPa and 950 hPa geopotential heights from gridded data of a 9-year period. For the most relevant principal components, a clustering technique was applied and results showed 19 CTs, one of which was related with 40% of torrential rains in the domain. A similar approach was followed by Esteban *et al.* (2005; 2006) within the Pyrenees and Western Europe spatial domain. They used a CTC technique which consisted of an s-mode PCA with a varimax rotation followed by a k-means cluster analysis. PCA helps removing colinearity from the data and thus improves the classification made by the cluster technique. Using reanalysis MSLP data in a 2.5º grid, they evaluated CTCs in relation to heavy rainfalls and snowfalls. This technique requires a pre-processing of the data and several assisted steps in which subjectivity may arise but results are consistent with previous knowledge of atmospheric circulation in the area and its use is suggested for weekly to daily phenomena.

Automatic based on cluster techniques group related atmospheric situations based on multivariate distances. Different configurations may be applied such as the kind of clustering (hierarchical or non-hierarchical), the number of groups used (pre-defined or as a result of the technique), the cluster linkage method (single, complete, average, etc.) the way to measure distances (i.e. Euclidean, Bray-Curtis), and consideration of extreme values, among others. Most of the cluster techniques rely on the non-hierarchical k-means algorithm. The k-means clustering aims at partitioning n observations into k clusters in which each observation belongs to the cluster with the nearest mean. The application of this algorithm favours having well separated and equally-sized CTs. Nevertheless, the physical interpretation of the results may be misleading (Huth *et al.*, 2008). Enke and Spekat (1997) used several daily upper air pressure variables (geopotential heights of several pressures and thickness of air mass between different geopotential heights) to determine, thanks to a cluster technique, CTs over the Atlantic-European domain in a 30-year period, for weather downscaling purposes. They used a minimum distance method of clustering

which consisted on i) subjectively choosing the most dissimilar pressure patterns as starting partition, ii) assigning all remaining weather patterns to their most similar class by calculating Euclidean distances, and iii) rearranging weather patterns iteratively to reach a stable final state. Only CTs with more than 5% of the observations were kept. Resulting CTs showed good agreement with previous knowledge of climate patterns in relation to temperature and sunshine duration when seasonal data were used. Within the Spanish domain, Petisco *et al.*, (2005) have developed a method of CTC for precipitation downscaling purposes. As a starting point to the downscaling process, they searched to establish a database of CTs for the 1961-1990 period, using daily 500 hPa and 1000 hPa geopotential heights. First, they run a correlation analysis to find the leader days following Lund (1963) methodology; second, they used k-means classification to expose the main CTs. The main problem of this method is that in the search of leader pressure maps, if the correlation coefficient value is too high, most of the found CTs are very similar. Philipp *et al.* (2007) used a newly implemented clustering scheme combining the concepts of Simulated ANnealing and Diversified RAndomization (SANDRA) to determine changes in CTs over North-Atlantic European region using daily SLP data of a 150-year time span. SANDRA allowed reduce the influence of chance in the cluster assignment (respect to k-means), leading to CTs that are more stable and reproducible. Nevertheless, selecting the number of meaningful CTs is not yet well established.

2.2.4 Alternative methods

The COST733 Action summarizes most of the methods that may be used to classify atmospheric circulation patterns in Europe. Nevertheless, some other approaches exist and have already been tested for different purposes.

According to Kuebler *et al.* (2002), the classification and regression tree (CART) method is one of the most common statistical tools used to identify patterns. From a multivariate database (comprising several independent variables and a dependent variable), the method partitions the observations into sub-groups by selecting the most important patterns of independent variables that help to explain the variability of the dependent variable (based on correlation). For each splitting, two groups are formed and the method is re-run in each of the sub-groups. A predictive tree for the dependent variable is built according to the values of the independent variables. Based on this recursive binary partition, CART is able to detect patterns and is therefore, useful to evaluate AQ issues (dependent) in relation to meteorological data (independent). CART is a supervised method that introduces subjective criteria when deciding the thresholds at each splitting step, making it difficult to automatize the process of classification for large databases thus its use is limited for the purposes of this proposal.

Some other approaches use multiple linear regressions (Stadlober *et al.*, 2008). Others rely on nonlinear multiple regressions or artificial neural networks (Papanastasious *et al.*, 2007).

Singh *et al.* (2012) compared linear and nonlinear modelling approaches for NO_2, SO_2 and PM prediction in an urban area in India. They found that, in general, nonlinear methods (neural networks and multivariate polynomial regression) performed better than linear ones (partial least square regression)

In certain cases, back trajectory modelling has been used, in combination with chemical species and/or synoptic maps to identify long-range transport sources of polluted air masses that may have an impact on local pollution. Jorba *et al.* (2004) analysed 4-day back trajectories in the Barcelona area for the period 1997-2002 to summarize and quantify the flow characteristics of long-range tropospheric transport. After a clustering process of back-trajectories based on wind speed and direction, results pointed to westerlies as the main wind direction. Nevertheless, there was a high variability of the speed, length and curvature of atmospheric masses and the importance of recirculations, depending on the season of the year, the height considered (5500, 3000, and 1500 m above sea level were analysed) and the relative North Atlantic Oscillation phase. It is noticeable that the Atlantic provenance dominated in all seasons except in summer when regional circulations predominated. Moreover, important decoupling of the lower from the middle troposphere was observed, especially during summertime.

Vardoulakis and Kassomenos (2008) identified the origin of PM10 pollution in two cities through the analysis of back-trajectories. They found that long-range transport of particles from continental Europe had a marked effect on PM10 background levels in Birmingham, while the local meteorology had a stronger influence on PM10 levels in Athens.

A more recent evaluation of clustered, 4-days back-trajectories at 1500 m above sea level near Barcelona (Izquierdo *et al.*, 2012) showed annual dominance of western flows when comparing 1980s to 2000s decades. Nevertheless, an increased contribution from central Europe and Northern-Africa were detected, particularly in autumn-winter and summer respectively.

2.3 Methods

A synoptic classification is sensitive not only to the classification technique (clt) but also to other factors as the number of CTs considered (nCT) (Michelangeli *et al.*, 1995; Philipp *et al.*, 2007; Fereday *et al.*, 2008, Philipp *et al.*, 2014), the large-scale input meteorological variable used as proxy (iv) (Casado and Pastor, 2013), the vertical level of the input meteorological variable (vl) (Erpicum *et al.*, 2008), the temporal resolution (tr) (Casado and Pastor, 2013), performing an annual or seasonal classifications (se) (García-Valero *et al.*, 2012), the horizontal resolution (hr), and the domain size (d) (Jiménez *et al.*, 2009; Demuzere *et al.*, 2009; García-Bustamante *et al.*, 2012; Beck *et al.*, 2013). Sensitivity tests have been performed to identify the most objective set-up possible for the synoptic

classification used in the air quality characterization (Table 2-2). The software used to derive the classifications is the open source cost733class software version 1.2. It was developed during the COST733 Action for easily creating, comparing and evaluating classifications (Philipp *et al.*, 2014).

The analyses cover the climatic period of 1983-2012 and use ERA-Interim reanalysis data (Dee *et al.*, 2011; http://apps.ecmwf.int/datasets/data/interim-full-daily/) from the European Centre for Medium-Range Weather Forecasts (ECMWF). The reanalysis dataset provides reliable gridded meteorological variables over a global domain every six hours, at several horizontal resolutions, both at the surface and staggered at 37 vertical levels up to 1 hPa geopotential height.

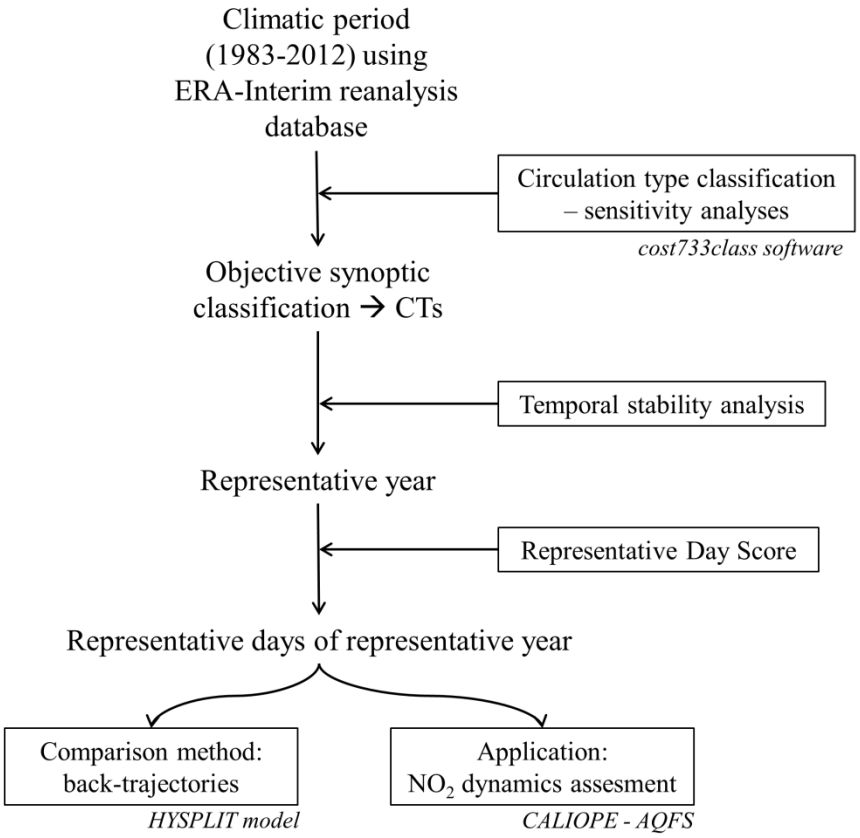

Figure 2-1. Methodological flowchart to obtain representative days of the objective CTC. Methodologies are shown in boxes and tools are indicated in italics

An optimum classification maximizes the separability of the identified CTs while minimizing the within-type variability. The Explained Variation (EV) index is a measure of the classification quality (Equation 2-1). EV is the result of the ratio between the internal variance of all the CTs (WSS) and the total variance of all the elements without clustering (TSS). WSS is the distance among samples in one CT calculated as within CT sum of squares (Equation 2-2), and TSS is the total sum of squared differences between all elements and the overall mean.

$$EV = 1 - (WSS/TSS) \quad \text{(Equation 2-1)}$$

$$WSS = \sum_{j=1}^{k} \sum_{i \in CT_j} D(X_i, \bar{X}_j)^2 \quad \text{(Equation 2-2)}$$

In Equation 2-2, k is the number of CTs, CT_j is the j of the k CTs, and D is the Euclidean distance between the sample (X_i) and its CT centroid ($\bar{X}_j$). The Euclidean distance is calculated considering the meteorological variable used in the classification on all grid cells. The sensitivity analyses are evaluated through the EV, which ranges from 0 to 1. CTs are more meaningful in terms of explaining the original amount of information when EV is closer to 1. According to Demuzere *et al.* (2011), the choice of an appropriate CTC should be based on an objective evaluation of the explanatory power of the CTs on the region they are derived for and the purpose of the classification. Therefore in this research, the choice of the configuration has been done attending not only to the quality of the classification (expressed by the EV) but also to its main purpose, which is the identification of typical CTs to study their influence on air quality dynamics over the IP.

The Rand Index (RI) is used as a measure of the agreement between two classifications with the same or a different number of CTs (Rand, 1971). RI ranges from 0 to 1. High values of RI imply that the identified CTs are similar in both classifications.

The identified CTs are characterized by describing the atmospheric dynamics from a synoptic point of view. The description includes the relative location of the action centres, which determine the direction and speed of air masses both at the surface and 500 hPa geopotential height (Z500). Z500 is situated at a level which the weight of the air column above and below it are alike enabling an estimation of the vertical structure of the atmosphere. Moreover, a quantitative description of each CT is given including the climatic frequency, the monthly distribution, the transitions between CTs which is useful for predictability at medium term (James, 2007), and the mean and maximum persistence. Cahynová and Huth (2009) defined persistence as the length of a sequence of days that are classified with one CT, while preceded and succeeded by another CT.

A temporally stable synoptic classification is able to identify similar CTs when using meteorological databases for different periods. An evaluation of the temporal stability of the classification is performed following a cross-validation process similar to that used in Fereday *et al.* (2008) and García-Valero *et al.* (2012). The synoptic classification of each year is compared to the 1983-2012 classification. The total stability is defined as the percentage of days within the year that are classified in the same CT in both classifications. Higher total stability indicates more similar results between the yearly and the 1983-2012 CTC. The year with the highest stability is selected as the representative year.

To confirm the consistency of CTs with the main sources of air masses directed towards the IP (Martín-Vide and Olcina, 2001), a comparison with ensemble back-trajectories on a representative day of each CT is performed. To adequately sample the history of the mass, the HYSPLIT model is used to determine 60-h back-trajectories ending at several locations (Madrid, Barcelona, Seville, Bilbao, Zaragoza, Santiago de Compostela and Palma de Mallorca, Figure 2-2a). The ensemble back-trajectories (27 members) are derived at 1500 and 5500 magl (approximately equivalent to Z850 and Z500, respectively) using the global reanalysis database Global Data Assimilation System (on a 1º x 1º grid) from National Centers for Environmental Prediction.

To objectively select a representative day for each CT, a daily score is designed to minimize the differences between the daily grid and the average grid of a given CT. For each day (*t*) within a given CT, the Day Score (*DS*) is calculated as the sum of the absolute value of the differences between the daily value and the average value of the meteorological variable of the CT for each cell (*i*) of the grid (Equation 2-3).

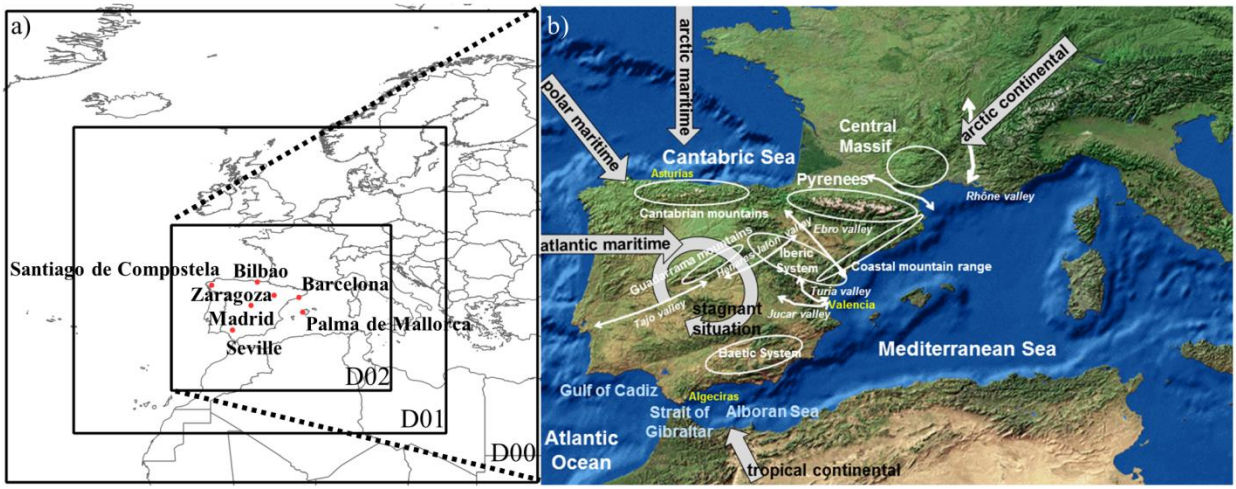

Figure 2-2. (a) Evaluated spatial domains. D00 (18.75N – 76.5N / 33.75W – 31.5 E), D01 (24.75N – 62.25N / 25.5W – 20.25 E), D02 (30N – 50.25N / 13.5W – 13.5 E) and origin of back-trajectories. (b) Topographic characteristics of interest. The arrows indicate the main advection of air masses towards the IP according to Martín-Vide and Olcina (2001)

$$DS_t = \sum_{i=1}^{n} |v_{t,i} - \overline{v_i}| \qquad \text{(Equation 2-3)}$$

In Equation 2-3, *n* is the number of cells of the grid; and $\overline{v_i}$ is the arithmetic mean of the input variable on each *i* cell of the domain for all days belonging to the CT. The Representative Day Score (*RDS*) minimizes the value of the DS identifying the representative day for each CT (Equation 2-4).

$$RDS = \min(DS_t) \qquad \text{(Equation 2-4)}$$

The RDS is a spatially explicit score useful to rank all days belonging to a given CT according to their similarity to the average value of the input variable of the 1983-2012 period. In addition, an extra criterion is established for the selection of the representative day. The day selected as representative has to be a day belonging to the month in which the CT is most frequent in the climatic period.

Table 2-2. Characteristics of sensitivity tests performed for the climatic period, 1983-2012. Elements between commas indicate the tested variable in each case study

# test	Studied factor	Variability range
1	Classification technique (clt)	1) Correlation techniques LND: Lund overall correlation coefficient KIR: Kirchofer partial correlation for each lat/lon ERP: Erpicum similarity index based on geopotential direction 2) Principal Component Analysis (PCA) PCT: obliquely rotated t-mode PCA PTT: orthogonally rotated t-mode PCA PXE: s-mode PCA with VARIMAX rotation PXK: t-mode PCA followed by a k-means cluster analysis 3) Clustering techniques HCL: hierarchical cluster KMN: k-means. Random seeds. DKM: Dk-means. Most dissimilar seeds. CKM: Ck-means. Most dissimilar seeds. 5% minimum frequency of each cluster. SAN: Simulated Annealing and Normalization
2	Number of circulation types (nCT)	From 2 to 15, 18, 27, 50
3	Meteorological variable used as proxy (iv)	Mean sea level pressure (mslp), 10-meter U and V wind components (UV10), 1000-hPa vorticity (Vort1000), 2-meter temperature (T2m), relative humidity (RH)
4	Vertical level (vl)	Surface, 11 geopotential levels from 1000 to 1 hPa each 100 hPa
5	Temporal resolution (tr)	Data each 6, 12, 24 hours, 06 h mean
6	Seasonality (se)	Winter, spring, summer, autumn, annual (an)
7	Horizontal resolution (hr)	0.125º x 0.125º, 0.25º x 0.25º, 0.75º x 0.75º, 1.5º x 1.5º, 3º x 3º
8	Spatial domain (d)	D00 (18.75N – 76.5N / 33.75W – 31.5 E), D01 (24.75N – 62.25N / 25.5W – 20.25 E), D02 (30N – 50.25N / 13.5W – 13.5 E)

2.4 Results and discussion

2.4.1 Determination of the reference synoptic classification set-up

Sensitivity tests to the classification technique and other factors affecting the results of the classification are performed (Table 2-2). Each test is run on a climatic basis (1983-2012) and evaluated in terms of EV. Within-type Standard Deviation and the Fast Silhouette Index are other metrics that inform about the classification quality. The results of these metrics are convergent with the EV and are presented as supplementary material (Annex I, Figure AI-1). The analyses are run with only one factor varying each time.

2.4.1.1 Classification technique

Test one (Table 2-2) analyses the effect of the automatic technique considered on the synoptic classification quality. The automatic techniques included in the cost733class software belong to three families of classification techniques: (1) correlation techniques, (2) Principal Component Analysis (PCA), and (3) clustering techniques. The techniques differ depending on the multivariate statistics used. A complete explanation of the 12 techniques used, their acronyms, and their implementation in the cost733class software is presented in Philipp *et al.* (2014) and references therein.

On average, cluster techniques have 15% and 60% higher EV than PCA techniques and correlation techniques respectively. The classification techniques that present the highest EV are the non-hierarchical clustering techniques (as in Casado and Pastor, 2013) (Figure 2-3a). Several variants of the k-means clustering (KMN, CKM and DKM), rank the highest EV together with the Simulated ANealing and Diversified Randomization (SAN). The k-means clustering has been widely used to derive synoptic classifications (Huth, 1996; Romero *et al.*, 1999; Rasilla, 2003; Jiménez *et al.*, 2009). KMN uses random seeds for the initialization of the clustering process, which can lead to suboptimum classifications. In contrast, CKM and DKM use the most dissimilar seeds possible (calculated in a previous step of the classification), enabling an optimum clustering. Unlike DKM, CKM does not allow the creation of CTs with less than 5% of the original data, in order to avoid the creation of extreme or infrequent CTs. As this work aims to obtain CTs that are related to the most common air quality patterns CKM is chosen. SAN is a clustering technique that has performed better than CKM in classifications made by other authors (Philipp *et al.*, 2007; Fereday *et al.*, 2008). In this case CKM and SAN perform similarly (EV = 0.474 and 0.478, respectively). Based on the higher computational cost of running classifications with SAN compared to CKM, the latter is chosen as the reference classification technique.

The robustness of the identified CTs between classification techniques is evaluated by means of the RI. The highest similarity is observed between all techniques based on k-

means (RI> 0.88 on average; CKM and DKM rank RI = 0.99) (Figure 2-4). With respect to CKM, PCA-based techniques range from 0.71 (PTT) to 0.79 (PXE), whereas correlation-based techniques range from 0.63 (ERP) to 0.78 (LND). These results indicate that k-means techniques determine similar CTs and reinforce the decision to use CKM as the classification technique.

2.4.1.2 Number of circulation types

Test two (Table 2-2) studies the effect of the number of CTs on the synoptic classification quality. In general terms, EV increases with the number of CTs, but the increase is not linear (Figure 2-3b). The number of CTs should be a balance between the EV and having an appropriate number of situations for air quality characterizations. For cluster techniques there is not a specific criterion to select the reference number of CTs. A 5% increase threshold in the EV is established to determine the most appropriate number of CTs. This leads to consider six CTs. Considering CKM, the EV is 0.48 using 6 CTs and 0.50 using 7 CTs. A complete table with the EV values is shown in the supplementary material (Annex I, Table AI-1). The obtained value of EV using CKM and six CTs is in the same range to those obtained by García-Valero *et al.* (2012) for a seasonal classification over Spain.

2.4.1.3 Meteorological variable used as proxy

Test three (Table 2-2) evaluates the effect of using different large-scale meteorological variables as a proxy on synoptic classification. Several classifications use the mean sea level pressure (mslp) as proxy meteorological variable because it is useful for relating the classification to variables influenced directly by the low levels of the atmosphere like surface temperature (Philipp *et al.*, 2007; Cassou *et al.*, 2005; Yiou *et al.*, 2008), sea surface temperature (Fereday *et al.*, 2008), wind (Jiménez *et al.*, 2009) and air quality.

Five meteorological variables (iv) available in the ERA-Interim database are tested: mslp, 10-meter wind components (UV10), 1000-hPa vorticity (Vort1000), 2-meter air temperature (T2m) and relative humidity (RH). T2m shows the highest EV (0.80), followed by mslp (EV = 0.48), RH (EV = 0.40) and UV10 (EV = 0.26) (Figure 2-3c). Similar results are obtained when using KMN, DKM, and SAN (Annex I, Figure AI-3). An analysis (not shown here) of the annual distribution of the identified CTs using T2m as meteorological variable indicates that the identified CTs were more related to seasonality than to atmospheric circulation. Thus, mslp is chosen as the meteorological reference variable. Atmospheric pressure is valuable because it provides information about the stability/instability of the atmosphere and the wind speed and direction, critical features to understand pollution transport dynamics.

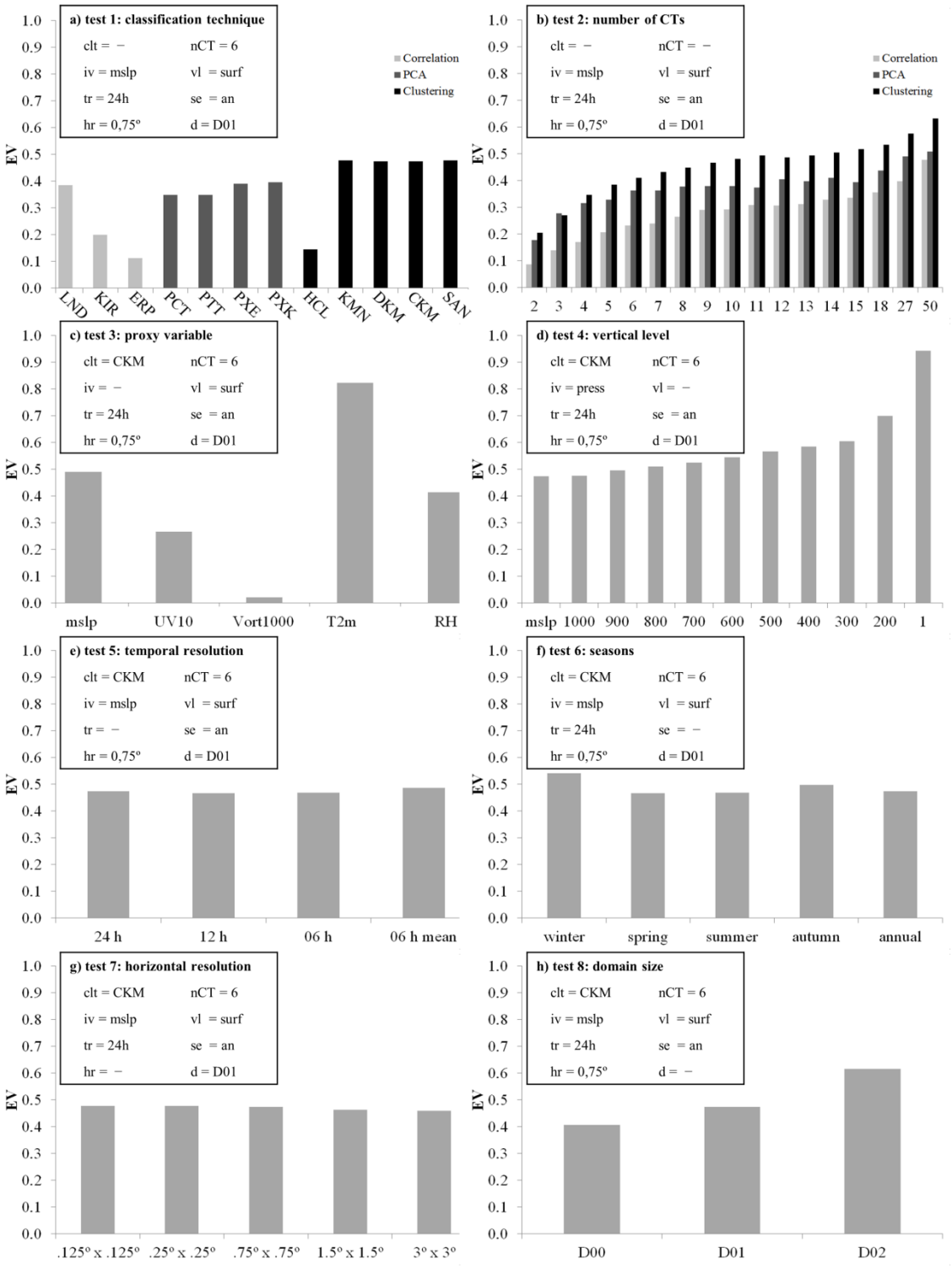

Figure 2-3 Explained Variation (EV) for the sensitivity tests (Table 2-2): a) test 1, classification technique; b) test 2, number of CTs (mean EV for correlation techniques, PCA techniques and clustering techniques); c) test 3, meteorological variable used as proxy; d) test 4, vertical level; e) test 5, temporal resolution; f) test 6, seasons; g) test 7, horizontal resolution; and h) test 8, domain size. Every single plot shows the fixed (box) and variable (bars) factor described in Table 2-2

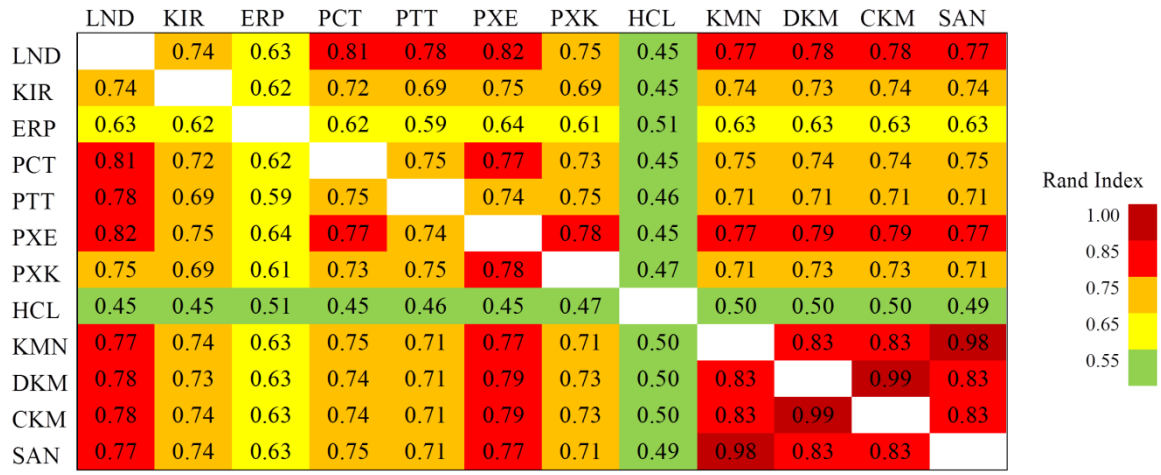

Figure 2-4 Rand Index matrix between classifications derived with the reference set-up and other classification techniques, calculated on a climatic basis (1983-2012)

2.4.1.4 Vertical level

Test four (Table 2-2) examines the effect of the vertical level on the classification quality. Surface data have typically been used to derive classifications (Kirchhofer 1974; Yiou and Nogaj 2004; Casado *et al.*, 2010). To a lesser extent, the geopotential height at 500 hPa (Z500) and 850 hPa (Z850) have been used in other studies (Kruizinga, 1979; Erpicum *et al.*, 2008; Casado and Pastor, 2013).

Classifications are obtained at different altitudes from 1000 hPa to 1 hPa by 100 hPa increments. EV increases from the surface to upper vertical levels (Figure 2-3d). Below 850 hPa the atmospheric circulation is strongly influenced by the topography, leading to complex and diverse pressure patterns to classify (EV~ 0.48).

At higher vertical levels where the complexity of the atmospheric circulation is lower, the identification of CTs is easier (higher EV). Many processes involved in air quality dynamics (emission, diffusion, advection, chemistry, deposition, etc.), together with effects of pollution on human health and the environment occur within the lower troposphere. Although ranking as the lowest EV (0.48), the reference vertical level is established at the surface (mslp), considering that the purpose of this synoptic classification is to identify CTs for air quality dynamics characterization.

2.4.1.5 Temporal resolution

Test five (Table 2-2) studies the impact of the temporal resolution. ERA-Interim reanalysis provides data every 6 hours (00:00, 06:00, 12:00, and 18:00 UTC). Resolutions used in the classification are 24-h (at 12:00 UTC), 12-h (using data at 00:00 and 12:00 UTC), 6-h (at 00:00, 06:00, 12:00 and 18:00 UTC) and 06-h mean (mean of 00:00, 06:00, 12:00 and 18:00 UTC). Results show that EV does not significantly change with the increase of the temporal resolution (Figure 2-3e), with EV = 0.48 for both 6-h and 12-h resolution. On the other hand, results show a very slight improvement in the classification quality when using the 6-h mean (EV = 0.49). However, in order to reduce the computational cost of the classification the reference temporal resolution is set to 24-h.

2.4.1.6 Seasonal classification

Test six (Table 2-2) evaluates the impact of considering either seasonal or annual data on the classification quality. Winter and autumn EV are 14% and 5% higher than the annual EV, respectively (Figure 2-3f). However, spring (EV= -2%) and summer (EV = -1%) are in the same range of quality as the annual classification. Overall, the mean seasonal EV is 0.019 higher than the annual EV.

An annual synoptic classification is chosen considering that a reduced number of CTs is desirable to facilitate the air quality dynamics characterization and that the total increase of seasonal EV respect to the annual classification EV is less than 4%.

2.4.1.7 Horizontal resolution

Test seven (Table 2-2) studies the impact of the horizontal resolution of the input data on the classification quality. Five resolutions 0.125º x 0.125º (110467 cells), 0.25º x 0.25º (27784 cells), 0.75º x 0.75º (3162 cells), 1.5º x 1.5º (864 cells), and 3º x 3º (238 cells), are considered. A higher resolution enables the description of more complex dynamics but may hinder the identification of CTs by introducing complexity to the input database.

Overall, horizontal resolution has a low impact on the EV (Figure 2-3g). For resolutions higher than 0.75º x 0.75º the increase in EV is less than 1%, whereas lower resolutions decrease the EV by 2.6% (1.5º x 1.5º) and 3.1% (3º x 3º). The 0.75º x 0.75º resolution guarantees high classification quality with fewer data, reducing the computational cost and storage requirements. It requires only 3% of the storage requirements compared to the 0.125º x 0.125º classification.

2.4.1.8 Domain size

Test eight (Table 2-2) analyses the effect of domain size on the classification quality. Three spatial domain sizes (D00 = $28x10^6$ km^2; D01 = $15x10^6$ km^2; D02 = $5x10^6$ km^2) centred over the IP have been studied (Figure 2-2a).

Results indicate that EV significantly varies with the domain size, with the highest EV at D02 (0.62) and the lowest at D00 (0.41) (Figure 2-3h). The increase in EV when considering D02 instead of D01 is almost 30%. This result is due to the fact that within a smaller domain the heterogeneity of atmospheric circulation is lower than in bigger domains, leading to an easier identification of CTs (Beck and Philipp, 2010). Similar results are obtained by Beck *et al.* (2013) when analysing the influence of the domain size on the classification quality, using 8 domains from $0.77x10^6$ to $18.5x10^6$ km^2.

The analysis of the spatial, temporal, and dynamic characteristics of the identified CTs over the different domains indicates that the domain size exerts an important influence on the results of a synoptic classification. For instance, around 50% of the days belonging to a given CT on D01 are not classified on the same CT on D02. This lack of consistency on the classification results between both domains indicates that the identified CTs are domain dependent.

D01 is the most suitable domain for this synoptic classification because it contains the usual locations of the more relevant action centres that affect the transport of air masses towards the IP (Martín-Vide and Olcina, 2001). The IP is greatly affected by the position of the Azores high and the British Isles low, which determine flows from the North-eastern Atlantic Ocean, the Western Mediterranean, Northern Africa, and Northern and Western Europe (all of them included in domain D01). Domain D00 also considers these areas but it ranks lower (EV =0.41) than D01, and is therefore less advisable as a reference domain.

2.4.1.9 Summary of the reference set-up

According to the results of the eight sensitivity tests, the reference set-up for the CTC uses the cluster-based CKM classification technique on 24-h (12:00 UTC) mean sea level pressure data with a horizontal resolution of 0.75º x 0.75º. The classification is performed without seasonalization on the intermediate D01 domain. Six CTs explain 48% of the 1983-2012 synoptic circulation variability.

2.4.2 Characterization of circulation types

This section characterises the six synoptic CTs identified for 1983-2012 with the reference set-up (Figure 2-5, Table 2-3).

Table 2-3. Characteristics of derived CT with the reference set-up (section 3.1) for the climatic period (1983-2012) and reference year 2012

Acronym		NWadv CT1	IBtl CT2	ENEadv CT3	AtlHi CT4	WSWadv CT5	ZonWadv CT6
Description		NW advection	Summer reduced surface pressure gradient	E/NE advection	Atlantic high with polar maritime advection	W/SW advection	Western Atlantic zonal advection
Criteria	Period						
Frequency (%)	1983-2012	23.9	22.4	21.3	12.0	10.4	10.1
	2012	21.9	21.6	8.8	17.8	20.5	9.3
Most frequent month	1983-2012	JUL	AUG	MAY	JAN	APR/OCT	JAN
	2012	JUL	AUG	FEB	JAN	APR/NOV	DEC
Seasonal frequency (%): DJF/ MAM/ JJA/ SON	1983-2012	10.1/26.1/ 43.5/ 20.3	11.7/26.2 /35.8/ 26.3	25.9/28.5/ 23.5/22.0	49.8/19.9/ 4.4/25.9	26.0/28.7/ 10.4/35.0	54.3/16.4/ 1.9/27.4
	2012	2.5/37.5/ 37.5/22.5	15.2/20.3 / 43.0/21.5	56.3/43.8/ 0.0/ 0.0	56.9/21.5/ 6.2/15.4	5.3/21.3/ 29.3/44.0	50.0/5.9/ 5.9/38.2
Mean / Max persistence (days)	1983-2012	2.9 / 23	2.9 / 22	3.8 / 19	2.7 / 27	3.0 / 17	2.9 / 19
	2012	3.6 / 10	2.6 / 8	4.6 /18	3.8 /15	3.0 /10	3.5 / 10
Transitions	1983-2012	IBtl	NWadv	IBtl	ZonWadv	NWadv	AtlHi
	2012	IBtl / WSWadv	NWadv / WSWadv	AtlHi	IBtl	NWadv / IBtl	WSWadv

NWadv is the most frequent CT overall (23.9% of the climatic frequency), especially common in summertime. Two action centres determine the surface pressure structure over Western Europe. They are the Azores high (~1020 hPa) and a low pressure system (~1008 hPa) over Scandinavia (Figure 2-5a). Between them isobars are arranged in a NW-SE orientation enabling the arrival of NW advection to the north of the IP. This synoptic situation leads to atmospheric instability and relative low pressure areas (~1012 hPa) over the Balearic Islands and the Spanish Mediterranean coast. The Cantabrian coast (north of IP) has high mslp (1016 hPa). At Z500, the geopotential isolines are in W-E direction and describe a slight through over Western Europe. This atmospheric situation leads to arctic maritime advection from the West of the British Isles towards the IP (Martín-Vide and Olcina, 2001).

IBtl is the second most frequent CT (22.4%). The intense solar radiation over the IP in summer leads to the formation of a thermal low (Millán *et al.*, 1991) (Figure 2-5b). IBtl is characterized by a reduced surface pressure gradient over the IP and Western Europe

(~1016-1018 hPa), which enable the development of mesoscale processes such as land-sea and mountain-valley breezes, especially along the Spanish Mediterranean coast (Baldasano *et al.*, 1994; Millán *et al.*, 1997; Azorin-Molina *et al.*, 2009). At Z500 there is a moderate geopotential height ridge that affects Western Europe enabling tropical continental advection from Northern Africa towards the IP (Martín-Vide and Olcina, 2001) (Figure 2-2b). IBtl is usually replaced by NWadv which is the most frequent summer pattern, and vice versa. IBtl corresponds with the S2 pattern (stagnant situation with SW circulation aloft) of the pseudo-subjective classification by García-Valero *et al.* (2012).

ENEadv takes place evenly throughout the year (21.3%) but it is more frequent at the end of winter and during spring (Table 2-3). ENEadv is associated with a blocking anticyclone located over the North Sea that affects the entire domain (Figure 2-5c). There are high isobaric patterns over Central Europe (> 1024 hPa), as well as in the IP (1020 hPa), leading to an E-NE advection towards the IP. It is usually replaced by IBtl when the high pressure subsides. At Z500 the 5580 m isoline describes a geopotential height ridge that descends longitudinally from the British Isles to the IP. This situation provokes an arctic continental advection from NE Europe to the IP (Martín-Vide and Olcina, 2001).

AtlHi accounts for 12% of the climatic frequency and typically occurs during the end of autumn and wintertime. AtlHi is characterized by high surface pressure (1024-1030 hPa) over the IP derived from the presence of the Azores high over the Cantabrian Sea (Figure 2-5d). AtlHi determines the arrival of Atlantic air masses to the Cantabrian coast. The north, centre and eastern IP are dominated by the influence of N and NE winds. The geopotential height field structure at 500 hPa is similar to that at the surface showing an air flow reaching the northern and central IP with a maritime origin. However, in the south-western IP air masses have a southern origin. AtlHi is usually replaced by ZonWadv in which the Atlantic advective features are more stressed. CT4 corresponds with the A1 pattern (anticyclone over the IP at all vertical levels) derived in García-Valero *et al.* (2012).

WSWadv typically occurs during transitional seasons (spring and autumn), although it is the second least frequent CT (10.4%). The Azores high (~1020 hPa) is in contrast to a low pressure area (~996 hPa) centred over western Ireland that affects Western Europe, leading to atmospheric instability over the IP (Figure 2-5e). A horizontal pressure gradient is established from NW (~1008 hPa) to SE (~1016 hPa) over the IP, enabling maritime advection towards western IP, as described by Martín-Vide and Olcina (2001). At Z500 air masses are advected western from the Atlantic Ocean. WSWadv is similar to C1 (extratropical cyclone at the NW IP) described by García-Valero *et al.* (2012), especially frequent in spring.

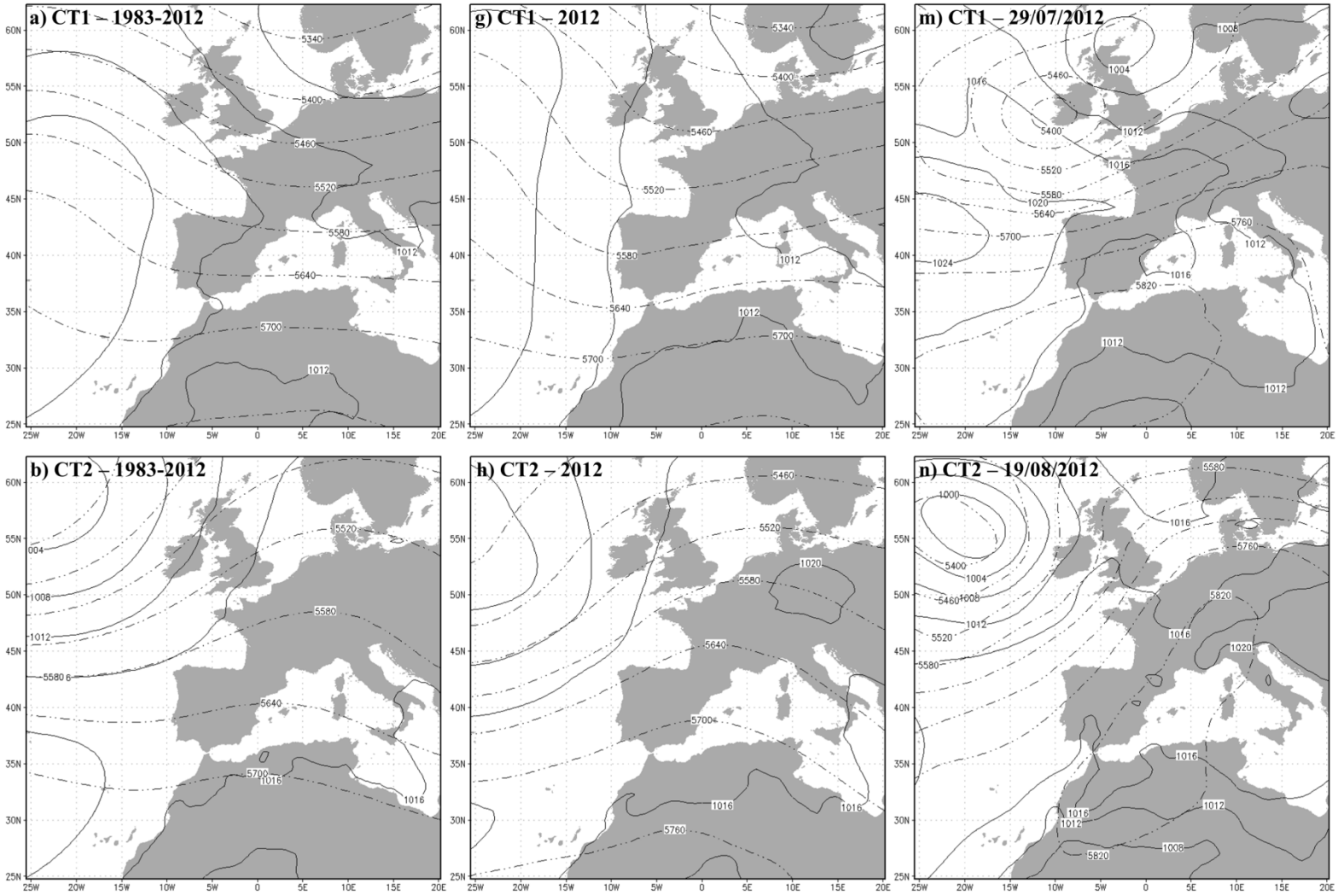

Figure 2-5. CTs derived with the reference set-up for the climatic 1983-2012 period (left), the representative year 2012 (centre) and representative day of each CT (right). Solid contours show mslp isobars (hPa) and dashed-dotted contours indicate Z500 isolines (masl)

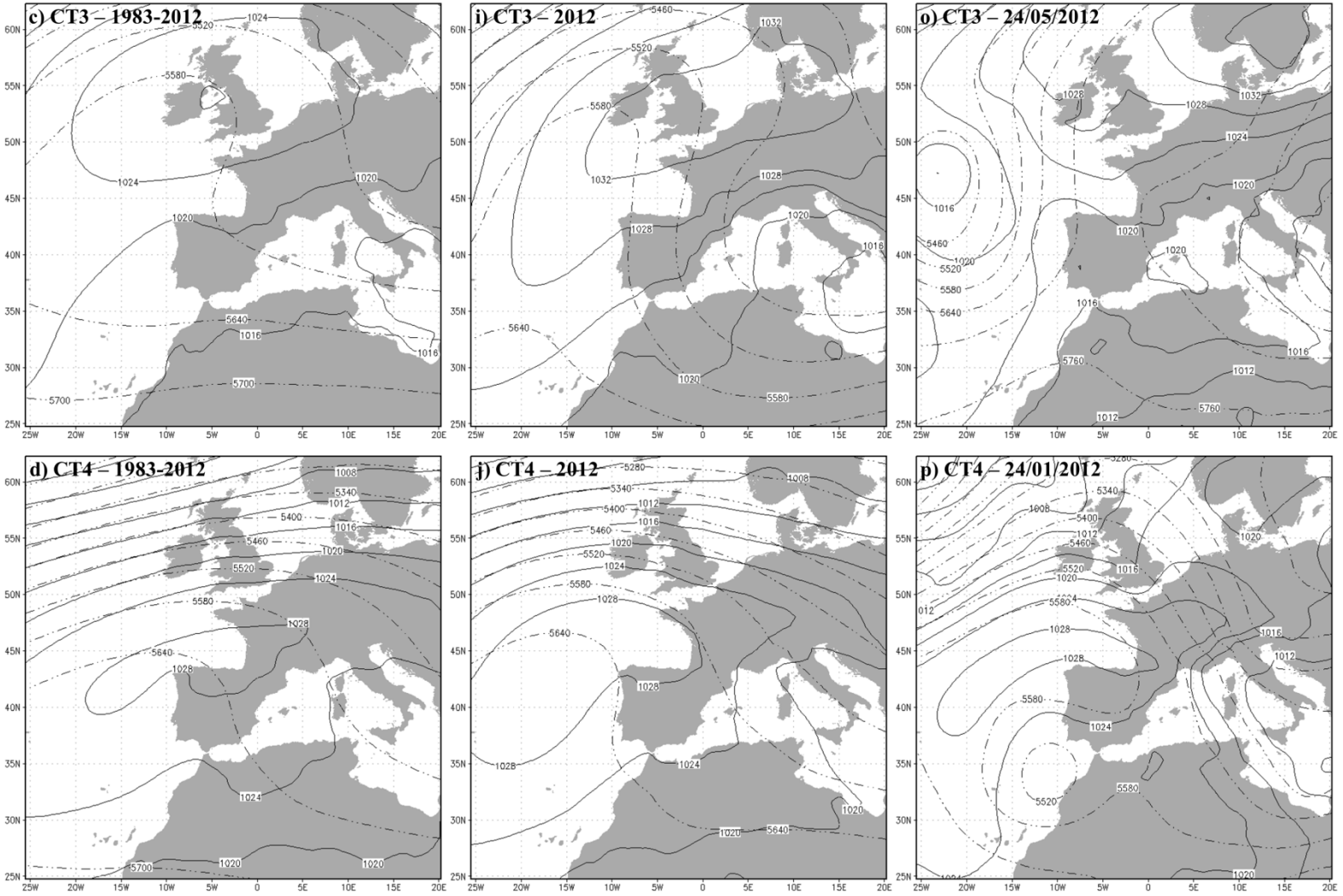

Figure 2-5. Continued

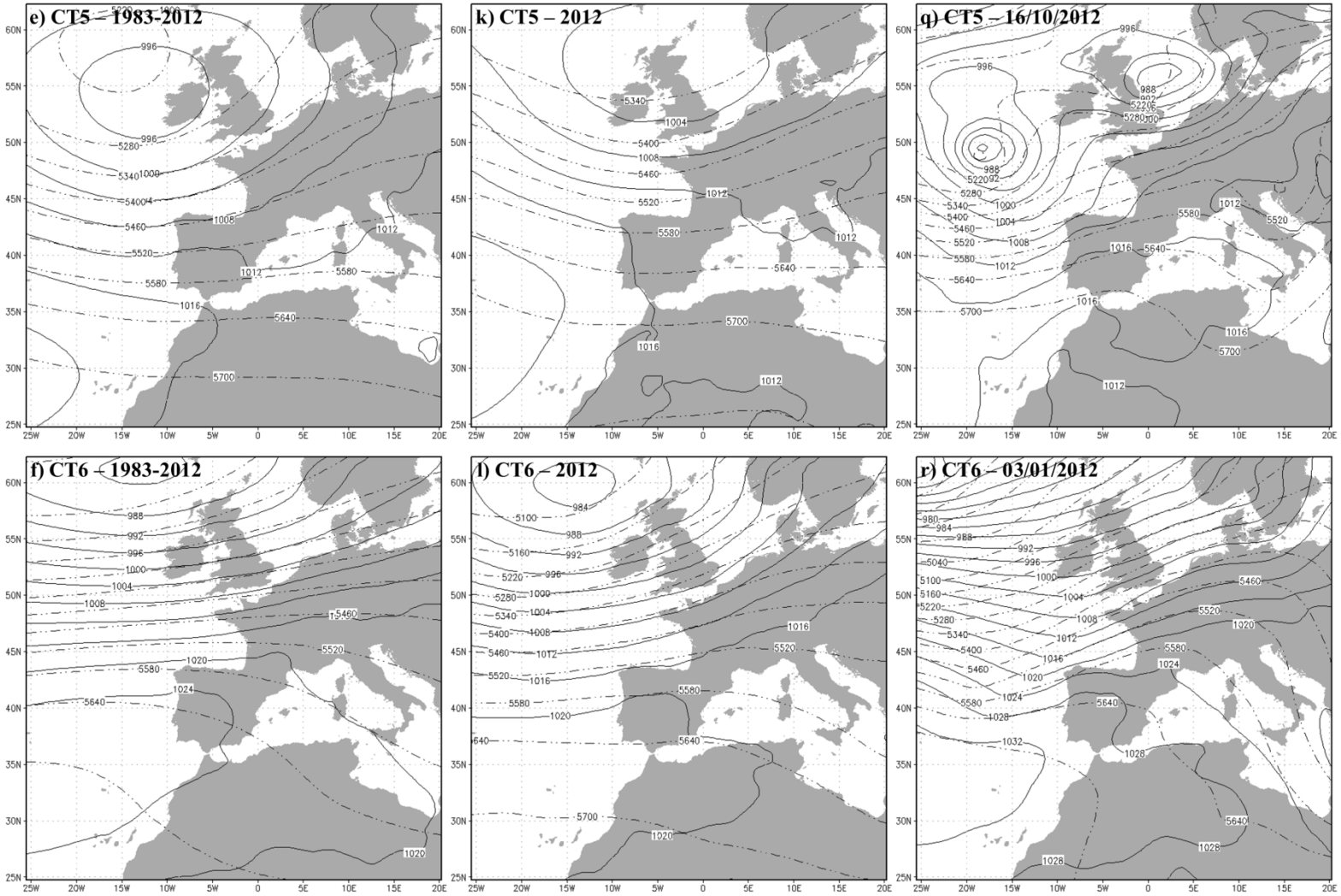

Figure 2-5. Continued

ZonWadv is the least frequent CT (10%) and occurs in winter, especially in January. In ZonWadv the Azores high (~1024 hPa) is located over the Canary Islands and southeastern IP (Figure 2-5f) and the Icelandic low is located between the British Isles and Iceland with high intensity (984 hPa). Between both action centres a significant horizontal pressure gradient over Western Europe is established. There is zonal advection from the Western Atlantic affecting Western Europe and northern IP. The geopotential height field structure at 500 hPa is similar to that at the surface. When the pressure gradient dissipates ZonWadv is usually replaced by AtlHi. Nevertheless, when the Icelandic low is in a southern location ZonWadv is replaced by WSWadv, characterized by W-SW advection. ZonWadv has been identified by García-Valero *et al.* (2012) as an extratropical cyclone close to the British Isles with zonal flow aloft over the IP (Z1). Unlike CT6 only the western and central IP are affected by Atlantic advection in WSWadv.

Concerning the persistence, the mean persistence for all CTs is 3 days. A similar result (3.4 days) was obtained by Cahynová and Huth (2009) when performing an automatic synoptic classification over a similar spatial domain (IP and Western Mediterranean 17W/9E – 31N/48N) and temporal range (1957-2002) using ERA-40 reanalysis database and a k-means cluster technique. The maximum persistence is 27 days (AtlHi) and several episodes of 23 consecutive days occur in summer (NWadv and IBtl).

2.4.3 Temporal stability of the classification and yearly classification

Results of temporal stability range from 34% for the year 1988 to 68% for the year 2012 with a mean of 51% for the 30 years (Figure 2-6a). There is not a clear trend in the temporal stability over the period. Consecutive years can rank similar (1998-1999, 57% to 56%) or very different (1988-1989, 34% to 55%) total stability. The heterogeneity of the results indicates the inter-annual variability of synoptic circulation over the area.

The year 2012 stands out as the most similar to the climatic period which makes it especially useful to characterize CTs based on the data for that year only. Comparisons of the climatic CTs with 2012 CTs depict that overall, the position of the action centres and the spatial structure of the pressure fields (mslp and Z500) are equivalent to those discussed for the climatic period. The main differences between climatic and 2012 CTs are found in NWadv and WSWadv. In NWadv, there is NW surface advection over the 1983-2012 period whereas it is N in 2012 (Figure 2-5g) most likely caused by the latitude of the Azores high being 10º higher (50ºN) than in the climatic period (40ºN). Regarding WSWadv (Figure 2-5k), the low pressure system over the British Isles is deeper in the climatic period (994 hPa) than in 2012 (1000 hPa), which establishes W advection in 2012 and SW over 1983-2012.

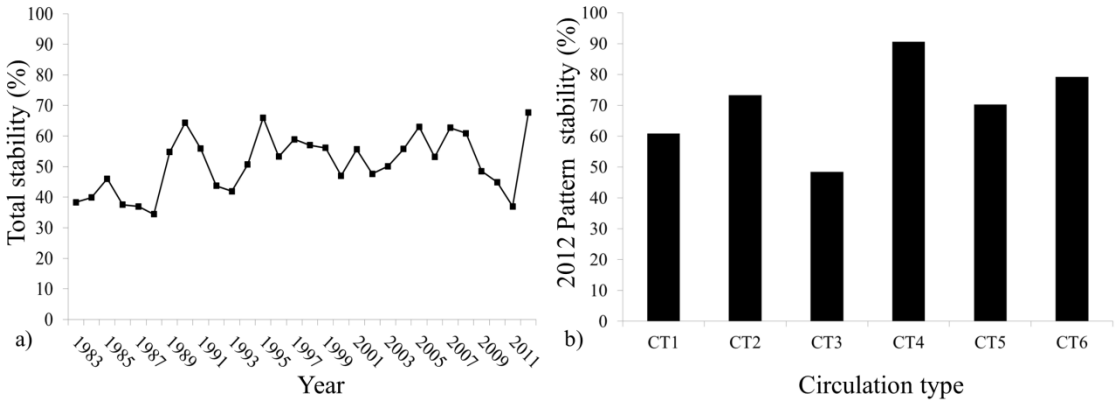

Figure 2-6. Temporal stability of the classification. (a) Total stability by years: yearly percentage of days classed in the same CT as in the climatic classification. (b) Stability for the year 2012: percentage of days within 2012 classes in the same CT as in the climatic classification for every CT

NWadv and IBtl are the most frequent CTs in both periods (Table 2-3). AtlHi and WSWadv are two times more frequent during 2012 than in the climatic period, whereas ENEadv is rarer in 2012. The least frequent climatic CT (ZonWadv) has a similar frequency compared with 2012. The period of the year in which each CT is more frequent is alike for both classifications except for ENEadv. Whereas in the climatic period this anticyclonic CT is equally present in all months, it only appears in winter and the beginning of spring in 2012.

During 2012 the mean persistence for the six CTs is 3.5 days (0.5 days higher than the climatic mean) nevertheless there is a prominence of short-lived (1-day) CTs. The maximum persistence in 2012 is lower than the one found in 1983-2012.

Considering the temporal stability by CT derived for 2012 (Figure 2-6b), the most stable is AtlHi with 91% of the data evenly classified, followed by ZonWadv, IBtl and WSWadv with 79%, 73% and 70%, respectively. ENEadv is the least stable of all the CTs with only half of the 2012 days classified in the same CT as in 1983-2012.

This characterization has also been performed for the 2nd and 3rd most stable years (1990 and 1995 respectively), showing similar results as those of 2012. The characteristics of the identified CTs and their associated pressure maps are provided as supplementary material (Annex I, Table AI-2 and Figure AI-4).

2.4.4 Identification of representative days

A representative day of each CT is selected for further analysis of pollution dynamics. The idea is to objectively choose one day for each CT of all the possible options in the representative year 2012 (Figure 2-7). The representative day of each CT minimizes the Representative Day Score, a score that computes the distance from the daily grid to the

average CT grid. On the representative day of each CT, the atmospheric circulation over the IP domain corresponds with the one characterising each CT at the surface and for Z500 (Figure 2-5m to Figure 2-5r). This selection of days is critical as the chosen days will be used for further analysis; specifically, the characterisation of pollution dynamics performed in Chapter 4 (NO_2 dynamics of the biggest cities and industrial areas in Spain), in Chapter 5 (analysis of power plants SO_2 and NO_2 plume dynamics), and in Chapter 6 (O_3 dynamics associated to on-road emissions from Madrid and Barcelona). The obtained conclusions from these pollution dynamics characterisations are considered as representative of the existing synoptic variability over the IP for the present climate (1983-2012). The representative day of each CT in 2012 are the 29th July (NWadv), 19th August (IBtl), 24th May (ENEadv), 24th January (AtlHi), 16th October (WSWadv), and 3rd January (ZonWadv), respectively (Table 2-4).

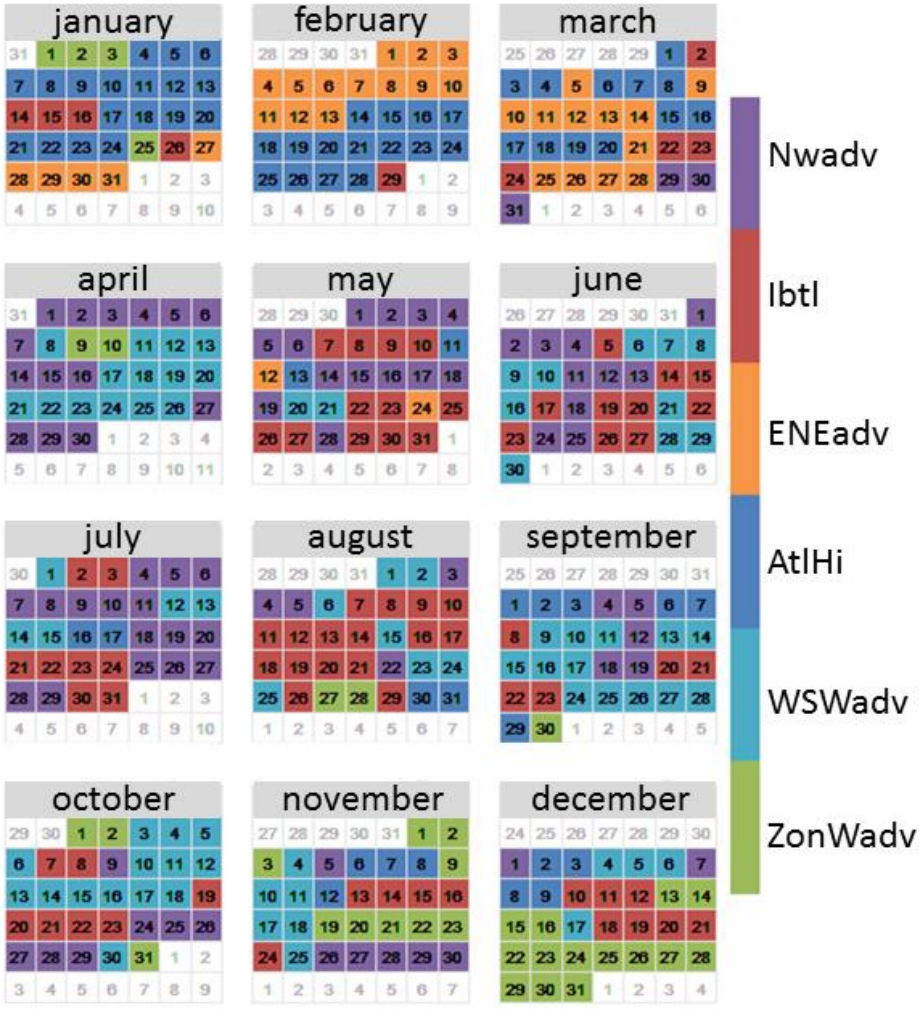

Figure 2-7. 2012 calendar showing the distribution of days for the identified CTs affecting the Iberian Peninsula

Table 2-4. Representative day of each of the six typical circulation types in 2012.

CT	1983-2012 frequency	2012 frequency	Representative day
NW advection (NWadv)	23.9%	21.9%	Sunday 29/07/2012
Iberian thermal low (IBtl)	22.4%	21.6%	Sunday 19/08/2012
E/NE advection (ENEadv)	21.3%	8.8%	Thursday 24/05/2012
Atlantic high (AtlHi)	12.0%	17.8%	Tuesday 24/01/2012
W/SW advection (WSWadv)	10.4%	20.5%	Tuesday 16/10/2012
Zonal Western advection (ZonWadv)	10.1%	9.3%	Tuesday 03/01/2012

2.4.5 HYSPLIT back-trajectories on representative days

For 2012 representative days, back-trajectories ending at the cities cited in Figure 2-2a are obtained by means of the HYSPLIT model (Figure 2-8 for single back-trajectories and Annex I, Figures AI-5 to AI-11, for ensemble back-trajectories). Back-trajectories at 1500 magl for July 29th (NWadv) show a NW origin in Santiago de Compostela, Bilbao, and Seville whereas in Madrid, Zaragoza, Barcelona and Palma the Mallorca the advection is from the W or SW. At 5500 magl back-trajectories mainly show a NW origin, confirming the maritime polar advection identified by the synoptic classification (ensemble back-trajectories are homogenous both at surface and Z500).

On August 19th (IBtl) there is a dominance of S winds at 1500 magl over the inland IP, as well as in the Cantabrian coast. Although in the Mediterranean coast (Palma de Mallorca) the advection is mainly from the E. At 5500 magl there is a net transport of air masses from Morocco towards the IP derived from the presence of a high pressure system over the Northwestern Mediterranean Basin. Except for Santiago de Compostela, 5500 magl back-trajectories and their ensembles show African advection which is consistent with the synoptic pattern characterized by IBtl.

On May 24th (ENEadv) 1500 magl back-trajectories in the eastern IP have a N-NE origin, coming mainly from France as shown in the ensemble back-trajectories at Barcelona, Bilbao and Zaragoza (Figure 2-8). Nevertheless, the continental advection from the NE is not clearly depicted in the southern and western IP. Similarly at 5500 magl, back-trajectories are from the N-NE in the northeastern IP and the Balearic Islands (Bilbao, Zaragoza, Barcelona and Palma).

Polar maritime advection that characterizes AtlHi is confirmed by the back-trajectories, both single and ensemble, on January 24th that show a N-NW origin for all the considered cities both at 1500 and 5500 magl.

In the western and central IP, 1500 magl back-trajectories on October 16th (WSWadv) have an Atlantic origin (W/NW). However, in the Spanish Mediterranean coast (Barcelona and Palma) the advection is from the S-SE. At 5500 magl all of the back-trajectories depict Atlantic maritime advection (ensembles are homogenous). There is an anticyclone over Italy that establishes S winds in the Spanish Mediterranean coast.

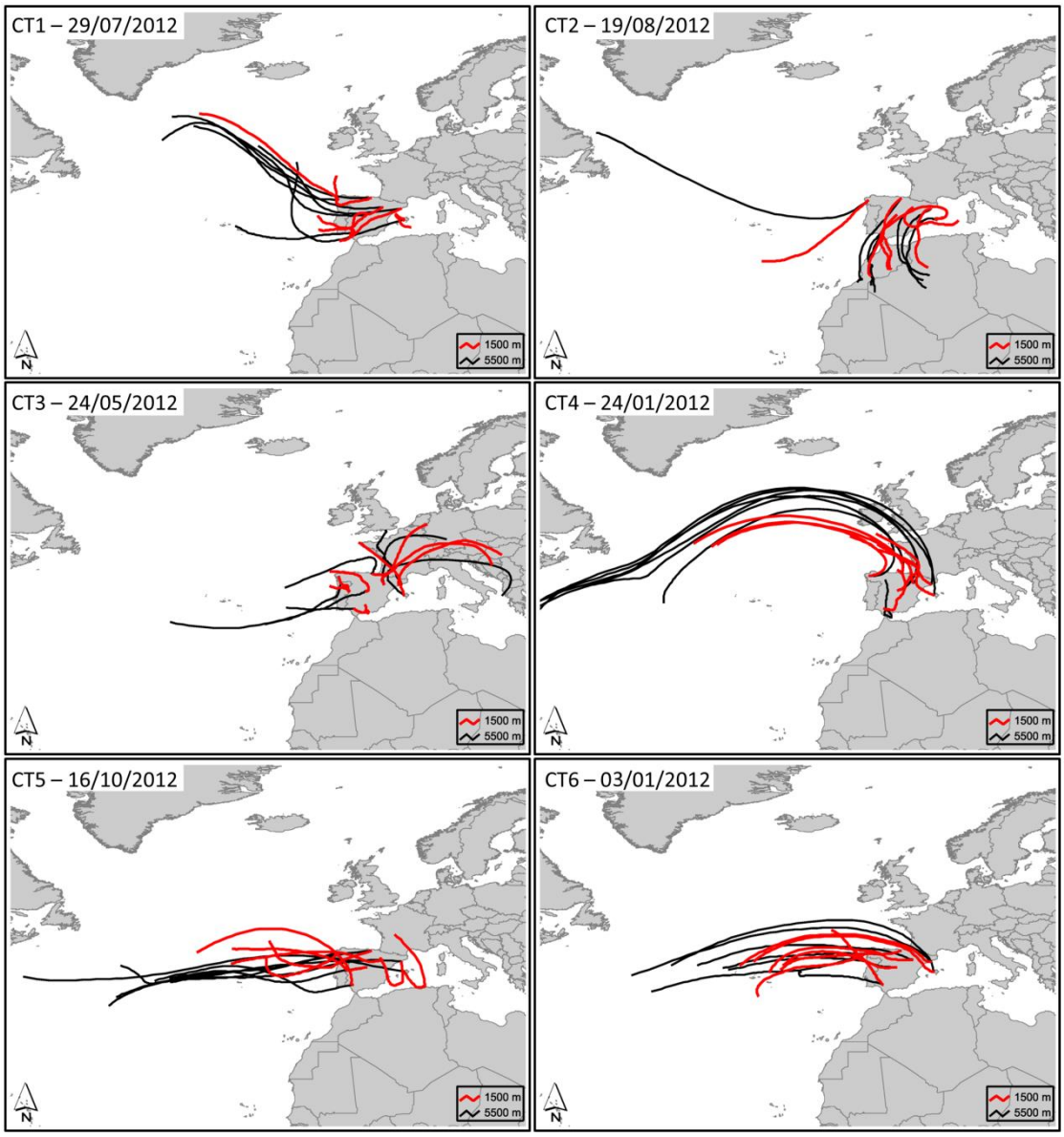

Figure 2-8. HYSPLIT 60 hour back-trajectories at 1500 magl (red line) and 5500 magl (black line) for representative days in 2012 corresponding to each CT: July 29th (NWadv-CT1), August 19th (IBtl-CT2), May 24th (ENEadv-CT3), January 24th (AtlHi-CT4), October 16th (WSWadv-CT5) and January 3rd (ZonWadv-CT6). The trajectories arrive at the cities of Santiago de Compostela, Bilbao, Barcelona, Zaragoza, Madrid, Seville and Palma de Mallorca (Figure 2-2a)

Zonal Atlantic advection, characteristic of ZonWadv, is clearly depicted in the single and ensemble back-trajectories of its representative day (January 3rd), both at 1500 and 5500

magl for all the considered cities. Contrary to WSWadv, at 1500 magl the strong westerlies are not obstructed by topographic barriers affecting the atmospheric dynamics in the Spanish Mediterranean coast.

Overall, the obtained results of single and ensemble back-trajectories are consistent with the origin of the air masses depicted in the CTs. Path and speed of the air masses as calculated by the HYSPLIT model confirm that the synoptic circulation is in agreement with the one described in each CT both at 1500 and 5500 magl.

2.5 Conclusions

The present work has established an objective procedure to establish a CTC on a climatic basis (1983-2012) to characterize air quality dynamics over the IP. Considering that there is not a single synoptic classification that best fits for all purposes (Huth *et al.*, 2008), sensitivity analyses to several classification techniques and factors affecting it have been performed in order to objectivize the set-up that maximizes its quality. Automatic classification techniques based on k-means clustering perform better in terms of EV than correlation-based and PCA-based techniques. Within the k-mean techniques, CKM guarantees the identification of non-extreme CTs, with maximum separability and minimum within-type variability using a reasonable amount of computing resources. The classification quality increases with the number of CTs, although this relation is not linear. A 5% increase threshold in EV is established in order to settle an appropriate number of CTs leading to a selection of six CTs. Surface pressure is the reference proxy variable chosen because it obtains the best EV (among the non-seasonalised variables) and informs about the stability/instability of the atmosphere and the wind speed and direction, which helps understanding air quality dynamics. Although surface level depicts lower EV than higher vertical levels (below 700 hPa), the surface is selected in the reference set-up because most of the processes involved in air quality occur within the lower levels of the atmosphere. The domain size is a critical factor when performing synoptic classifications because the identified CTs for each domain have different spatial, temporal, and dynamic characteristics. The medium-sized domain (D01) is selected in the reference set-up because it covers areas that are the origin of the air masses towards the IP while ranking an average EV (0.48).

The three most common CTs account for 67.6% of climatic frequency (NWadv, IBtl, and ENEadv) and mainly occur in summertime, replacing one another. While CT1 (23.9%) is a NW advective pattern characterized by the arrival of polar maritime air masses towards the IP determined by the presence of the Azores high, IBtl (22.4%) depicts a reduced pressure surface gradient, enabling the development of the Iberian thermal low; although stagnant conditions dominate at the surface in IBtl, there is a net advection of North African air masses at Z500. Despite being present throughout the year, ENEadv (21%) is especially

frequent in spring and summer as a result of a blocking anticyclone over central Europe that leads to E-NE advection towards the IP. When the high pressure system subsides, ENEadv tends to be replaced by IBtl. In winter two CTs are especially frequent, AtlHi (12%) and ZonWadv (10%). The former is an anticyclonic situation that enables the arrival of Atlantic air masses towards the IP, whereas the latter is characterised by zonal Atlantic maritime advection. Finally, WSWadv (10%) presents unstable conditions over the IP with W-SW winds and precipitation, and it is typical of transitional seasons. Topographic barriers in the central and eastern IP (Iberic System, Baetic System, Catalan mountain range) are overcome by westerlies on their way to the Spanish Mediterranean coast in ZonWadv but not in WSWadv.

Although inter-annual variability exists, the classification is temporally stable showing consistent CTs when using yearly data. The year 2012 is the representative year of this climatic period because its CTs show the highest temporal stability (67.8%). The CTs obtained with the reference set-up for the climatic period and 2012 are consistent with synoptic patterns over the IP found in the literature (Martín-Vide and Olcina, 2001; García-Valero *et al.*, 2012, Figure 2-2b). A representative day of 2012 for each CT has been objectively identified by means of the Representative Day Score. Single and ensemble Back-trajectories obtained with the HYSPLIT model confirm the synoptic flows depicted by each CT on representative days.

3. Modelling system: setup and evaluation

This chapter is based on:

Valverde V, Pay MT, Baldasano JM. 2015 A model-based analysis of SO_2 and NO_2 dynamics from coal-fired power plants under representative synoptic circulation types over the Iberian Peninsula. Science of the Total Environment **541**: 701-713. DOI: 10.1016/j.scitotenv.2015.09.111.

Valverde V, Pay MT, Baldasano JM. 2015 Ozone attributed to Madrid and Barcelona on-road transport emissions: characterization of plume dynamics over the Iberian Peninsula. Science of The Total Environment **543**: 670-682. DOI: 10.1016/j.scitotenv.2015.11.070.

3.1 The CALIOPE air quality forecast system

The CALIOPE air quality forecast system (CALIOPE-AQFS) is the result of a long-term effort started at the Environmental Modelling Laboratory of the Technical University of Barcelona and followed at the Earth Sciences Department of the Barcelona Supercomputing Centre-Centro Nacional de Supercomputación (BSC-CNS) to obtain a reliable modelling system to analyse and forecast air quality in Europe and Spain. CALIOPE is the acronym of the scientific project that aimed at establishing the air quality modelling system in an operational workflow: *CALIdad del aire OPeracional para España*. The CALIOPE-AQFS (www.bsc.es/caliope) is a state-of-the-art operational system for gases and aerosols that provide 24h and 48h forecasts for Europe and Spain.

A comprehensive list of publications regarding the CALIOPE-AQFS developments throughout its history can be found at the project webpage (http://www.bsc.es/caliope/en/publications?language=en). This section highlights some of the essential publications of the history of the research group according to its main focus: meteorological modelling (Soriano *et al.*, 2001; Jorba *et al.*, 2004; Pérez *et al.*, 2004); emission modelling (Costa and Baldasano, 1996; Parra *et al.*, 2006; Baldasano *et al.*, 2008a; Guevara *et al.*, 2013; 2014a; 2014b; 2014c); chemical transport modelling (Baldasano *et al.*, 1994; Jiménez and Baldasano, 2004; Jiménez *et al.*, 2005; 2006a; 2006b; Baldasano *et al.*, 2008b; Gonçalves *et al.*, 2009; Baldasano *et al.*, 2010; Pay *et al.*, 2012a; 2012b; Gonçalves *et al.*, 2012; Pay *et al.*, 2014a; 2014b); mineral dust modelling (Pérez *et al.*, 2006a; 2006b; Basart *et al.*, 2012a; 2012b); and post-processing of data (Gonçalves *et al.*, 2010; Sicardi *et al.*, 2012).

Moreover, the system has been used in case studies for air quality management purposes (Gonçalves *et al.*, 2008; Soret *et al.*, 2011; 2014; Baldasano *et al.*, 2014).

The CALIOPE-AQFS involves a set of coupled state-of the-art models that run in the Mare Nostrum supercomputer of the BSC-CNS. The models are run offline, that is to say, without considering the feedbacks of the chemistry on the meteorology which favours the system being computationally efficient (Figure 3-1). The models included in CALIOPE-AQFS are the High-Elective Resolution Modelling Emissions System (HERMES) emission model (Guevara *et al.*, 2013), the Weather Research and Forecasting model-Advanced Research WRF (WRF-ARW) meteorological model (Skamarock and Klemp, 2008), the Community Multiscale Air Quality (CMAQ) chemical transport model (Byun and Schere, 2006) and the Barcelona Supercomputing Center Dust REgional Atmosphere Model 8 bins (BSC-DREAM8b) mineral dust model (Pérez *et al.*, 2006a; 2006b; Basart *et al.*, 2012a).

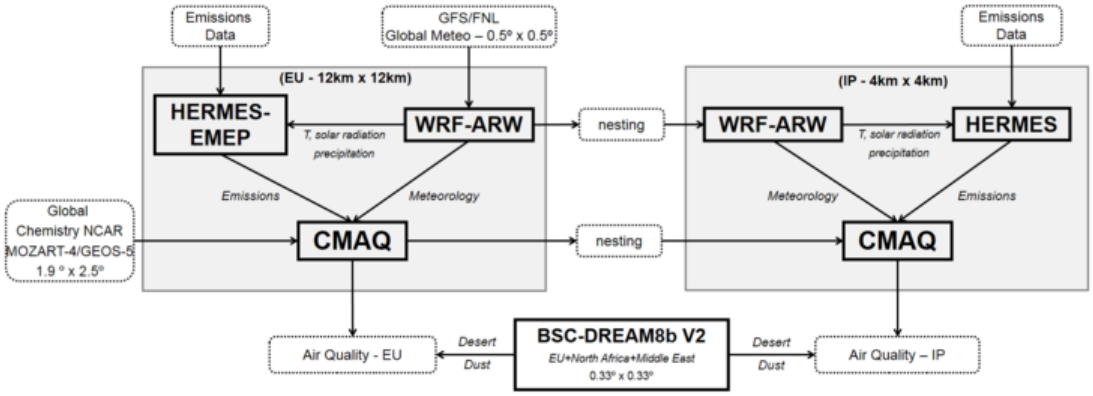

Figure 3-1. Modular structure of the CALIOPE-AQFS used to simulate air quality dynamics in Europe (EU domain) and in the Iberian Peninsula (IP domain). Squared boxes with solid lines represent the main models of the framework. Boxes with dashed lines represent input/output dataset. Lines connecting boxes represent the information flow (Baldasano *et al.*, 2011)

The HERMES model (http://www.bsc.es/earth-sciences/hermes-emission-model), which has been developed in-house at the Earth Sciences Department of BSC-CNS, estimates emissions, both natural and anthropogenic, with high spatial and temporal resolution of 1 h and 1 km^2 on 11 vertical levels. It calculates emissions using up-to date information and the state-of-the-art methodologies for emission estimations The current HERMES version (v 2.0) computes emissions based on a combination of activity factors and emission factors for all the sectors considered in the Selected Nomenclature for reporting of Air Pollutants (SNAP) (1) power stations (2) refineries (3) domestic and commercial fossil fuel use (4) manufacturing industries (including the industrial sectors of cement, lime, glass, fine ceramics, pulp and paper. iron and steel, bricks and tiles, chemistry, and non-ferrous metallurgy) (5) domestic and industrial solvent use (6) on-road transport (7) ports (8) airports (9) incinerators (10) agricultural activities (including machinery and the use of fertilizers for the management of crops) and (11) vegetation. It is worth mentioning that

for Spanish power plants, HERMESv2 calculates emissions using real facility activity and measured emissions factors from 2009 (OCEM-CIEMAT, personal communication).

WRF (http://www.wrf-model.org/index.php) is a mesoscale numerical, fully compressible, Eulerian and non-hydrostatic model which uses the Advanced Research WRF dynamical solver (ARW). Essentially, the WRF-ARW has been developed by the National Center for Atmospheric Research (NCAR), the National Centers for Environmental Prediction (NCEP), and the US Air Force Weather Agency (AFWA). It is widely used both for atmospheric research and operational forecasting. The WRF-ARW model provides meteorological fields to HERMES to adjust the calculations of biogenic and evaporative NMVOC emissions (temperature, accumulated precipitation, solar radiation).

CMAQ (https://www.cmascenter.org/cmaq/) is a 3-D Eulerian atmospheric chemistry and transport model that simulates multi-pollutants throughout the troposphere across spatial scales ranging from local to hemispheric. The model has been developed by the US Environmental Protection Agency (EPA) and it includes the state-of-the-art of physical and chemical processes involving the modelling of gaseous and particulate matter pollutants. The HERMES model provides emission fluxes (g km^{-1} h^{-1}) that match the requirements of CMAQ in terms of spatial and temporal resolution, as well as chemical speciation.

The BSC-DREAM8b mineral dust model (http://www.bsc.es/projects/earthscience/BSC-DREAM/) has been developed at the BSC-CNS based on a simpler version of the model by Nickovic *et al.* (2001). In the context of the forecasting system, this model improves the estimates of PM10 concentration over Europe and Spain by including the contribution of Saharan dust intrusions. However, for the purposes of this Ph.D. Thesis that focuses on gaseous pollutants, the contributions of the BSC-DREAM8 model have not been considered in the discussions of the SO_2, NO_2, and O_3 pollution dynamics in Chapters 4, 5, and 6.

The CALIOPE-AQFS provides forecast for a European domain (EU12) at 1 hour temporal resolution and at 12 km x 12 km spatial resolution (Figure 3-2). In order to provide reliable modelling results, high-resolution is especially needed in regions with complex topography like Spain (Palau *et al.*, 2005; Jiménez-Guerrero *et al.*, 2008). That is why a higher-resolution nest (4 km x 4 km) is performed over the IP. The Iberian Peninsula domain (IP4) is one-way nested on the EU12 domain (the mother domain). The CALIOPE-AQFS also provides forecast for specific Spanish domains (Catalonia, Madrid, Andalucía and the Canary Islands) that have not been used in this Ph.D. Thesis.

The meteorological boundary and initial conditions for the EU12 domain are provided by a global meteorological model. The initial and boundary conditions for the IP4 domain are downscaled from the EU12 domain by means of a one-way nest. The chemical boundary

conditions are either constant, based on climatologies for the main gases and aerosols or they are provided by a global model.

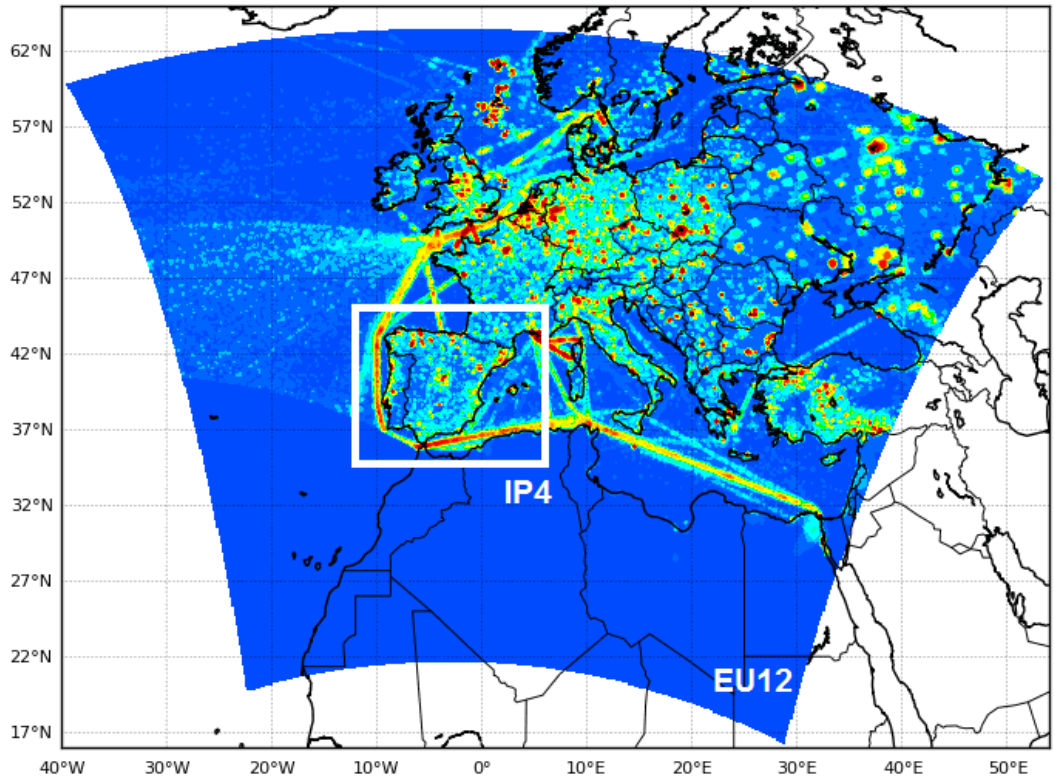

Figure 3-2. CALIOPE-AQFS domains: Europe at 12 km x 12 km horizontal resolution (EU12) and the nested Iberian Peninsula 4 km x 4 km resolution (IP4)

Regarding the CALIOPE-AQFS performance, the system is evaluated in near-real time against hourly air quality observations from more than 400 ground-level stations from the Spanish monitoring network including vertical profiles to establish confidence in the modelling system (Gonçalves *et al.*, 2010). There are also annual evaluations of the system that provide robustness to the results (Pay *et al.*, 2010; Baldasano *et al.*, 2011 and its supplementary material; Pay and Baldasano, 2012; Arévalo *et al.*, 2014).

3.2 CALIOPE-AQFS configuration and setup

The operational configuration of the CALIOPE-AQFS is described in Arévalo *et al.*, 2014. Whereas the operational outputs from the CALIOPE-AQFS were used for the analysis performed in Chapter 4, two specific simulations were run for the pollution dynamics characterisations of Chapters 5 and 6. For the latter, this section presents the setup of the CALIOPE-AQFS system that was used.

The meteorological model, WRF-ARW, version 3.5.1 runs over EU12 using initial and boundary conditions from the Global Forecast System (GFS/FNL) dataset that has 6-h

temporal resolution and 0.5º x 0.5º horizontal resolution (http://rda.ucar.edu/datasets/ds083.2/). In order to heat the model, a 12-hour spin-up is used prior the 24-h run of each simulated day. Vertically, WRF-ARW is configured with 38 σ vertical levels from the surface up to 50 hPa, with 11 levels characterizing the planetary boundary layer (PBL). The configuration and setup of CALIOPE-AQFS for Chapters 5 and 6 is shown in Table 3-1.

Table 3-1. CALIOPE-AQFS setup

Meteorological model	WRF-ARWv3.5.1
Initial and boundary meteorological conditions	GFS-FNL (1.5ºx1.5º, 6h)
Meteorological spin-up period	12 hours
WRF mother domain 12 km x 12 km resolution over Europe (nx, ny, nz)	480 x 400 x 38
WRF nested domain 4 km x 4 km over the Iberian Peninsula (nx, ny, nz)	399 x 399 x 38
WRF parametrizations	Boundary layer: YSU Microphysics: WSM5 Cumulus Scheme: no cumulus parametrization Land Surf physics: unified Noah land-surface model Long Wave: RRTM Short Wave: Dudhia Surface Layer: Revised MM5 Monin-Obukhov scheme
Emission model	HERMESv2
Base year of the emission	2009
Chemical Transport Model	CMAQv5.0.1 (Chapter 5) / CMAQv5.0.2 (Chapter 6)
Chemical mechanism	cb05cl_ae5_aq (Chapter5) / cb05-TUCL-aero6 (Chapter 6)
Chemical boundary conditions	MOZART4-GEOS5 forecast (1.7º x 2.5º, 6h)
CTM spin-up period	3 days (Chapter 5) / 7 days (Chapter 6)
ISAM tracked species	O_3, NO_x, NMVOC (Chapter 6)
Mother domain 12 km x 12 km resolution over Europe (nx, ny, nz)	478 x 398 x 15
Nested domain 4 km x 4 km over the Iberian Peninsula (nx, ny, nz)	397 x 397 x 15
CMAQ parametrizations	Horizontal/Vertical advection scheme: Horiz.: Yamartino mass-conserving/ Vert.: Piecewise Parabolic Method (PPM) Vertical diffusion module: Asymmetric Convective Model v2 (ACM2) Eddy diffusivity approach Dry deposition routine: Models-3 + Cl species

The Meteorology-Chemistry Interface Processor of CMAQ (MCIPv4.1) is used to collapse the 38 σ levels of WRF into 15 vertical layers, 12 of which are below 1500 meters above ground level (magl). The chosen diffusion and advection schemes are shown in Table 3-1.

It has been proven that using daily time and space varying chemical boundary conditions improves air quality model skills over Europe respect seasonal or invariant boundary conditions (Szopa *et al.*, 2009; Akritidis *et al.*, 2013). This is why the CALIOPE-AQFS uses the outputs of a global chemistry model as boundary conditions for the CMAQ model. However, the choice of chemical boundary conditions is an important factor of variability of the performance of an area-limited air quality modelling system (Marécal *et al.*, 2015). For example, a recent study by Terrenoire *et al.* (2015) over Europe using the CHIMERE CTM shows that there is an overestimation of O_3 concentrations related to an underestimation of NO_2 and an overestimation of O_3 concentrations of the chemical boundary conditions (from the global model Laboratoire de Météorologie Dynamique-INteraction avec la Chimie et les Aérosols – LMDz-INCA–; Hauglustaine *et al.*, 2014). Pay *et al.* (2015) recently analysed the performance of two state-of-the-art 3-D global CTMs – the Model for OZone And Related chemical Tracers, Version 4 (MOZART4, Emmons *et al.*, 2010) and the Monitoring Atmospheric Composition and Climate model (MACC, Inness *et al.*, 2013) – in the simulation of O_3 vertical profiles in several sites in Europe. To that end, they evaluated the 15-day averaged O_3 concentration from ozone-sondes against the model outputs. Their results proved that MACC performs better than MOZART-4 for O_3 vertical profiles. The same conclusion was obtained when using MOZART-4 and MACC as boundary conditions of the EU12 domain within the CALIOPE-AQFS and evaluating the O_3 surface concentration against AirBase monitoring stations in the same 15-day period as in Pay *et al.* (2015) (Table 3-2).

Table 3-2. CALIOPE-AQFS performance in EU12 domain for surface O_3 concentration in Europe using two different chemical boundary conditions: MACC and MOZART-4. Average of 198 rural background stations from AirBase on the 21-31 July 2012 period

	Mean Bias (μg m^{-3})	Root Mean Square Error (μg m^{-3})	Correlation coefficient
MACC/CMAQ	-6.12	28	0.69
MOZART-4/CMAQ	-8.07	28	0.68

For the CALIOPE-AQFS simulations performed in this Ph.D. Thesis, the lack of MACC data for all the periods of study lied to the use of MOZART-4 as chemical boundary conditions for CMAQ in the EU12 domain. This model, developed by the US National Center for Atmospheric Research (NCAR) (https://www2.acom.ucar.edu/gcm/mozart) is an offline global chemical transport model particularly suited for studies of the troposphere. A comprehensive description of the model and its chemical mechanism, and a

thorough evaluation over the 2000–2007 period can be found in Emmons *et al.* (2010). MOZART-4 is driven by the Atmospheric Global Climate Model Goddard Earth Observing System Model, Version 5 (GEOS-5). GEOS-5 is developed by –US National Aeronautics and Space Administration (NASA) to support its research in the fields of climate and weather prediction (http://geos5.org/wiki/index.php?title=GEOS-5_Earth_System_Modeling_and_Data_Assimilation).

The MOZART-4/GEOS-5 outputs contain 80 variables including the concentration of the main atmospheric gases and aerosols and they can be downloaded in netCDF format from a web repository (http://www.acd.ucar.edu/gctm/mozart/subset.shtml). The temporal resolution is 6 hours. The horizontal resolution is Latitude 1.9º x Longitude 2.5º. Vertically, the model is configured with 56 hybrid sigma pressure levels. The anthropogenic emissions are provided by the Argonne National Laboratory (University of Chicago) emission inventory developed for the Arctic Research of the Composition of the Troposphere (ARCTAS) project (http://bio.cgrer.uiowa.edu/arctas/emission.html) whereas the fire emissions come from the Finish Fire INventory from NCAR, Version 1.0 (FINN-v1) model that proved 1 km resolution, global estimates of the trace gas and particle emissions from open burning of biomass.

A time-independent vertical concentration profile was used to settle the initial chemical conditions and a 3-day and 7-day spin-up was used to heat the model, respectively for experiments in Chapters 5 and 6.

Regarding the CTM, two different versions have been used in this Ph.D. Thesis, version 5.0.1 (Chapter 5) and version 5.0.2 (Chapter 6). Both versions contain the updated carbon bond gas-phase mechanism (CB05) with new toluene chemistry (Whitten *et al.*, 2010). The last release of CMAQ (Version 5.0.2) has an update on the aerosol module (AERO6 with ISORROPIA v2.1 inorganic chemistry) that is needed to perform source apportionment studies and that is the reason why the 5.0.2 version had to be used. The CB05 chemical mechanism is chosen because it performs better than other gas-phase mechanisms (SAPRC-99, CB4) implemented in CMAQ (Luecken *et al.* 2008; Pay *et al.*, 2012c).

3.3 Evaluation of the CALIOPE-AQFS performance

3.3.1 Introduction

In order to give confidence to a modelling system an evaluation of its performance is needed. The model evaluation has been defined by the EEA (2011) as the "sum of processes that need to be followed in order to determine and quantify the model's performance capabilities, weaknesses and advantages in relation to the range of applications for which it has been designed". Several approaches exist to analyse the

performance of an air quality model. Dennis *et al.* (2010) proposed a set of statistical indicators that are widely used by the air quality modelling community: the Mean Bias (MB), the Root Mean Squared Error (RMSE), and the correlation coefficient (r). These indicators provide complementary information on the capability of a model to reproduce the pollutant concentration measured at a monitoring site. The Joint Research Center of the European Commission has developed a complimentary tool intended for model evaluation: The DELTA TOOL (Thunis and Cuvelier, 2015). It is a harmonised tool that is useful to assess the model quality objectives that indicate the level of accuracy considered to be acceptable for regulatory applications according to the Ambient Air Quality Directive 2008/50/EC taking into account the observation uncertainty. The tool facilitates the depiction of graphical outputs such as time series, scatter plots, and Target plots.

This section presents the results of the evaluation of the air quality simulation of the CALIOPE-AQFS over the IP4 domain for the periods of interest (Chapter 2, section 2.4.4). Regarding the WRF-ARW performance, refer to the annual meterological modelling evaluation over the IP by Baldasano *et al.* (2011). In general terms, the meteorological model is performant in terms of spatial and temporal variability for key meteorological variables such as the 2-meter temperature, 2-m dew point temperature, and 10-m wind speed and direction.

As for the evaluation of the CTM, an analysis of the performance of the system has been done for the representative day of each CT against validated observations from the Spanish air quality monitoring network (Figure 3-3). The considered pollutants are NO_2, SO_2, and O_3. The choice of these pollutants is based on the fact that they are the three most problematic gasesous pollutants in Spain and because their dynamics are further characterised in Chapters 4, 5, and 6.

According to the Air Quality Directive, only monitoring stations with at least 75% of the daily data have been considered (Directive 2008/50/EC). Depending on the day of study, and the pollutant, the total number of stations varies. On average, the number of stations is ~320 for SO_2, ~400 for NO_2, and ~335 for O_3. On the one hand, a spatio-temporal analysis based on the MB, RMSE, and r is performed (Section 3.3.2). On the other hand the DELTA TOOL v5.1. (Thunis and Cuvelier, 2015) is used to assess the model quality objectives as defined in the Air Quality Directive based on the use of the Target Plot (Section 3.3.3).

Figure 3-3. Location of validated stations from the Spanish air quality monitoring network (RedESP) used for the evaluation of the CALIOPE-AQFS

3.3.2 Evaluation with classic statistics

One specific CALIOPE-AQFS simulation was run in order to analyse the SO_2 and NO_2 pollution dynamics associated to the emissions in a selection of coal-fired power plants (Chapter 5). Another CALIOPE-AQFS simulation was run to characterise the O_3 dynamics in Spain attributed to on-road transport emissions (Chapter 6). The set-up of the system for both runs is alike except for the slight change in the CMAQ version and the use of a larger spin-up period in the second simulation. This section presents an evaluation of the temporal and spatial skills of the modelling system of the simulation used in Chapter 6 based on the MB, the RMSE, and the r that have been computed for thse three pollutants and each CT against validated observations from the Spanish monitoring network (RedESP). Note that only stations with more than 75% of the hourly data over the selected period have been considered as defined in the Air Quality Directive.

On average for all the considered locations in Spain, the CALIOPE-AQFS properly reproduces NO_2, O_3, and SO_2, concentrations as shown by the general statistics (Table 3-3,

Table 3-4, and Table 3-5, respectively) calculated on an hourly basis for the representative day of each CT.

Table 3-3. Statistical evaluation of the CALIOPE-AQFS: NO_2 concentration at available stations during the representative day of each CT. Mean Bias (MB, µg m^{-3}), Root Mean Square Error (RMSE, µg m^{-3}), correlation coefficient (r), average of the observations (OBS) and average of the model (MOD)

	NWadv	IBtl	ENEadv	AtlHi	WSWadv	ZonWadv
# stations	415	432	396	390	381	389
MB (µg m^{-3})	-1	-2	-9	-11	-9	-11
RMSE (µg m^{-3})	14	18	21	23	19	20
r	0.5	0.4	0.6	0.6	0.7	0.7
OBS (µg m^{-3})	12.3	14.4	22.1	28.0	22.7	25.9
MOD (µg m^{-3})	11.0	12.4	13.7	17.4	14.0	15.0

Table 3-4. Statistical evaluation of the CALIOPE-AQFS: O_3 concentration at available stations during the representative day of each CT. Mean Bias (MB, µg m^{-3}), Root Mean Square Error (RMSE, µg m^{-3}), correlation coefficient (r), average of the observations (OBS) and average of the model (MOD)

	NWadv	IBtl	ENEadv	AtlHi	WSWadv	ZonWadv
# stations	356	353	323	324	332	326
MB (µg m^{-3})	5	16	2	21	13	17
RMSE (µg m^{-3})	25	28	29	30	24	25
r	0.6	0.6	0.6	0.6	0.7	0.6
OBS (µg m^{-3})	73.2	62.3	75.7	32.9	46.7	34.7
MOD (µg m^{-3})	78.3	78.0	77.1	54.4	59.3	51.7

Table 3-5. Statistical evaluation of the CALIOPE-AQFS: SO_2 concentration at available stations during the representative day of each CT. Mean Bias (MB, µg m^{-3}), Root Mean Square Error (RMSE, µg m^{-3}), correlation coefficient (r), average of the observations (OBS) and average of the model (MOD)

	NWadv	IBtl	ENEadv	AtlHi	WSWadv	ZonWadv
# stations	333	344	319	305	305	309
MB (µg m^{-3})	-1	-1	-3	-3	-2	-3
RMSE (µg m^{-3})	8	11	14	10	5	7
r	0.4	0.1	0.2	0.2	0.2	0.2
OBS (µg m^{-3})	4.4	4.8	5.0	5.6	3.9	5.3
MOD (µg m^{-3})	2.8	3.9	2.4	3.2	1.8	2.0

The SO_2 and NO_2 concentrations tend to be underestimated; on average for the six CTs, the MB are -2.2 $\mu gSO_2\ m^{-3}$ and -7.2 $\mu gNO_2\ m^{-3}$. Larger underestimations occur in winter CTs (AtlHi and ZonWadv) for both pollutants. However, the general temporal variability is well captured, with an r-SO_2 = 0.21 and r-NO_2 = 0.58. For NO_2 there is a peak during the morning and another in the evening associated to transport and domestic electricity consumption patterns, which are correctly simulated by the model on all the CTs (Figure 3-4). The daily SO_2 cycle presented in Figure 3-6 has to be examined with care because it considers many locations with little concentration of the pollutant. Despite this fact, it is possible to see that the model is able to reproduce the daily peaks and minimum concentrations at night. For NO_2, the highest error is found for the AtlHi (RMSE = 23 $\mu g\ m^{-3}$) and it is minimum for the NWadv episode (RMSE = 14 $\mu g\ m^{-3}$). For SO_2, the lowest error is found for the WSWadv (RMSE = 5 $\mu g\ m^{-3}$) and are alike for the other CTs (RMSE ~ 9 $\mu g\ m^{-3}$).

The daily O_3 variability is well captured by the modelling system for all the CTs with maximum concentrations at midday and minimum at night (Figure 3-5). The correlation coefficient is alike for all the CTs ~0.6. However, there is a general overestimation of O_3 particularly during the night, in line with the evaluation performed by Appel *et al.* (2012) over Europe with CMAQv5.0. In the spring/summer daytime, the O_3 is slightly underestimated (Figure 3-5a and Figure 3-5c). This peak underestimation is in line with Vivanco *et al.* (2009) who also found a general underestimation of O_3 concentration in large areas of Spain in a multi-year evaluation using the CHIMERE model in Spain. In autumn and winter CTs the CALIOPE-AQFS tends to overestimate the O_3 concentration AtlHi (Figure 3-5d), ZonWadv (Figure 3-5e) and WSWadv (Figure 3-5f).

Nocturnal O_3 concentration is overestimated for all the CTs. This fact may be explained by the underestimation of the planetary boundary layer (PBL) height by the WRF model (Banks *et al.*, 2015) that leads to higher surface concentration, especially at night when the PBL height is low. Moreover, the overall O_3 overestimation can be related to the underestimation of NO_2 that limits the O_3 titration by NO_2. The RMSE (26 $\mu g\ m^{-3}$ on average) is slightly higher than the annual error of the CALIOPE-AQFS operational forecast for 2013 (21.1 $\mu g\ m^{-3}$; Arévalo *et al.*, 2014) but it is in the range of RMSE of the median MACC-II ensemble daily forecast (20-26 $\mu g\ m^{-3}$) in the Mediterranean area (Marécal *et al.*, 2015). Finally, another factor that can explain the general overestimation of O_3 is related to the contribution of the boundary conditions in the western IP domain (O_3 and precursors coming from North America and the Atlantic) which is of special relevance in the IP due to its location in Western Europe as suggested in the area apportionment study by Pay *et al.* (2014b).

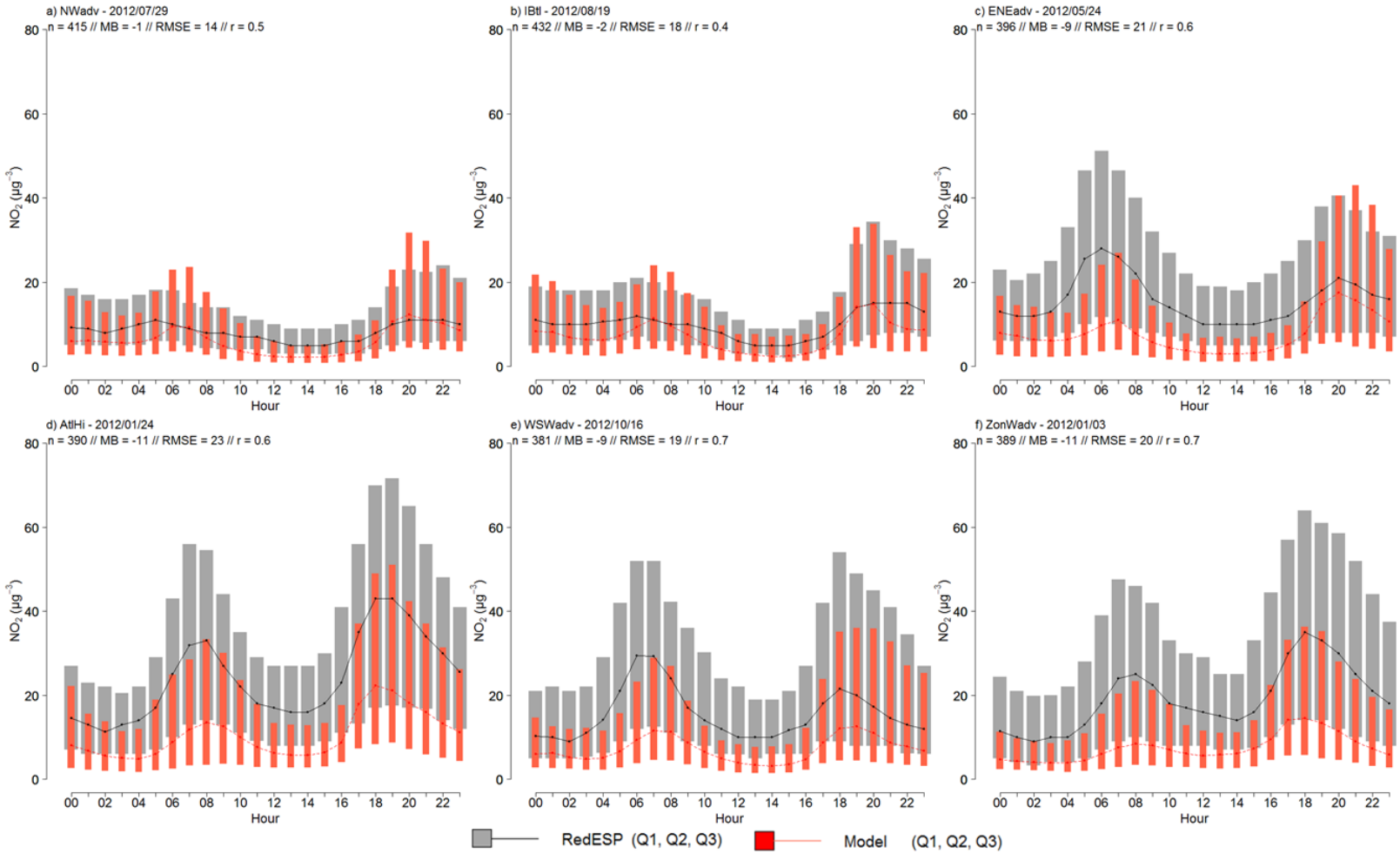

Figure 3-4. Daily cycle (hours in GMT) of observed (RedESP) and modelled (CALIOPE-AQFS) NO_2 surface concentrations (µg m^{-3}) on the representative day of each CT. n: number of air quality monitoring stations from RedESP considered; MB: mean bias (µg m^{-3}); RMSE: root mean square error (µg m^{-3}); r: correlation coefficient (unitless). Q1: 1st quartile; Q2: median; Q3: 3rd quartile

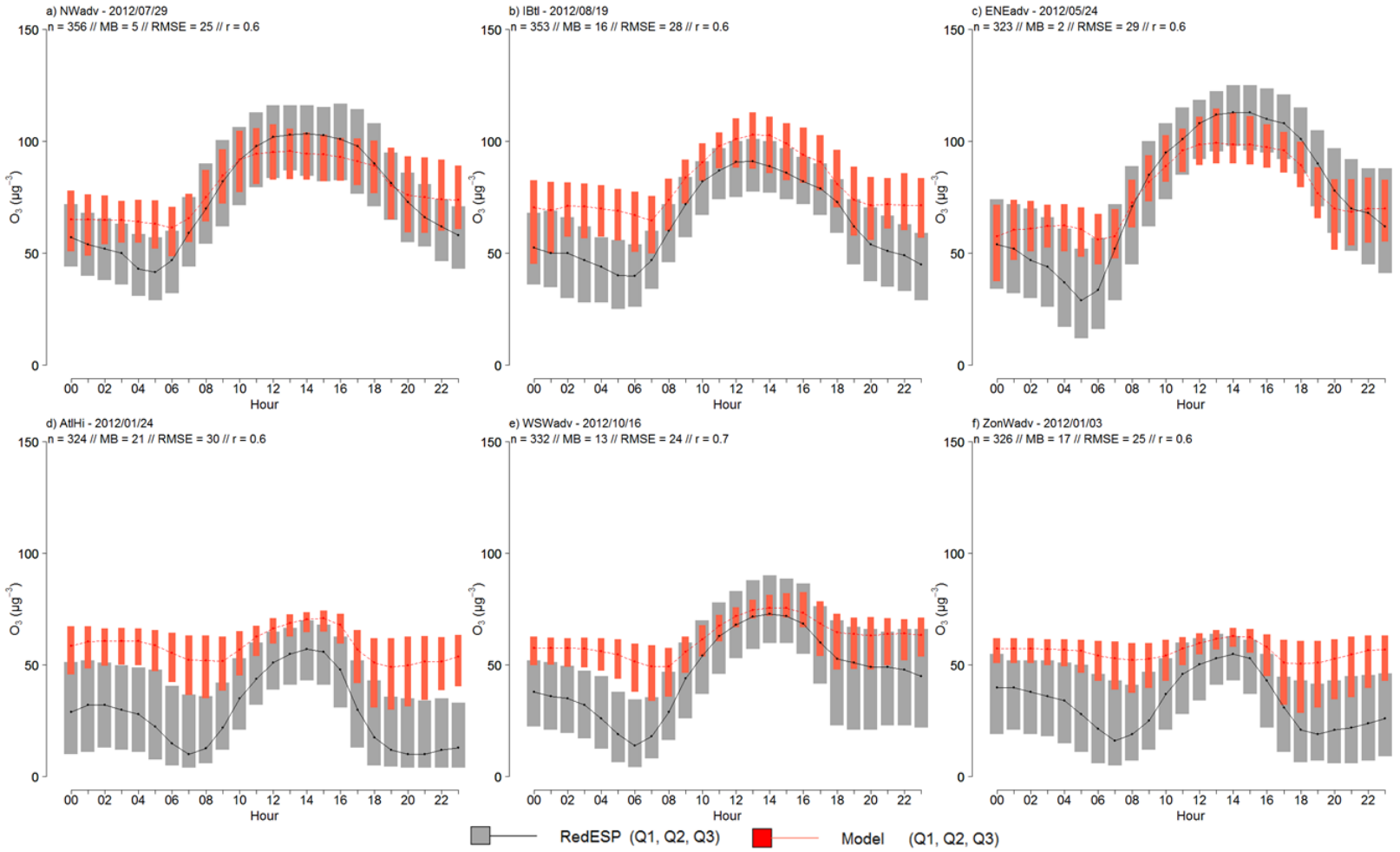

Figure 3-5. Daily cycle (hours in GMT) of observed (RedESP) and modelled (CALIOPE-AQFS) O_3 surface concentrations (µg m^{-3}) on the representative day of each CT. n: number of air quality monitoring stations from RedESP considered; MB: mean bias (µg m^{-3}); RMSE: root mean square error (µg m^{-3}); r: correlation coefficient (unitless). Q1: 1st quartile; Q2: median; Q3: 3rd quartile

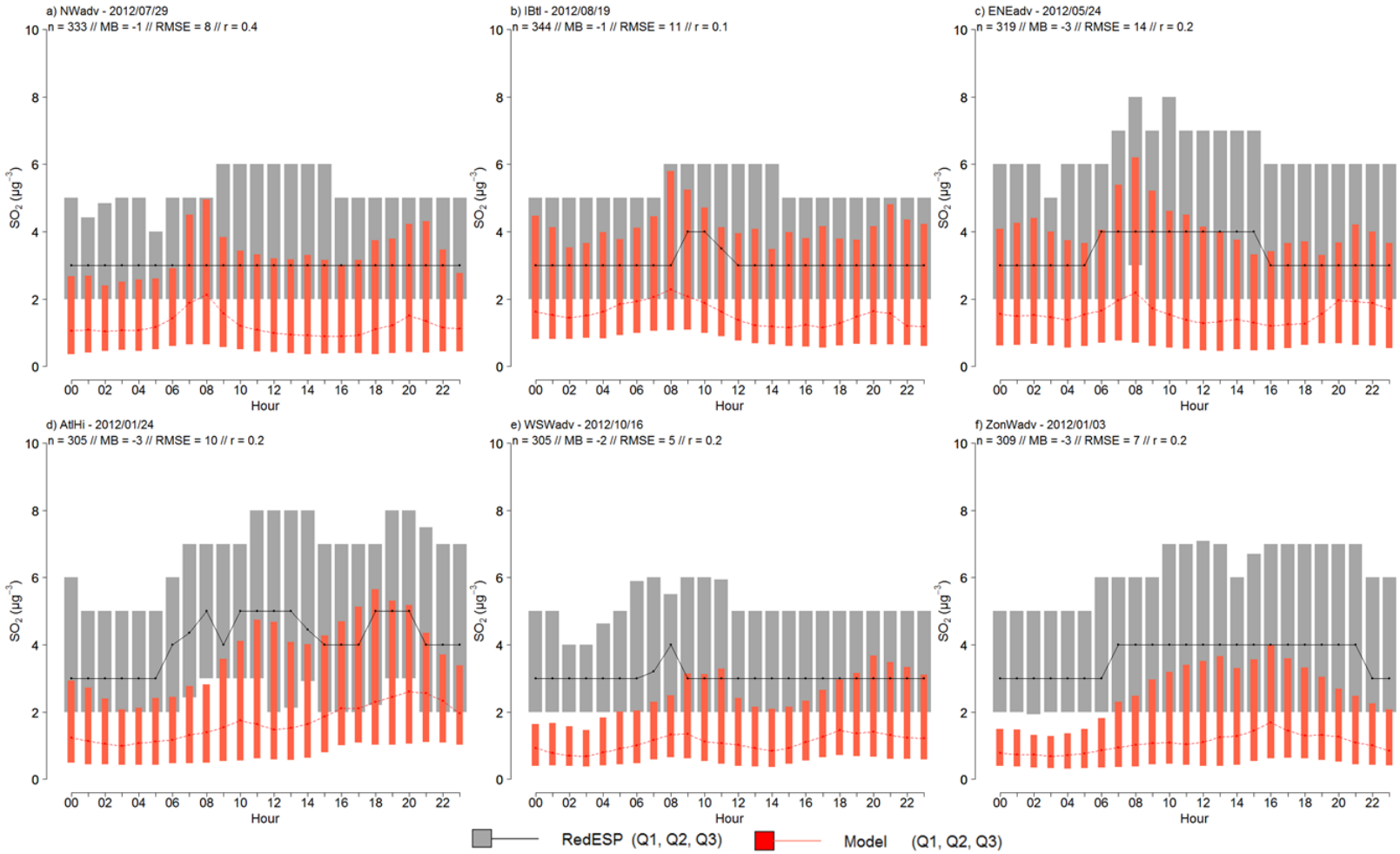

Figure 3-6. Daily cycle (hours in GMT) of observed (RedESP) and modelled (CALIOPE-AQFS) SO_2 surface concentrations (µg m^{-3}) on the representative day of each CT. n: number of air quality monitoring stations from RedESP considered; MB: mean bias (µg m^{-3}); RMSE: root mean square error (µg m^{-3}); r: correlation coefficient (unitless). Q1: 1st quartile; Q2: median; Q3: 3rd quartile

In order to have a better understanding of the CALIOPE-AQFS's performance on the representative day of each CT, a spatial evaluation has been performed for the aforementioned pollutants and statistics. The current quality criteria colour code used in the reporting system of the CALIOPE-AQFS (Arévalo *et al.*, 2014) has been used (Table 3-6). The ranges for the statistics in Table 3-6 are defined based on previous evaluations of the system (Pay *et al.*, 2010; Baldasano *et al.*, 2011).

Table 3-6. Quality criteria for the evaluation of the performance of the CALIOPE-AQFS based on the Mean Bias (MB μg m^{-3}), Root Mean Square Error (RMSE μg m^{-3}), and correlation coefficient (r) of pairs of observed/modelled concentrations of pollutants

Pollutant	Model performance category	MB (μg m^{-3})	RMSE (μg m^{-3})	r
NO_2	Very good	|MB| < 5	RMSE < 5	0.60 < r
	Good	5 < |MB| < 10	5 < RMSE < 15	0.40 < r < 0.60
	Acceptable	10 < |MB| < 20	15 < RMSE < 25	0.20 < r < 0.40
	Bad	20 < |MB| < 30	25 < RMSE < 35	0.10 < r < 0.20
	Very Bad	30 < |MB|	35 < RMSE	r < 0.10
O_3	Very good	|MB| < 5	RMSE < 10	0.70 < r
	Good	5 < |MB| < 10	10 < RMSE < 20	0.50 < r < 0.70
	Acceptable	10 < |MB| < 20	20 < RMSE < 30	0.30 < r < 0.50
	Bad	20 < |MB| < 30	30 < RMSE < 40	0.10 < r < 0.30
	Very Bad	30 < |MB|	40 < RMSE	r < 0.10
SO_2	Very good	|MB| < 3	RMSE < 5	0.40 < r
	Good	3 < |MB| < 5	5 < RMSE < 15	0.30 < r < 0.40
	Acceptable	5 < |MB| < 10	15 < RMSE < 25	0.20 < r < 0.30
	Bad	10 < |MB| < 20	25 < RMSE < 35	0.10 < r < 0.20
	Very Bad	20 < |MB|	35 < RMSE	r < 0.10

The simulations of NO_2 show a "*very good*" and "*good*" performance in terms of MB in 50%-75% of the locations depending on the CT (Figure 3-7). The largest problems occur in areas affected by large traffic emissions such as Madrid, Barcelona, and the Basque Country. Regarding the r, the results are "*very bad*" or "*bad*" especially in locations along the Atlantic Coast such as Galicia, Asturias, and Huelva (Figure 3-8). The largest values of the RMSE occur in the area of Madrid, particularly in the winter CTs (Figure 3-9).

The CALIOPE-AQFS's performance for O_3 shows the largest MB at rural locations along the Mediterranean coast and over areas of the centre of the IP, where the concentrations tend to be high (Figure 3-10). The r is qualified as "*very bad*" or "*bad*" mainly in winter CTs in areas of the NW Spain such as Galicia, Leon, and Asturias (Figure 3-11). The RMSE for O_3 is categorized as "*acceptable*" or better in at least 75% of the locations for all the CTs.

The location of the very bad stations varies depending on the CT, however the Basque Country houses several stations with bad performance on most of the CTs (Figure 3-12).

Finally, the performance of the system for SO_2 is "*very good*" or "*good*" in at least 75% of the locations when considering the MB (Figure 3-13). The underestimations of the SO_2 are larger where the SO_2 concentration is high, close to power plants such as the one in Andorra (Teruel), in the mining area of Leon or in the industrial area of Puertollano (Ciudad Real). In these same locations, the correlation tends to be better than in areas with low SO_2 concentration such as in large urban areas (like Madrid, Seville, or Valencia) and in rural locations (Figure 3-14). The modelled SO_2 concentration is "*very good*" or "*good*" at 90% of the locations as measured through the RMSE (Figure 3-15). Again, the largest errors occur in areas where the concentration is higher than the average.

All in all, the evaluation for the six CTs shows a similar performance of the CALIOPE-AQFS for NO_2, SO_2, and O_3 (except for the overestimation under winter CTs). Although there are slight differences between the CTs, no significant variations in either the spatial distribution or the distribution of the model performance categories for the three used statistics (MB, r, and RMSE) are found.

The evaluation of the CALIOPE-AQFS on the representative day of the CTs by the environment type (rural, suburban, and urban) and the dominant emission source (traffic, industrial, and background) indicates that the largest positive bias and errors regarding the NO_2 occur at urban traffic locations (Figure 3-16). In general terms, CALIOPE-AQFS shows a high agreement with observations at background locations and urban stations at big cities like Madrid and Barcelona in agreement with previous evaluations (Baldasano *et al.*, 2011).

The modelling results for O_3 are quite alike for all kinds of types and dominant source of emissions (Figure 3-17). The overestimation of O_3 that occurs in all CTs is largest in urban and suburban locations but the correlation coefficient is also larger in these locations than in rural ones. The RMSE is higher in suburban and urban locations than in rural ones for all CTs except in NWadv.

Considering the dominant emission source, the industrial locations are those where the modelled SO_2 shows highest RMSE and a largest underestimation. However, the industrial sites are where the r is the highest for all CTs (Figure 3-18). Regarding the environment type, there is not a clear pattern of a best performance of the system considering the three statistics.

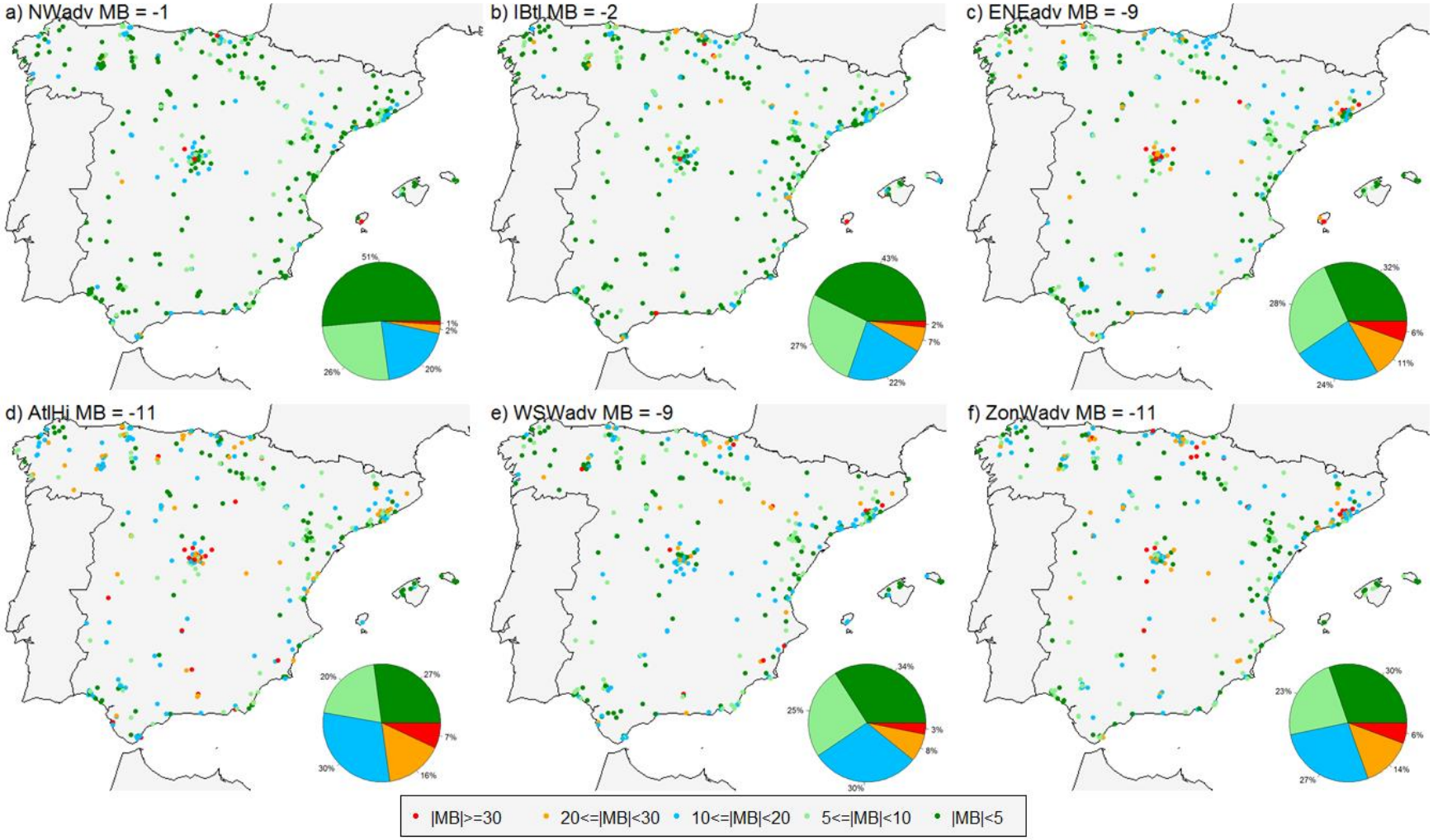

Figure 3-7. Evaluation of the CALIOPE-AQFS performance for NO_2 against validated observations from the Spanish air quality monitoring network on the representative day of each CT. Spatial distribution of the mean bias (MB) per model performance category, distribution of the number of monitoring stations for every model performance category (pie chart) and average MB for all the stations

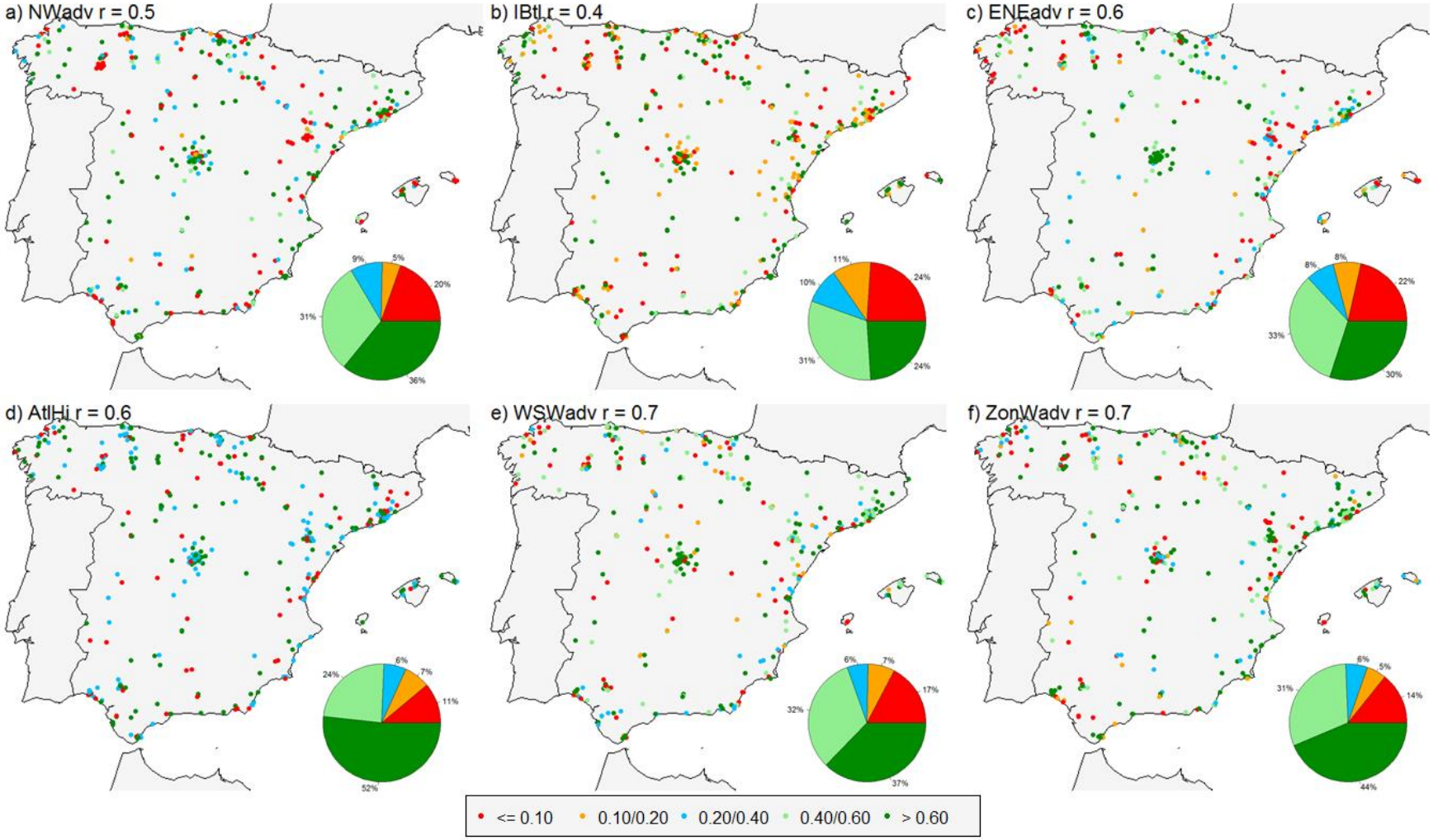

Figure 3-8. Evaluation of the CALIOPE-AQFS performance for NO_2 against validated observations from the Spanish air quality monitoring network on the representative day of each CT. Spatial distribution of the correlation coefficient (r) per model performance category, distribution of the number of monitoring stations for every model performance category (pie chart) and average r for all the stations

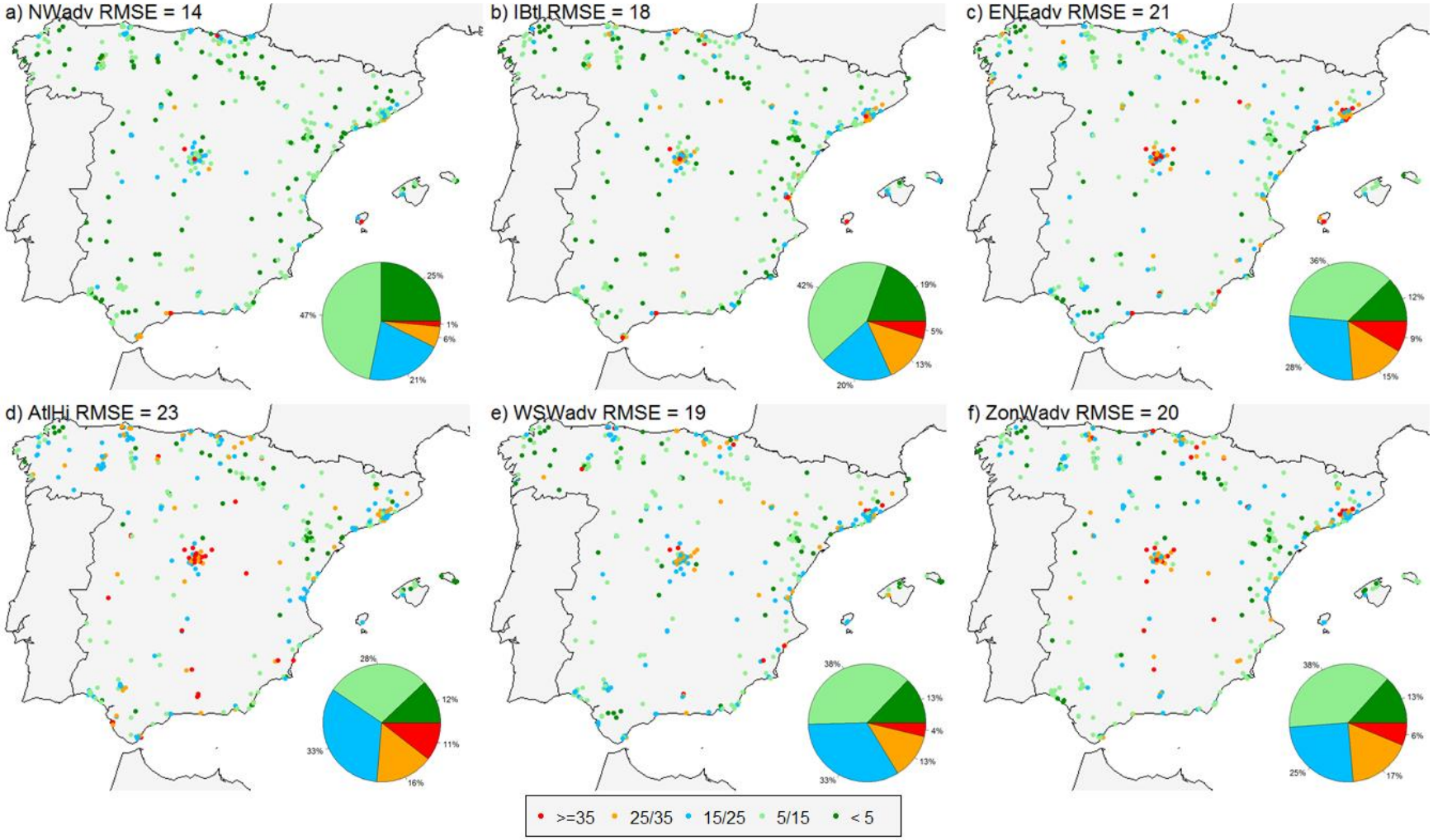

Figure 3-9. Evaluation of the CALIOPE-AQFS performance for NO_2 against validated observations from the Spanish air quality monitoring network on the representative day of each CT. Spatial distribution of the root mean square error (RMSE) per model performance category, distribution of the number of monitoring stations for every model performance category (pie chart) and average RMSE for all the stations

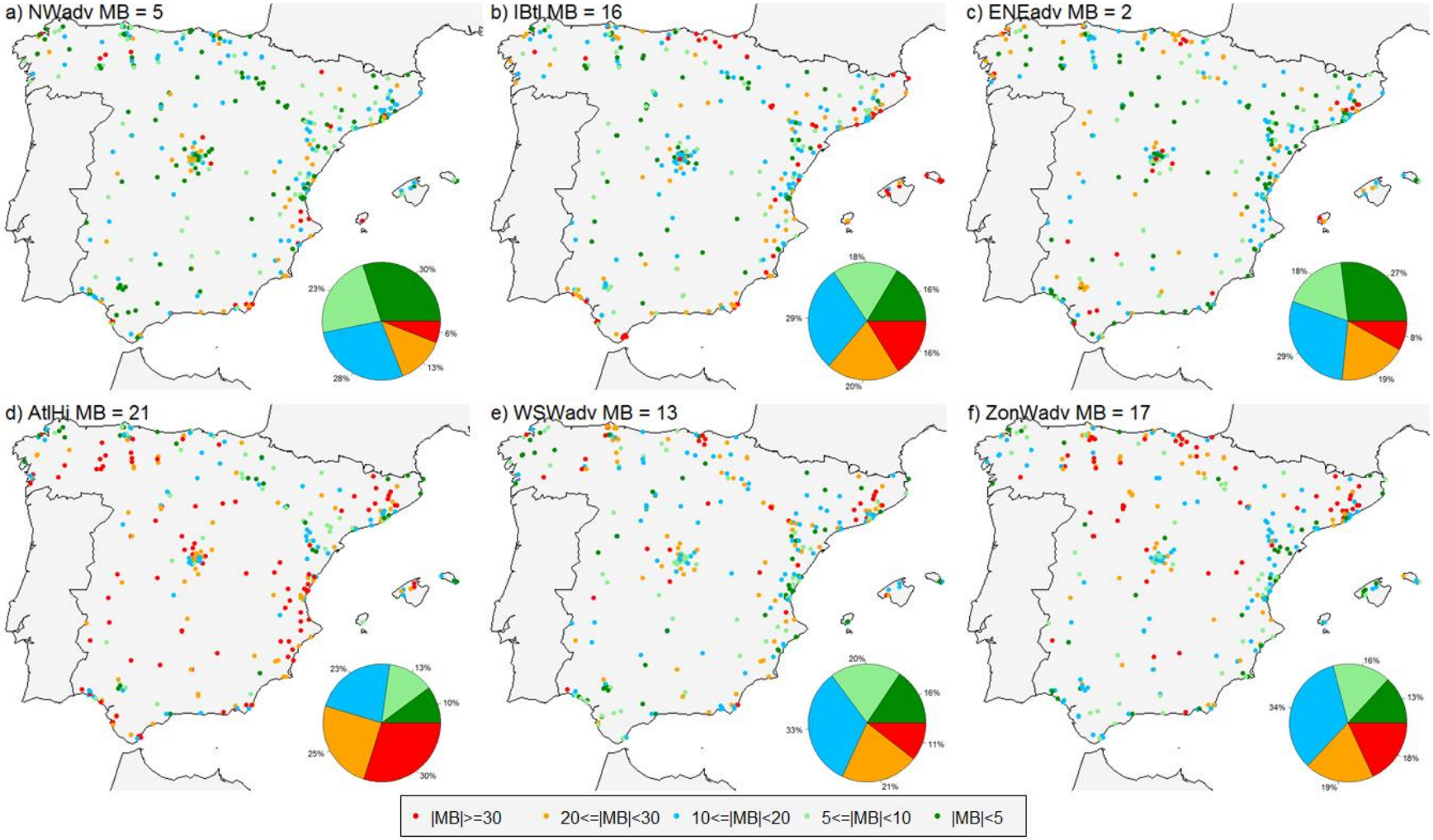

Figure 3-10. Evaluation of the CALIOPE-AQFS performance for O_3 against validated observations from the Spanish air quality monitoring network on the representative day of each CT. Spatial distribution of the mean bias (MB) per model performance category, distribution of the number of monitoring stations for every model performance category (pie chart) and average MB for all the stations

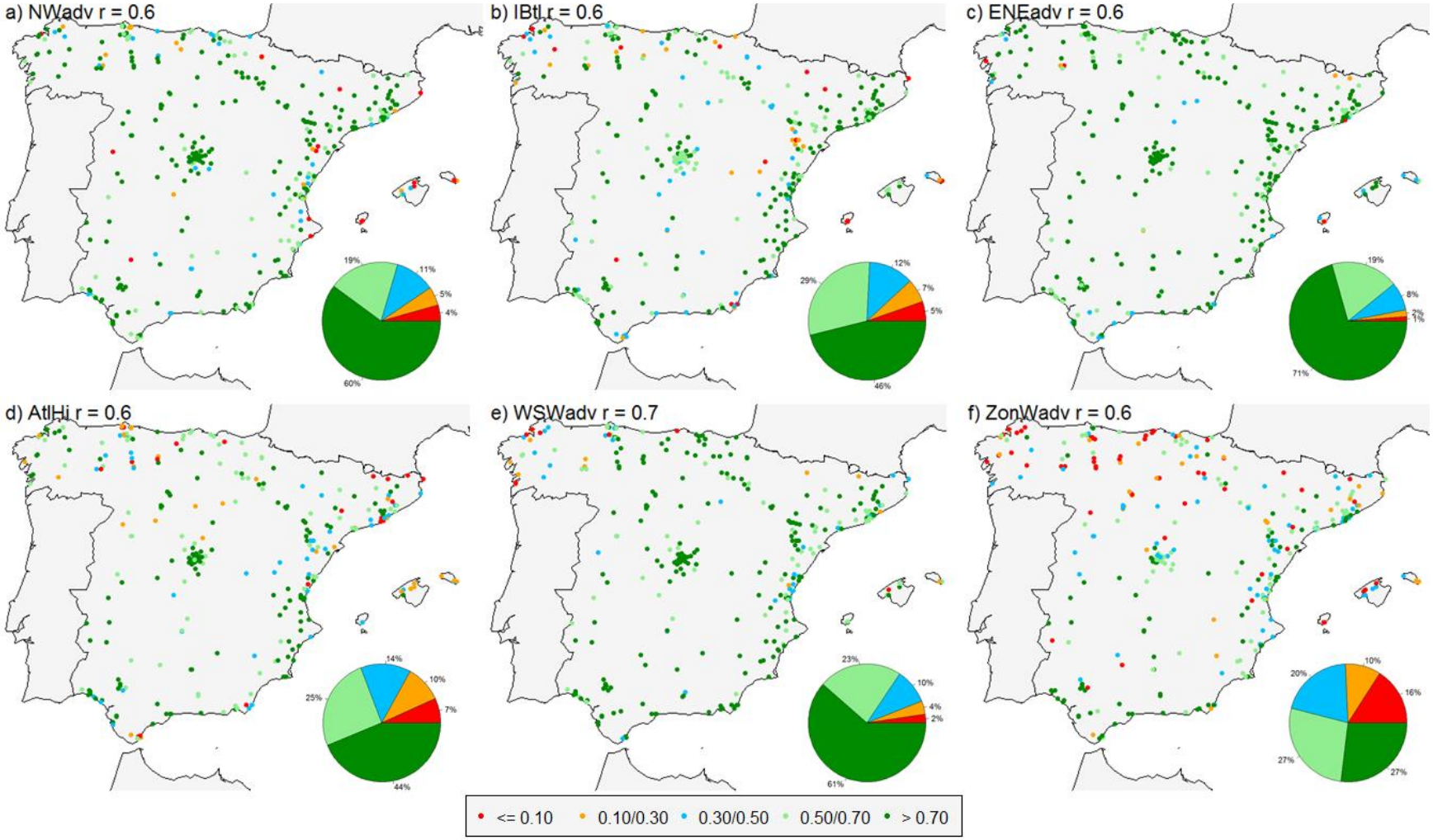

Figure 3-11. Evaluation of the CALIOPE-AQFS performance for O_3 against validated observations from the Spanish air quality monitoring network on the representative day of each CT. Spatial distribution of the correlation coefficient (r) per model performance category, distribution of the number of monitoring stations for every model performance category (pie chart) and average r for all the stations

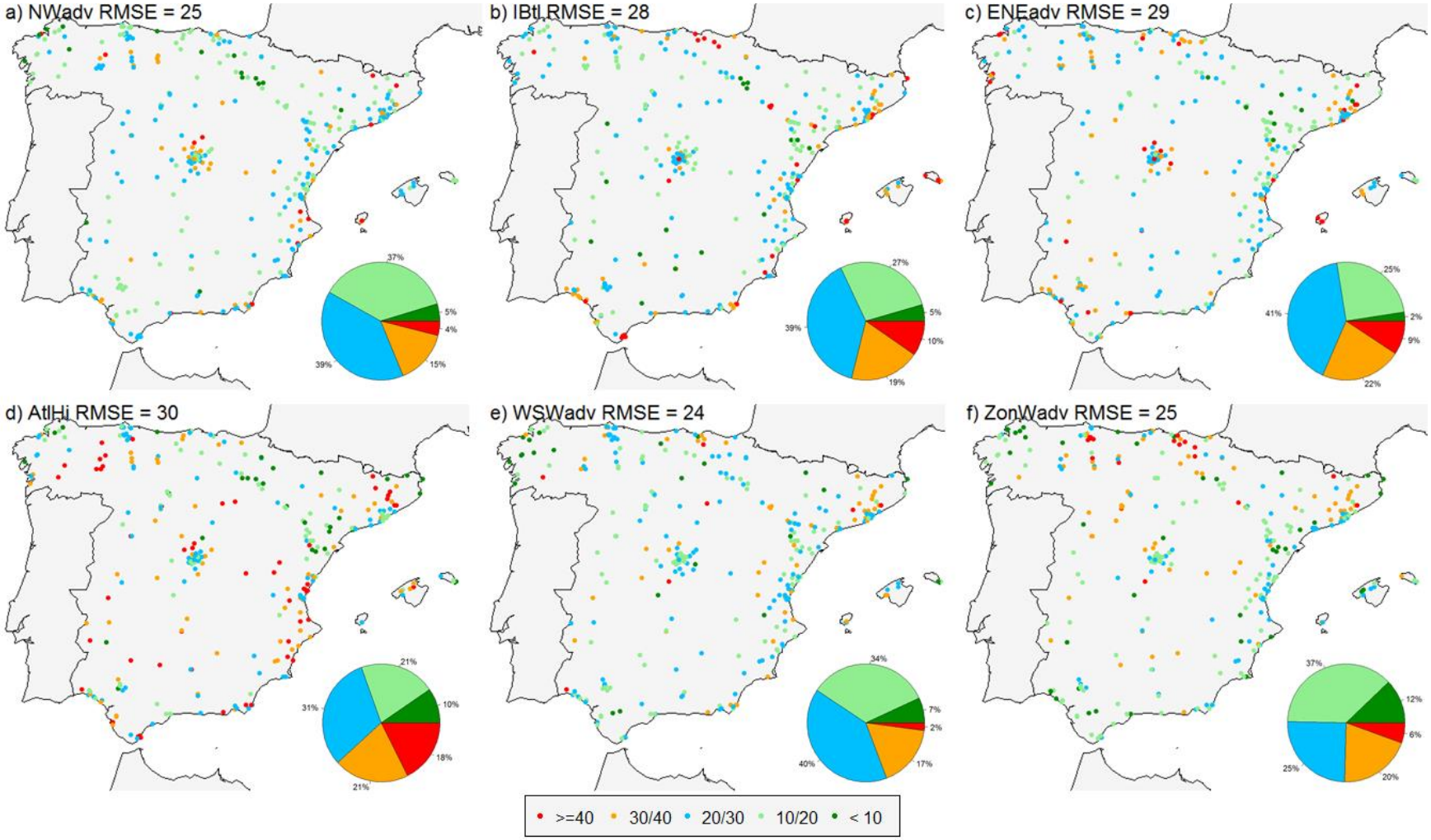

Figure 3-12. Evaluation of the CALIOPE-AQFS performance for O_3 against validated observations from the Spanish air quality monitoring network on the representative day of each CT. Spatial distribution of the root mean square error (RMSE) per model performance category, distribution of the number of monitoring stations for every model performance category (pie chart) and average RMSE for all the stations

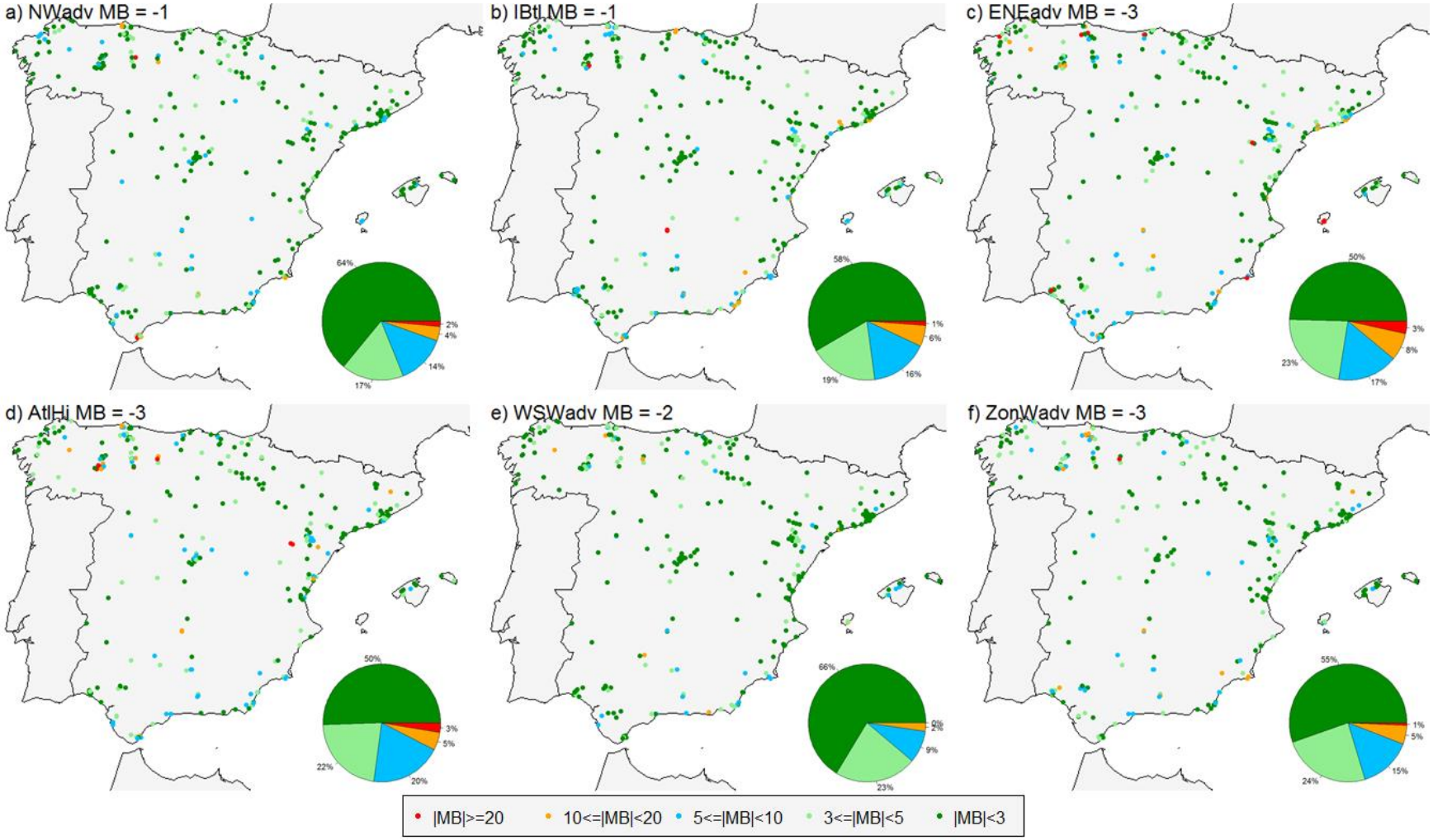

Figure 3-13. Evaluation of the CALIOPE-AQFS performance for SO_2 against validated observations from the Spanish air quality monitoring network on the representative day of each CT. Spatial distribution of the mean bias (MB) per model performance category, distribution of the number of monitoring stations for every model performance category (pie chart) and average MB for all the stations

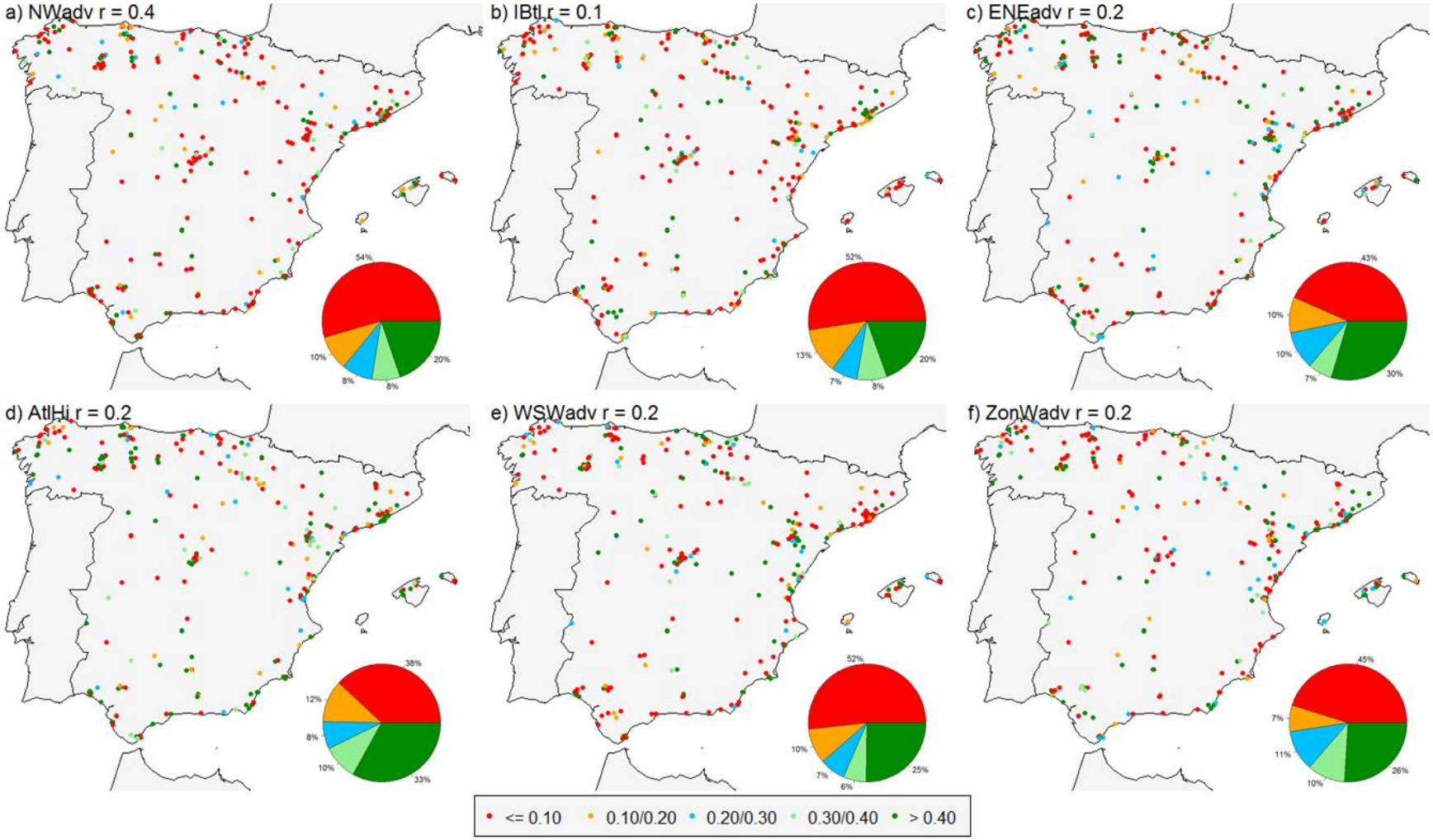

Figure 3-14. Evaluation of the CALIOPE-AQFS performance for SO_2 against validated observations from the Spanish air quality monitoring network on the representative day of each CT. Spatial distribution of the correlation coefficient (r) per model performance category, distribution of the number of monitoring stations for every model performance category (pie chart) and average r for all the stations

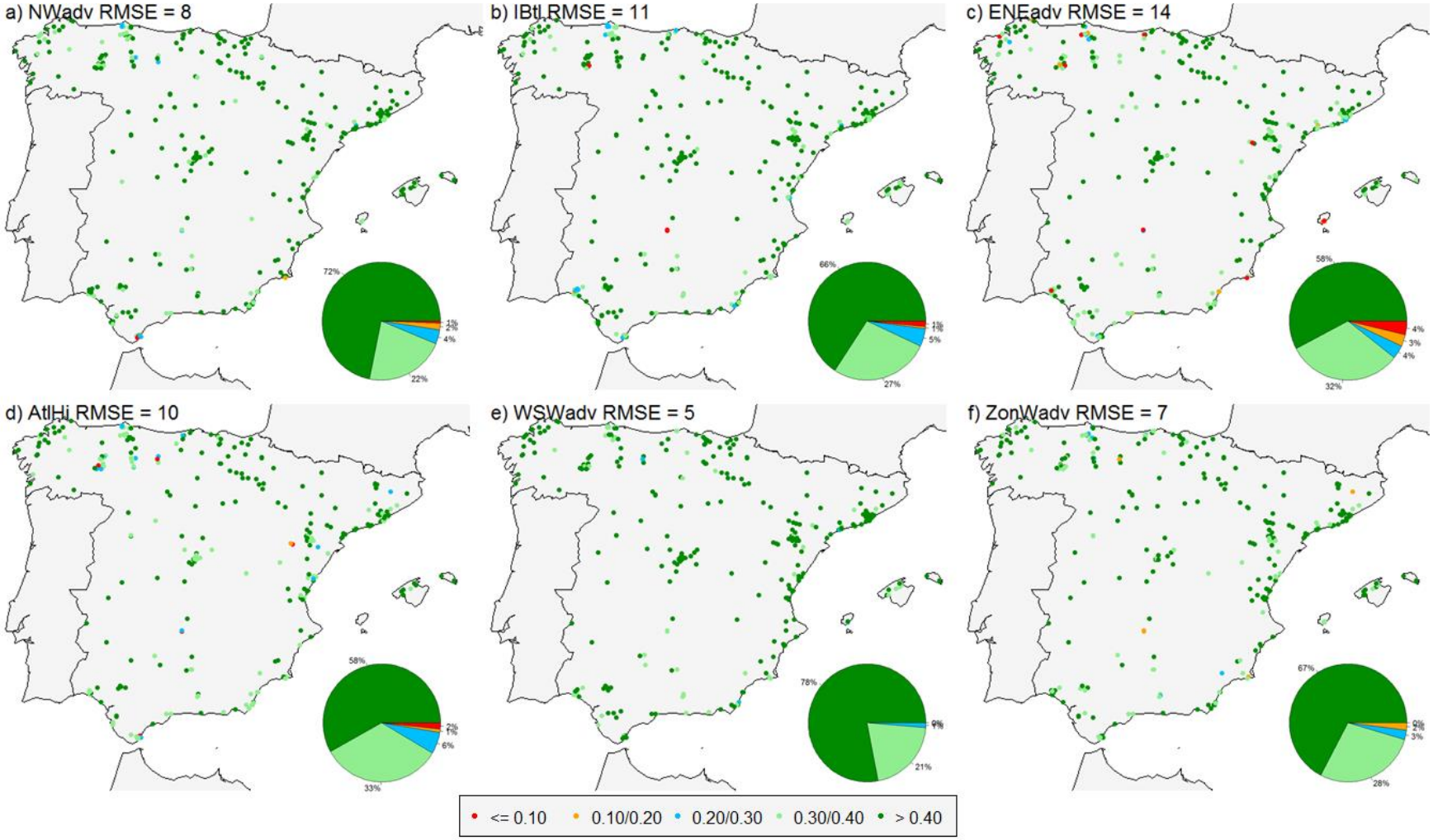

Figure 3-15. Evaluation of the CALIOPE-AQFS performance for SO_2 against validated observations from the Spanish air quality monitoring network on the representative day of each CT. Spatial distribution of the root mean square error (RMSE) per model performance category, distribution of the number of monitoring stations for every model performance category (pie chart) and average RMSE for all the stations

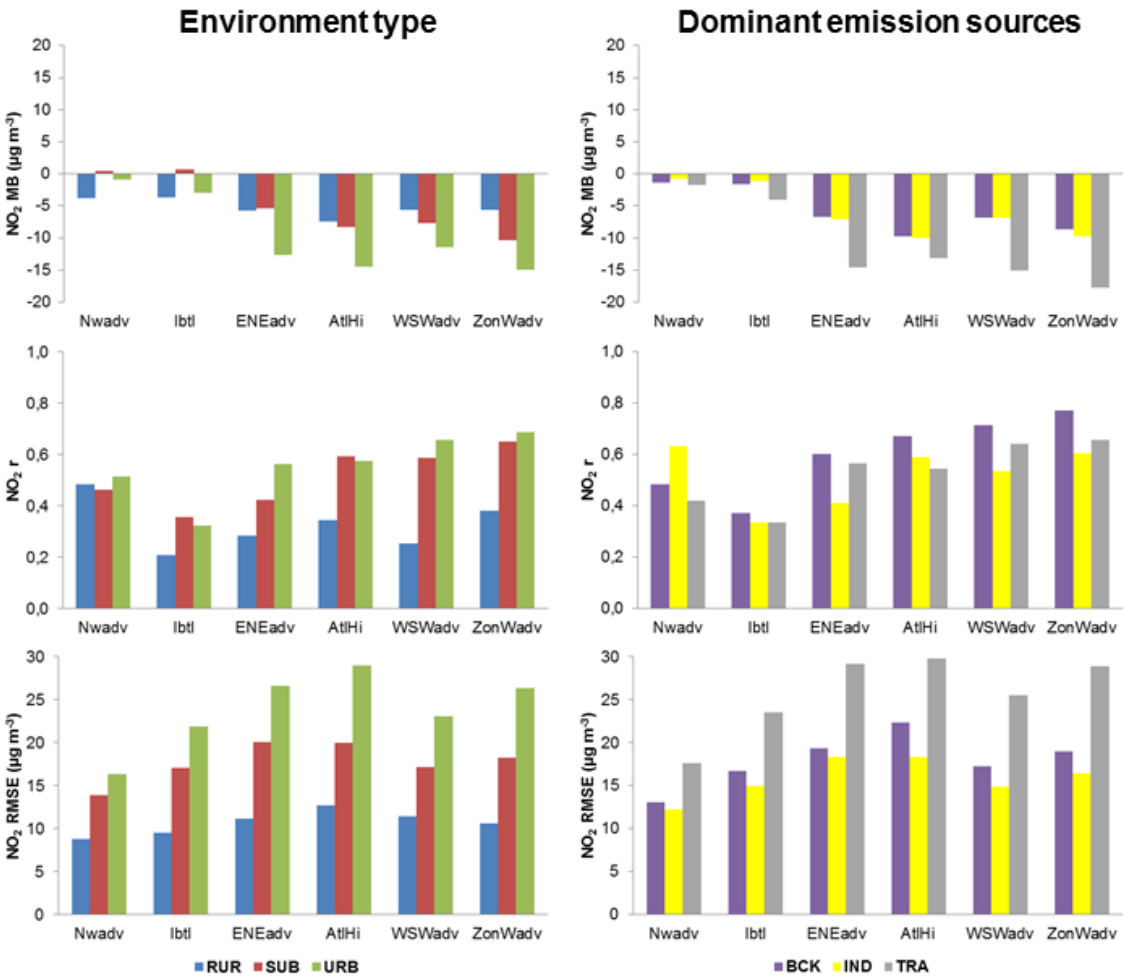

Figure 3-16. Evaluation of the CALIOPE-AQFS performance for NO_2 against validated observations from the Spanish air quality monitoring network on the representative day of each CT averaged over each environment type (RUR: rural, SUB: suburban, and URB: urban) and dominant emission sources (BCK: background, IND: industrial, and TRA: traffic). MB: mean bias. r: correlation coefficient. RMSE: root mean square error

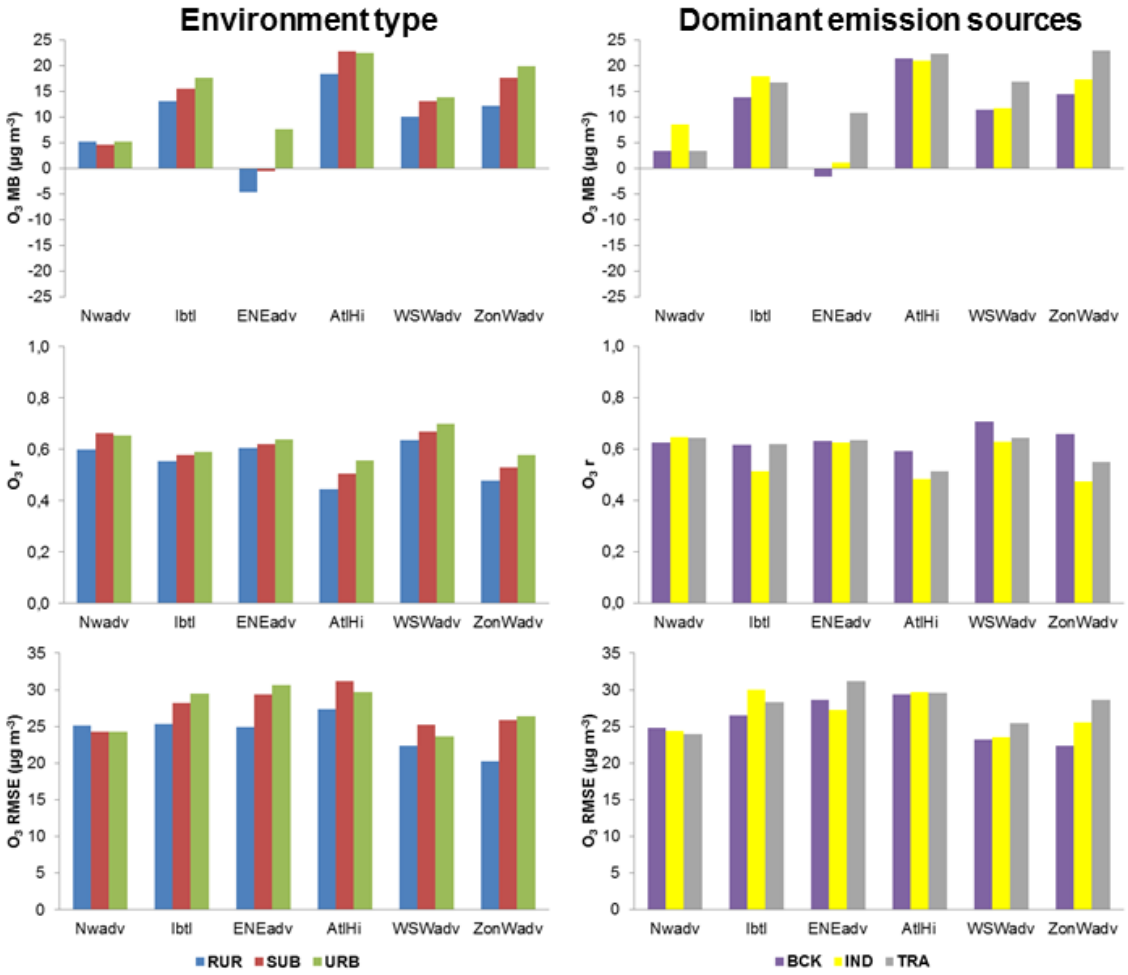

Figure 3-17. Evaluation of the CALIOPE-AQFS performance for O_3 against validated observations from the Spanish air quality monitoring network on the representative day of each CT averaged over each environment type (RUR: rural, SUB: suburban, and URB: urban) and dominant emission sources (BCK: background, IND: industrial, and TRA: traffic). MB: mean bias. r: correlation coefficient. RMSE: root mean square error

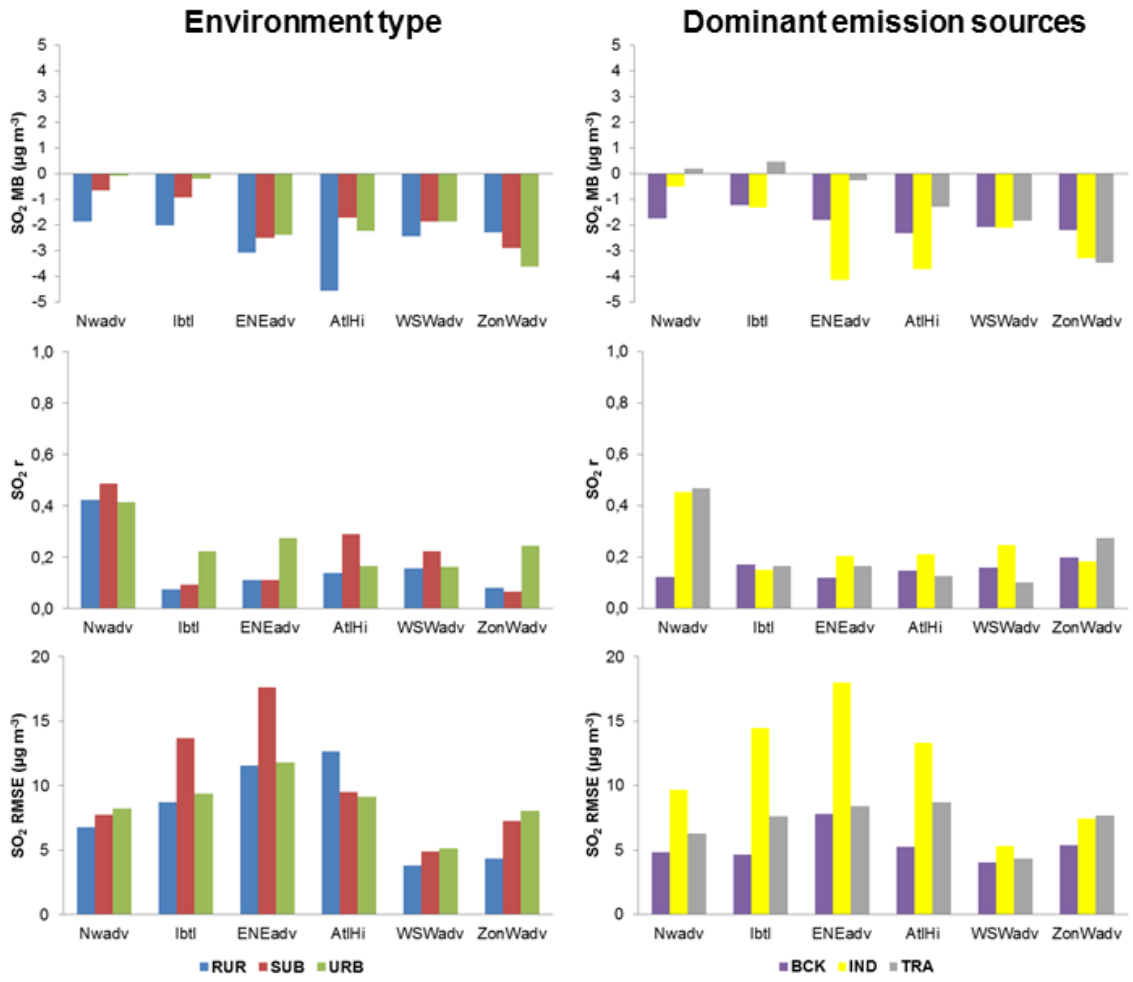

Figure 3-18. Evaluation of the CALIOPE-AQFS performance for SO_2 against validated observations from the Spanish air quality monitoring network on the representative day of each CT averaged over each environment type (RUR: rural, SUB: suburban, and URB: urban) and dominant emission sources (BCK: background, IND: industrial, and TRA: traffic). MB: mean bias. r: correlation coefficient. RMSE: root mean square error

3.3.3 Evaluation with the DELTA TOOL

The DELTA TOOL version 5.1 has been used to evaluate the CALIOPE-AQFS performance for each representative day considering all the available air quality stations differentiating their typology. In this tool's version, the SO_2 Target plot is not available because there is no parametrization to estimate SO_2 measurements uncertainty. Furthermore, the DELTA TOOL aims at analysing seasonal and annual O_3 and not individual days. As a result only results for NO_2 are discussed (Figure 3-19, Figure 3-20, and Figure 3-21, for rural, suburban and urban stations, respectively). In the Target Plot, stations located in the green area fulfil the model quality objectives based on bias, correlation, error, and observation uncertainty. The number of stations fulfilling the target criteria, indicated as a percentage in the plots, ranges from 67% to 98%. According to the AQD, the minimum expected performance of a model is 90%. The results for rural locations are good enough

under all the CTs whereas in suburban and urban locations, the performance depends on the CT. The percentage of stations fulfilling the AQD criteria range 80%-90% in suburban locations and 67%-87% in urban ones. Considering the results by CT for all kinds of stations, the worst results are obtained for the ENEadv and IBtl probably related to a combination of high NO_2 emissions together with stagnant conditions over large parts of the IP that make it difficult to properly model the transport dynamics. On the contrary, the best results are recorded under Atlantic advection conditions (ZonWadv, WSWadv and NWadv). Overall, there is a negative bias for surface concentration, especially for low values (< 10 μg m^{-3}). Moreover, the target plots highlight that correlation errors dominate over the standard deviation error.

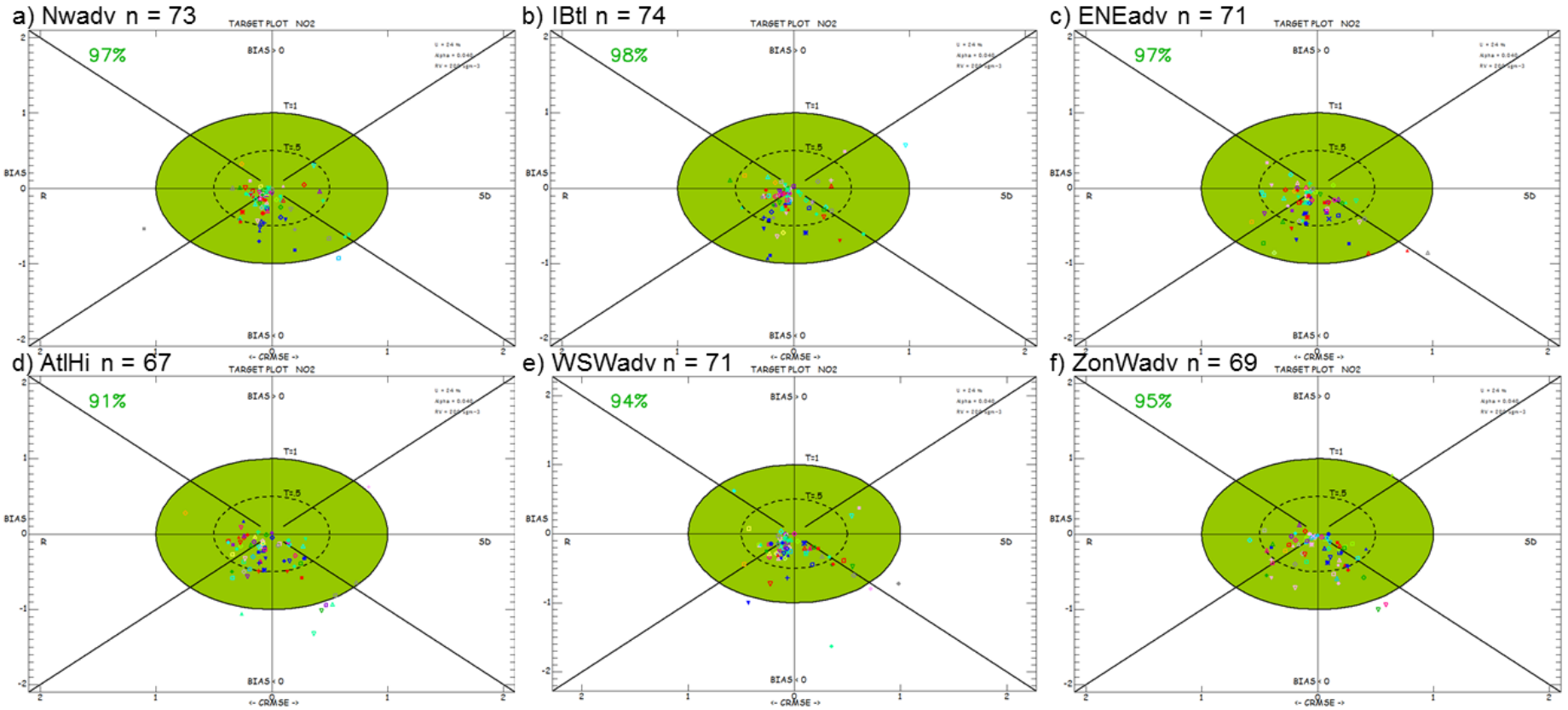

Figure 3-19. Evaluation of the CALIOPE-AQFS performance for NO_2 against validated observations at rural stations from the RedESP, for each CT. Target plot from DELTA TOOL for hourly pairs of observed-modelled concentrations. n: number of stations. Symbols and colours represent the different stations. The percentage indicates stations fulfilling the model quality objective target criteria

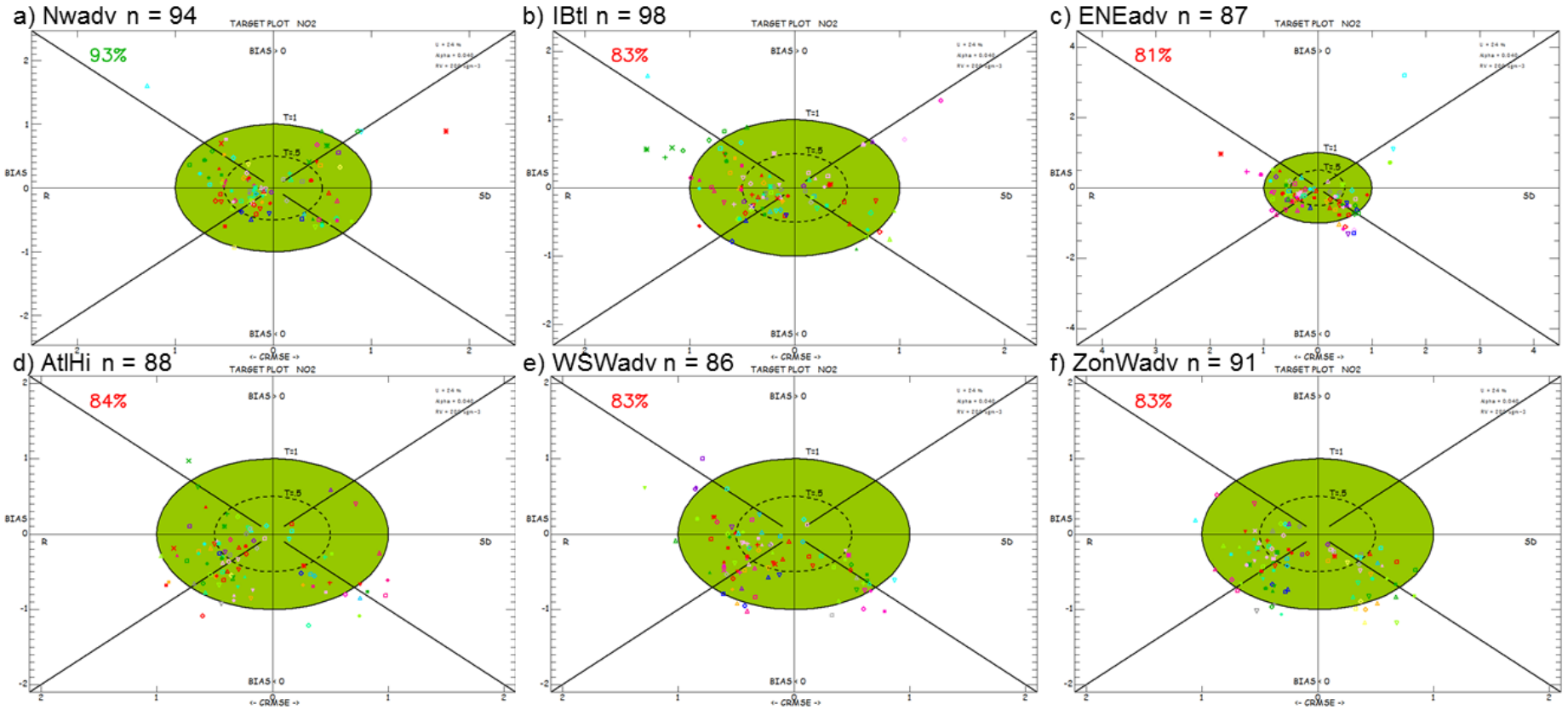

Figure 3-20. Evaluation of the CALIOPE-AQFS performance for NO_2 against validated observations at suburban stations from the RedESP, for each CT. Target plot from DELTA TOOL for hourly pairs of observed-modelled concentrations. n: number of stations. Symbols and colours represent the different stations. The percentage indicates stations fulfilling the model quality objective target criteria

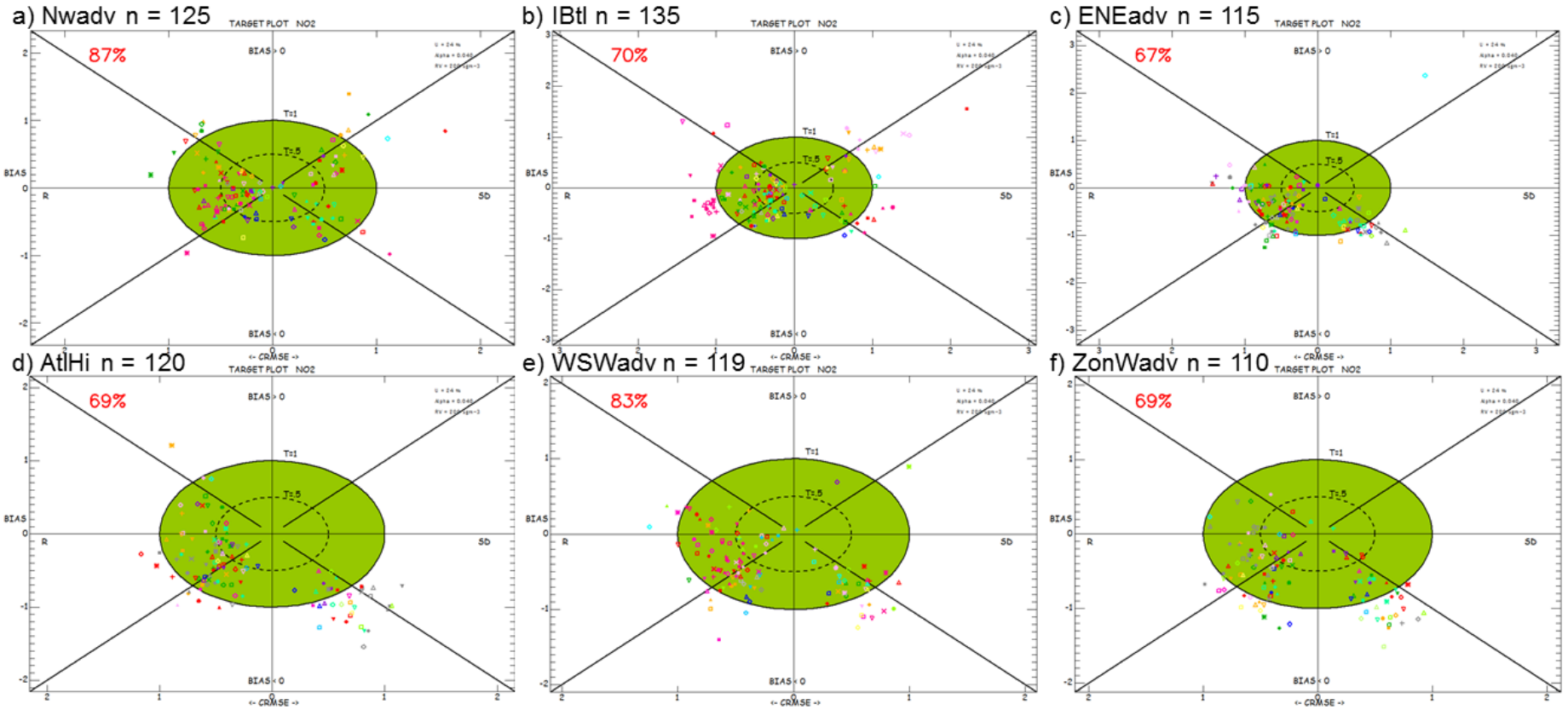

Figure 3-21. Evaluation of the CALIOPE-AQFS performance for NO_2 against validated observations at urban stations from the RedESP, for each CT. Target plot from DELTA TOOL for hourly pairs of observed-modelled concentrations. n: number of stations. Symbols and colours represent the different stations. The percentage indicates stations fulfilling the model quality objective target criteria

3.4 Conclusions

The Earth Science Department of the BSC-CNS has developed along the years a state-of-the-art air quality forecast system for Europe and Spain, the CALIOPE-AQFS. The system is based on a set of interlinked models (emissions, meteorology, chemistry and transport, and mineral dust) that run on the MareNostrum supercomputer and provide an operational forecast for the main pollutants at high spatial and temporal resolution. In this Ph.D. Thesis, the CALIOPE-AQFS has been used in study cases to analyse pollution dynamics under typical CTs affecting the IP.

The CALIOPE-AQFS is able to reproduce NO_2, O_3, and SO_2 concentration as shown by statistics (MB, RMSE, and r) calculated on an hourly basis. Although NO_2 tends to be under estimated the general dynamics are well captured. The highest errors are found in urban stations and lowest in rural ones where more than 90% of the monitoring stations are aligned with the quality criteria defined by the Air Quality Directive. As for O_3, the model tends to overestimate the concentration, particularly during the night and in urban and suburban locations. However, the daily trends are well captured. The simulation of SO_2 is challenging because the concentration of the pollutant is low in most areas of the country. However, close to the main sources of SO_2, the CALIOPE-AQFS is able to reproduce the variability despite slightly underestimating the measured values.

The results of the CALIOPE-AQFS evaluation regarding NO_2 and O_3 are consistent with other authors. For example, a recent chemical transport model inter comparison evaluation over Europe using four offline models (CHIMERE, EMEP, MATCH and MOCAGE) and two approaches of meteorological driver (ERA-Interim reanalysis and outputs from a Global Climate Model) consistently shows an underestimation of NO_2 and an overestimation of O_3 annual concentrations respect to Airbase measurements (Colette *et al.*, 2011; Watson *et al.*, 2015). For both pollutants, the bias appears to be mainly correlated to the boundary layer height.

The CALIOPE-AQFS performance, when run at high spatial and temporal resolution over the IP, is inline with the Air Quality Directive quality criteria despite Spanish complex topography. Even if some improvements need to be done (regarding the choice of chemical boundary conditions) it is a powerful tool to analyse air pollution dynamics in Spain and it has therefore been considered as the main tool to provide insight in the causes, mechanisms and dynamics of air pollution in this Ph.D. Thesis. No correction factors have been applied to the outputs of the CALIOPE-AQFS as the focus of the research is done over dynamics rather than on the quantification of concentration levels. However, the results and discussions in the following Chapters have to consider the limitations presented in this evaluation of the modelling system.

4. Pollution dynamics associated to NO_2 from urban and industrial sites

*This chapter is based on: Valverde V, Pay MT, Baldasano JM. 2014. Circulation-type classification derived on a climatic basis to study air quality dynamics over the Iberian Peninsula. International Journal of Climatology **35**. DOI: 10.1002/joc.4179.*

4.1 Introduction

This Chapter presents the first effort that was performed during the Ph.D. Thesis to characterise air pollution dynamics under the typical CTs that were identified over the IP in Chapter 2. The aim of the Chapter is to present a characterization of NO_2 dynamics associated to emissions in the biggest urban and industrial areas in Spain through the analysis of NO_2 concentration maps obtained from the operational CALIOPE-AQFS on the representative day of each CT.

Special focus is done over five areas within the IP that frequently show high NO_2 concentrations (1h-maximum > 40 $\mu g\, m^{-3}$). They are the two biggest cities of Spain (Madrid and Barcelona > 5 million inhabitants), the urban-industrial area of Valencia (1.5 million inhabitants), the industrial area of Algeciras (there are two power plants, a refinery and it is a hotspot of maritime traffic), and the energy generation area of Asturias (there are five power plants and three cocking plants).

4.2 Methods

NO_2 concentration maps over the IP domain on the representative day of each CT (Table 2-4) are provided by the operational forecast of the CALIOPE-AQFS described and evaluated in Chapter 3. The forecast system model versions at the time of the experiment (2012) were the WRF-ARWv3.0.1 (Skamarock and Klemp, 2008), the HERMESv2 emission model (Guevara *et al.*, 2013), the CMAQv4.5 (Byun and Schere, 2006), and the BSC-DREAM8b mineral dust model (Pérez *et al.*, 2006a; 2006b; Basart *et al.*, 2012a).

4.3 Results and discussion

On July 29th, 2012 (NWadv, Figure 4-1, CT1), northwesterlies in the Cantabrian coast reach 10-15 m s^{-1} and transport NO_2 emissions from Asturias towards the S (40 μg m^{-3} at 40 km) till the Cantabrian Mountains (2000 masl). Synoptic northerlies follow the Portuguese coastline reaching the Gulf of Cadiz and become westerlies in Algeciras (10-15 m s^{-1}) transporting the NO_2 plume towards the E (40 μg m^{-3} at 115 km) during the morning; then the wind becomes weak enabling the transport of locally emitted NO_2 through sea breeze till 30 km to the NW (60 μg m^{-3}). The Guadarrama Mountains (2200-2400 masl), with a NE-SW orientation north of the metropolitan area of Madrid, prevent the arrival of N-NW winds (~5 m s^{-1}) towards the capital, leading to more stagnant atmospheric conditions; thus, Madrid urban plume remains within the metropolitan area (~20 km, 80 μg m^{-3}). Northern synoptic winds, channelled between the Pyrenees and the French Central Massif favour the establishment of an anticyclonic atmospheric circulation in the area of Barcelona that transport NO_2 towards the S during dawn (50 μg m^{-3} at 40 km) and to the SW, parallel to the coast (~40 km) during the morning reaching 30 μg m^{-3}; in the afternoon southern winds towards Barcelona transport the plume to the N (30 μg m^{-3} at 30 km). In Valencia, the development of mesoscale processes control NO_2 transport; sea breezes penetrate inland through the Jucar Valley.

August 19th, 2012 is characterised by a reduced surface pressure gradient over Western Europe (IBtl, Figure 4-1, CT2), that enables a mesoscale control of surface dynamics. The plume in Asturias is transported without a dominant direction. NO_2 emissions from Algeciras are mainly transported by easterlies towards the Gulf of Cadiz reaching 40 μg m^{-3} at 100 km; meanwhile in the evening there is a short-distance transport to the NW from the area of emissions (60 μg m^{-3} at 20 km). Madrid's urban plume remains stationary with a maximum displacement of 20 km (southern winds ~5 m s^{-1}, 80 μg m^{-3}). Along the Mediterranean coast, NO_2 dynamics are dominated by land-sea breezes that drive plumes on a daily cycle: towards the sea at night, inland at noon and perpendicular to the coast in the morning and the afternoon.

Under a blocking anticyclone over the North Sea, E-NE advection is established towards the IP (ENE, Figure 4-1, CT3), as observed in May 24th, 2012. NE winds in the Cantabrian coast (~15 m s^{-1}) transport Asturias NO_2 towards the W (30 μg m^{-3} at 50 km). In Algeciras, strong E winds favour NO_2 transport (40 μg m^{-3}) towards the Gulf of Cadiz (~150 km). In the urban area of Madrid, the synoptic E-NE winds are channelled through the Tajo Valley (NE-SW orientation) leading to a SW transport of the urban plume (40 μg m^{-3}, up to 40 km). Strong northerlies (~25 m s^{-1}) are channelled through the Rhone Valley favouring an anticyclonic circulation over the Balearic Islands that lead to a transport of Barcelona's plume in an E direction during the morning (up to 40 km) and N-NE in the afternoon (up to 30 km from the city). In Valencia, synoptic winds arrive from the E leading to a net

transport of the plume (~30 μg m^{-3} up to 30 km) towards the NW through the Turia Valley, and the W through the Jucar Valley.

On January 24th, 2012 (AtlHi, Figure 4-1, CT4) northerlies (~10 m s^{-1}) arriving to the northern IP shift into easterlies when they reach the coast, transporting NO_2 from Asturias (40 μg m^{-3}) towards the W reaching 40 km. In Algeciras, transport is dominated by westerlies during the morning (40 μg m^{-3} are reached till 120 km); in the afternoon, the strengthening of a low pressure system located S of the Gulf of Cadiz initiates a change of dominant wind direction, enhancing easterlies to transport Algeciras's plume (40 μg m^{-3}) 100 km to the W. In the Madrid area, northerlies (~5 m s^{-1}) are channelled through the Tajo Valley transporting the NO_2 urban plume towards the SW; nevertheless, wind speed is higher in AtlHi than in ENEadv and the urban plume goes further, reaching the same concentration (40 μg m^{-3}) at 70 km. N-NW synoptic winds are channelled between the Pyrenees and the French Central Massif, establishing N winds towards the NW IP (15 m s^{-1}), transporting Barcelona's urban plume (40 μg m^{-3}) to the S-SE (100 km) during the morning; in contrast, in the evening and at night, NO_2 (40 μg m^{-3}) is transported to the NE parallel to the coast and forced by the Pre-coastal mountain range reaching 85 km away from Barcelona. With AtlHi, surface westerly winds are weakened as they pass through the IP, leading to mesoscale control of NO_2 transport over Valencia; during the night, land-breezes transport NO_2 towards the sea up to 20 km (40 μg m^{-3}), whereas during the day, the urban plume is transported by sea-breezes towards the NW, channelled by the Turia Valley, up to 40 km.

Under the W-SW advective CT5, on October 16th, 2012 (WSWadv, Figure 4-1, CT5), southwesterlies and westerlies reach up to 15 m s^{-1} and transport Asturias' plume to the NE (10 μg m^{-3}, 50 km). In the southern IP there is a short-range (20 km) transport of NO_2 towards the SE of the Algeciras Bay (80 μg m^{-3}) in the morning, followed by short-range W transport at noon (40 μg m^{-3} at 20 km). Westerlies arriving to Madrid (10-15 m s^{-1}) during the night transport the urban plume (30 μg m^{-3}) towards the E-NE up to 60 km; in the afternoon Madrid's NO_2 urban plume (50 μg m^{-3}) is channelled through the Henares and Jalon Valleys (NE orientation) and transported 80 km away. The Spanish Mediterranean coast is less affected by the synoptic W-NW advection because winds are weakened by topographic barriers (Iberian System, Baetic System, Catalan mountain range) on their way to the east. Thus, Barcelona's urban plume is mainly controlled by land-sea breezes; NO_2 is transported towards the NE parallel to the Pre-coastal mountain range during the day (30 μg m^{-3} at 50 km). In Valencia, the transport of NO_2 is dominated by easterlies and channelled by the Jucar Valley (40 μg m^{-3} at 30 km).

Atlantic zonal winds arriving to the IP (ZonWadv, Figure 4-1, CT6), are present on January 3rd, 2012. Strong westerlies (30 m s^{-1}) arrive to the Cantabrian coast transporting Asturias' plume towards the E-NE, reaching up to 100 km at dawn (10 μg m^{-3}). In Algeciras, westerlies transport the NO_2 plume to the E reaching the Alboran Sea (200 km, 30 μg m^{-3}).

Madrid's urban plume (40 μg m^{-3}) is channelled in a NE direction through the Henares and Jalon Valleys up to 150 km, especially in the evening. Western synoptic winds are strong enough to overcome the topographical barriers and reach the Mediterranean coast. In Barcelona and Valencia areas, westerlies transport NO_2 towards the Mediterranean Sea (40 μg m^{-3} at 90 and 60 km away, respectively); nevertheless, in the afternoon, westerlies become weak leading to short-distance dispersion without a dominant direction.

Locally high NO_2 concentrations are observed in Asturias under NWadv, IBtl and AtlHi; during these CTs the plume is transported at short distance associated to weaker winds compared to those in ENEadv, WSWadv, and ZonWadv when there is a dominance of stronger winds that enhance the dispersion of NO_2. In the Algeciras area, the transport is mainly controlled by easterlies (IBtl, ENEadv, and AtlHi) and westerlies (NWadv, WSWadv, and ZonWadv) derived from synoptic circulation; nevertheless, for the most frequent patterns when there is a shift in wind direction the local transport towards the NW leads to high NO_2 concentration in the Algeciras area. In the central IP synoptic circulation together with the Guadarrama Mountains control the NO_2 transport towards the SW, channelled by the Tajo Valley during ENEadv and AtlHi or in a lesser frequency towards the NE channelled through the Henares and Jalon Valleys under WSWadv and ZonWadv. The progression of Atlantic synoptic air masses is weakened in their way towards the Spanish Mediterranean coast in four CTs (69% of climatic frequency), enabling mesoscale recirculation of NO_2 (driven by land-sea and mountain-valley breezes) perpendicular to the coast along the Barcelona and Valencia areas. Only under the influence of E-NE advection (21% of climatic frequency) and Western Atlantic zonal advection (10%), synoptic circulations control NO_2 transport along the Spanish Mediterranean coast.

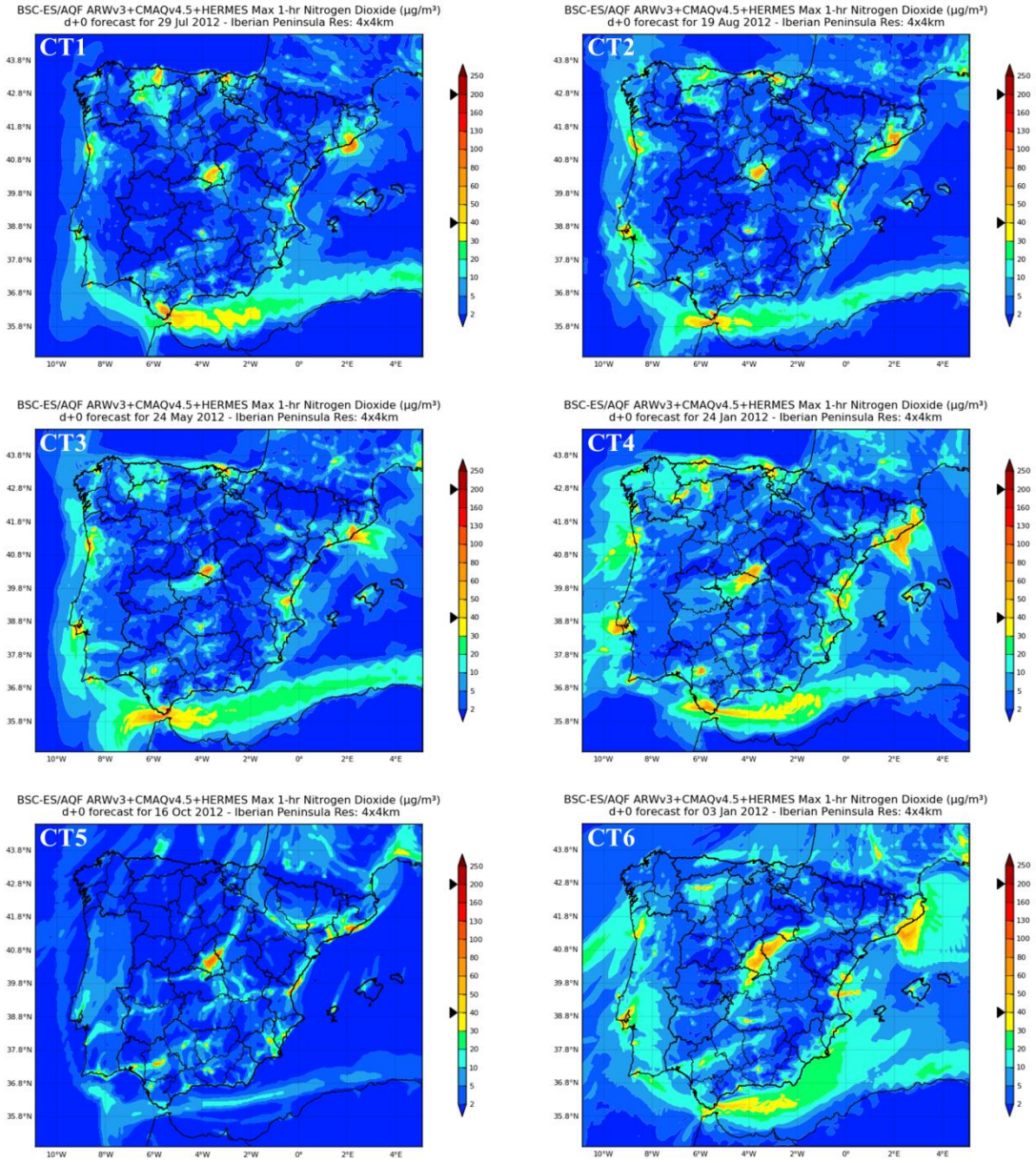

Figure 4-1. 1h-maximum NO_2 concentration (µg m^{-3}) maps from CALIOPE-AQFS for representative days in 2012 corresponding to each CT: July 29th (CT1), August 19th (CT2), May 24th (CT3), January 24th (CT4), October 16th (CT5) and January 3rd (CT6)

Complementary, modelled daily NO_2 concentrations from CALIOPE-AQFS at air quality stations belonging to the Spanish air quality monitoring network over the previously discussed five areas have been boxplotted per CT, using daily data of year 2012 (Figure 4-2). Overall, IBtl that is characterised by a reduced surface pressure gradient presents the highest mean NO_2 concentration. Despite being a typical summertime pattern when NO_2 emissions are at its annual minimum (Guevara *et al.*, 2013), the lack of surface advection favours the accumulation of NO_2 during consecutive days, enhancing high NO_2 concentrations. On the other hand ZonWadv, which is the most infrequent pattern, shows the second highest NO_2 concentrations of all the CTs, in the Mediterranean coastal areas

and Madrid. In Madrid, these concentration records are probably related with a low planetary boundary layer height (300 masl at 12:00 UTC, as forecasted by the WRF-ARW model, compared to ~600 masl for AtlHi; 1500 masl for ENEadv and WSWadv; and 1800 masl for NWadv and IBtl).

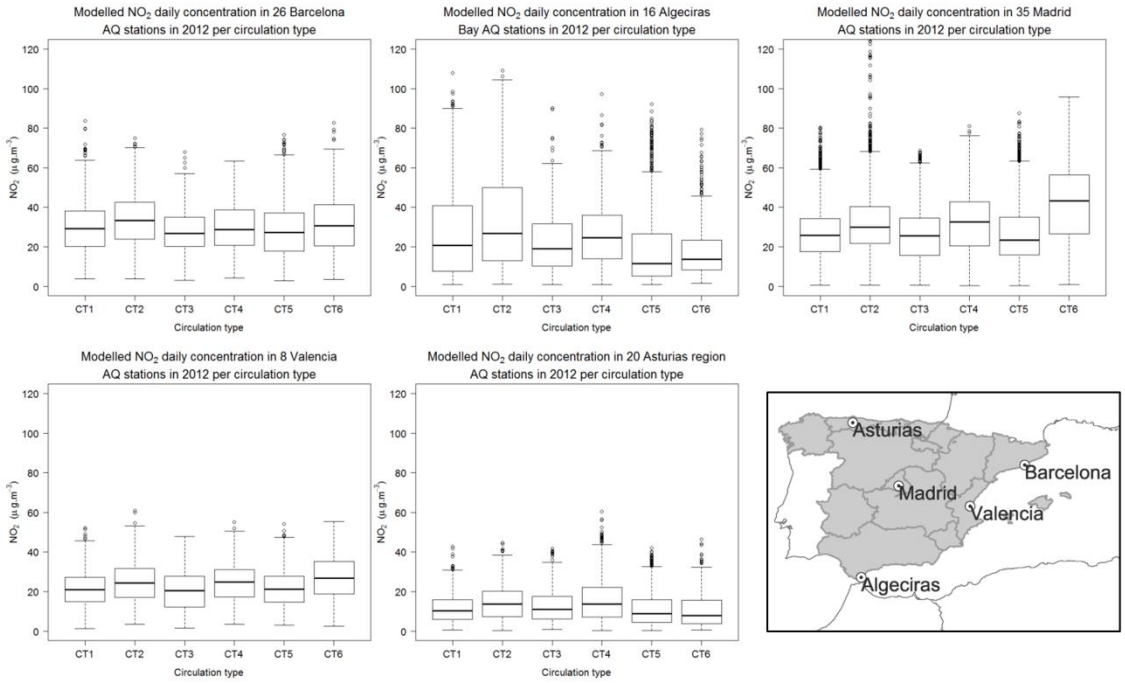

Figure 4-2. Daily mean NO_2 surface concentration (µg m^{-3}) of the year 2012 modelled by the CALIOPE-AQFS in points belonging to the Spanish air quality monitoring network per CT. The number of considered locations is 35 for Madrid, 26 for Barcelona, 8 for Valencia, 16 for Algeciras, and 20 for Asturias

4.4 Conclusions

The analysis of NO_2 concentration maps over the IP associated with the six CTs in 2012 shows that synoptic circulation contributes to explain the spatial distribution of urban and industrial NO_2 plumes. Synoptic circulation influences the intensity of the advection and the planetary boundary layer height favouring or limiting the air pollutant dispersion. Regarding the influence of the CT on NO_2 transport, two main regions within the IP are distinguished: 1) areas of central, northern, and southern IP where there is a synoptic control of NO_2 under all of the CTs; and 2) Mediterranean coastal areas, where in 4 CTs (69% of climatic frequency) synoptic forcing is weakened, and a combined approach of synoptic and mesoscale dynamics control the NO_2 concentrations. Explaining the spatiotemporal dynamics of air pollution patterns under typical CTs is useful to properly develop air quality plans and atmospheric pollution risk assessments.

5. Pollution dynamics associated to SO_2 and NO_2 from coal-fired power plants.

This chapter is based on: Valverde V, Pay MT, Baldasano JM. 2015 A model-based analysis of SO_2 and NO_2 dynamics from coal-fired power plants under representative synoptic circulation types over the Iberian Peninsula. Science of the Total Environment **541**: 701-713. DOI: 10.1016/j.scitotenv.2015.09.111.

5.1 Introduction

Air pollution is a threat for human health (Brunekreef and Holgate, 2002; Gurjar *et al.*, 2010; WHO, 2013) and the environment (de Vries *et al.*, 2014). In the last years, the European Union has established limits to the emission of air pollutants (National Emission Ceilings Directive 2001/81/EC) and legally binding limit values for air quality (Directive 2008/50/EC) in order to reduce the exposition of people and ecosystems to harmful concentrations of pollutants. Partially due to these policy actions, during the 2001-2012 period, the SO_2 and NO_2 concentration at the remote rural EMEP stations in Spain declined 3.6 to 7.7%/year and 2.8 to 3.7%/year, respectively (Querol *et al.*, 2014).

Despite the increase in renewable electricity production in Spain by 50% in the 2008-2012 period (REE, 2013) and the use of cleaner technologies and fuels (ORDEN PRE/77/2008), the contribution of coal-fired power plants to the electricity generation pool was 19.3% in 2012, 54 721 GWh for the Spanish IP (REE, 2013), being the second technology in electricity generation in 2012 after nuclear (22.1%) and before wind power (18.1%). Although SO_2 and NO_2 emissions from energy industry (SNAP01) have been reduced by 29.7% and 12.5% during the period 2008-2012, respectively (MAGRAMA, 2014); they were still significant in 2012 corresponding to a 41% and 22% of the SO_2 and NO_2 total Spanish emissions, respectively. The emissions from coal-fired power plants were the main contributor within the SNAP01 with 79% and 55% of SO_2 and NO_2 emissions, respectively.

The synoptic scale circulation is considered to play a significant role in air pollution both transporting primary and secondary pollutants through long distances (Vivanco *et al.*, 2012; Zhang *et al.*, 2012; Putero *et al.*, 2014) and controlling the effect on the local meteorological conditions (Kassomenos *et al.*, 1998; Menut *et al.*, 1999, Segura *et al.*, 2013). Several studies

relate how different CTs establish dissimilar effects on health for respiratory (Jamason *et al.*, 1997; de Pablo *et al.*, 2013), cardiovascular, and digestive diseases (Morabito *et al.*, 2006, de Pablo *et al.*, 2008).

Circulation-type classification summarises a complex series of synoptic conditions into a catalogue containing a small number of predominant modes of atmospheric circulation or CTs (Barry and Perry, 1974; Beck and Philipp, 2010; Philipp *et al.*, 2014). Each CT is associated with a number of distinctive meteorological behaviours and predominant flow characteristics (Shahgedanova *et al.*, 1998). Several CT classifications have been performed over the IP for different applications. Recently, an objective classification based on a climatic database has been developed for air quality purposes and could be used to analyse the plume dynamics under representative CTs (Valverde *et al.*, 2014).

The dispersion of the pollutants emitted at high stacks relies on combination of meteorological fields and is affected by topography (Palau *et al.*, 2005; 2009). Plume dispersion at power plants, refineries and incinerators has been analysed in impact assessments studies under particular pollution episodes over Spain (Salvador *et al.*, 1992; Hernández *et al.*, 1995; 1997; Puig *et al.*, 2008; Baldasano *et al.*, 2014). However, there is no a comprehensive characterization of the plume dynamics from coal-fired power plants considering the influence of (1) the facilities characteristics, (2) the topography, and (3) the synoptic conditions affecting the IP. Understanding the plume dynamics and the specific contribution of power plants to air pollution under representative CTs can improve the power grid management in the context of environmental sustainability.

The objective of this work is twofold. First, to characterize the plume dynamics for selected Spanish coal-fired power plants under representative CTs over the IP, describing the role of emissions, meteorology, and topography. Second, to determine the contribution of SO_2 and NO_2 surface concentration of each power plant under each CT.

This chapter is organized as follows. Section 5.2 describes the methods and data used. Section 5.3 characterises the power plants' plume dynamics and analyses their contribution to surface SO_2 and NO_2 concentration. Finally, Section 5.4 discusses the synoptic circulation role on plume dynamics over the IP.

5.2 Methods

This section presents the facilities that have been chosen for this study together with the CTC used. The CALIOPE-AQFS (Chapter 3) is used in an ad-hoc experiment to characterise the power plants plume's dynamics.

5.2.1 Power plants selection

There are currently sixteen Spanish coal-fired power plants (combustion installations with boilers > 300MWt) in the IP. Seven facilities have been selected for this study considering those with highest contribution in terms of energy generation (> 950 GWh $year^{-1}$) (Table 5-1 and Figure 5-1). They represent 63.7% of the installed capacity and 79.4% of the 2009 electricity production of coal-fired power plants.

Table 5-1. Characteristics of the coal-fired power plants considered in this study (2009 Data used in HERMESv2)

Power plant / acronym / PRTR register code / Altitude (masl)	**Installed capacity / production***	**# stacks and stack height (magl)**	**Type of fuel**	**SO_x emissions* (Gg $year^{-1}$)**	**NO_x emissions* (Gg $year^{-1}$)**
As Pontes / ASP / 3536 / 360	1 468 MW / 5 815 GWh	4 x 356	Brown lignite	4.99	7.46
Aboño/ ABO / 2928/ 42	921 MW / 4 876 GWh	1 x 175 + 1 x 225	Coal + anthracite	5.83	8.13
Compostilla II / COM) / 8246 / 590	1 341 MW / 2 819 GWh	2 x 270 + 2 x 290	Coal + anthracite	3.79	8.38
Guardo/Velilla / GUA / 3590/ 1120	498 MW / 980 GWh	1 x 70 + 1 x 176	Coal + anthracite	0.82	3.07
Andorra / AND / 3530/ 612	1 101 MW / 2 717 GWh	3 x 343	Black lignite	11.71	10.00
Litoral de Almería, Carboneras / CAR / 3537/ 13	1 159 MW / 5 804 GWh	2 x 200	Imported coal	13.99	9.80
Los Barrios / LBB / 3531/ 11	568 MW / 3 219 GWh	1 x 230	Imported coal	2.53	5.39

*based on year 2009

Figure 5-1. Topographic map of the Iberian Peninsula and location of the studied coal-fired power plants according to Table 5-1

5.2.2 Plume dynamics characterization: methods and data

In order to understand the relationship between each CT and the plume dynamics the present analysis takes into account the location, the stack height and the emission rates of each facility, meteorological fields, and SO_2 and NO_2 concentration profiles. The characterisation of pollution dynamics is performed on the representative day of each CT (Table 2-4, Figure 5-2).

At each power plant, meteorological hourly fields are extracted from the MCIP module. Wind speed, wind direction and vertical vorticity at different vertical layers enable an analysis of horizontal and vertical plume transport close to the power plant. Positive vertical vorticity causes counter clockwise circulation and upward movement of the air mass, whereas negative values cause clockwise circulation and downward movement.

As different plume behaviours are expected when emission occurs under and above the PBL, the PBL height (PBLH, magl) was also analysed using data from the MCIP module. SO_2 and NO_2 hourly concentrations are estimated by the CMAQ model for the representative day of each CT. A brute-force also known as zero-out approach (running two equal simulations but setting the emissions from the seven selected facilities to zero in

one of them) is used to obtain the contribution of the power plants in terms of air quality concentrations. Two complimentary approaches are considered to analyse these data. On the one hand, N-S and W-E cross-sections up to 3000 masl passing by the power plant are obtained (daily maximum and hourly concentration are used). Cross-sections plots help characterising the plumes diffusion and their relationship to topography. On the other hand, SO_2 and NO_2 surface concentration maps and total column mass maps allow describing the horizontal plume transport. The plume length (km) is calculated as the maximum distance from the facility that has a surface contribution higher than the remote background concentration (RBC) in Spain. RBC is calculated as 2003-2012 average of 10 Spanish EMEP stations corresponding to 4.3 $\mu gNO_2\,m^{-3}$ and 1.2 $\mu gSO_2\,m^{-3}$.

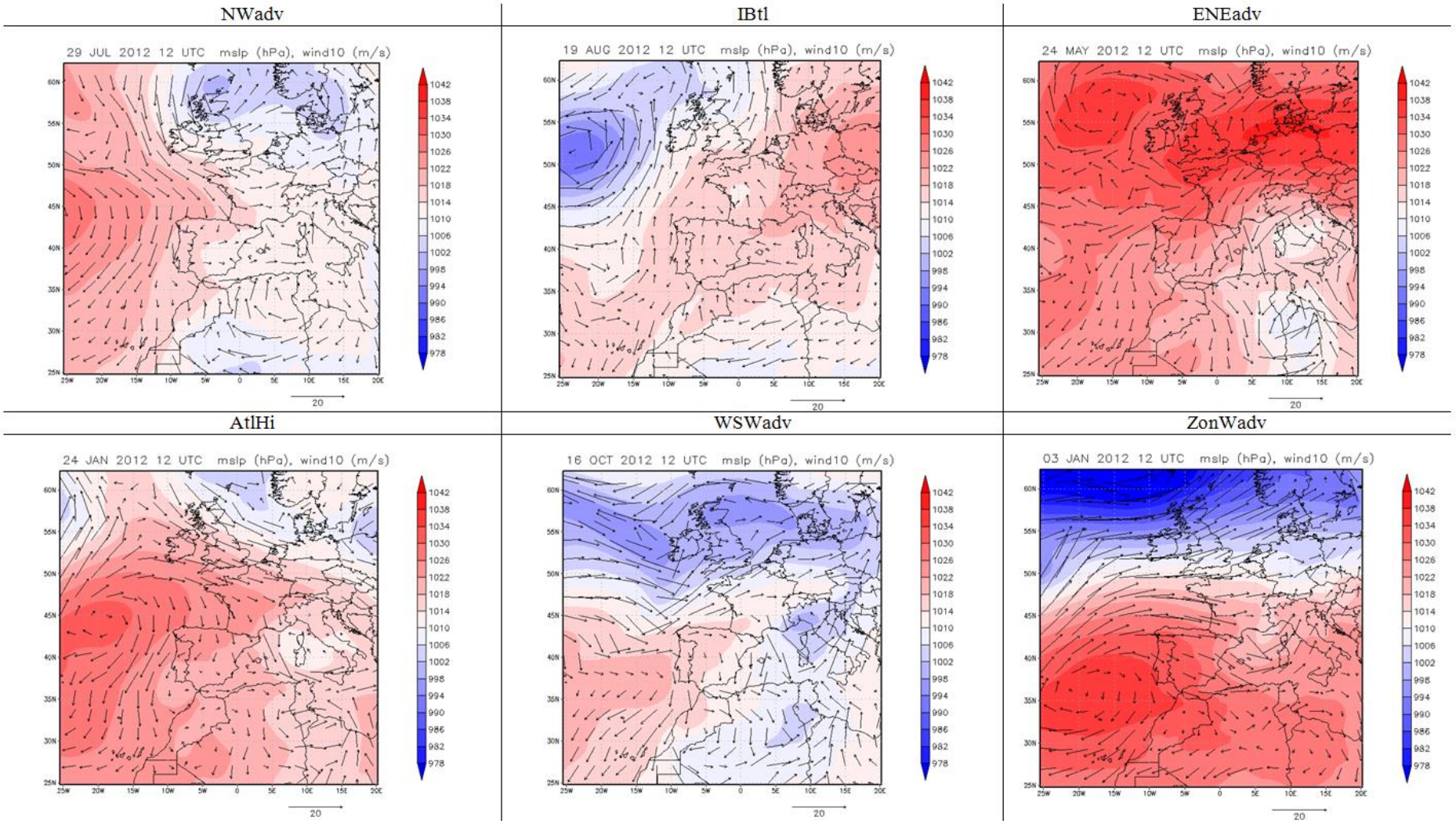

Figure 5-2. Mean sea-level pressure (hPa) and 10-m wind (m s^{-1}) of the representative day of each CT in 2012 (12:00 UTC) over the IP

5.3 Results and discussion

5.3.1 Emissions characterization

To explain the power plants' plume dynamics it is necessary to characterize the temporal emissions variability. The power plants emissions depend on the electricity demand and therefore change throughout the year and along the day (the emission rates for each facility along the representative day of each CT for SO_2 and NO_2 are presented in Figure 5-3 and Figure 5-4, respectively). In general terms, the emission rates are the highest during winter CTs AtlHi and ZonWadv, both with a representative day in January 2012. For the seven power plants, the daily emission rate ranges 250-3400 $kgSO_2\,day^{-1}$ and 900-2900 $kgNO_2\,day^{-1}$. In ASP however, the maximum rates are reached in NWadv (1310 $kgSO_2\,day^{-1}$ and 1960 $kgNO_2\,day^{-1}$). In August, during the IBtl, the emissions are minimal in the seven power plants ranging, 50-2000 $kgSO_2\,day^{-1}$ and 190-900 $kgNO_2\,day^{-1}$.

Superimposed to the seasonal variations, the emission rates change following a daily cycle. Emission rates are the lowest at night and rises in the early morning showing their maximum at 12:00. A second maximum is reached at 20:00-21:00. There are larger variations on emission rates along the daily cycle during winter CTs than during summer, especially for power plants with an emission rate lower than 20 $kg\,h^{-1}$ (GUA, LBB).

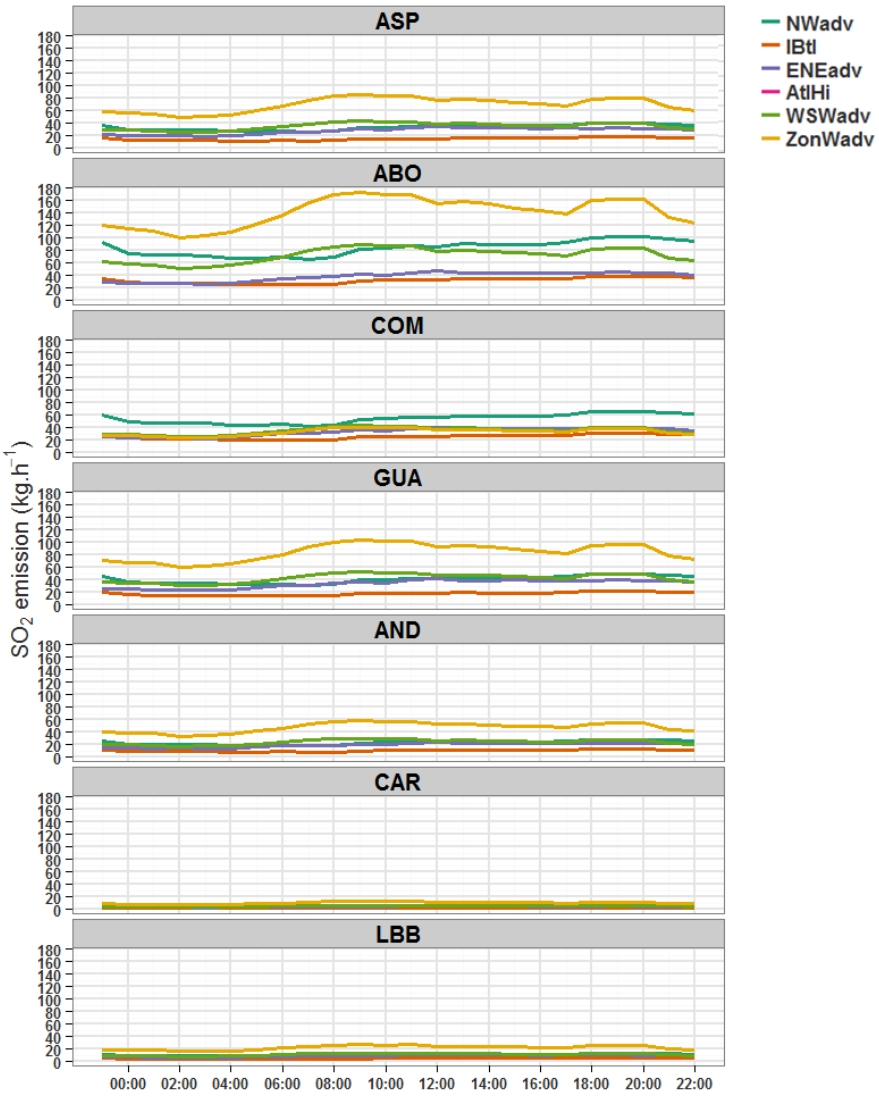

Figure 5-3. SO_2 emission rates (kg h^{-1}) along the representative day of each CT at the 4 km x 4 km cell where the seven selected power plants are located

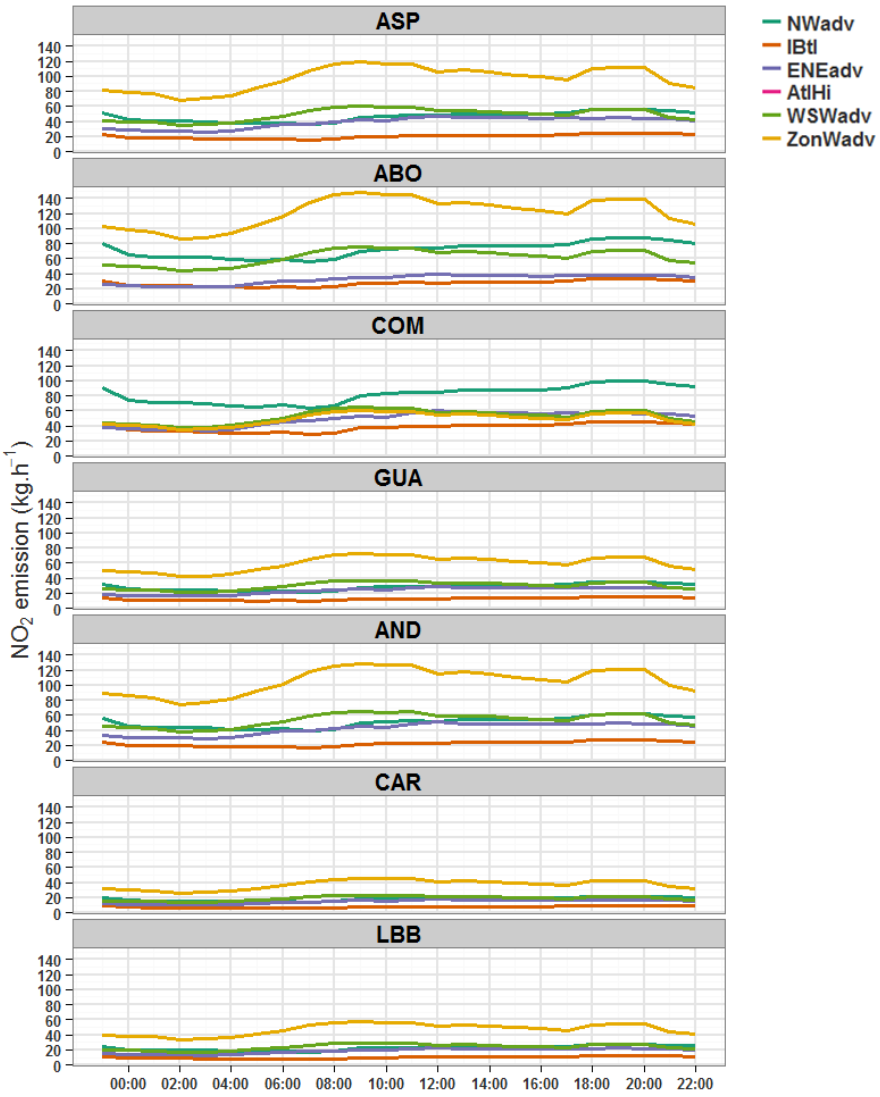

Figure 5-4. NO_2 emission rates (kg h^{-1}) along the representative day of each CT at the 4 km x 4 km cell where the seven selected power plants are located

5.3.2 Plume dynamics from Spanish power plants

In this section, the SO_2 and NO_2 plume dynamics are described on the representative day of each CT using i) maps for the daily maximum surface concentration (Figure 5-5 and Figure 5-6 for SO_2 and NO_2, respectively), ii) maps for the daily maximum total column mass (Figure 5-7 for SO_2 and Figure 5-8 NO_2, respectively), iii) cross-sections at the power plants for the daily maximum concentration (Figure 5-10 to Figure 5-16, for SO_2 and Figure 5-17 to Figure 5-23 for NO_2, respectively) and, iv) daily cycle at the power plant for the hourly PBLH, wind speed and direction and, the vertical vorticity (Annex II, Figures AII-1 to AII-7).

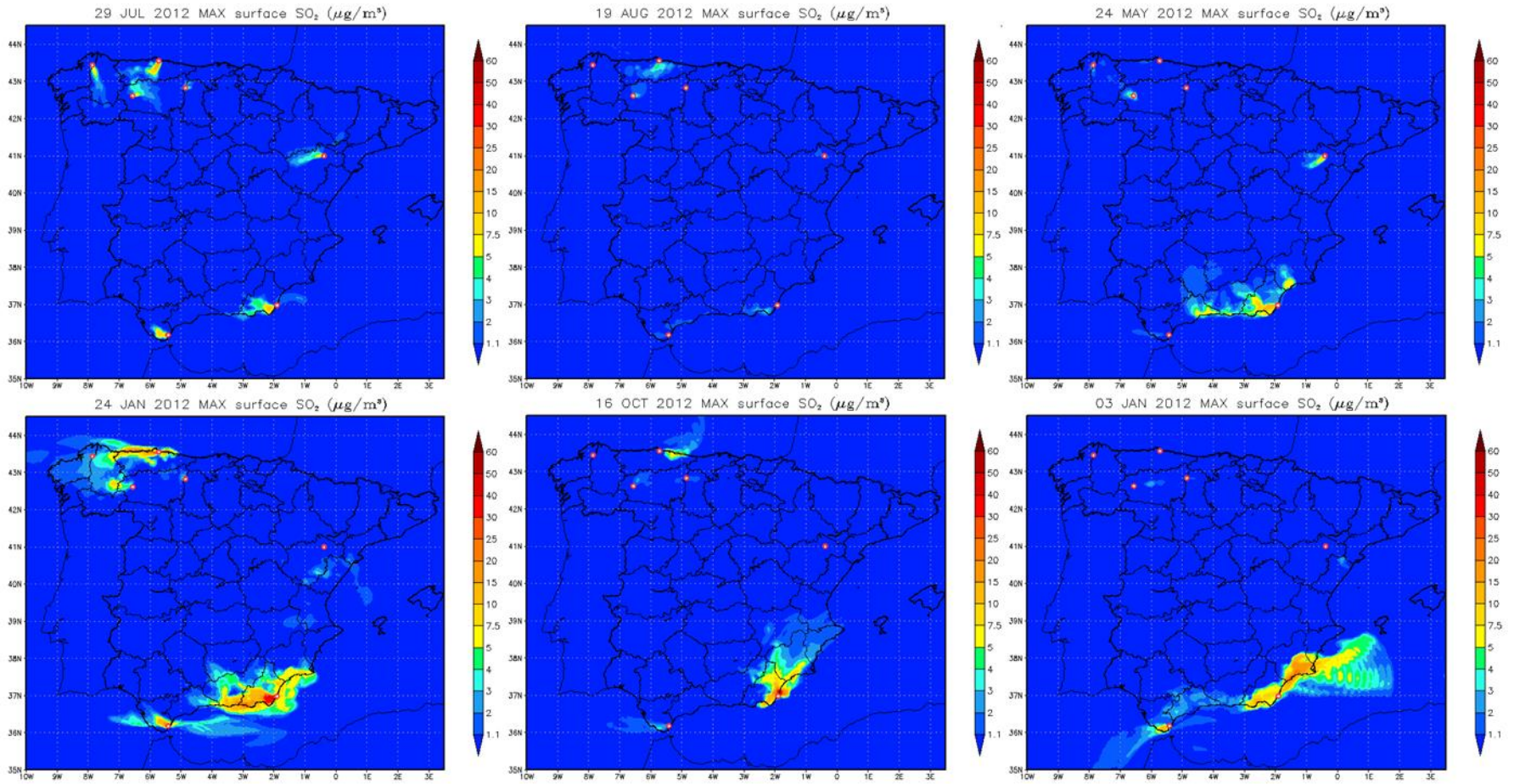

Figure 5-5. Daily maximum SO_2 surface concentration (μg m^{-3}) associated to the emissions in the seven analysed power plants on the representative day of each CT

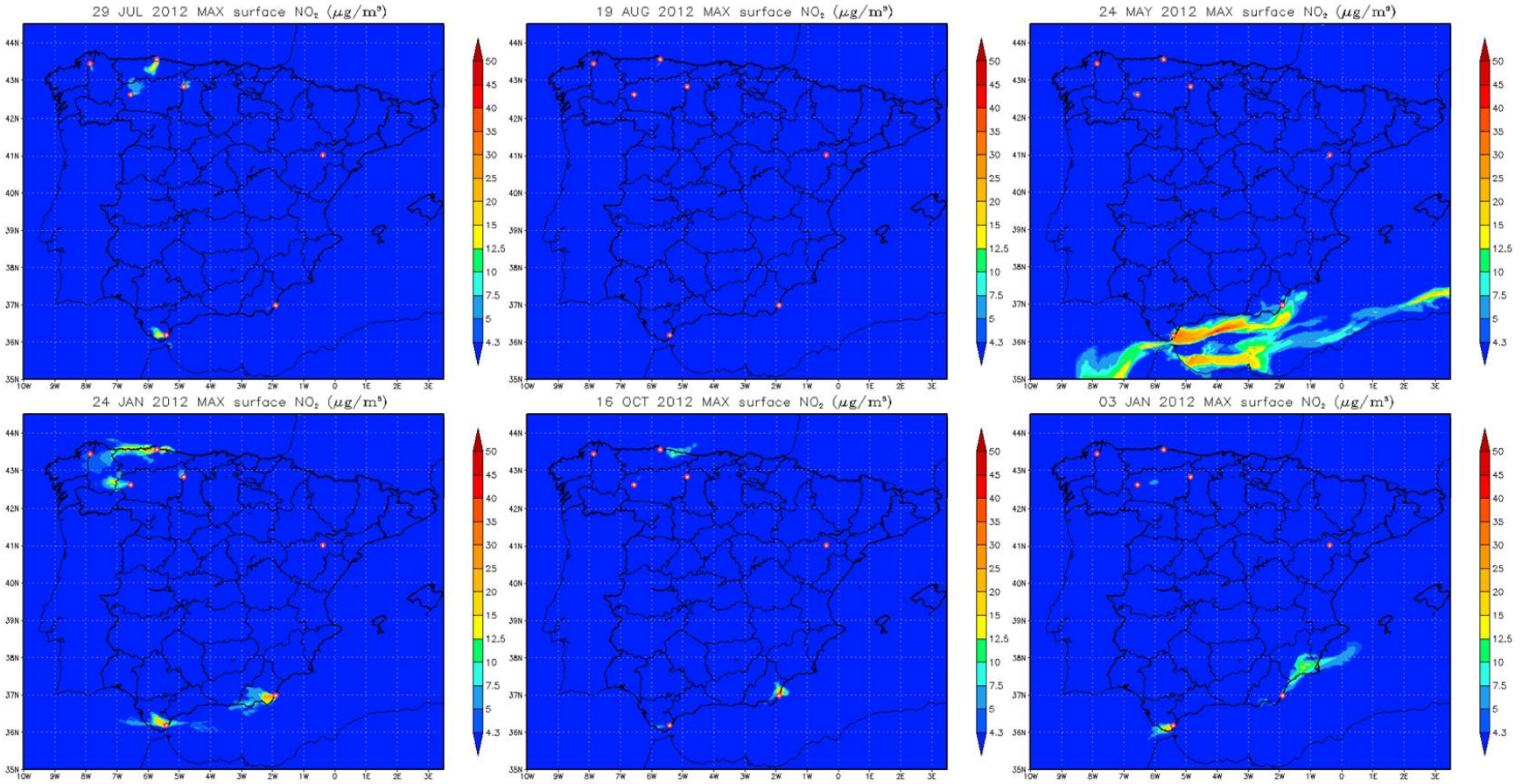

Figure 5-6. Daily maximum NO_2 surface concentration (µg m^{-3}) associated to the emissions in the seven analysed power plants on the representative day of each CT

5.3.2.1 NWadv

ASP and ABO, located the Atlantic coast, are reached by N/NW winds along the day (Figure 5-2). The plume from ASP reaches 1250 meters above injection height (maih, computed as altitude of the facility plus stack height, Figure 5-10 and Figure 5-17) and it is oriented towards the SE/E (Figure 5-5, Figure 5-7, Figure 5-6, and Figure 5-8) reaching 125 km for SO_2 and 25 km for NO_2 (Figure 5-9). At ABO, the plume is transported southwards (60 km for SO_2 and 50 km for NO_2) attaining ~700 maih (Figure 5-11 and Figure 5-18). There is a fumigation process occurring at both power plants at midday leading to a maximum increase in surface concentration close to the source (10-15 km) of 7.3 $\mu gSO_2\ m^{-3}$ and 6.5 $\mu gNO_2\ m^{-3}$ in ASP and 14.3 $\mu gSO_2\ m^{-3}$ and 16.4 $\mu gNO_2\ m^{-3}$ in ABO. This fumigation process at noon is related to i) the injection is done within the PBL which height is maximum at midday (ASP ~ 1000 magl, ABO ~ 600 magl) due to thermal heating of the ground (Figure AII-1, AII-2); and ii) between 13:00 and 17:00 the vertical velocity is negative, favouring a vertical transport of the emissions towards the ground. The main difference between ASP and ABO is that in the former, although the emission rates for SO_2 and NO_2 are higher than in ABO, the emissions are injected at higher altitude ($ASP_{injection\_height}$ = 716 masl > $ABO_{injection\_height}$ = 267 masl) favouring a larger pollutants dispersion (in ASP there is little plume formation for NO_2, Figure 5-6).

COM and GUA are located in Northern Spain in areas with complex topography (Figure 5-1). The Cantabrian Mountains (2000 masl with W-E orientation) situated to the North of COM and GUA behave as an orographic barrier reducing the influence of the Atlantic Ocean over these areas. Synoptic NW winds towards COM and GUA are transformed into westerlies that blow parallel to the Cantabrian Mountains along the day (Figure AII-3 and AII-4) transporting the SO_2 and NO_2 plumes to the E/NE. COM plumes reach ~850 maih and ~75 km for SO_2 and ~55 km for NO_2. The maxima surface contributions are registered at 10 km from the facility and are 6.4 $\mu gSO_2\ m^{-3}$ and 8.6 $\mu gNO_2\ m^{-3}$. In GUA, the plume of both pollutants attains 400 maih (Figure 5-13 and Figure 5-20) and 25 km. The maximum contribution is disclosed at 7 km from the source (3.7 $\mu gSO_2\ m^{-3}$ and 10.5 $\mu gNO_2\ m^{-3}$). As in ASP and ABO, in COM and GUA, there is also a fumigation process from 10:00 that explains the pollutants diffusion towards the ground although the PBLH is higher (~1400 magl) than in the Atlantic power plants. The length and width of GUAs plumes is lower than those of COM (Figure 5-7 and Figure 5-8) due to a combination of factors: lower SO_2 and NO_2 emission rates at GUA, lower plume altitude (the emissions are less dispersed because they are exposed to weaker winds) and because GUA is under the influence of mountain-valley winds which favour recirculations close to the source (Figure AII-4).

The Ebro valley, where AND is located, connects the Iberian's Peninsula Mediterranean and Atlantic coasts. Under NWadv, northwesterlies are channelled by the Ebro Valley. At night, the wind is oriented down valley towards the Mediterranean Sea (Figure AII-5).

However, during the day, the wind is up valley (SE) driven by strong sea-land breezes. Moreover, orographic mountain-valley winds originated in the close Gúdar Mountains (1600 masl, 40 km south of the power plant, Figure 5-1) increase wind complexity in the region. The SO_2 and NO_2 plumes from AND drift without a dominant direction during the morning until mesoscale sea breezes are more intense and drive the plumes towards the W/NW (Figure 5-7 and Figure 5-8). The plume reaches 1750 maih for SO_2 and 1350 maih for NO_2 (Figure 5-14 and Figure 5-21). There is a differential behaviour between pollutants due to their different diffusivity in ambient air (the SO_2 and NO_2 diffusivity at 296 K are: 12532 ± 1733 Pa cm^2 s^{-1} and 14132 ± 4933 Pa cm^2 s^{-1}, respectively according to Tang *et al.* (2014). The NO_2 plume does not reach the ground, whereas the SO_2 plume affects first the Arcos Mountains (700 masl, 20 km westward from AND) contributing to 6.1 μgSO_2 m^{-3} and is further transported up to 100 km from the source.

Under NWadv, CAR is reached by easterlies during night hours transporting the plume towards the sea (SE). However, during the day, mesoscale sea-land breezes drive wind dynamics at surface and at injection height (Figure AII-6) carrying the pollutants inland (W/SW) at 800 maih for SO_2 (Figure 5-15) and up to 500 maih for NO_2 (Figure 5-22). The emissions are injected above the PBL ($PBLH_{max}$ < 300 magl) favouring its horizontal transport where the plume reaches 150 km and 30 km for SO_2 and NO_2, respectively. The difference in the maximum plume length between SO_2 and NO_2 is caused by the large SO_2 emission rate in the fuel used in CAR (Figure 5-3). Moreover, the SO_2 plume affects the Alhamilla Mountains (1300 masl, ~30 km from the power plant, Figure 5-15) contributing with 11.4 μgSO_2 m^{-3} to the surface concentration.

The Strait of Gibraltar is a complex topographic region that receives Mediterranean and Atlantic influences. In this region, NWadv is characterised by western synoptic winds (Figure 5-2). However, the SO_2 and NO_2 plumes from LBB are transported to the E during the early morning and around 9:00-10:00 there is a shift in wind direction (Figure AII-7) and E/SE winds drive the plume towards the NW (~50 km, at 600 maih). During the shift in the advection direction, negative vertical vorticity is registered at LBB favouring a fumigation process. The eastern façade of the Algeciras Mountains (Figure 5-1, 15 km from the source) is reached by the plumes of LBB contributing to 10.6 μgSO_2 m^{-3} and 15.0 μgNO_2 m^{-3} to surface concentration (Figure 5-16 and Figure 5-23). It is also noteworthy that from 20:00 the PBLH is < 35 magl. This nocturnal layer enhances the concentration of pollutants at surface level.

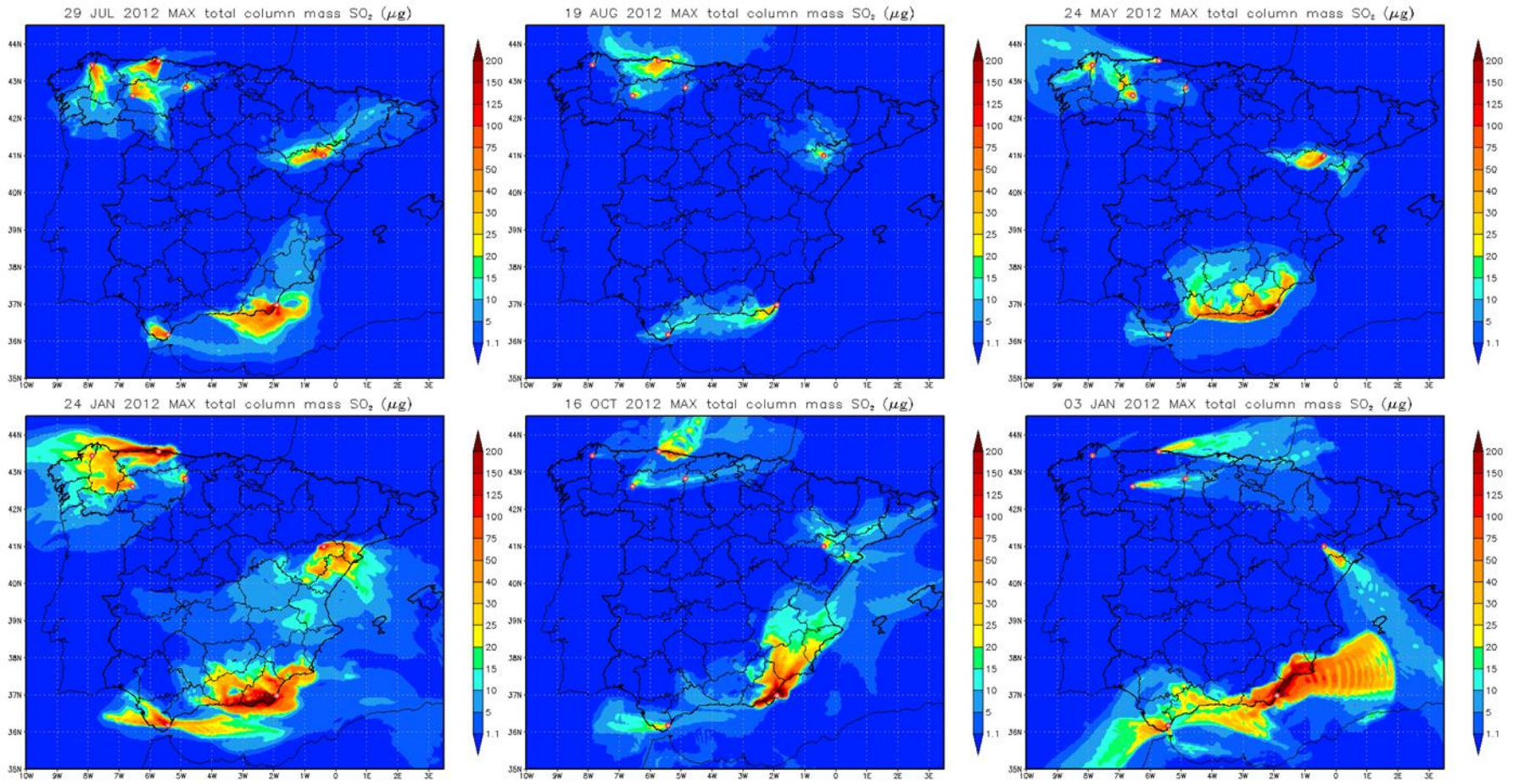

Figure 5-7. Daily maximum SO_2 total column mass (μg) associated to the emissions in the seven analysed power plants on the representative day of each CT

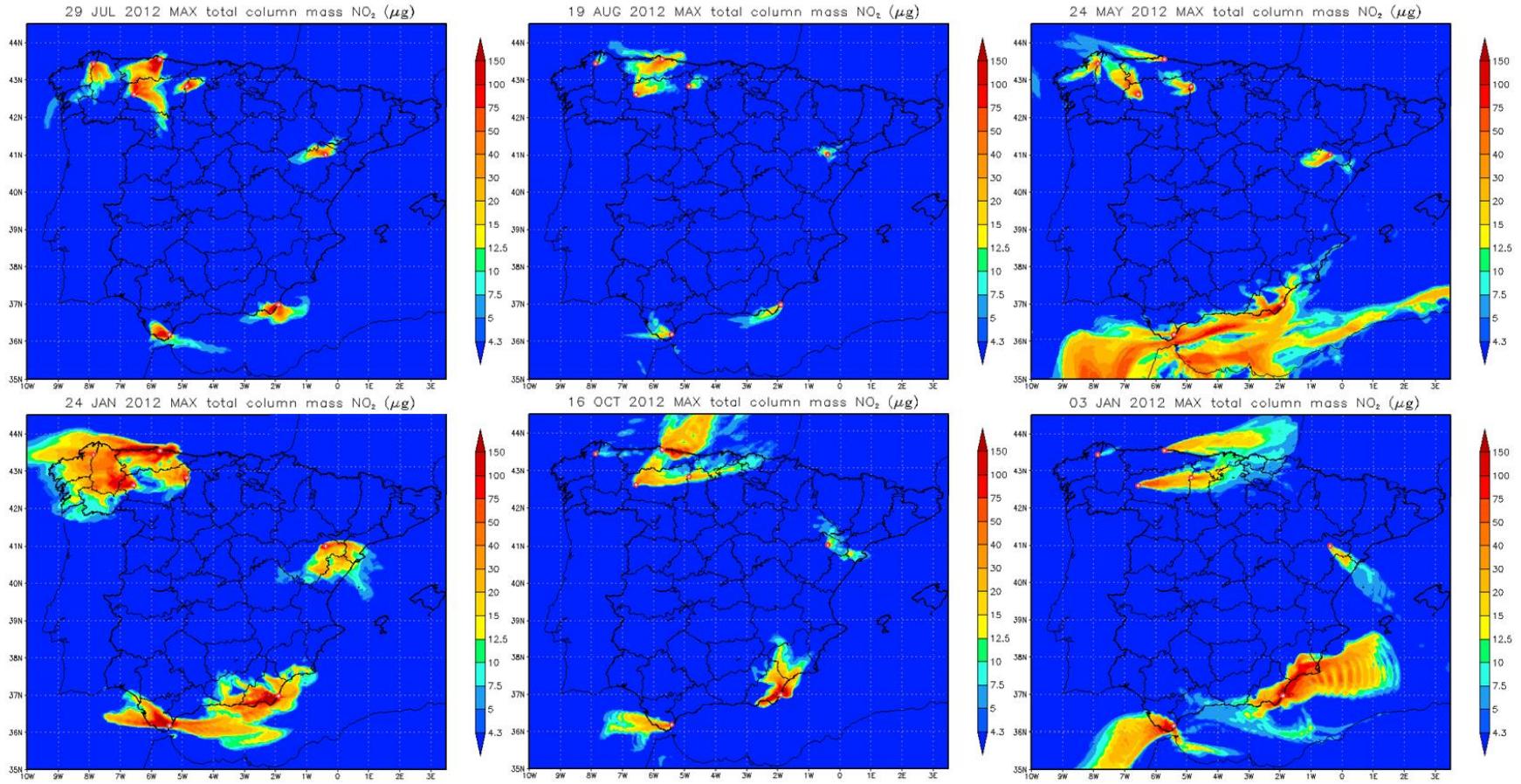

Figure 5-8. Daily maximum NO_2 total column mass (µg) associated to the emissions in the seven analysed power plants on the representative day of each CT

5.3.2.2 IBtl

Under IBtl, the North-Western IP is under the cyclonic influence of the Icelandic Low (Figure 5-2). The emissions at ASP are the lowest of all the representative days (30 $kgSO_2$ h^{-1} and 40 $kgNO_2$ h^{-1}), which hinders the formation of distinctive plumes. Although the PBLH at midday is ~1000 magl (Figure AII-1) and the injection is done within the PBL, there is positive vertical vorticity during this time-span (11:00-14:00), which prevents fumigation towards the ground.

The Cantabrian Mountains disconnect ABO from the southwards synoptic advection affecting the IP. Plume dynamics in ABO are driven by a mesoscale vortex that favours sea-land dispersion during the day and land-sea during the night at 500 maih (Figure 5-11 and Figure 5-18). The emissions are injected above the PBL (~400 magl) which favours its horizontal transport. The SO_2 and NO_2 plumes contact the ground at 95 and 25 km from the source, respectively. The contribution from the power plant in terms of surface concentration is maximal at 18 km south of the facility (< 5 $\mu g\ m^{-3}$ for SO_2 and NO_2).

Inland the IP, during the summer IBtl, the PBL reaches its maximum in COM (~1900 magl), GUA (~2000 magl) and AND (~2100 magl). Although the emissions at midday are injected within the PBL in these three facilities, there is little transport towards the ground. This can be explained by i) the SO_2 and NO_2 emission rates are the lowest of all the CTs (Figure 5-3, Figure 5-4) due to lower electricity demand, and ii) the vertical vorticity at midday is mainly positive due to soil heating. The maximum surface contribution occurs in COM at 7 km from the source: 4.7 $\mu gSO_2\ m^{-3}$ and 6 $\mu gNO_2\ m^{-3}$. Considering the total column, the SO_2 and NO_2 plumes from COM and GUA are driven by southerlies northwards towards the Cantabrian Mountains that are a topographic block that avoids longer dispersion (Figure 5-7 and Figure 5-8). At AND, the winds are weak without dominant direction enabling that AND plumes remain close to the point source and reach 1500 maih for SO_2 and 1000 maih for NO_2 (Figure 5-14 and Figure 5-21).

At CAR, the wind blows from the E/NE along the day (Figure AII-6). In LBB, however, the wind is from the E (Figure AII-7). The plumes of CAR are transported in altitude 680 maih for SO_2, 380 maih for NO_2 (difference due to the larger SO_2 than NO_2 emission rate in CAR) towards the SW (Figure 5-7 and Figure 5-8) whereas in LBB, the plume is oriented to the W reaching 360 maih for both pollutants (Figure 5-16 and Figure 5-23). In both cases, the injection is done above the PBL favouring its horizontal transport. The SO_2 plumes from CAR and LBB have a maximum length of 97 and 81 km from the source, respectively.

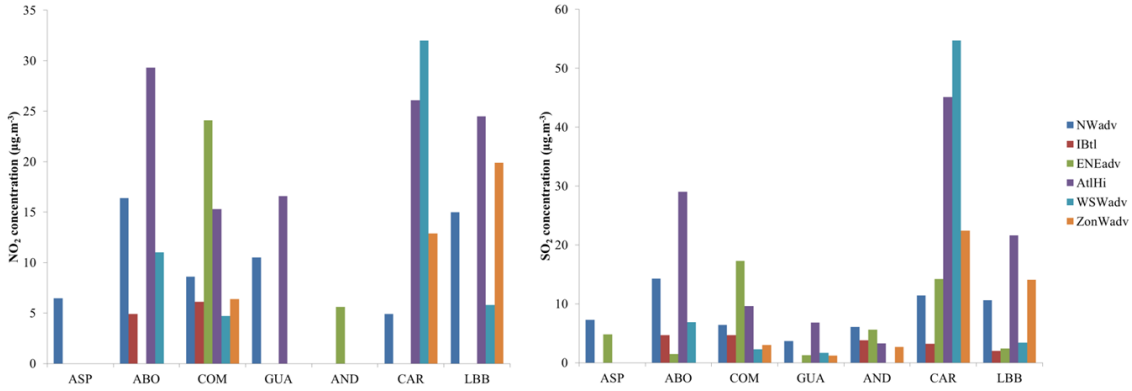

Figure 5-9. Daily maximum NO_2 (left) and SO_2 (right) contribution to surface concentration (µg m^{-3}) for the seven power plants under each CT. Different scales in the y-axis are applied

5.3.2.3 ENEadv

The blocking anticyclone over Central Europe that characterises ENEadv leads to the arrival of easterlies towards ASP, ABO, COM and GUA. However, this general advective pattern is modulated by the Cantabrian Mountains. Winds arriving at ASP are from the SE/E during 00:00-12:00 and from NE/E from 15:00 onwards (Figure AII-1). The plumes from ASP are transported northwards during the morning (at 1200 maih) and after the change in wind direction, the plumes go towards the SW/S (Figure 5-7 and Figure 5-8). At midday, the injection is done within the PBL favouring fumigation towards the ground (< 5 µg m^{-3} for both pollutants).

In ABO, the advection is from the E, parallel to the coastline at surface and at the injection height (Figure AII-2). For both pollutants, the plume is oriented towards the W at 230 maih (Figure 5-7 and Figure 5-8). The injection is done above the PBL along the day which hinders the fumigation towards the ground and favours the horizontal transport where the SO_2 plume reaches up to 59 km whereas the NO_2 does not even reach the ground (Figure 5-18).

The easterlies arriving at COM drive the SO_2 and NO_2 plumes towards the W/NW. However, there is little horizontal plume advection (Figure 5-5 and Figure 5-6). The plume dynamics are dominated by the vertical vorticity (the maximum plume altitude is > 1500 maih). At midday negative vorticity combined with emission injection within the PBL ($PBLH_{max}$ = 1800 magl) enhances fumigation towards the ground, close to the source. The maximum contributions to surface concentrations occur at 3.5 km from the source and attain 17.3 µgSO_2 m^{-3} and 24.1 µgNO_2 m^{-3}. GUA plumes are also transported to the W without affecting the ground at 300 maih (Figure 5-13 and Figure 5-20).

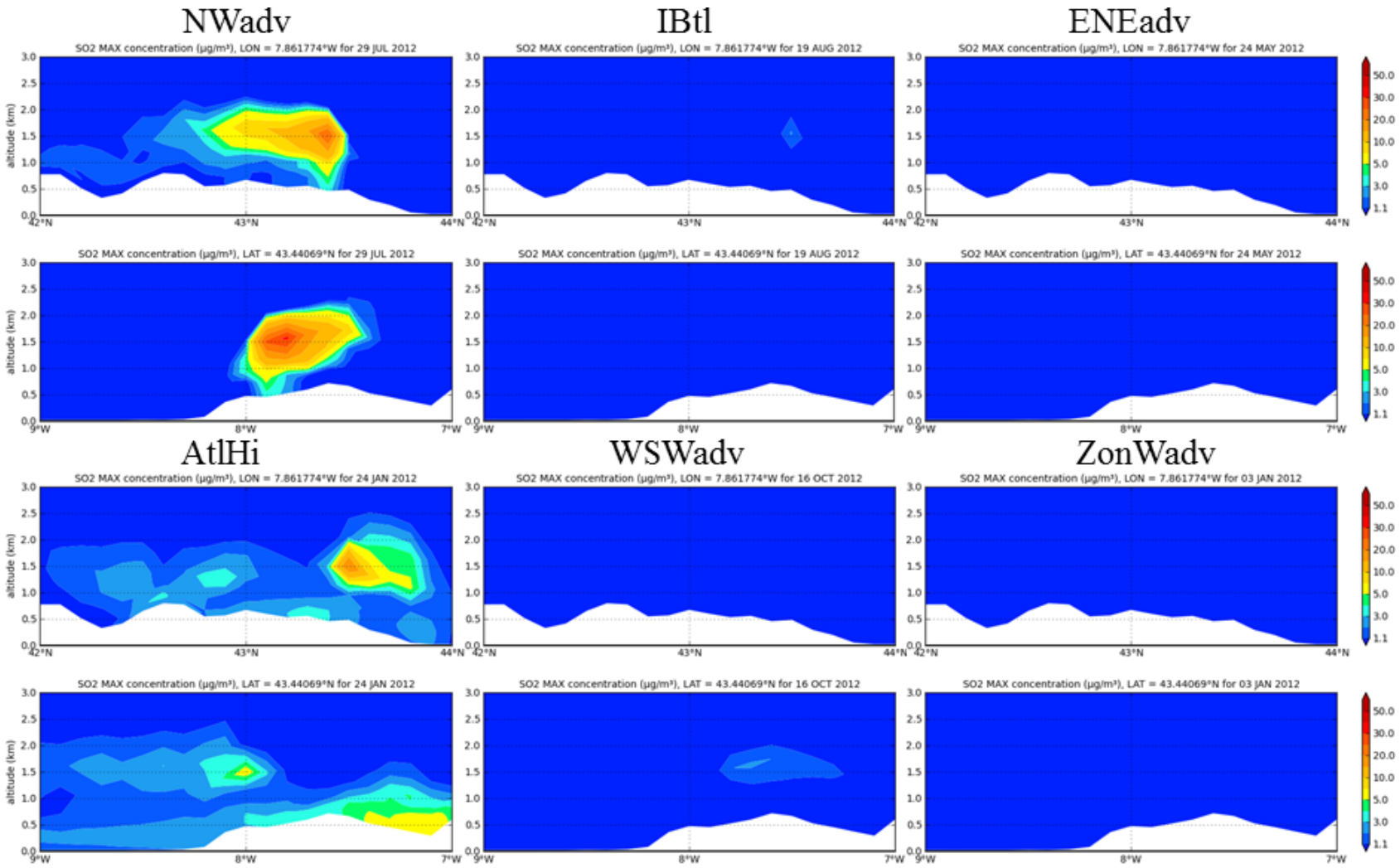

Figure 5-10. Daily maximum vertical SO_2 concentration (µg m^{-3}) N-S and W-E cross-sections passing by ASP for each CT

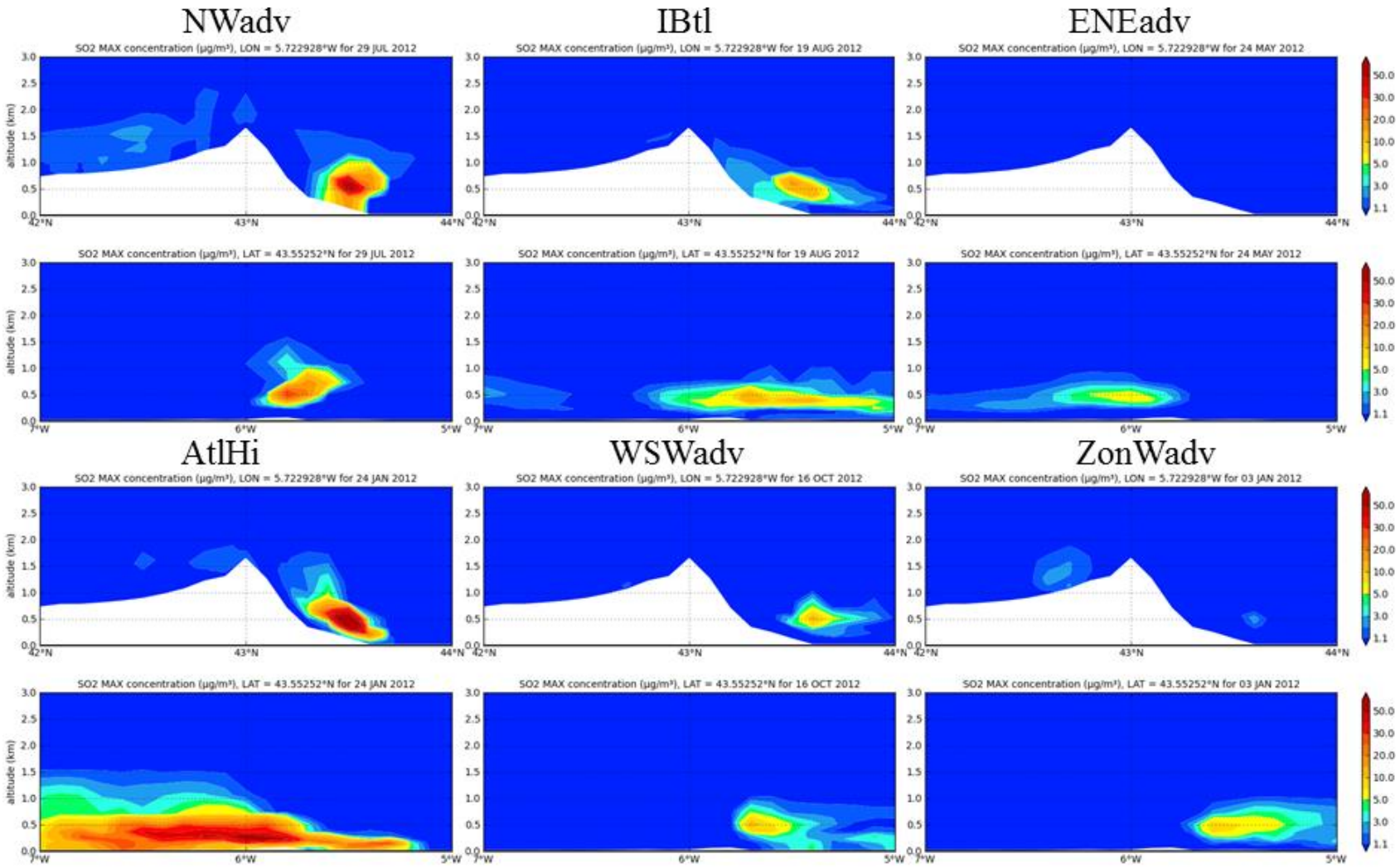

Figure 5-11. Daily maximum vertical SO_2 concentration (µg m^{-3}) N-S and W-E cross-sections passing by ABO for each CT

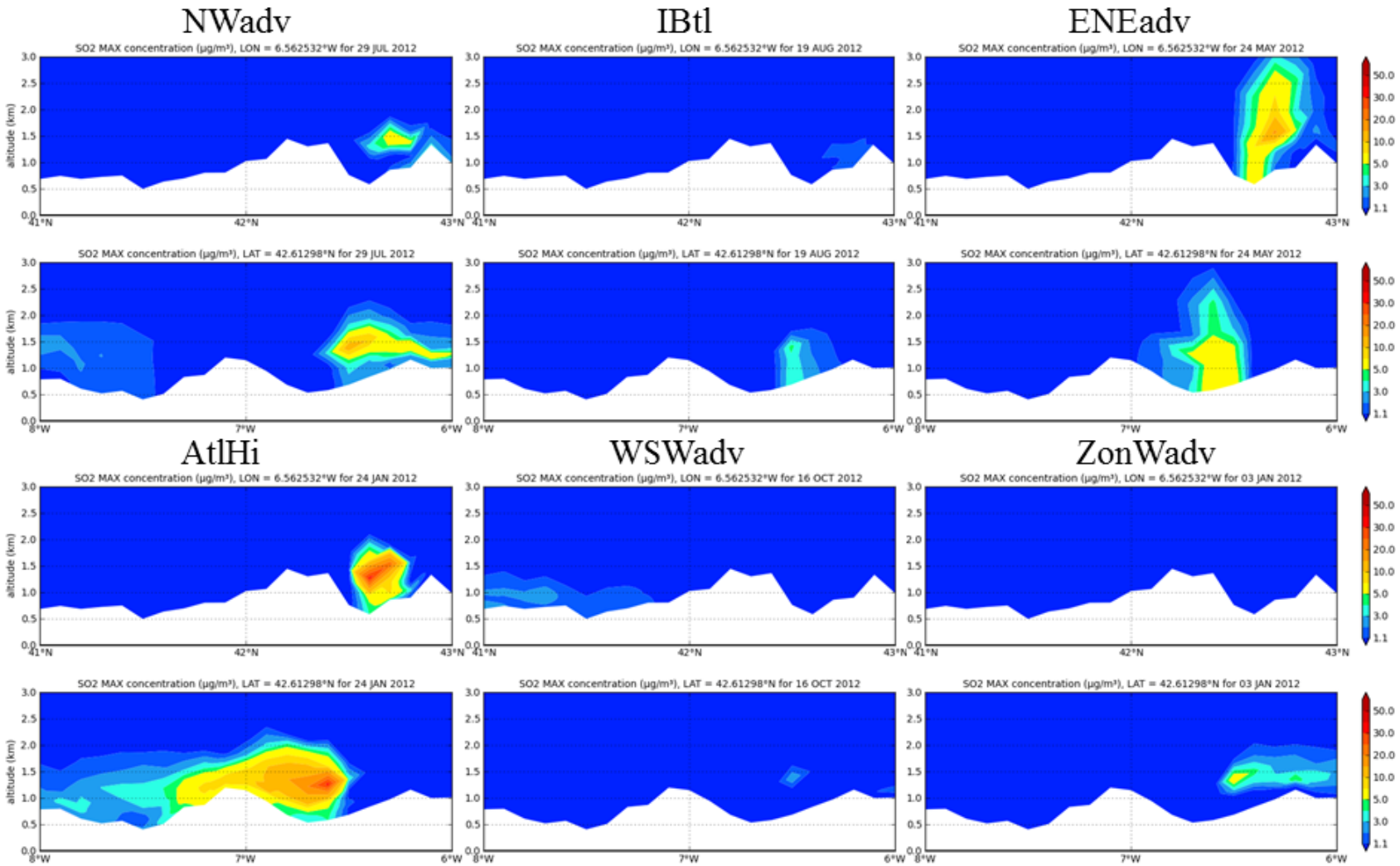

Figure 5-12. Daily maximum vertical SO_2 concentration (µg m^{-3}) N-S and W-E cross-sections passing by COM for each CT

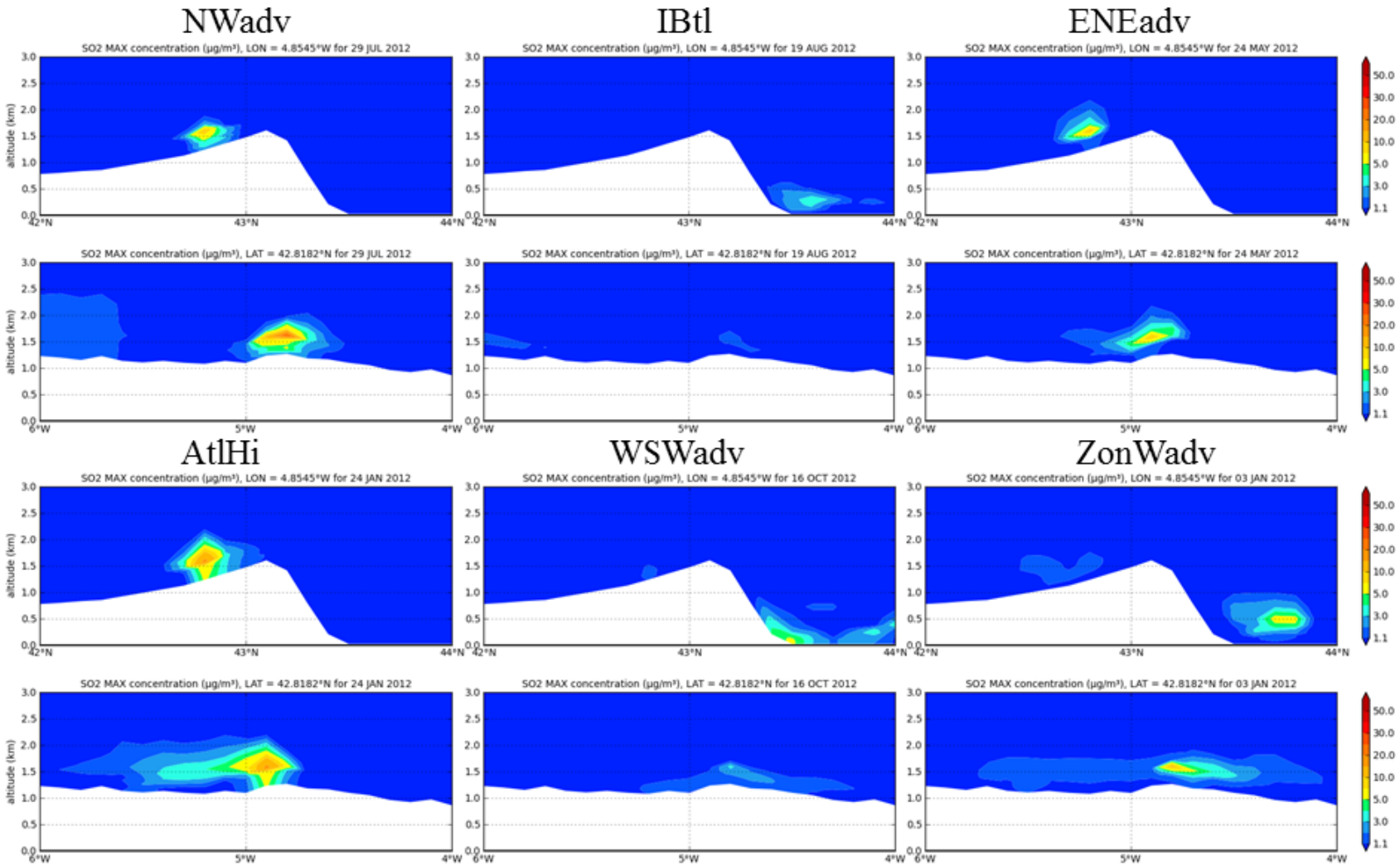

Figure 5-13. Daily maximum vertical SO_2 concentration (µg m^{-3}) N-S and W-E cross-sections passing by GUA for each CT

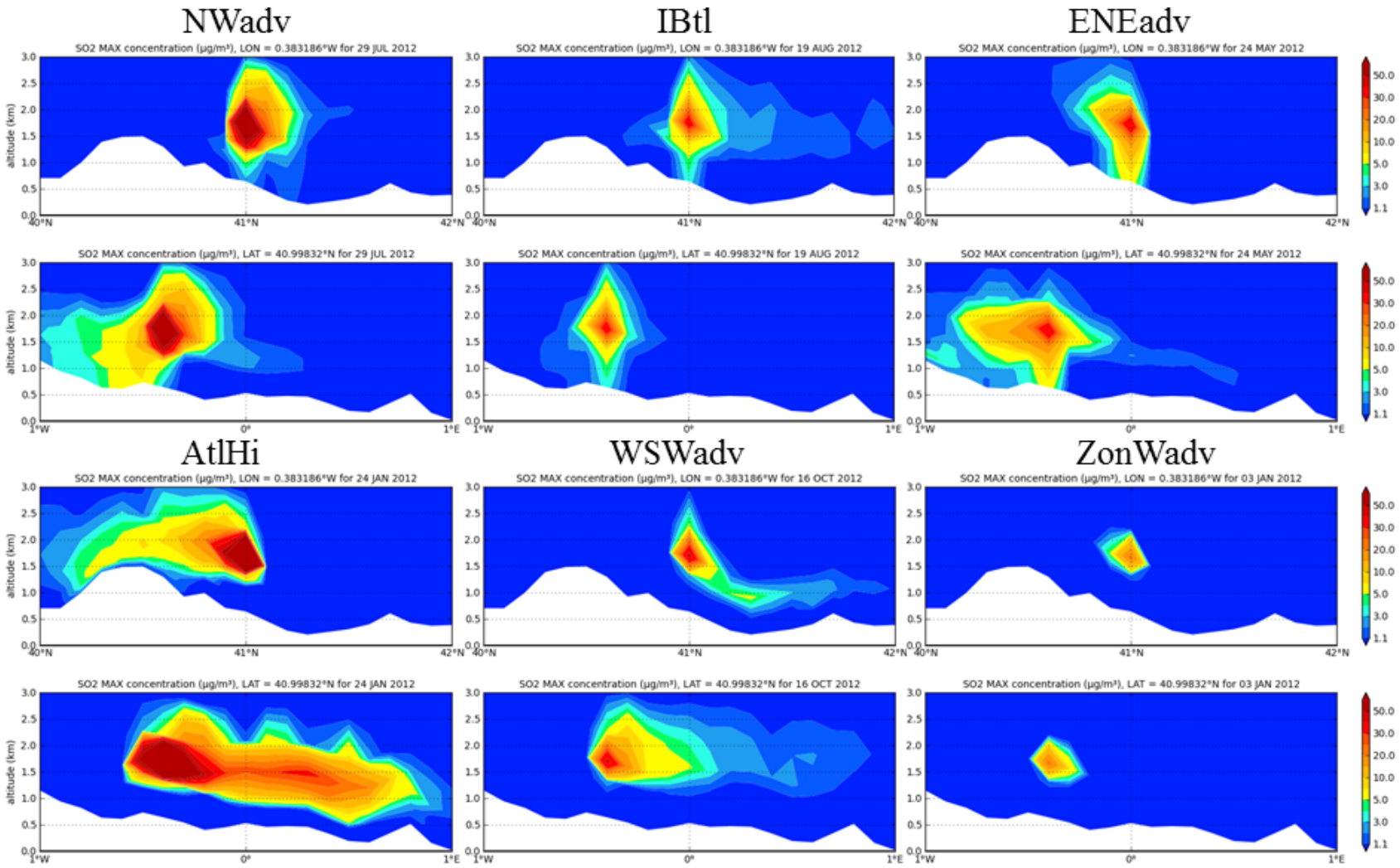

Figure 5-14. Daily maximum vertical SO_2 concentration (µg m^{-3}) N-S and W-E cross-sections passing by AND for each CT

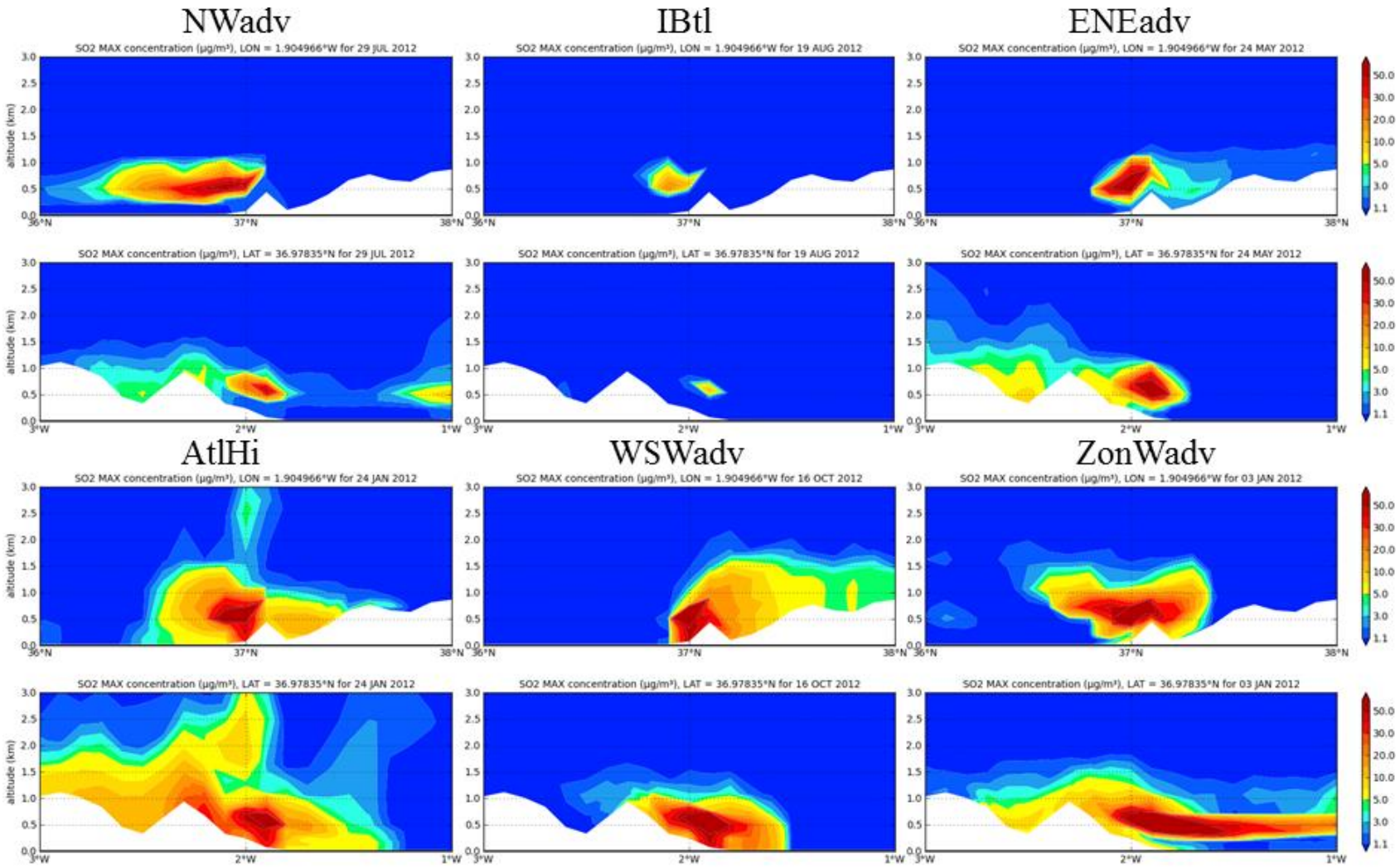

Figure 5-15. Daily maximum vertical SO_2 concentration (µg m^{-3}) N-S and W-E cross-sections passing by CAR for each CT

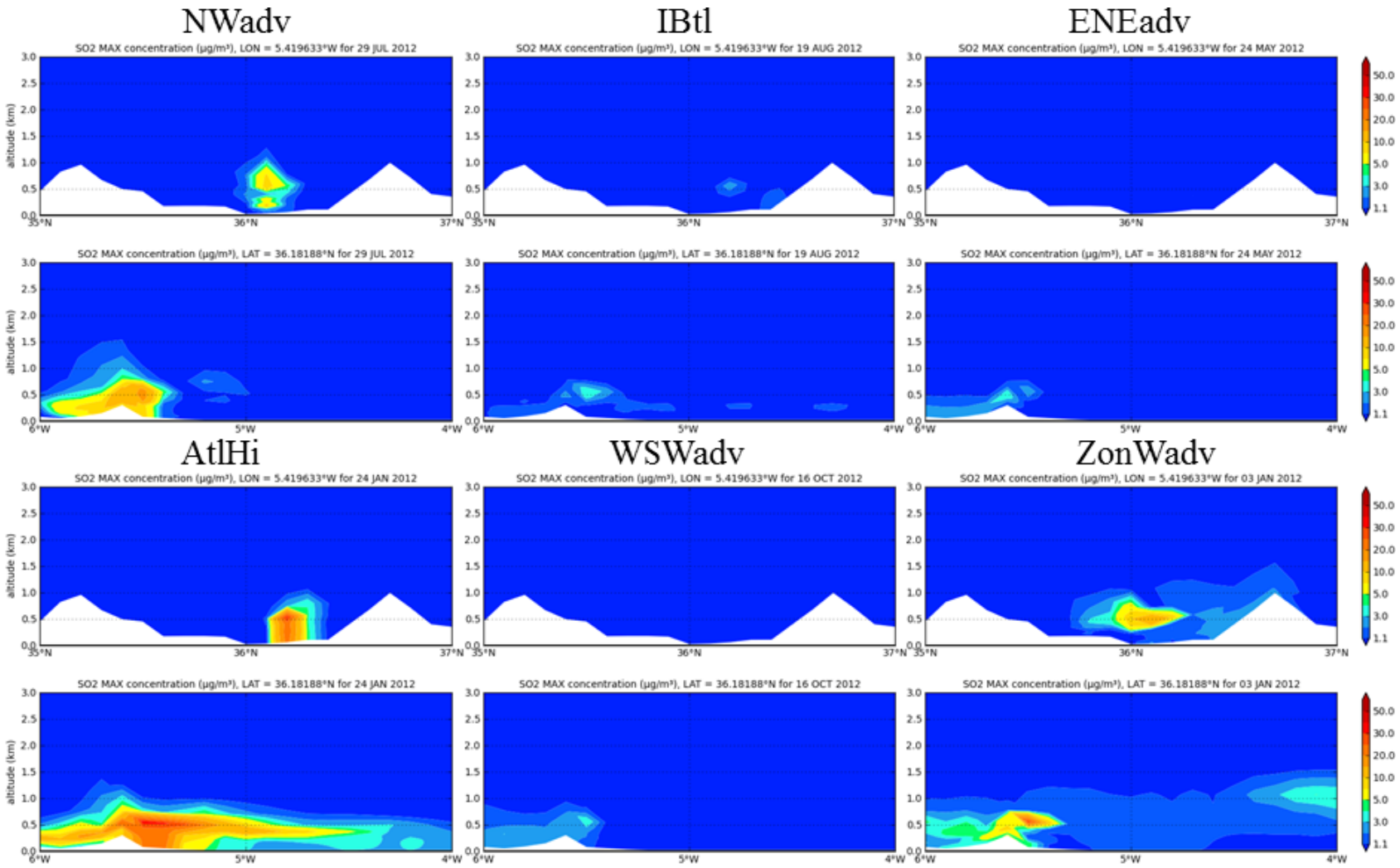

Figure 5-16. Daily maximum vertical SO_2 concentration (µg m^{-3}) N-S and W-E cross-sections passing by LBB for each CT

The advection under ENEadv at AND is from the North channelled by the Ebro valley (Figure 5-2). The simulation shows a complex situation with a superposition of the synoptic northerlies, sea-land breezes from the Mediterranean and downslope winds from the Gúdar Mountains (Figure AII-5). The plumes from AND are transported to the SE during the morning (maximum altitude: 1350 maih for SO_2 and 1050 for NO_2, Figure 5-14 and Figure 5-21). At midday with the development of sea-land breezes, the plumes turn westwards and are oriented towards the SW from the facility (Figure 5-7 and Figure 5-8). The change in wind direction at midday at AND together with negative vertical vorticity and emission injection within the PBL ($PBLH_{max}$ ~1800 magl) enables a fumigation process. The maximum contribution to surface concentration is at 9 km from AND (5.6 $\mu gSO_2\ m^{-3}$ and 5.6 $\mu gNO_2\ m^{-3}$).

In Southern Spain, the ENEadv is characterised by easterlies (Figure 5-2). The CAR plumes are transported towards the SW and W with a maximum altitude of ~800 maih. As the emission is done above the PBL ($PBLH_{max}$ < 200 magl, Figure AII-6) the horizontal transport is enhanced enabling long plumes up to 200 km away from the stack (Figure 5-7 and Figure 5-8). It is noteworthy that the marine boundary layer is a barrier to the vertical movement of the plume favouring the transport of the pollutants inland. The plume affects the ground when it reaches the nearby Alhamilla Mountains, W of CAR (Figure 5-15 and Figure 5-22) with up to 14.2 $\mu gSO_2\ m^{-3}$ and 7.5 $\mu gNO_2\ m^{-3}$ (Figure 5-9).

In LBB the plumes are transported westwards (~100 km) close to the ground (~200 maih). The maximum contribution to surface concentration is 2.4 $\mu gSO_2\ m^{-3}$ and 20 $\mu gSO_2\ m^{-3}$ over the Algeciras Mountains, 20 km W of the source. The difference between pollutants is due to the emission rates (10 $kgSO_2\ h^{-1}$ and 20 $kgNO_2\ h^{-1}$). Moreover, during the night hours, there is a nocturnal layer (PBLH is < 50 magl) that increases surface concentration close the source (Figure AII-7).

5.3.2.4 AtlHi

Under the winter AtlHi there is a low PBLH at the seven power plants locations (PBLH < 500 magl). This fact enables that the emission injection occurs above the PBL favouring their dispersion. On the other hand, AtlHi together with ZonWadv are the CTs characterised by highest emission rates (Figure 5-3, Figure 5-4).

On the Cantabrian coast, AtlHi advection is depicted by northerlies that turn westwards when reaching the coastline. The plumes from ASP are transported westwards reaching ~1100-1200 maih without contacting the surface. The region of ASP is affected by quick easterlies coming from Asturias transporting SO_2 and SO_2 concentrations from ABO along the surface (Figure 5-10 and Figure 5-17). In ABO, the plumes are parallel to the Atlantic coast (E-W orientation) and reach long distances (268 km for SO_2 and 204 km for NO_2) because there are not topographic barriers that stop them (0-600 maih, Figure 5-11 and Figure 5-18). The highest contributions to surface concentration from ABO occur within 23 km from the source (~29

$\mu g\ m^{-3}$ for both pollutants). The high emission rates together with high dispersive conditions favour the formation of wide multi-source plumes on North-Western IP during AtlHi (Figure 5-7 and Figure 5-8).

The COM plumes are also oriented westwards but the transport is partially stopped by the Galician Massif (40 km to the W) affecting the surface concentration in that area (Figure 5-12 and Figure 5-19, 9.6 $\mu gSO_2\ m^{-3}$ and 15.3 $\mu gNO_2\ m^{-3}$). The plumes from COM have a length of ~100 km and a maximum altitude of ~1100 maih. In COM and ABO, the PBL is very close to the ground (PBLH < 50 magl) during the night, enhancing the concentration of the pollutants at the surface (Figures AII-2 and AII-3).

During the day, the plume from GUA is transported towards the W (27 km, ~500 maih for NO_2 and ~700 maih for SO_2). However, the nocturnal downslope winds from the nearby mountains drive the plume towards the S (Figure 5-13 and Figure 5-20). At midday (12:00-15:00) the PBLH is high enough (~500 magl) to enable the emission injection within the PBL favouring the increase of surface concentration close to the source (< 3 km, 6.8 $\mu gSO_2\ m^{-3}$ 16.6 $\mu gNO_2\ m^{-3}$).

Under AtlHi, the northern advection towards AND is channelled by the Ebro valley (Figure 5-2) driving the plumes down valley towards the SE/E (Figure 5-14 and Figure 5-21) at 1650 maih for SO_2 and 1150 maih for NO_2. The differential diffusivity of the pollutants explains this difference in altitude. The plumes reach 130-140 km from the source and the contribute little to surface concentrations (< 4 $\mu g\ m^{-3}$).

Westerlies are characteristic of the AtlHi on the Strait of Gibraltar as well over the Alboran Sea (Figure 5-2). However, winds blow from the NE in CAR (Figure AII-6) showing a complete disconnection from the main synoptic advection caused by an anticyclonic eddy located on the Mediterranean, 60 km away from the coastline. The plumes from CAR are transported to the SW/W. The Alhamilla Mountains blocks the progress of the plume westwards and enhances the concentration of pollutants on its eastern side 15-20 km from the source (45.1 $\mu gSO_2\ m^{-3}$ and 26.1 $\mu gNO_2\ m^{-3}$; Figure 5-15 and Figure 5-22). The SO_2 and NO_2 plumes reach 2800 maih and 1200 maih and up to 250 and 180 km away from the source, respectively.

The plume from LBB is driven by westerlies into the Mediterranean during the morning (00:00-10:00). However, at midday there is a change in wind direction (E advection) and the LBB plume is transported towards the W (~180 km and 500-600 maih). When the wind changes its main direction there is a significant diffusion of SO_2 and NO_2 from the stack to the ground at midday that contributes up to 21.6 and 24.5 $\mu g\ m^{-3}$., respectively (Figure 5-9).

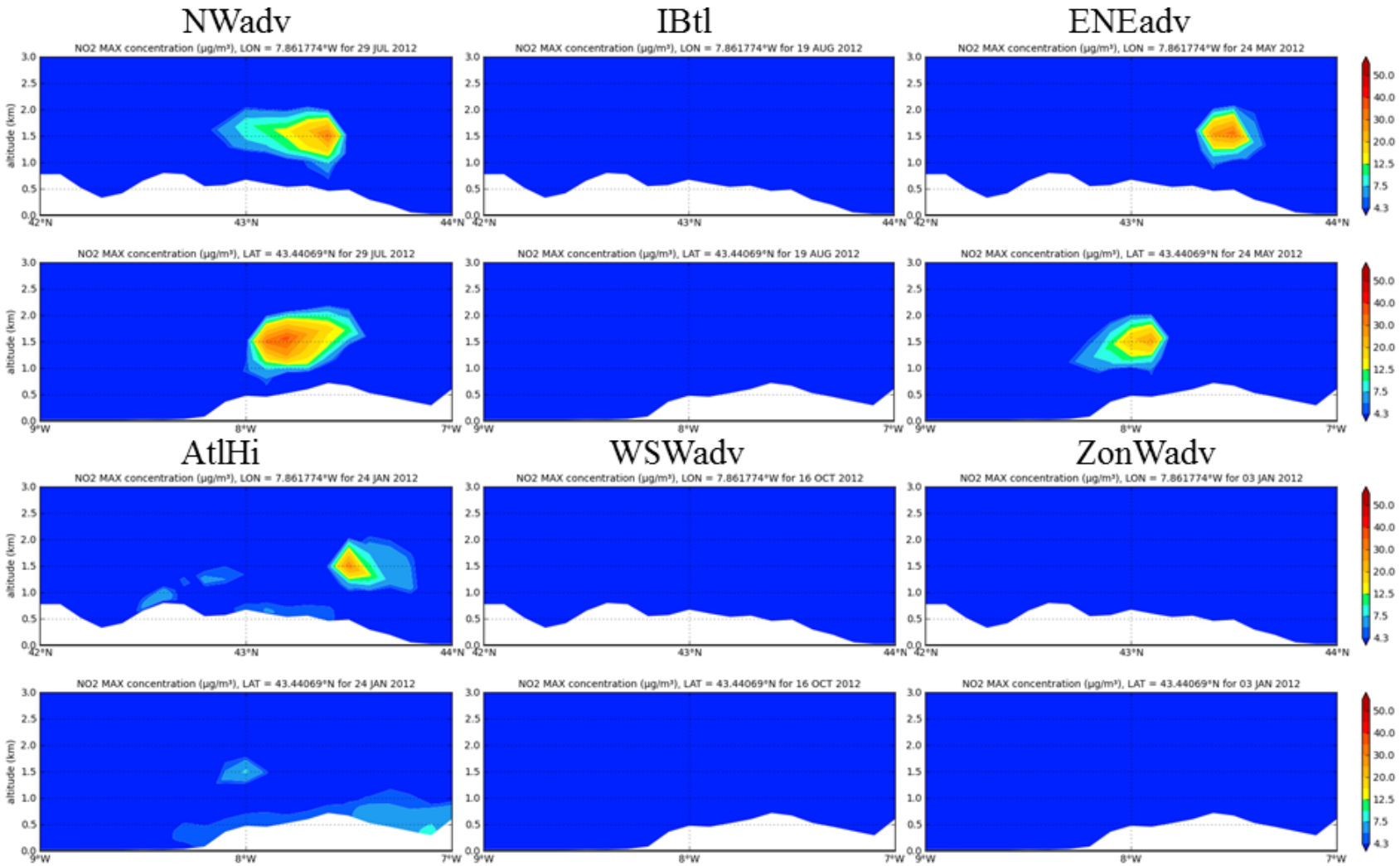

Figure 5-17. Daily maximum vertical NO_2 concentration (µg m^{-3}) N-S and W-E cross-sections passing by ASP for each CT

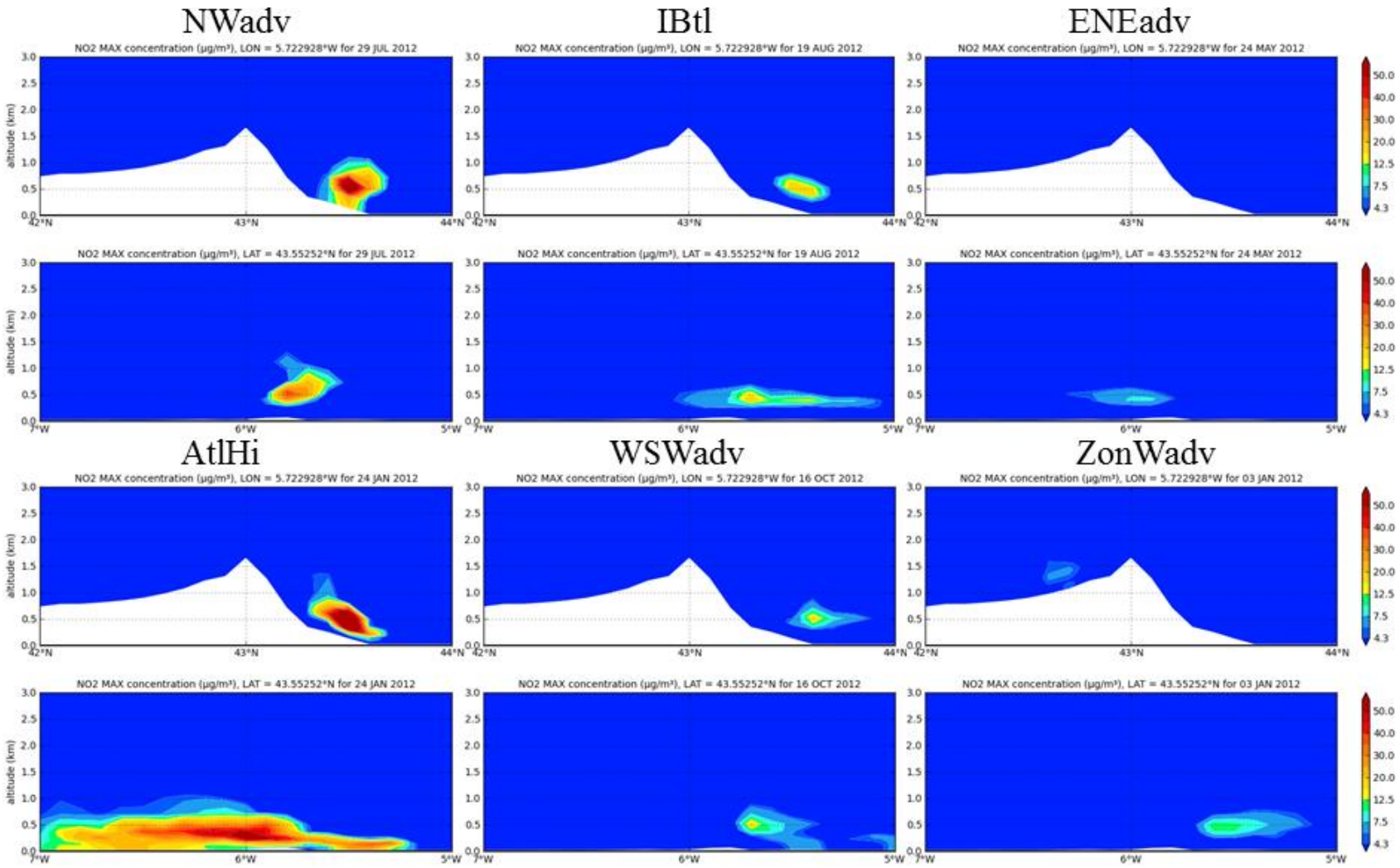

Figure 5-18. Daily maximum vertical NO_2 concentration (µg m^{-3}) N-S and W-E cross-sections passing by ABO for each CT

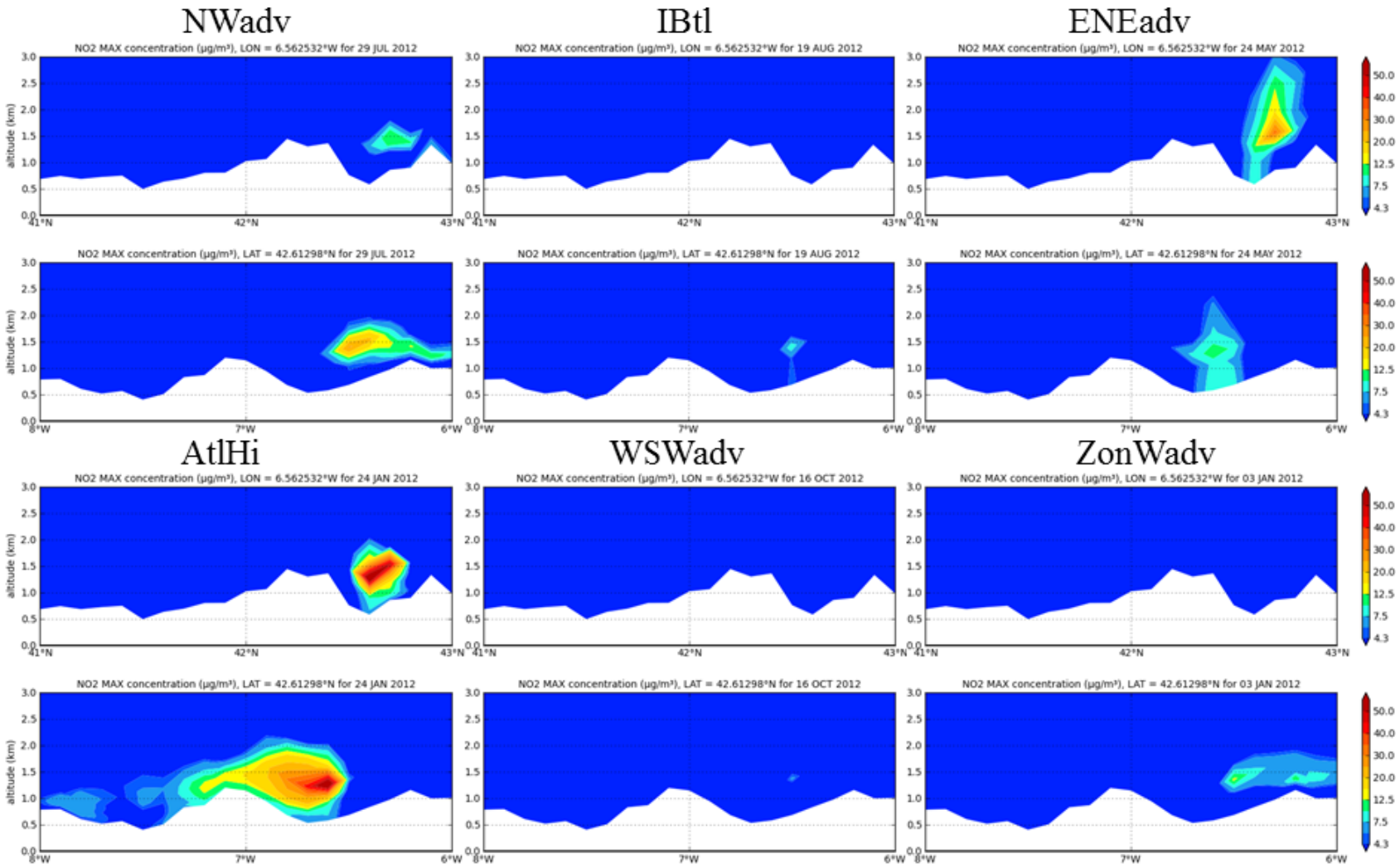

Figure 5-19. Daily maximum vertical NO_2 concentration (µg m^{-3}) N-S and W-E cross-sections passing by COM for each CT

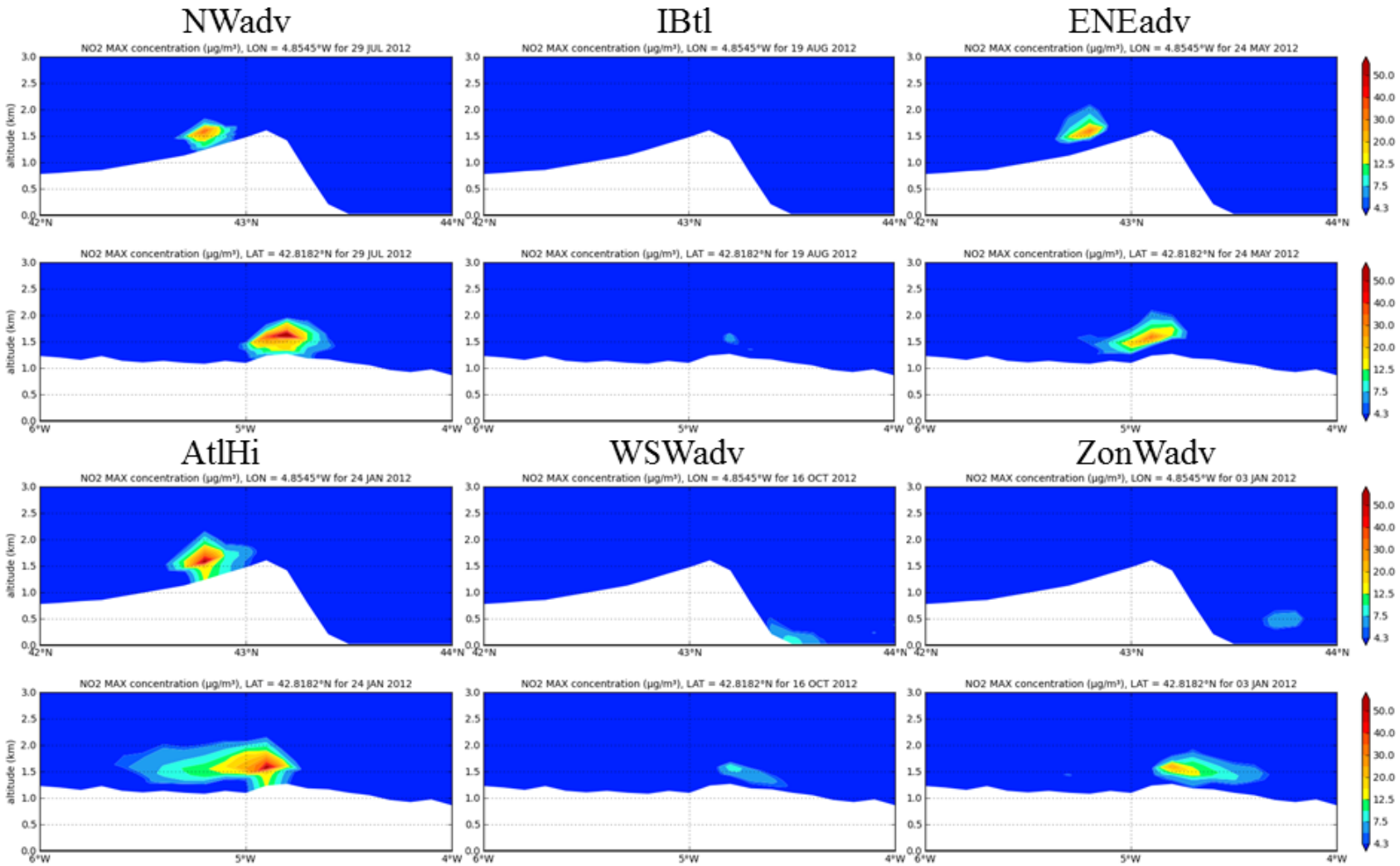

Figure 5-20. Daily maximum vertical NO_2 concentration (µg m^{-3}) N-S and W-E cross-sections passing by GUA for each CT

5.3.2.5 WSWadv and ZonWadv

In ASP the wind fields of WSWadv and ZonWadv are similar with a dominant SW surface advection coming from the Atlantic Ocean. However, at the injection height, ZonWadv presents clear western advection whereas under WSWadv, the advection is from the SW (Figure AII-1). High wind speed at the facility on both days together with emission injection above the PBL favours their horizontal dispersion towards the E/NE (Figure 5-7 and Figure 5-8) without attaining the surface in any moment.

Under WSWadv, the SW winds at ABO lead to a NE/N transport of the plumes at ~400 maih towards the Ocean reaching 160 km for SO_2 and 110 km for NO_2. The ABO contribution to surface concentration occurs at ~40 km east of the source (6.9 $\mu gSO_2\ m^{-3}$ and 11.0 $\mu gNO_2\ m^{-3}$). On the other hand, under ZonWadv westerlies disperse the plume towards the E at a maximum altitude of ~400 maih without affecting the surface (Figure 5-11 and Figure 5-18).

The synoptic winds that characterise WSWadv reach COM and GUA from the SW. The plumes are driven towards the NE at an altitude that ranges 300-500 maih and are stopped by the southern façade of the Cantabrian Mountains (contributing with < 5 $\mu g\ m^{-3}$ for both pollutants, 20-30 km from the sources). Under ZonWadv, W winds are faster than at WSWadv, both at surface and along the column (Figures AII-3 and AII-4) driving the plumes of COM and GUA towards the E without affecting the surface (Figure 5-5 and Figure 5-6).

In AND, under WSWadv the horizontal plume dynamics are a combination synoptic advection and mesoscale breezes (Figure AII-5). During the night the plumes are driven by northwesterlies towards the S however during the day sea-land breezes dominate, leading to a N/NE transport at a maximum altitude of 1650 maih for SO_2 and 1050 for NO_2 (Figure 5-14 and Figure 5-21). Under ZonWadv the westerlies are channelled by the Ebro Valley driving the plumes down-valley going beyond the Mediterranean coastline without affecting the surface (Figure 5-7 and Figure 5-8).

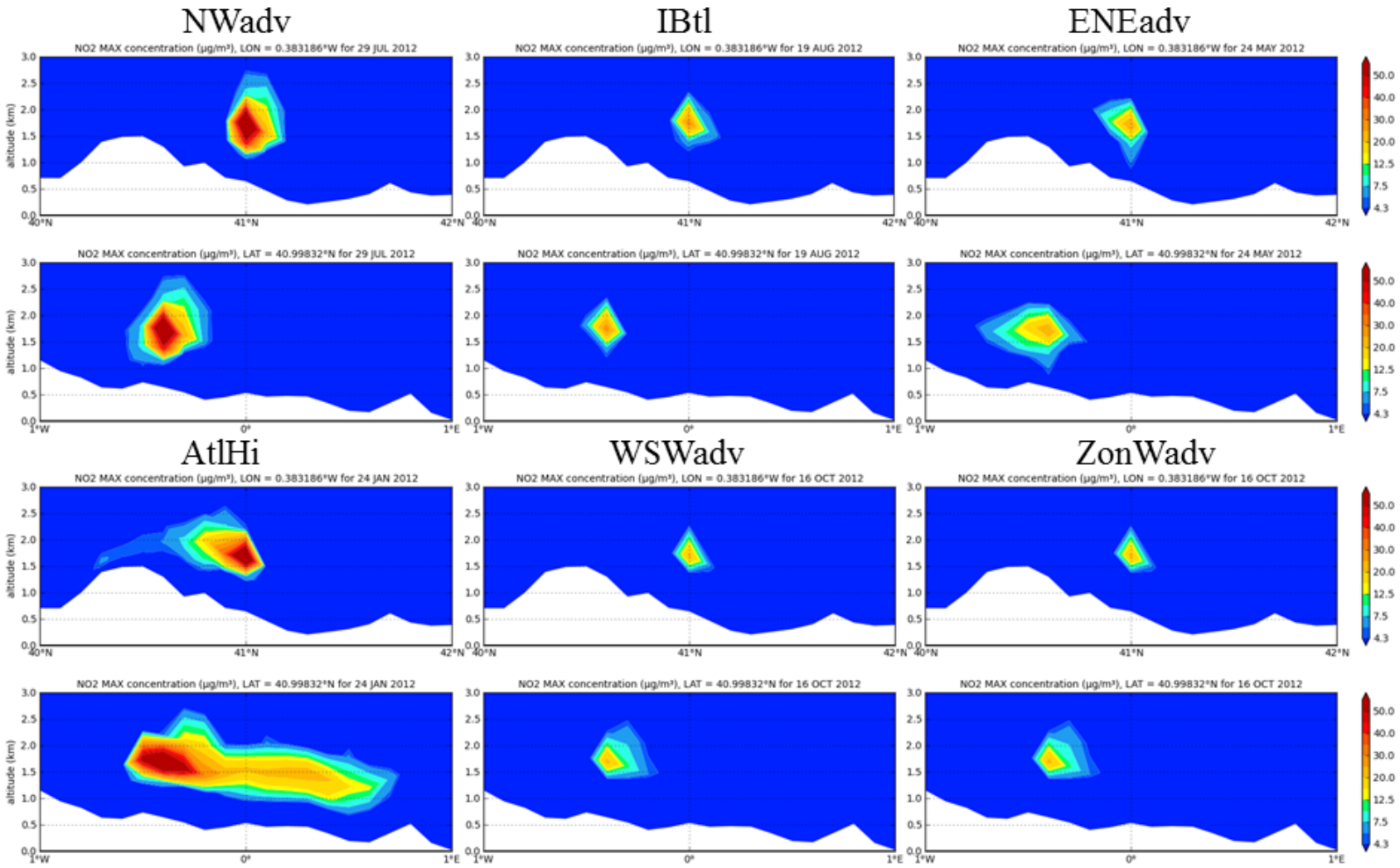

Figure 5-21. Daily maximum vertical NO_2 concentration (µg m^{-3}) N-S and W-E cross-sections passing by AND for each CT

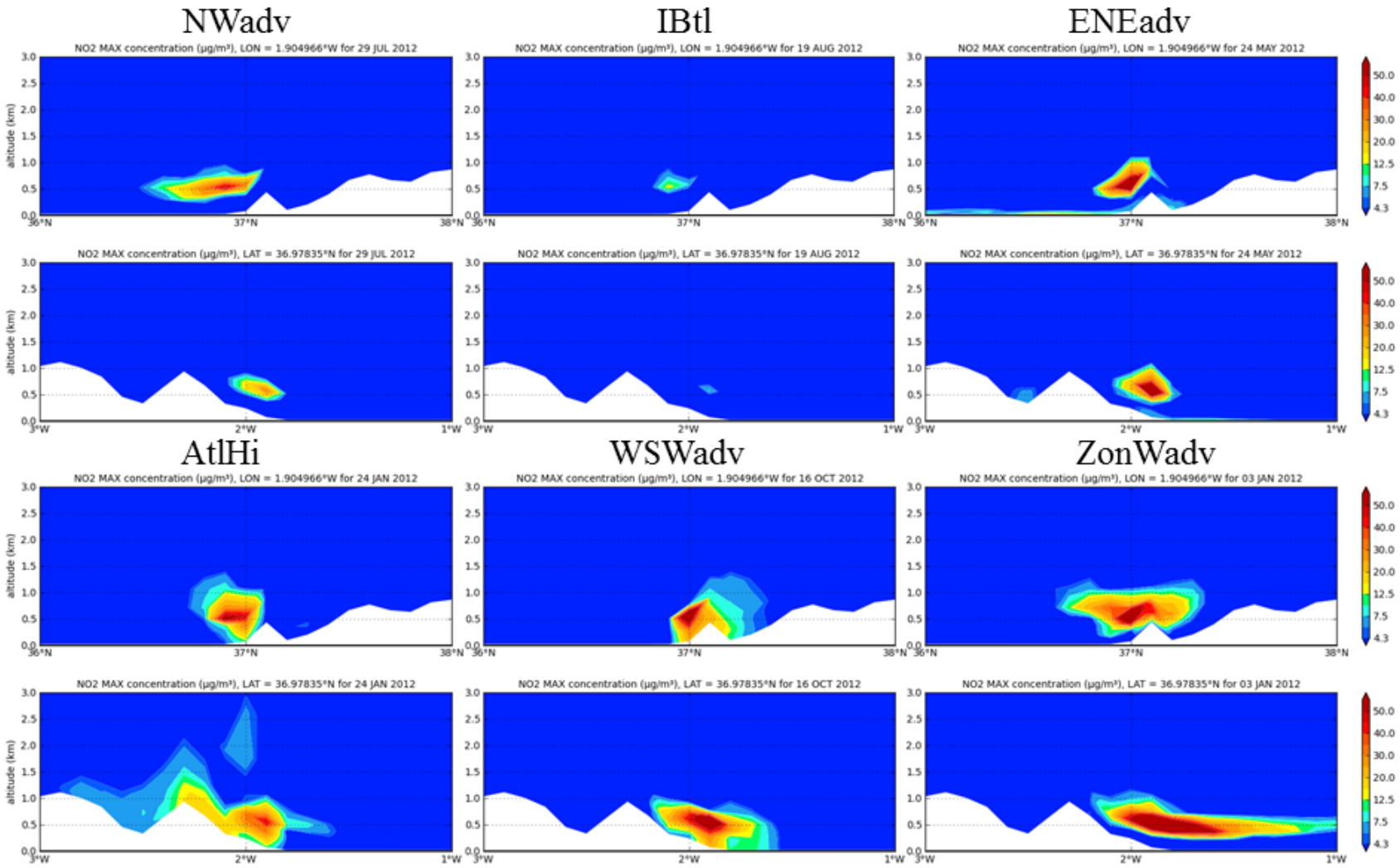

Figure 5-22. Daily maximum vertical NO_2 concentration (µg m^{-3}) N-S and W-E cross-sections passing by CAR for each CT

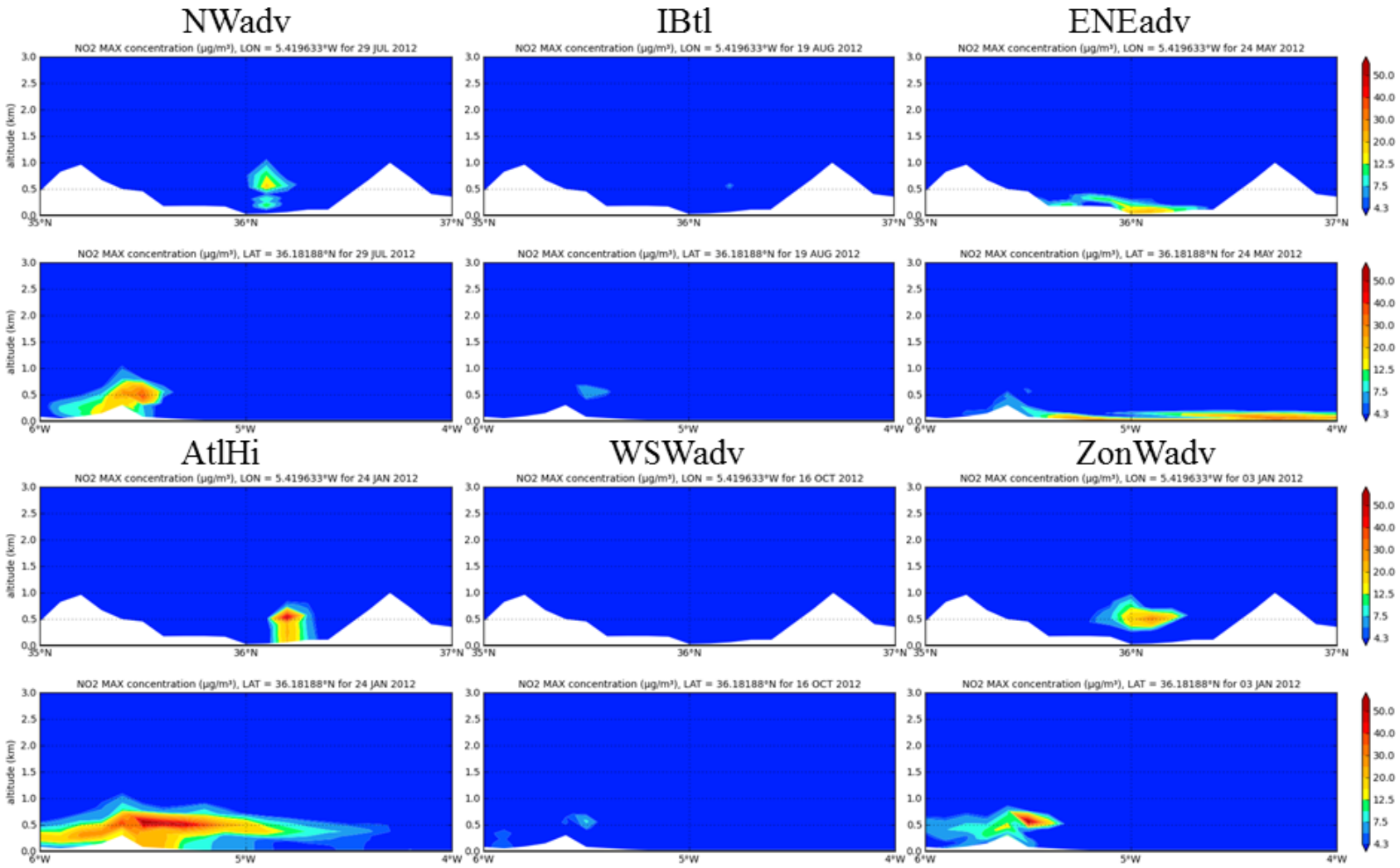

Figure 5-23. Daily maximum vertical NO_2 concentration (µg m^{-3}) N-S and W-E cross-sections passing by LBB for each CT

The simulated wind field at CAR shows a complex behaviour. Under WSWadv the sea-land breezes together with an anticyclonic vortex located over the Alboran Sea drive the CAR plumes towards the NE during the morning, towards the N at midday and towards the W in the afternoon (Figure 5-22). This CT is characterised by atmospheric instability with negative vertical vorticity that enhances the fumigation of the plume. The maximum contribution to surface concentration is reached at 4-6 km from the source (54.7 $\mu gSO_2\ m^{-3}$ and 32.0 $\mu gNO_2\ m^{-3}$). Furthermore, the SO_2 plume is transported up to 290 km from CAR (at an altitude of 1300 maih) and the NO_2 plume reaches 50 km (700 maih). Under ZonWadv, sea breezes are coupled with synoptic westerlies driving the plumes towards the NE, parallel to the coastline from surface up to 800-1200 maih (Figure 5-15and Figure 5-22). The strong wind speed at the surface (15-20 m s^{-1}) and over the column that characterise the ZonWadv, favour the formation of long plumes (> 250 km). The maximum contribution to surface concentration (22.4 $\mu gSO_2\ m^{-3}$ and 12.9 $\mu gNO_2\ m^{-3}$) is reached far away from the source (66 km for SO_2 and 116 km for NO_2).

Despite the Atlantic advection that affects the IP under WSWadv and ZonWadv, the area of the Strait of Gibraltar is disconnected from this general pattern and it is dominated by Mediterranean winds under both CTs. The SO_2 plumes from LBB, driven by easterlies at surface and at injection height, reach 170 km and 250 km W of the source at 260 maih and 560 maih for WSWadv and ZonWadv, respectively (Figure 5-16 and Figure 5-23). The NO_2 plumes share the same transport pattern but they are shorter (55 and 85 km, respectively). The main difference between WSWadv and ZonWadv at LBB is that the emission rates during the latter (22 kg $SO_2\ h^{-1}$ and 48 kg $NO_2\ h^{-1}$) duplicate those of WSWadv (11 kg $SO_2\ h^{-1}$ and 24 kg $NO_2\ h^{-1}$) leading to a larger contribution at surface level (14.1 $\mu gSO_2\ m^{-3}$ and 19.9 $\mu gNO_2\ m^{-3}$) over the eastern Algeciras Mountains façade.

5.4 Conclusions

The CALIOPE-AQFS used with a zero-out approach is useful to characterize coal-fired power plants' SO_2 and NO_2 plume dynamics under representative synoptic CTs, and to quantify their contribution to air quality concentrations. The results regarding the plume dynamics and the SO_2 and NO_2 surface contributions are different under each CT and for each of the seven studied facilities.

It is possible to define two kinds of facilities depending on their plume dynamics. On the one hand, there are power plants whose plume dynamics are mainly driven by the synoptic conditions (the plume follows the characteristic of the advective pattern). This is the case of ASP, ABO and COM, located on the Atlantic IP. On the other hand, there are facilities whose plumes are driven by a combination of the synoptic advection and mesoscale processes such as sea-land breezes and wind-channelling by river valleys (AND, CAR and LBB, located over the Mediterranean). GUA is in an intermediate situation because its plume follows the synoptic advection under IBtl, ENEadv, WSWadv and ZonWadv. However, under NWadv and AtlHi mesoscale winds related to its complex topographic context (wind-channeling by the valley) influences the horizontal plume motions.

The plume lengths have been quantified using a novel approach based on the maximum distance from the facility in which the power plant contribution to surface concentration is higher than the Spanish remote background concentration. On average for the seven facilities and six CTs, the maximum plume lengths are 230 km for SO_2 and 112 km for NO_2 (with plumes up to 250-300 km for SO_2 and 200-250 km for NO_2). The plume lengths are larger for CTs characterised by Atlantic advection (NWadv, AtlHi, WSWadv and ZonWadv) than for CTs with non-Atlantic advection (IBtl and ENEadv). The average SO_2/NO_2 plume length for Atlantic and non-Atlantic CTs is 110/54 km and 66/6 km, respectively. The high coal-fired power plants stack height (70-356 magl), which enable an injection of the emissions at high altitude where the atmosphere is more dispersive, explain these remarkable plume lengths. It is noteworthy that within the CALIOPE-AQFS the use of plume-rise calculations, which dynamically allocate the emissions to the most appropriate vertical layers of CMAQ, have not proven to robustly improve the system performance (Guevara *et al.*, 2014b).

The power plant contributions to SO_2 and NO_2 surface concentration occur mainly close to the source (< 20 km). On average for the six CTs, the contributions range 2-25 $\mu gSO_2\ m^{-3}$ and 1-15 $\mu gNO_2\ m^{-3}$. The largest contributions are registered in CAR (25 $\mu gSO_2\ m^{-3}$, 15 $\mu gNO_2\ m^{-3}$), ABO (9 $\mu gSO_2\ m^{-3}$, 14 $\mu gNO_2\ m^{-3}$), and LBB (9 $\mu gSO_2\ m^{-3}$, 10 $\mu gNO_2\ m^{-3}$) whereas the lowest occur in ASP and AND (<5 $\mu gSO_2\ m^{-3}$, 1 $\mu gNO_2\ m^{-3}$), the power plants with higher stack heights. The stack height also explains why ASP and AND plumes reach higher altitudes than those of the other facilities. The contributions are more significant when the emissions are injected within the PBL enabling fumigation processes, usually at midday. When the PBLH is lower than the injection height horizontal plume dispersion is favoured. However, if the emission rates are low, even when the meteorological conditions are favourable for vertical diffusion towards the ground, the pollutants are dispersed horizontally (IBtl at ASP for NO_2 for example).

Within Eulerian photochemical models, the proper simulation of surface pollutant concentration has been related to the accurate determination of PBLH and vertical diffusion (Athanassiadis *et al.* 2002; Byun *et al.*, 2007). The WRF models the PBL following the Yonsei Univeristy parametrization although it is not clear which PBL scheme performs best for the IP (Banks *et al.*, 2015). Moreover, the CMAQ models the diffusion using the ACM2 scheme which tends to predict smaller concentrations of primary pollutants at the surface (Pleim, 2007). Considering these modelling uncertainties the described fumigation dynamics have to be taken with caution.

The plume dynamics for each power plant under the six CTs shows similar patterns for SO_2 and NO_2. However, the absolute values of plume length, altitude and contribution to surface concentration differ depending on the emission rates (that are type-fuel dependent) and on the pollutant diffusivity in the air (higher for NO_2 than SO_2). Further research is needed to determine if differences in deposition velocity between SO_2 and NO_2 under the representative CTs is an added factor of the plume dynamics differential behaviour.

The obtained results over the IP confirm that the pollution dynamics associated to coal-fired power plants depend on a combination of interlinked variables: location and topographic characteristics, stack height, emission rates, and synoptic and mesoscale meteorology.

6. Pollution dynamics of O_3 attributed to on-road transport emissions

This chapter is based on: Valverde V, Pay MT, Baldasano JM. 2015 Ozone attributed to Madrid and Barcelona on-road transport emissions: characterization of plume dynamics over the Iberian Peninsula. Science of The Total Environment **543**: 670-682. DOI: 10.1016/j.scitotenv.2015.11.070.

6.1 Introduction

Tropospheric O_3 is a matter of concern because it is responsible of ~17 400 premature deaths each year in the European Union (EEA, 2014a), it is a greenhouse gas with positive radiative forcing (0.40 ± 0.2 W m^{-2}, Myhre *et al.*, 2013) that favours the global warming, and it is a powerful oxidant that can damage vegetation and reduce crop productivity (Chuwah *et al.*, 2015).

O_3 is photochemically produced close to the ground from a series of precursors emitted by anthropogenic and natural sources, and it is transported over intercontinental scales favoured by its lifetime (c.a. 25 days) in the atmosphere (EEA, 2013; Monks *et al.*, 2015). Wild and Akimoto (2001) have suggested that Europe is the continent of the Northern Hemisphere most prone to be affected by intercontinental effects due to rapid transport of O_3 and its precursors from North America.

In Europe, the O_3 rural background concentration doubled between the 1950s and 2000 (The Royal Society, 2008; Cooper *et al.*, 2014) and it has had a negative trend (-1.44%) in the 2003-2012 decade (EEA, 2014a; EMEP, 2015). However, the target value for the protection of the human health, as defined by the Air Quality Directive 2008/50/EC, is still exceeded in large areas of Southern and Central Europe where high temperature and solar radiation occur in summer (EEA, 2013). In Spain, there is not a clear trend in O_3 concentration in the last decade (2001-2012), despite a decrease of NO_x emissions and an increase in surface solar radiation (Querol *et al.*, 2014). On average for the 2010-2012 period, the O_3 target value was exceeded in 48 of the 135 Spanish AQZ (close to urban and industrial areas, mainly in the center and south of the country and along the Mediterranean coast, MAGRAMA, 2013b).

In Spain, the emission of NO_x, NMVOC and CO has decreased by 32%, 38%, 27%, respectively, in the 2001-2012 period due to a combination of emission reduction policies and the effect of the economic crisis (EEA, 2014b). The on-road transport is the anthropogenic activity with the largest contribution to the O_3 precursor's emissions in Madrid and Barcelona cities, the two biggest Spanish urban areas. However, there are not studies quantifying the contribution of on-road transport emissions from main Spanish urban areas to O_3 concentration in Spain.

Identifying the activity sources and the areas contributing to pollutant concentration is a fundamental task to design and implement effective abatement strategies and air quality plans as stated in the Air Quality Directive 2008/50/EC. Source apportionment modelling techniques such as the Integrated Source Apportionment Method (ISAM) within the Community Multi-scale Air Quality Model (CMAQ) can be used to analyse the contributions of different areas and sources to O_3 pollution and support the diagnosis of the origin of the problem (Cohan *et al.*, 2005; Tran *et al.*, 2014; Kwok *et al.*, 2015). Furthermore, in order to establish efficient mitigation measures that minimize the impact of O_3 on population and ecosystems, it is vital to understand the O_3 transport dynamics which depend on meteorological conditions (Kassomenos *et al.*, 1998; Jacob and Winner, 2009; Santurtún *et al.*, 2015).

The objective of the present work is twofold. First, to determine the contribution of on-road transport emissions to the surface O_3 concentration within the area of influence of Madrid and Barcelona O_3 plumes. Second, to characterize the O_3 plume dynamics attributed to urban on-road transport emissions in Madrid and Barcelona areas under the typical synoptic conditions that affect the IP.

The chapter is organized as follows. Section 6.2 describes the target areas as well as the CALIOPE-AQFS setup for O_3 source apportionment studies. Section 6.3 quantifies the relative contribution of Madrid and Barcelona on-road transport emissions to the total O_3 concentration under typical CTs, and it analyses the O_3 plume dynamics attributed to those sources over the IP. Finally, conclusions are given in Section 6.4.

6.2 Methods

6.2.1 Target areas

Madrid and Barcelona metropolitan areas are taken as source areas to be tagged because they are the two biggest cities in the country in terms of population (6 and 5 million inhabitants, respectively) and number of vehicles (13.7% and 11.4% of total vehicles in Spain in 2012 in Madrid and Barcelona provinces, respectively. DGT, 2015). Furthermore, those areas have dissimilar topographic constraints and weather conditions that can lead to

different O_3 plume dynamics. On the one hand, in the Madrid area the climate is Mediterranean continental and the main topographic features are the Tajo valley in the S/SE and the Guadarrama Mountains (2200–2400 masl) with a NE–SW orientation, north of the metropolitan area of Madrid (Figure 6-1c). On the other hand, the Mediterranean climate in the Barcelona area is strongly influenced by its complex topography (Figure 6-1d) with two sets of mountain ranges parallel to the coast, the Pre-coastal (1000-1500 masl) and the Coastal chains (~500 masl).

Madrid and Barcelona metropolitan areas have been defined according to the Spanish Ministry of Public Works and Transport (MFom, 2013) which define the boundaries taking into account the number of inhabitants per municipality, population density, demographic and commuting dynamics, and transport networks (Madrid ~1 000 km^2; Barcelona ~3 200 km^2; Figure 6-1b). On-road transport in Madrid and Barcelona is the most important contributor to the overall emissions of O_3 precursors. In the Madrid metropolitan area, the total on-road transport emissions fluxes range 22-36 $kg_{NO2}\ day^{-1}\ km^{-2}$; 5.8-9.7 $kmol_{NMVOCs}\ day^{-1}\ km^{-2}$; and 1.7-2.8 $kg_{CO}\ day^{-1}\ km^{-2}$; the same order of magnitude as in the Barcelona metropolitan area where they range 22-31 $kg_{NO2}\ day^{-1}\ km^{-2}$; 4.8-6.2 $kmol_{NMVOCs}\ day^{-1}\ km^{-2}$; and 1.9-2.8 $kg_{CO}\ day^{-1}\ km^{-2}$ (Guevara *et al.*, 2014c). In Madrid/Barcelona, on-road transport contributes 65%/59% of NO_x, 40%/33% of NMVOC, and 67%/85% of CO emissions (Guevara *et al.*, 2014c). The relative contribution of on-road transport to the total NO_x and NMVOC emissions in Barcelona is lower than in Madrid due to the significant emission of the Barcelona harbour.

6.2.2 Air quality simulations and ISAM setup

The CALIOPE-AQFS is used in a case study to simulate the O_3 dynamics over the IP for one representative day of each of the six synoptic CTs that typically affect the IP (Table 2-4, Figure 5-2). These typical CTs and their representative day were identified by Valverde *et al.* (2014) using an objective CTC derived for air quality purposes over the present climate 1983-2012 (Chapter 2). The CALIOPE-AQFS is described and fully evaluated in Chapter 3. The chemical boundary conditions used for the mother domain (EU12, Figure 6-1a) are from the global MOZART-4 model (lat 1.9ºx lon 2.5º) driven by the GEOS-5 model run at NCAR. A summary of the modelling setup in the IP domain is available in the Chapter 3. Biogenic emissions are taken into account through the Model of Emissions of Gases from Nature (MEGANv2.04, Guenther *et al.*, 2006).

The ISAM is used within CMAQ to track the contribution of the Madrid and Barcelona on-road transport emissions to the total O_3. The ISAM approach attributes O_3 production to precursor sources based on the O_3 formation regime estimated using the $PH_2O_2/PHNO_3$ indicator ratio (Kwok *et al.*, 2015). ISAM-CMAQ is configured to estimate the O_3 concentration attributed to the on-road transport emissions in the Madrid and Barcelona metropolitan areas ($O_{3T\text{-}MAD}$ and $O_{3T\text{-}BCN}$, respectively). The contribution of the

remaining emissions (i.e. non-traffic activity sectors inside and outside the metropolitan areas and on-road transport outside the metropolitan areas) to O_3 concentration is computed in a single variable ($O_{3\text{-OTHER}}$). ISAM allows to track the O_3 coming from the boundaries of the study domain. Thus, this work estimates the O_3 transported to the IP boundaries ($O_{3\text{-BCON}}$) according to Figure 6-1a. The influence of O_3 initial condition is also monitored by ISAM ($O_{3\text{-ICON}}$). The contributions from ICON are minimised using a 7-day spin-up period for CMAQ.

The ISAM is a computationally expensive tool. The simulations for this experiment (6 episodes of 8 days each) took 65 000 CPU hours and were run in the Mare Nostrum supercomputer host at the Barcelona Supercomputing Center. The CMAQ-ISAM runs required 1 TB of disk.

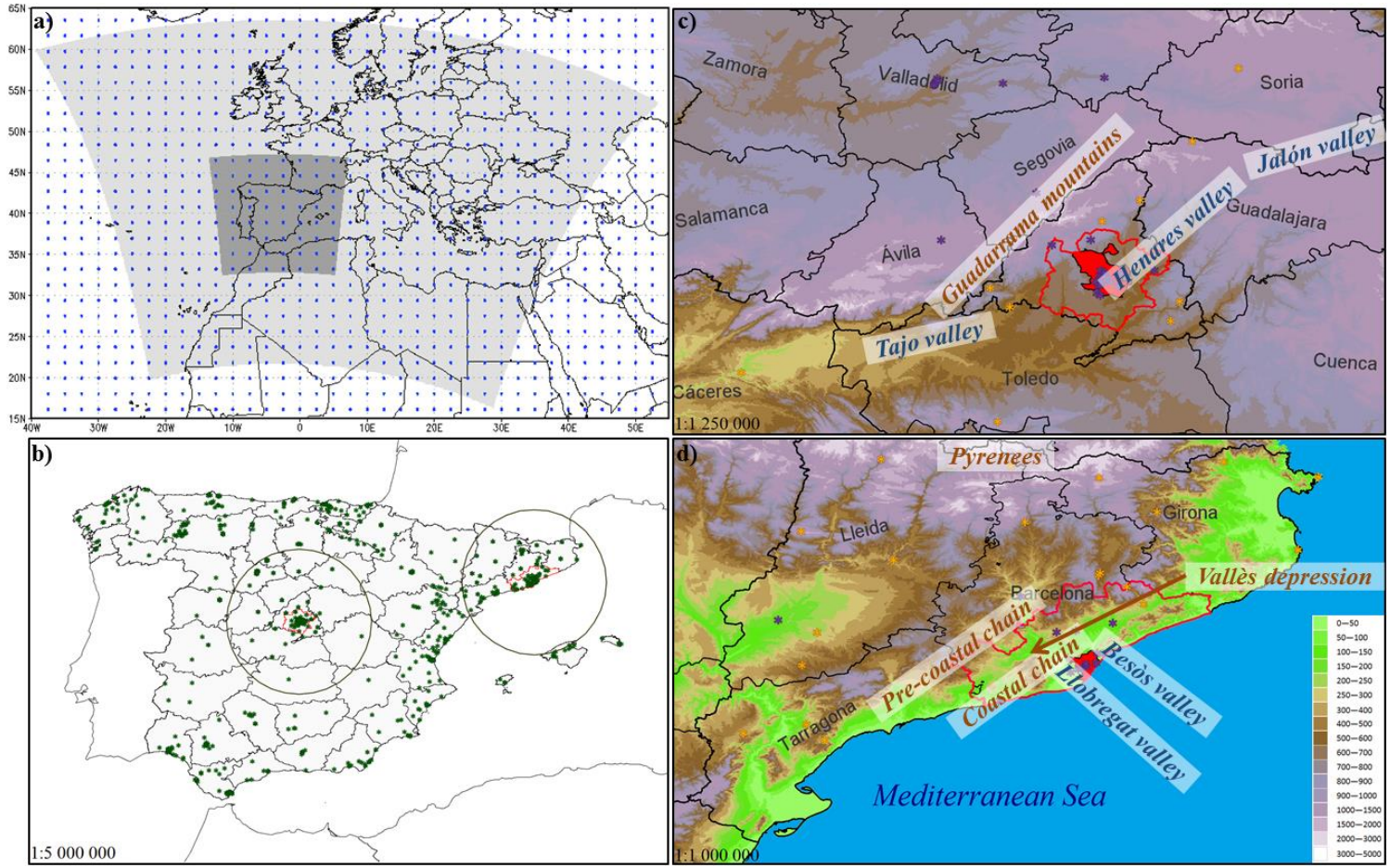

Figure 6-1. a) CALIOPE-AQFS simulation domains: European mother domain (light grey) and Iberian Peninsula nested domain (dark grey). The blue dots indicate the horizontal resolution of the MOZART model used as chemical initial and boundary conditions. b) Iberian Peninsula map where the circles indicate the 200 km radius of influence from Madrid and Barcelona city centres, and the green stars the air quality monitoring stations used for the model evaluation. Madrid (c) and Barcelona (d) metropolitan area (red line) and city limit (red area). Purple and orange stars indicate the location of urban traffic and rural background air quality monitoring stations, respectively, used for the source contribution analysis. Colour chart indicates terrain elevation (masl)

6.2.3 Source contribution analysis and plume dynamics characterization

The contributions of $O_{3T\text{-}MAD}$ and $O_{3T\text{-}BCN}$ concentrations are analysed along the main direction of the plumes and taking into account different environments (i.e. urban traffic and rural background). The locations of air quality stations have been used as reference for the analysis within 200 km radius from Madrid and Barcelona city centres (Figure 6-1b) considered as areas of influence of Madrid and Barcelona metropolitan areas according to our results. Results are analysed i) averaged per typology (between 50 and 61 monitoring stations depending on the CT) and, ii) at individual monitoring stations (2 in Madrid and 2 in Barcelona) along the daily cycle.

In order to increase the knowledge on the origin of O_3 it is important to know if its formation relies either on a NO_x-limited or VOCs-limited regime (Jiménez and Baldasano, 2004; Stein *et al.*, 2005; Zhang *et al.*, 2009). To complement the source apportionment analysis, we estimate the O_3 formation regimen coming from on-road transport emissions in rural background environments downwind Madrid and Barcelona for each CT. This is possible because ISAM calculates O_3 source apportionment based on the instantaneous attribution of O_3 either VOC or NO_x (Kwok *et al.*, 2015)

We characterize the plume dynamics of the $O_{3\text{-}TMAD}$ and $O_{3T\text{-}BCN}$ under each CT in terms of length, area and daily cycle for the maximum daily concentrations. The plume length is calculated considering a concentration baseline, which is established as the average of the remote background concentration (RBC) at the European Monitoring and Evaluation Programme (EMEP) monitoring stations in Spain over the 2003-2012 period (74.7 $\mu g\ m^{-3}$). The plume length is the maximum distance from the city centre to any cell which has higher concentration than the RBC. The plume area corresponds to the number of cells with daily maximum surface concentration above the winter RBC (60 $\mu g\ m^{-3}$). Finally, the plume daily cycle is described taking into account the O_3 photochemistry and the synoptic and the mesoscale patterns.

6.3 Results and discussion

6.3.1 Source contribution

On average at urban traffic (UT) monitoring stations within the area of influence of Madrid and Barcelona, the $O_{3T\text{-}MAD}$ (0.2%-23.5%) contributes more to the total O_3 concentration than the $O_{3T\text{-}BCN}$ (0.5%-7.7%), considering the average contribution during the sunlight hours of the day (Figure 6-2a and Figure 6-2b). At rural background (RB) stations, the contribution of $O_{3T\text{-}MAD}$ (Figure 6-2c) is slightly higher than the contribution of $O_{3T\text{-}BCN}$ (Figure 6-2d) ranging 1.8%-8.6% and 0.9%-6.2%, respectively. In general terms, both $O_{3T\text{-}}$

$_{MAD}$ and $O3_{T\text{-}BCN}$ are maximal for the CTs occurring in the O_3 season (April-September), mainly NWadv and ENEadv.

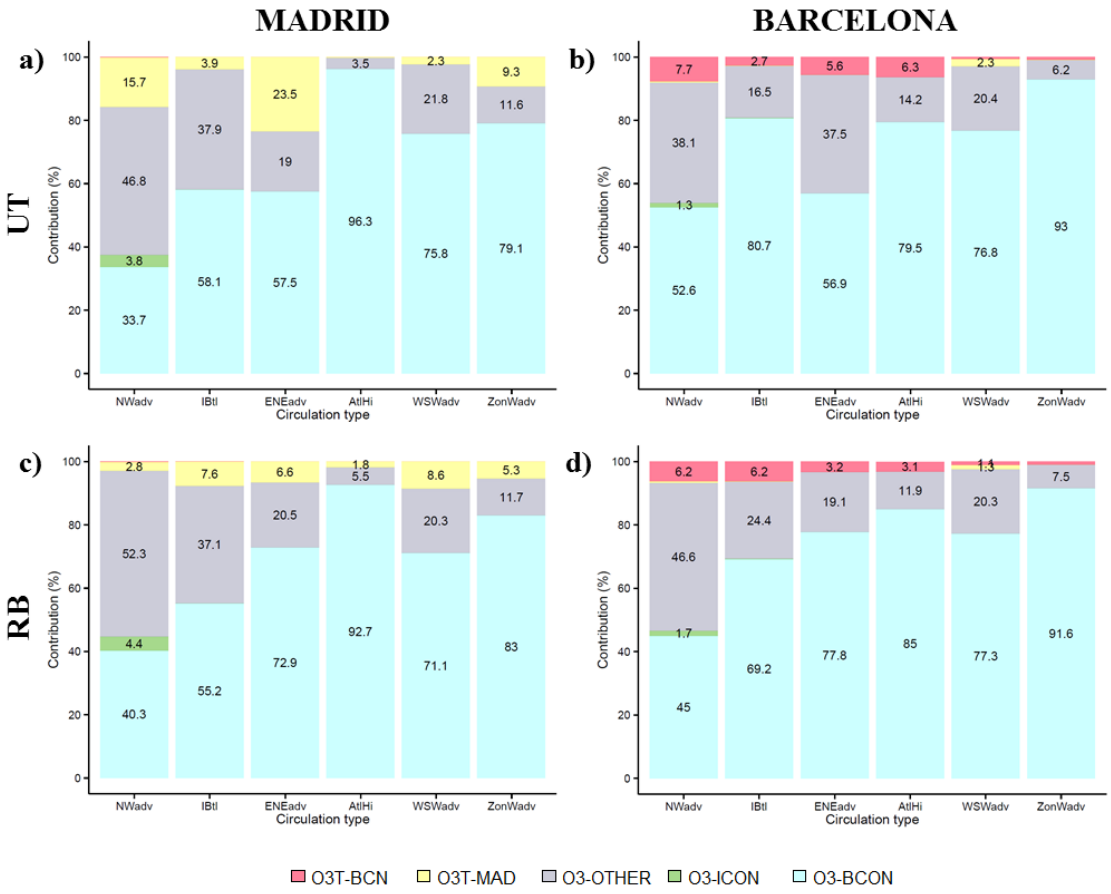

Figure 6-2. Mean source contribution (%) over sunlight hours to O_3 concentration over stations within a radius of 200 km from Madrid and Barcelona city centres and affected by the $O_{3T\text{-}MAD}/O_{3T\text{-}BCN}$ plume on the representative day of each CT: a) urban traffic (UT) stations around Madrid city, b) UT stations around Barcelona city, c) rural background (RB) stations around Madrid city; and d) RB stations around Barcelona city

Except for the NWadv CT, the major contributor to the total O_3 concentration in UT and RB stations is the long-range transport to the IP domain ($O_{3\text{-}BCON}$), both for Madrid and Barcelona (Figure 6-2). This behaviour is in agreement with previous source apportionment analysis in the IP which have used different modelling conditions; Pay *et al.* (2014b) used the CMAQ-ISAM with boundary conditions from the MACC model whereas Borrego *et al.* (2015) used CAMx-OSAT with MOZART4 boundary conditions. The $O_{3\text{-}BCON}$ represents 34%-96% of the total O_3 and its share is larger at rural stations and under AtlHi and ZonWadv, the CTs occurring in wintertime. The O_3 is advected from British Isles (NWadv), the Atlantic Ocean (AtlHi, WSWadv, ZonWadv), the continental European mass (ENEadv) or from Northern-Africa (IBtl). Finally, the O_{3OTHER} ranges 3.5%-52.3% and is in the same order of magnitude at UT and RB locations (Figure 6-2).

For a UT station located in the centre of Madrid (ES0118A) and Barcelona (ES1480A), there is a large variability of the contribution of $O_{3T\text{-}MAD}$ and $O_{3T\text{-}BCN}$ depending on the hour of the day (Figure 6-3 and Figure 6-4). The largest contributions tend to occur just after the morning traffic rush hour, both in Madrid and Barcelona. For the CTs occurring in the O_3 season (NWadv, IBtl, and ENEadv, Figure 6-3 and Figure 6-4), the $O_{3T\text{-}MAD}/O_{3T\text{-}BCN}$ contribution are key to explain the daily peaks of O_3 concentration. It is noteworthy that the total O_3 concentration and the $O_{3T\text{-}MAD}/O_{3T\text{-}BCN}$ are minimal during rush hours at these UT locations due to O_3 titration by NO_2 (Figure 6-3 and Figure 6-4). The average correlation coefficient between total O_3 concentration and $O_{3T\text{-}MAD}/O_{3T\text{-}BCN}$ at urban traffic stations is 0.58 for the CTs occurring in the O_3 season (NWadv, IBtl and ENEadv). At a RB station within the $O_{3T\text{-}MAD}/O_{3T\text{-}BCN}$ plume, the contribution is maximal 2-4 hours later, depending on the advective pattern of the CT (average correlation coefficient = 0.47).

The maximum contribution in an hour of $O_{3T\text{-}MAD}$ to the total O_3 concentration (Figure 6-5a) occurs under NWadv (45.5%; 80 μg m^{-3}) followed by the ZonWadv (44.8%; 23 μg m^{-3}). In both cases, the maximum contribution is reached 10-20 km from Madrid city centre within the metropolitan area. For $O_{3T\text{-}BCN}$, the maximum contribution to the total O_3 concentration in an hour (Figure 6-5b) is 53.2% (107 μg m^{-3}) under NWadv (occurring at 22 km from the Barcelona city centre). Under IBtl and ENEadv, the maximum contribution reaches ~46% (84 and 110 μg m^{-3}, respectively) at ~100 km from the city centre. Averaged over sunlight hours, the monitoring station with highest $O_{3T\text{-}MAD}/O_{3T\text{-}BCN}$ contribution (~20 μg m^{-3}) is an UT and a RB, respectively (Table AIII-1).

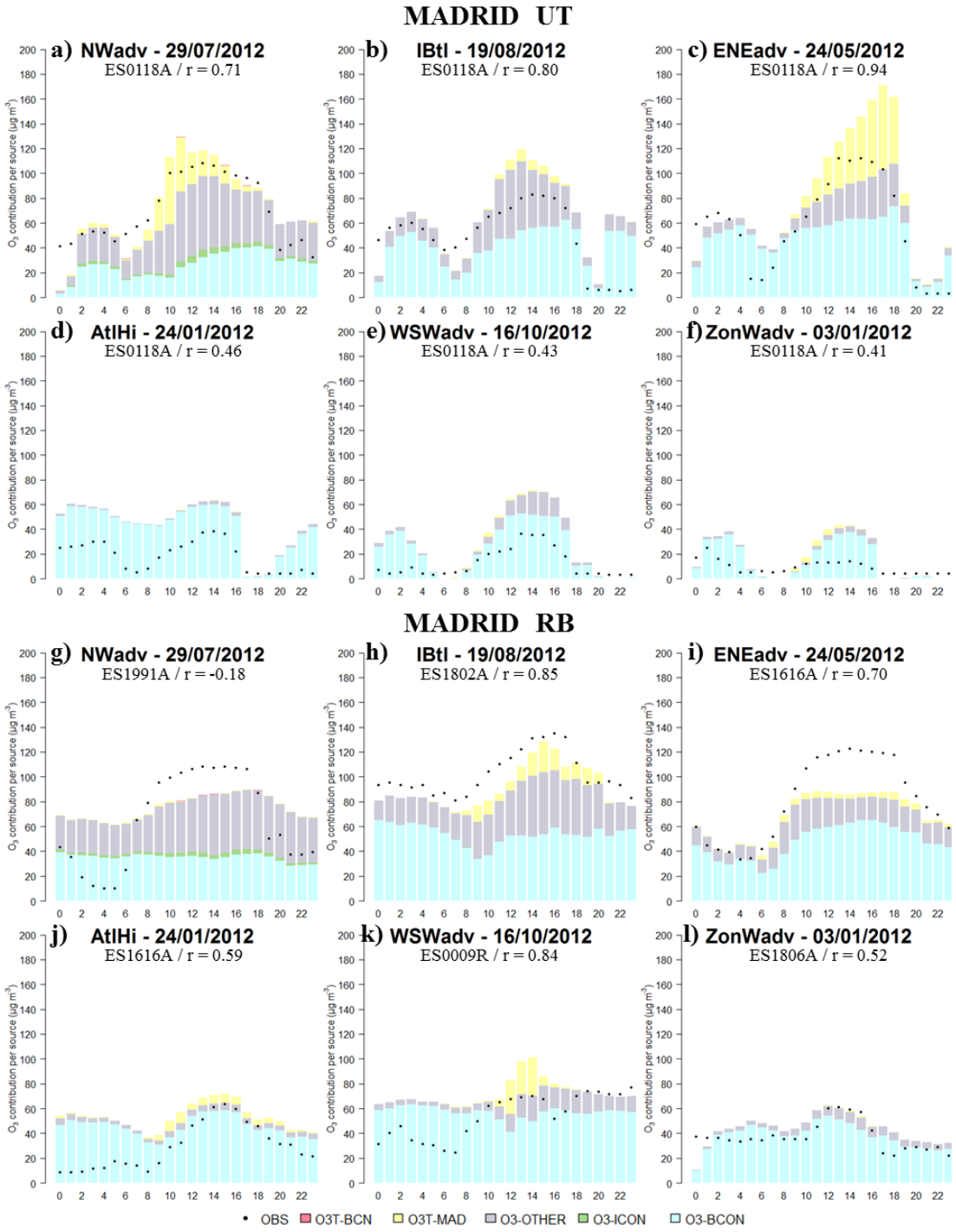

Figure 6-3. Daily cycle (hours in GMT) of observed and modelled O_3 concentration (µg m^{-3}) by source on the representative day of each CT at an urban traffic (top panel) and a rural background (bottom panel) monitoring station downwind emission sources from Madrid metropolitan area (located in Figure 6-7). The monitoring station codes are available in Table AIII-1a. r indicates the correlation coefficient between the total surface O_3 concentration and the $O_{3T\text{-}MAD}$ concentration

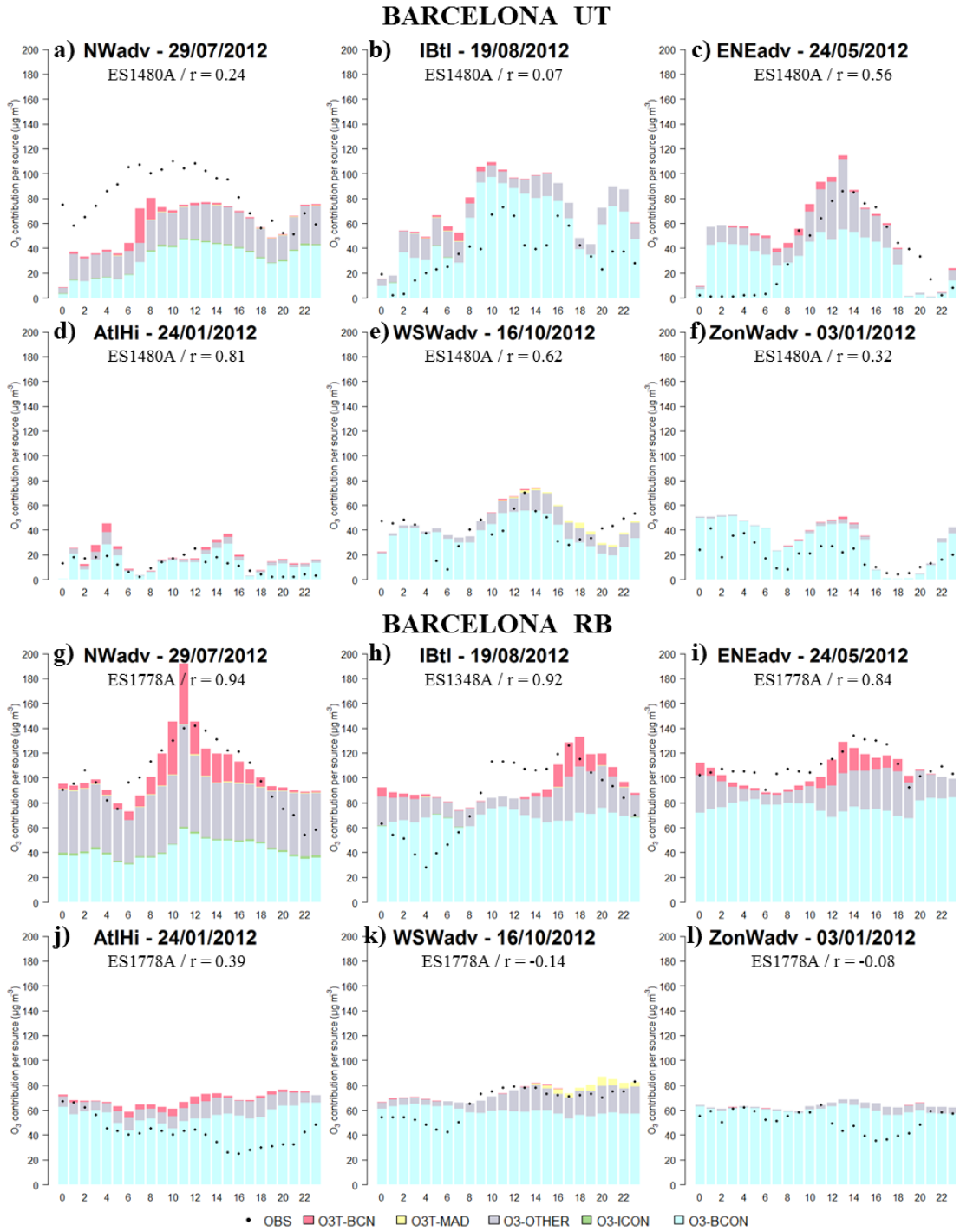

Figure 6-4. Daily cycle (hours in GMT) of observed and modelled O_3 concentration (µg m^{-3}) by source on the representative day of each CT at an urban traffic (top panel) and a rural background (bottom panel) monitoring station downwind emission sources from Barcelona metropolitan area (located in Figure 6-8). The monitoring station codes are available in Table AIII-1a. r indicates the correlation coefficient between the total surface O_3 concentration and the $O_{3T\text{-}BCN}$ concentration

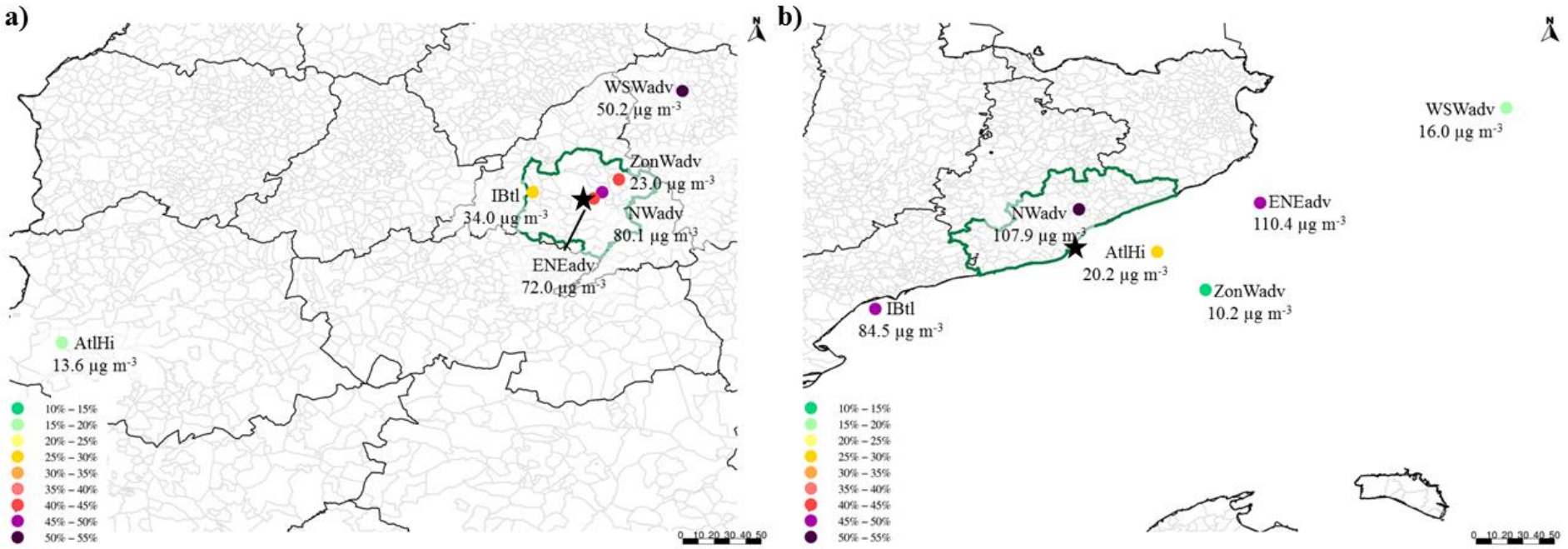

Figure 6-5. Location of the hourly maximum $O_{3T\text{-}MAD}$ (c) and $O_{3T\text{-}BCN}$ (d) on the representative day of each CT, where colour chart indicates the contribution in percentage over the total O_3. The green lines indicate the boundaries of the metropolitan areas

6.3.2 O_3 regime formation

The O_3 regime formation attributed to on-road transport emissions is studied considering the average behaviour at the rural background monitoring stations affected by the $O_{3T\text{-}MAD}/O_{3T\text{-}BCN}$ plume within 200 km from Madrid and Barcelona city centres (Figure 6-1c and Figure 6-1d). Madrid and Barcelona rural background areas have a similar regime under the six CTs (Figure 6-6). For NWadv, IBtl, and ENEadv occurring under summer warm conditions, the O_3 is mainly formed in a NO_x-limited ambient whereas under AtlHi, WSWadv, and ZonWadv, the O_3 formation relies both in NO_x-limited and VOC-limited atmosphere (Figure 6-6). The VOC emission from the on-road transport sector includes gasoline evaporative emissions that are temperature dependent (EEA, 2009). Therefore, VOC emissions are higher under NWadv, IBtl and ENEadv, the CTs that occur more frequently in spring-summer (Figures AIII-5 and AIII-6). This seasonal behaviour of VOC together with meteorological condition explains the difference in O_3 formation under different CTs. Under NWadv, IBtl, and ENEadv, which present the highest concentration of $O_{3\text{-}TMAD}$ and $O_{3T\text{-}BCN}$, small increases in NO_x emissions will lead to larger O_3 concentrations at rural sites. The same NO_x-limited regime has been described for the Porto area in Portugal (Borrego *et al.*, 2015).

6.3.3 $O_{3T\text{-}MAD}/O_{3T\text{-}BCN}$ plume dynamics under representative synoptic conditions

Once the contribution of on-road transport emissions to the total O_3 concentration has been characterised, this section analyses the plume dynamics of $O_{3T\text{-}MAD}/O_{3T\text{-}BCN}$ under the typical CTs affecting the IP focusing on the CTs whose representative day occurs in the O_3 season.

6.3.3.1 NW advection

Under the NWadv, the $O_{3T\text{-}MAD}$ concentration over Madrid city starts to rise progressively from 6:00 (night concentration < 10 μg m^{-3}); it reaches its maximum concentration at 9:00-10:00 (75-80 μg m^{-3}); it then remains constant till 17:00; and then it drops progressively reaching the night concentration at midnight (Figure AIII-1a). At UT stations, the $O_{3T\text{-}MAD}$ concentration is positively correlated with the 2-meter temperature but not with the solar radiation (Table AIII-2). The maximum values of the $O_{3T\text{-}MAD}$ are found within the metropolitan area (Figure 6-7a); however, the plume is transported by synoptic winds towards the NE, parallel to the Guadarrama Mountains, along the Henares and Jalon valleys. The $O_{3T\text{-}MAD}$ travels a longer distance than the NO_2 attributed to on-road transport emission in the metropolitan area of Madrid $NO_{2T\text{-}MAD}$ (Figure AIII-3a) because it is formed downwind.

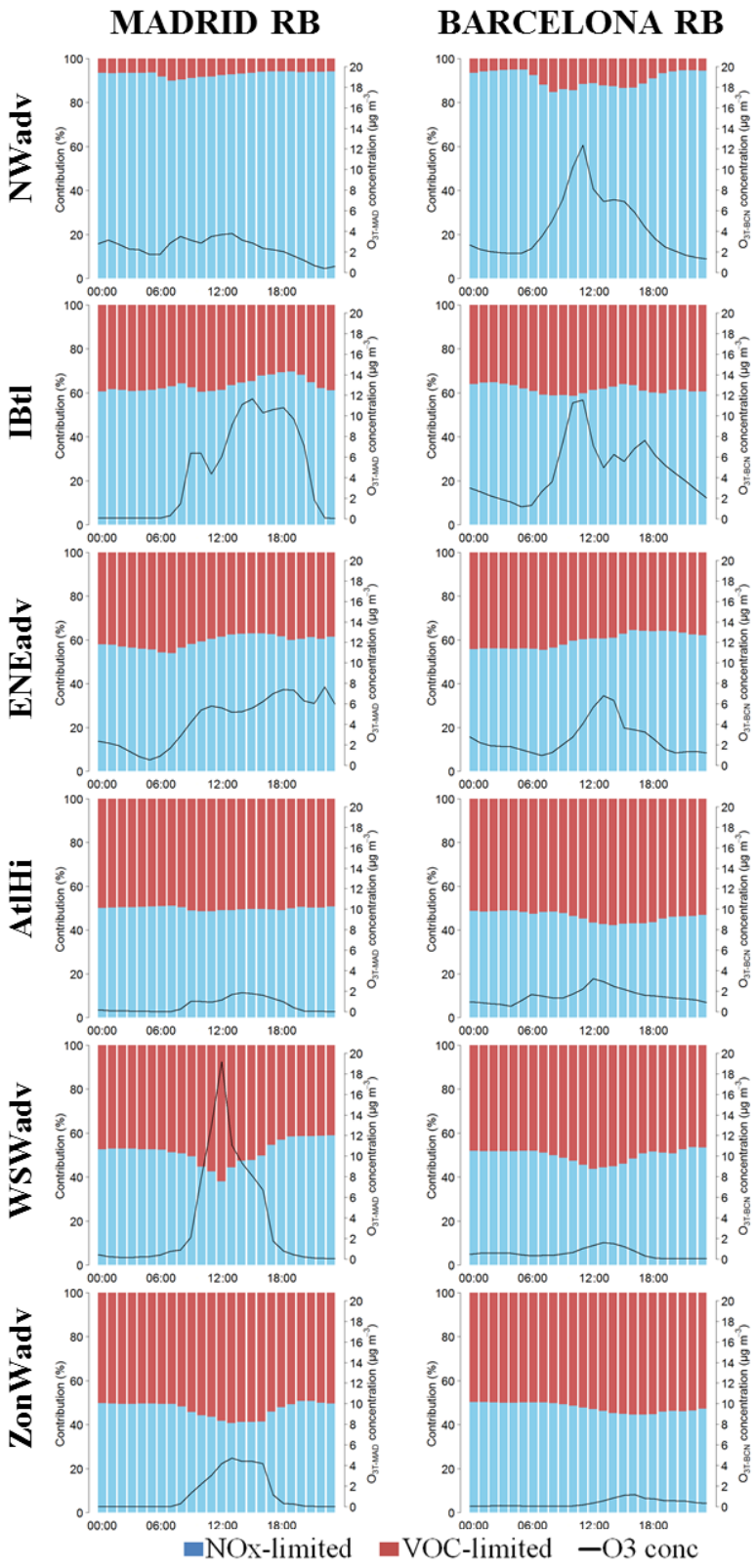

Figure 6-6. Daily cycle (hours in GMT) contribution (%) of NO_x-limited and VOCs-limited regimes to the O_3 concentration (black line, µg m^{-3}) attributed to on-road transport emissions, on average for rural background stations affected by $O_{3T\text{-}MAD}/O_{3T\text{-}BCN}$ plume and located in a radius of 200 km from Madrid (left) and Barcelona (right) city centres, on the representative day of each CT

North-western synoptic winds, channelled between the Pyrenees and the Central French Massif (Figure 6-1d), favour the establishment of an anticyclonic circulation in the area of Barcelona. The $O_{3T\text{-}BCN}$ plume is therefore transported inland, through the Llobregat valley towards the Vallès depression (Figure 6-8a). The daily maximum $O_{3T\text{-}BCN}$ concentration (80-100 μg m^{-3}), which is reached at 9:00 (Figure AIII-2a), is modelled within the Barcelona metropolitan area. At 11:00 the $O_{3T\text{-}BCN}$ contributes to the daily maximum concentration at ES1778A RB station, 50 km N of Barcelona city centre (Figure 6-5g).

6.3.3.2 Iberian thermal low

Mesoscale processes such as land–sea and mountain–valley breezes are enhanced under the IBtl, which is characterised by a low surface pressure gradient over the IP occurring mainly in summer (Valverde *et al.*, 2014). The $O_{3T\text{-}MAD}$ plume is transported from the Madrid metropolitan area towards the Guadarrama Mountains (Figure 6-7b) by upslope winds which are enhanced under the IBtl. The daily maximum $O_{3T\text{-}MAD}$ (~30 μg m^{-3}) is reached at ~20 km from Madrid city centre affecting the southern facade of the Guadarrama Mountains (Figure 6-5a). The $O_{3T\text{-}BCN}$ plume dynamics is controlled by the combination of sea-land breezes and anabatic winds over the Pre-Coastal chain (Figure 6-1d) that result in an anticyclonic behaviour (Figure 6-8b). The concentration rises from 7:00-8:00 (Figure AIII-2b) and the $O_{3T\text{-}BCN}$ is transported towards Tarragona parallel to the coast where it reaches its maximum ~80 μg m^{-3}; then around 11:00, the sea breeze favours it transport inland affecting large areas of central Catalonia (~30 μg m^{-3}); in the afternoon the $O_{3T\text{-}BCN}$ reaches Andorra and the Pyrenees, 120 km away from Barcelona city centre and then, the concentration starts to drop (Figure AIII-2b). The $O_{3T\text{-}BCN}$ plume pattern follows in space and time the $NO_{2T\text{-}BCN}$ and $VOC_{T\text{-}BCN}$ patterns (Figure AIII-4b and AIII-6b, respectively). It is noteworthy that under IBtl, the $O_{3T\text{-}BCN}$ photochemically produced during the day is accumulated during the night at RB locations (Figure AIII-2h) due to the recirculation of pollutants. In fact there are some locations over the sea and the land with an accumulated nocturnal $O_{3T\text{-}BCN}$ concentration up to 15 μg m^{-3}. This recirculation of O_3 has already been described by other authors in the geographical area of Barcelona under a weak surface pressure gradient at synoptic scale (Millán *et al.*, 1996; Toll and Baldasano, 2000; Gonçalves *et al.*, 2009).

.

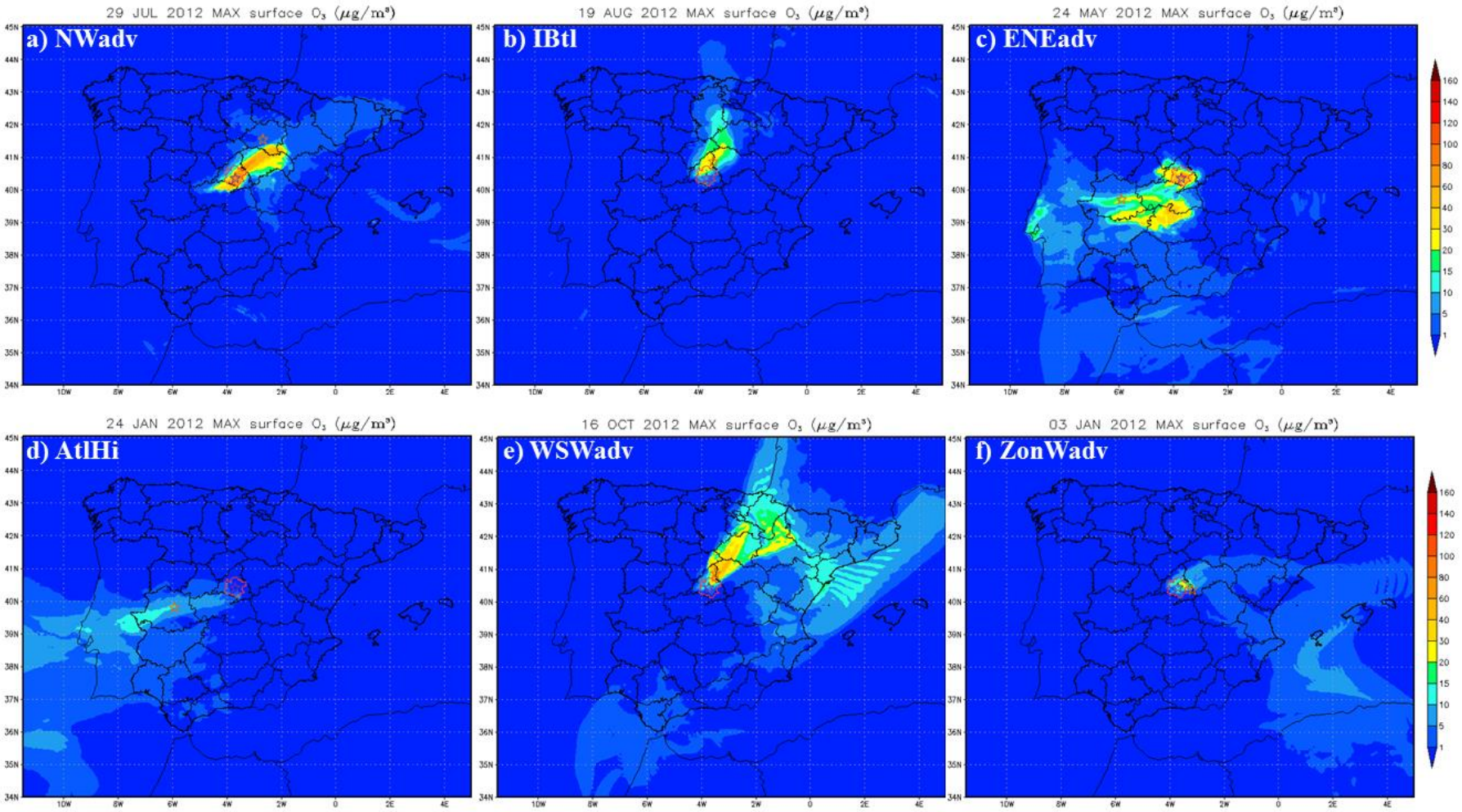

Figure 6-7. Daily maximum O_3 surface concentration (μg m^{-3}) attributed to on-road transport emissions from Madrid metropolitan area ($O_{3T\text{-}MAD}$) on the representative day of each CT: a) NWadv, b) IBtl, c) ENEadv, d) AtlHi, e) WSWadv; and f) ZonWadv. The purple and the orange stars indicate the location of the urban traffic and the rural background air quality monitoring stations, respectively, used for the source contribution analysis of Figure 6-3

6.3.3.3 ENE advection

The representative day of ENEadv, characterised by the arrival of an air mass from central Europe towards the IP, occurs in May under daily temperatures ranging 20-25 ºC and high solar radiation (~300 W m^{-2} $hour^{-1}$, Figure AIII-1c). During the morning, the $O_{3T\text{-}MAD}$ concentration rises in the SW of the Madrid autonomous region, along the Tajo valley. The plume is then transported down-valley, driven by synoptic easterlies, affecting large areas of central IP (Figure 6-7c). The daily maximum concentration of $O_{3T\text{-}MAD}$ ranges 60-80 μg m^{-3}. At midday, the $O_{3T\text{-}MAD}$ plume mainly affects the Madrid metropolitan area, and in the city centre (Figure 6-3c), the concentration reaches 60-70 μg m^{-3}.

The advection from continental Europe, channelled by the Rhone valley, leads to strong northerlies (25 m s^{-1}) at the Lyon Gulf that establish an anticyclonic circulation over the Balearic Islands. As a consequence, the $O_{3T\text{-}BCN}$ plume is transported towards the sea (Figure 6-8c). Over land, the areas affected by the $O_{3T\text{-}BCN}$ are the coast of Girona (40-60 μg m^{-3}) and the Vallès depression (30-40 μg m^{-3}) which is reached through the Besòs valley.

6.3.3.4 Atlantic high

Under AtlHi, northerlies arriving at the Madrid area are channelled by the Tajo Valley transporting the $O_{3T\text{-}MAD}$ plume towards the SW up to the Portuguese border ~350 km from Madrid city centre (Figure 6-7d). However, as this CT tends to occur in winter, the $O_{3T\text{-}MAD}$ concentration is low (~10 μg m^{-3}). The maximum $O_{3T\text{-}MAD}$ concentration (13.6 μg m^{-3}) is reached over relevant natural areas (Monfragüe National Park, Figure 6-5a).

The Atlantic synoptic winds are channelled between the Pyrenees and the French Central Massif establishing an anticyclonic circulation over the Barcelona area. The $O_{3T\text{-}BCN}$ peaks at 13:00-14:00, several hours after the traffic rush hour in the Barcelona metropolitan area (Figure AIII-2d and AIII-2j). $O_{3T\text{-}BCN}$ reaches 15-20 μg m^{-3} and it affects areas of the inner Barcelona province, and locations over the Barcelona and Girona coast (Figure 6-8d). Nocturnal $O_{3T\text{-}BCN}$ photochemically produced from emissions of the former day reach the Balearic Islands, 180 km south from Barcelona (~15 μg m^{-3}).

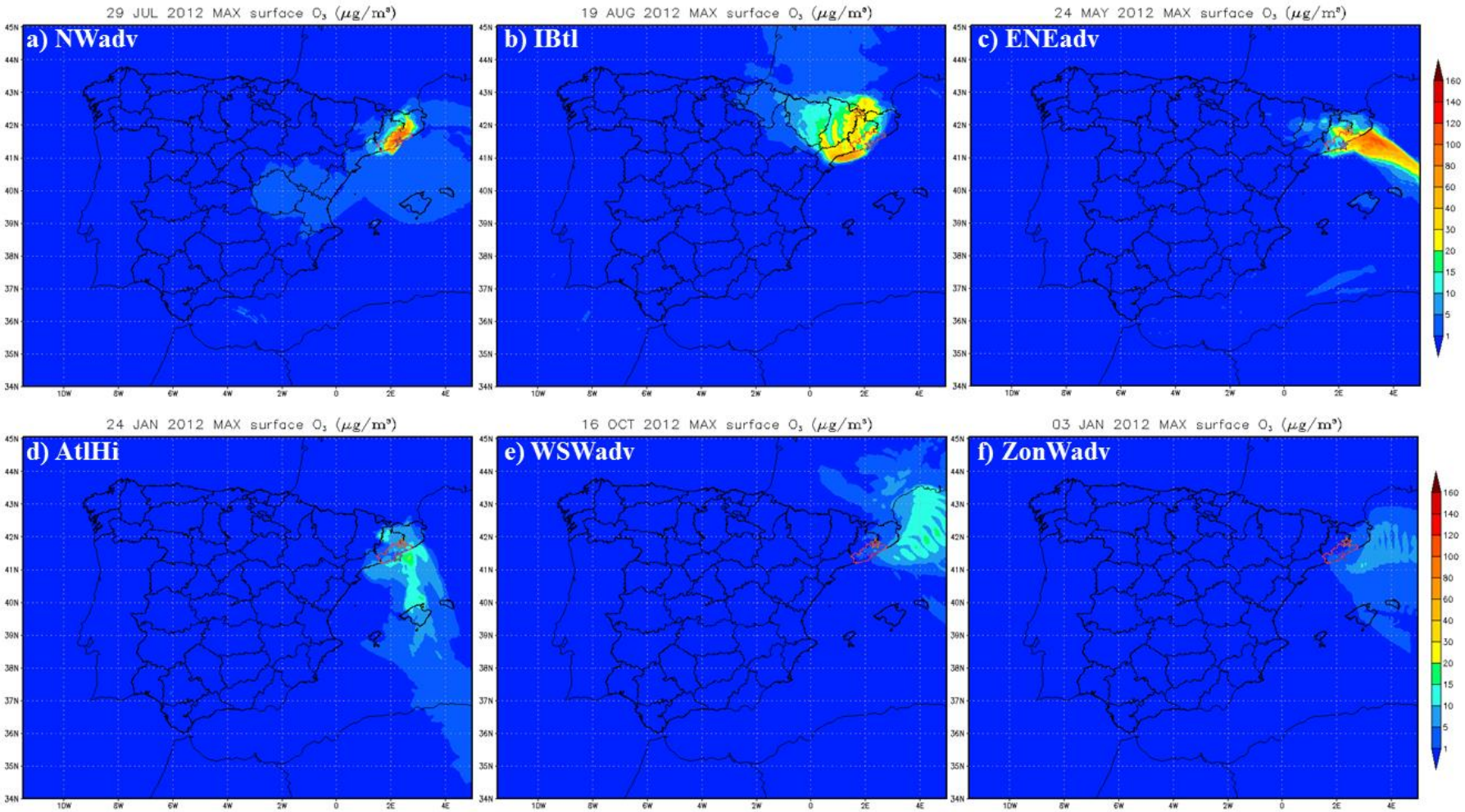

Figure 6-8. Daily maximum O_3 surface concentration (µg m^{-3}) attributed to on-road transport emissions from Barcelona metropolitan area ($O_{3T\text{-}BCN}$) on the representative day of each CT: a) NWadv, b) IBtl, c) ENEadv, d) AtlHi, e) WSWadv; and f) ZonWadv. The purple and the orange stars indicate the location of the urban traffic and the rural background air quality monitoring stations, respectively, used for the source contribution analysis of Figure 6-4

6.3.3.5 WSW advection

The synoptic westerlies arriving to the Madrid area transport the $O_{3T\text{-}MAD}$ plume towards the NE through the Henares and Jalon valleys (Figure 6-7e). The $O_{3T\text{-}MAD}$ concentration starts to rise progressively from 8:00; it reaches its daily maximum concentration at midday (50 $\mu g\ m^{-3}$), 80 km away from Madrid city centre; and it drops from 15:00 (Figures AIII-1e and AIII-1k). $O_{3T\text{-}MAD}$ daily maximum concentration reaches 40-50 $\mu g\ m^{-3}$ in the Guadalajara province, 80 km NE from Madrid (Figure 6-5a). The $O_{3T\text{-}MAD}$ reaches the Cantabrian Sea during the afternoon (10-15 $\mu g\ m^{-3}$) whereas nocturnal O_3 formed the previous day is transported by synoptic westerlies towards the Mediterranean. It is noteworthy that under WSWadv, the $O_{3T\text{-}MAD}$ is advected towards Barcelona and it arrives at Barcelona UT and RB stations in the afternoon (Figure 6-4e and Figure 6-4k, respectively), contributing to 2.5%-3% of O_3 concentration in Barcelona's area of influence (Figure 6-2d).

The $O_{3T\text{-}BCN}$ plume is driven by synoptic WSW winds towards the Lyon Gulf (Figure 6-8e) where it attains a maximum concentration of ~15 $\mu g\ m^{-3}$ 220 km from Barcelona city centre (Figure 6-5b). Over land, the $O_{3T\text{-}BCN}$ concentration reaches ~10 $\mu g\ m^{-3}$ affecting Girona coastal areas at midday. There is a remarkable difference between the concentration of $O_{3T\text{-}MAD}$ and $_{O3T\text{-}BCN}$ under WSWadv. This difference can be attributed to the lower VOCs concentration over the Gulf of Lyon (Figure AIII-6e) than over central IP (Figure AIII-5e) that limit the photochemical formation of $O_{3T\text{-}BCN}$. Furthermore, the MEGAN model has no biogenic emissions module for marine ecosystems which also limits the VOC availability for the O_3 photochemistry over the Gulf of Lyon area. Finally, the WRF simulation did not produce rain on that day in either Madrid or Barcelona areas that could explain the differences in $O_{3T\text{-}MAD}/O_{3T\text{-}BCN}$ concentrations.

6.3.3.6 Zonal Western advection

The ZonWadv CT is typical of winter when low O_3 concentrations are registered in Spain (EEA, 2014b). The $O_{3T\text{-}MAD}$ concentration starts to rise from 9:00 and the daily maximum concentration occurs at 12:00 (Figure 6-3f) within the Madrid metropolitan area reaching ~20 $\mu g\ m^{-3}$ (Figure 6-5a). The plume is transported eastwards by the zonal Atlantic winds (Figure 6-7f).

The lack of sufficient temperature (5-10 ºC) and solar radiation (~250 $Wm^{-2}\ hour^{-1}$) limit the photochemical production of O_3 from Barcelona on-road transport emissions. The $O_{3T\text{-}BCN}$ plume is advected towards the Mediterranean Sea by the zonal winds (Figure 6-8f). The maximum $O_{3T\text{-}BCN}$ concentration ~10 $\mu g\ m^{-3}$ is reached at midday over the sea (Figure 6-5b).

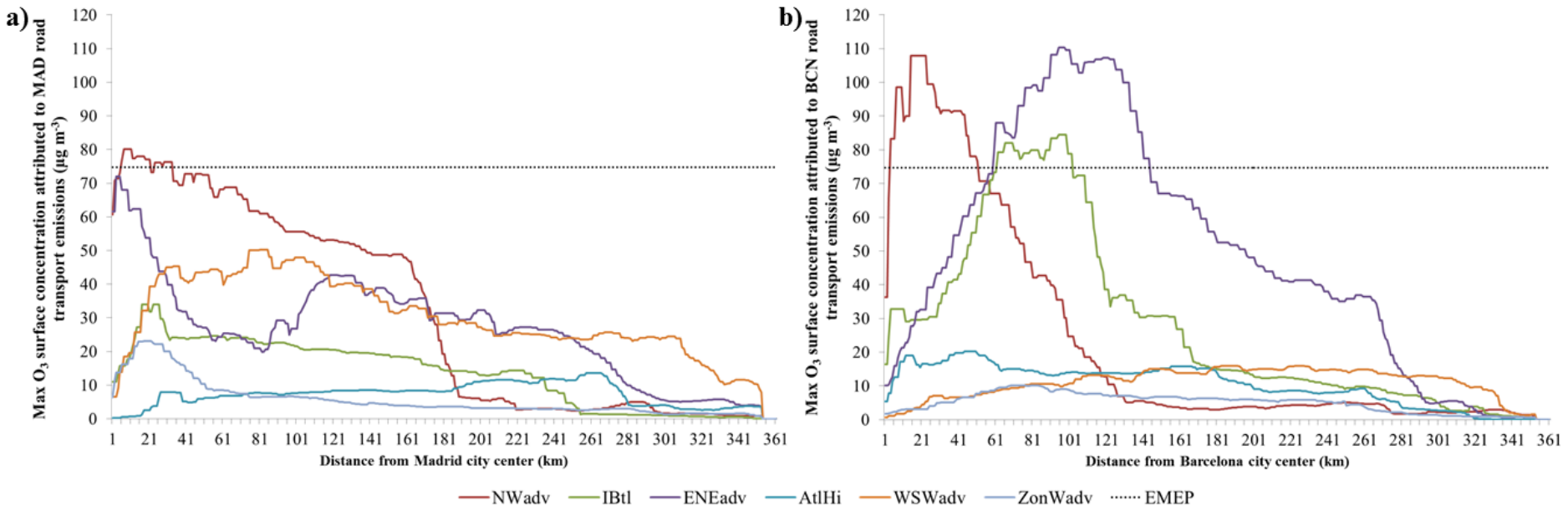

Figure 6-9. O_3 surface concentration from on-road transport (µg m^{-3}) as a function of the distance (km) from Madrid ($O_{3T\text{-}MAD}$, a) and Barcelona ($O_{3T\text{-}BCN}$, b) city centres (black star in Figure 6-5) for each CT. Dotted black line indicates the 2003-2012 average O_3 concentration at Spanish EMEP stations

6.3.4 $O_{3T\text{-}MAD}/O_{3T\text{-}BCN}$ plume length and area under representative synoptic conditions

Under NWadv, the plume of $O_{3T\text{-}MAD}$ with a concentration above the RBC reaches ~30 km away from Madrid city centre (Figure 6-9a) towards the NE. The $O_{3T\text{-}MAD}$ plume affects an area of 1400 km^2 (Figure 6-10a). The $O_{3T\text{-}BCN}$ plume reaches 50 km from Barcelona city centre (Figure 6-9b) affecting an area of 1500 km^2 (Figure 6-10b). In the case of Madrid, the affected area is bounded by the topography of the Henares and Jalon valleys leading to a narrow plume while in the case of Barcelona, the plume is dispersed by the anticyclonic circulation established over the area with the only topographic constraint of the Pyrenees.

The $O_{3T\text{-}MAD}$ does not exceed the EMEP RBC under the IBtl but the plume reaches ~125 km to the N of Madrid with a concentration above 20 $\mu g\ m^{-3}$ (Figure 6-9a). The $O_{3T\text{-}BCN}$ plume length is ~100 km from the city centre. Favoured by the recirculations over the area, the plume affects cities in Tarragona, Lleida and Barcelona provinces totalising an area of ~1100 km^2 (Figure 6-9b, Figure 6-10b).

On the ENEadv representative day, the $O_{3T\text{-}MAD}$ plume length above 20 $\mu g\ m^{-3}$ is ~260 km (Figure 6-9a) and the plume area is ~ 200 km^2 (Figure 6-10a). The $O_{3T\text{-}BCN}$ plume length is 145 km (Figure 6-9b) and the plume area is ~4 500 km^2 (Figure 6-10b) affecting mainly the Mediterranean Sea (Figure 6-8c).

For the CTs occurring more frequently outside the O_3 season (AtlHi, WSWadv and ZonWadv), the formation of $O_{3T\text{-}MAD}/O_{3T\text{-}BCN}$ is limited by temperature and VOC availability (Figures AIII-5d-f and AIII-6d-f). The concentration do not surpass the RBC not even the the winter RBC (60 $\mu g\ m^{-3}$) and therefore, the plume length and plume areas are not computable (Figure 6-10a and Figure 6-10b). For these three CTs and for both, the $O_{3T\text{-}MAD}$ and $O_{3T\text{-}BCN}$, the WSWadv CT is the one under which larger areas are affected by O_3 attributed to on-road emissions due to a larger VOC availability (Figure AIII-5e and AIII-6e) and the strong WSW winds that enhance the $O_{3T\text{-}MAD}$ dispersion.

The NWadv pattern, the most frequent CT, is the one under which the highest values of $O_{3T\text{-}MAD/}O_{3T\text{-}BCN}$ plume length and areas (over land) are reached. This situation is favoured by high temperatures that enhance biogenic VOC availability (Figure AIII-5a and AIII-5b) and O_3 photochemistry and the dispersive conditions in the case of Madrid and re-circulations in the case of Barcelona.

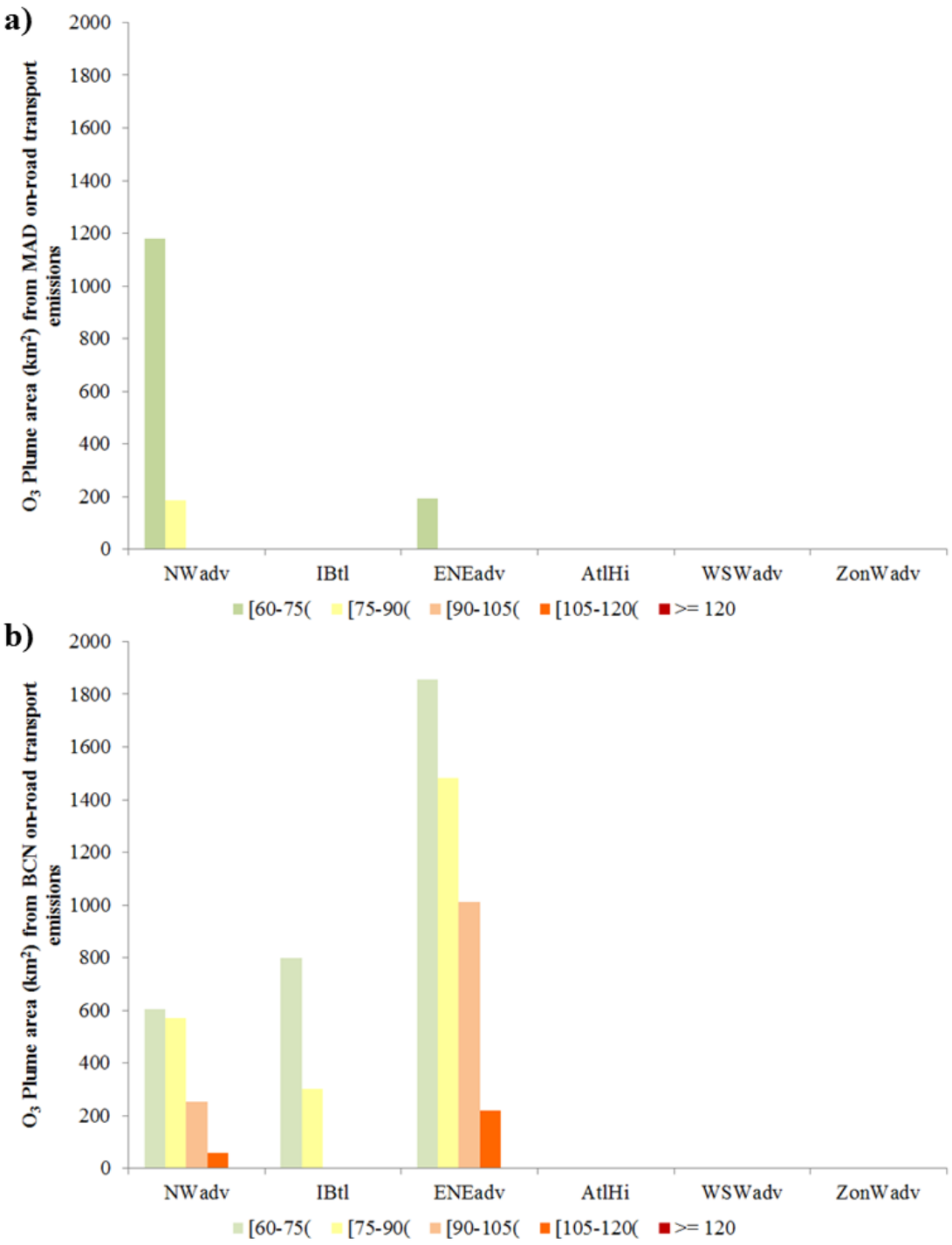

Figure 6-10. Daily maximum O_3 plume area (km^2) by concentration ranges ($\mu g\ m^{-3}$) attributed to on-road transport emissions in the metropolitan areas of Madrid $O_{3T\text{-}MAD}$ (a) and Barcelona $O_{3T\text{-}BCN}$ (b) on the representative day of each CT

6.4 Conclusions

The ISAM-CMAQ within the CALIOPE-AQFS has been applied to understand the effect of on-road transport emissions of Madrid and Barcelona to O_3 concentration and its dynamics. The results show that although the on-road transport is the major anthropogenic source emitter of O_3 precursors in the Madrid and Barcelona metropolitan areas accounting 65%/59% of NO_x, 40%/33% of NMVOC, and 67%/85% of CO, the daily maximum contribution of these emissions to the total O_3 concentration modelled under the most typical CTs affecting the IP is 23.5% for Madrid and 7.7% for Barcelona. For both Madrid and Barcelona areas of influence (~ 200 km) there is a background O_3 concentration of ~60 $\mu g\, m^{-3}$ on average for all the CTs. The photochemical activity attributed to traffic emissions from local sources increases the ambient O_3 concentration in such a way that the maximum total O_3 concentration occurs when the $O_{3T\text{-}MAD}/O_{3T\text{-}BCN}$ is maximal. Therefore, the O_3 attributed to on-road transport emissions is relevant to explain O_3 peak concentration and exceedances of the regulatory target values.

Furthermore, the source apportionment method shows that the O_3 attributed to the long-range transport (accounted as boundary conditions) is the main contributor to the total O_3 concentration for all the CTs, especially in winter (BCON 70-96%), when the O_3 photochemical activity is hindered by low temperatures and low VOC emissions.

Under CTs with high photochemical activity (warm CTs: NWadv, IBtl and ENEadv) the O_3 formation in rural background areas is limited by NO_x due to the high VOC emission. Under these scenarios, the implementation of mitigation strategies focused on on-road transport NO_x emissions could be effective to reduce the O_3 concentration within an area of 200 km around Madrid and Barcelona.

The plume attributed to the on-road transport emission from the Madrid metropolitan area ($O_{3T\text{-}MAD}$) depends on the synoptic advection and it affects large areas of the IP channelled by the Tajo and the Henares valley. The plume of $O_{3T\text{-}MAD}$ affects up to 1400 km^2 depending on the CT and can affect areas up to 200 km. The daily maximum $O_{3T\text{-}MAD}$ in an hour is higher for CTs characterised by NW advection (80 $\mu g\, m^{-3}$), ENE advection (72 $\mu g\, m^{-3}$), than for the other CTs, and it occurs within the metropolitan area of Madrid just after the morning traffic rush hour. In rural background locations, the O_3 traffic peak is delayed 2-4 hours. Under WSW advection, the $O_{3T\text{-}MAD}$ plume reaches the Barcelona metropolitan area.

The dynamics of the O_3 plume from Barcelona metropolitan area ($O_{3T\text{-}BCN}$) depend more on mesoscale processes (sea-land and mountain-valley breezes) than on the synoptic conditions and it affects areas of land and the Mediterranean Sea in a radius of 200 km. The $O_{3T\text{-}BCN}$ concentration is also higher for the CTs with highest temperature when VOCs emissions and O_3 photochemistry are higher: NWadv (maximum in an hour up to

108 μg m^{-3}), ENEadv (110 μg m^{-3}) and the IBtl (85 μg m^{-3}). Under frequent NWadv, the $O_{3T\text{-}BCN}$ plume reaches the Madrid area of influence.

The obtained results are conditioned by the technical apportionment approach considered within the ISAM-CMAQ. It is noteworthy that ISAM is also a useful tool to establish the length of the spin-up period in CMAQ. In our study, we used an a priori 7-day period which resulted as a good choice except for the NWadv case. Under this CT, the ICON contribution after 7 days of spin-up ranges 1.3%-4.4% of the total O_3 with larger contributions in the Madrid area related to recirculations over the centre of the IP. Due to the ISAM novelty, further scientific and computational improvements are expected that will enable future in-depth studies on source attribution and pollution dynamics.

7. Conclusions and perspectives

7.1 General conclusions

The scientific context, motivations, and objectives of the present Ph.D. Thesis were presented in the introductory Chapter 1. Chapter 2 presented a review of circulation type classifications and described the procedure to develop an objective and automated classification over the Iberian Peninsula for air quality purposes. The modelling system used throughout the Ph.D. has been comprehensively described and evaluated for the episodes of study in Chapter 3. The dynamics of NO_2 from the main Spanish urban areas (Madrid, Barcelona and Valencia) and two of the largest industrial/electricity generation areas of the country (Algeciras Bay and Asturias) have been characterised under the identified typical circulation types in Chapter 4. Chapters 5 and 6 have been devoted to the analysis of air pollution dynamics attributed to coal-fired power plants and on-road transport emissions, respectively. Chapters 2, 3, 4, 5, and 6 present a conclusion section where the main results and findings are discussed. This section, within the Conclusion Chapter, summarises the most relevant aspects of the conclusions presented in the aforementioned Chapters.

7.1.1 Circulation-type classification

The atmospheric circulation at the synoptic scale affects pollution transport at the regional scale (Flocas *et al.*, 2009). Therefore, in order to characterize air quality in a given territory, it is necessary to understand how the synoptic circulations control pollution dynamics at regional and local scale (Elminir, 2005; Giorgi and Meleux, 2007; Demuzere *et al.*, 2009). Circulation of air masses is dynamic, and the various states of the atmosphere are not clearly separated. Synoptic classifications enable the establishment of discrete CTs by categorizing the continuum of atmospheric circulation based on their similarities (Beck and Philipp, 2010, Philipp *et al.*, 2014). The work presented in Chapter 2 established an objective procedure to establish a CTC on a climatic basis (1983-2012) to characterize air quality dynamics over the IP. Considering that there is not a single synoptic classification that best fits for all purposes (Huth *et al.*, 2008), sensitivity analyses to several classification techniques and factors affecting it have been performed in order to objectivize the set-up that maximizes its quality. Automatic classification techniques based on k-means clustering perform better in terms of EV than correlation-based and PCA-based techniques. Within

the k-mean techniques, CKM guarantees the identification of non-extreme CTs, with maximum separability and minimum within-type variability using a reasonable amount of computing resources. The classification quality increases with the number of CTs, although this relation is not linear. A 5% increase threshold in EV is established in order to settle an appropriate number of CTs leading to a selection of six CTs. Surface pressure is the reference proxy variable chosen because it obtains the highest EV (among the non-seasonalised variables) and informs about the stability/instability of the atmosphere and the wind speed and direction, which helps understanding air quality dynamics. Although surface level depicts lower EV than higher vertical levels (below 700 hPa), the surface is selected in the reference set-up because most of the processes involved in air quality occur within the lower levels of the atmosphere. The domain size is a critical factor when performing synoptic classifications because the identified CTs for each domain have different spatial, temporal, and dynamic characteristics. The medium-sized domain (D01) is selected in the reference set-up because it covers areas that are the origin of the air masses towards the IP while ranking an average EV (0.48).

The three most common CTs account for 67.6% of climatic frequency (CT1, CT2, and CT3) and mainly occur in summertime, replacing one another. While CT1 (23.9%) is a NW advective pattern characterized by the arrival of polar maritime air masses towards the IP determined by the presence of the Azores high, CT2 (22.4%) depicts a reduced pressure surface gradient, enabling the development of the Iberian thermal low; although stagnant conditions dominate at the surface in CT2, there is a net advection of North African air masses at Z500. Despite being present throughout the year, CT3 (21%) is especially frequent in spring and summer as a result of a blocking anticyclone over central Europe that leads to E-NE advection towards the IP. When the high pressure system subsides, CT3 tends to be replaced by CT2. In winter two CTs are especially frequent, CT4 (12%) and CT6 (10%). The former is an anticyclonic situation that enables the arrival of Atlantic air masses towards the IP, whereas the latter is characterised by zonal Atlantic maritime advection. Finally, CT5 (10%) presents unstable conditions over the IP with W-NW winds and precipitation, and it is typical of transitional seasons. Topographic barriers in the central and eastern IP (Iberic System, Baetic System, Catalan mountain range) are overcome by westerlies on their way to the Spanish Mediterranean coast in CT6 but not in CT5.

Although inter-annual variability exists, the classification is temporally stable showing consistent CTs when using yearly data. The year 2012 is the representative year of this climatic period because its CTs show the highest temporal stability (67.8%). The CTs obtained with the reference set-up for the climatic period and 2012 are consistent with synoptic patterns over the IP found in the literature (Martín-Vide and Olcina, 2001; García-Valero *et al.*, 2012, Figure 2-2b). A representative day of 2012 for each CT has been objectively identified by means of the Representative Day Score. Single and ensemble

Back-trajectories obtained with the HYSPLIT model confirm the synoptic flows depicted by each CT on representative days.

7.1.2 Dynamics of SO_2 and NO_2 from coal-fired power plants.

The CALIOPE-AQFS, used with a brute-force approach, is useful to characterize Spanish coal-fired power plants' SO_2 and NO_2 plume dynamics under representative synoptic CTs, and to quantify their contribution to air quality concentrations.

The plume dynamics of the power plants located on the Atlantic IP (ASP, ABO and COM) are mainly driven by the advective pattern associated to each CT. However, the plumes from AND, CAR and LBB, located over the Mediterranean coast, are driven by a combination of the synoptic advection and mesoscale processes, namely sea-land breezes and wind-channelling by river valleys. The GUA plumes follow the synoptic advection under IBtl, ENEadv, WSWadv and ZonWadv. However, under NWadv and AtlHi, mesoscale winds related to its complex topographic context (wind-channeling by the valley) influence the horizontal plume motions.

On average for the seven facilities and six CTs, the maximum plume lengths are 230 km for SO_2 and 112 km for NO_2 (with plumes up to 250-300 km for SO_2 and 200-250 km for NO_2). The average SO_2/NO_2 plume length for CTs characterised by Atlantic advection (NWadv, AtlHi, WSWadv and ZonWadv) is 110/54 km whereas for CTs with non-Atlantic advection (IBtl and ENEadv), the SO_2/NO_2 plume length is 66/6 km. The high coal-fired power plants stack height (70-356 magl), which enable an injection of the emissions at high altitude where the atmosphere is more dispersive, explain these remarkable plume lengths.

The power plant contributions to SO_2 and NO_2 surface concentration occur mainly close to the source (< 20 km). On average for the six CTs, the contributions range 2-25 $\mu gSO_2\ m^{-3}$ and 1-15 $\mu gNO_2\ m^{-3}$. The largest contributions are registered in CAR (25 $\mu gSO_2\ m^{-3}$, 15 $\mu gNO_2\ m^{-3}$), ABO (9 $\mu gSO_2\ m^{-3}$, 14 $\mu gNO_2\ m^{-3}$), and LBB (9 $\mu gSO_2\ m^{-3}$, 10 $\mu gNO_2\ m^{-3}$) whereas the lowest occur in ASP and AND (<5 $\mu gSO_2\ m^{-3}$, 1 $\mu gNO_2\ m^{-3}$), the power plants with higher stack heights. The stack height also explains why ASP and AND plumes reach higher altitudes than those of the other facilities. The contributions are more significant when the emissions are injected within the PBL enabling fumigation processes, usually at midday. When the injection occurs above the PBL, horizontal plume dispersion is favoured. However, if the emission rates are low, even when the meteorological conditions favour vertical diffusion, the pollutants are dispersed horizontally.

Within Eulerian photochemical models, the proper simulation of surface pollutant concentration has been related to the accurate determination of PBLH and vertical diffusion (Athanassiadis *et al.* 2002; Byun *et al.*, 2007). The WRF models the PBL following the Yonsei University parametrization although it is not clear which PBL scheme performs best for the IP (Banks *et al.*, 2015). Moreover, the CMAQ models the diffusion using the

ACM2 scheme which tends to predict smaller concentrations of primary pollutants at the surface than other available schemes (Pleim, 2007). Considering these modelling uncertainties the described vertical diffusion dynamics have to be taken with caution. The use of a plume-in-grid module within CMAQ can help allocating the emission in the appropriate vertical layer but this approach has large data requirements (emission temperature, flow, stack dimensions, etc.) which are not easy to obtain (Guevara *et al.*, 2014b). A specific research regarding the choice of PBL parametrizations and diffusion schemes within WRF and CMAQ is necessary to adapt CALIOPE-AQFS to the study of pollution dynamics from high point sources such as power plants. A possible way of evaluating the modelling system is by gathering emission and inmission data from the corporate monitoring networks that are required by the Integrated Environmental Authorization in many facilities in the context of the Integrated Pollution Prevention and Control Directive (Directive 2008/1/EC).

The plume dynamics for each power plant under the six CTs shows similar patterns for SO_2 and NO_2. However, the absolute values of the plume length, the altitude and the contribution to surface concentration differ depending on the emission rates (that are type-fuel dependent) and on the pollutant diffusivity in the air (the SO_2 and NO_2 diffusivity at 296 K are: 12532 ± 1733 Pa cm^2 s^{-1} and 14132 ± 4933 Pa cm^2 s^{-1}, respectively according to Tang *et al.,* 2014). Differences in SO_2 and NO_2 deposition – wet and dry – needs to be studied to further explain the dissimilarities in their plume dynamics.

The obtained results over the IP confirm that the pollution dynamics associated to coal-fired power plants depend on a combination of interlinked variables: location and topographic characteristics, stack height, emission rates, and synoptic and mesoscale meteorology.

The differences observed in the pollution dynamics between the CTs might be due to a combination of seasonal variations in meteorological conditions and human behaviour. The concentration of pollutants is higher in winter than in spring/summer CTs because during winter there are increased emissions associated to heating necessities. In winter CTs, the PBLH is lower compared to summer CTs and there are also more temperature inversions in the cold season that help trapping the pollutants in the PBL. In summer CTs, concentrations are lower due to higher PBLH, lower emissions than in winter CTs, and due to increased rates of photochemical oxidation of NO_2 (Henschel *et al.*, 2015).

7.1.3 Dynamics of O_3 attributed to on-road transport from Madrid and Barcelona metropolitan areas.

Currently, tropospheric O_3 is a matter of concern in Spain as the target value for the protection of human health is frequently exceeded in spring and summer in large areas of the Mediterranean coast and the centre and South of Spain (Figure 1-13e). The O_3

concentration is particularly high in areas downwind the cities of Madrid and Barcelona (Figure 1-13f) leading to exceedances of the information threshold (> 180 μg m^{-3} averaged during one hour between April and September). Considering that the on-road transport is the main contributor to the anthropogenic emission of O_3 precursors in big cities, a characterisation of O_3 dynamics attributed to these emissions has been performed under the typical CTs affecting the IP.

The ISAM-CMAQ within the CALIOPE-AQFS has been applied to understand the effect of on-road transport emissions of Madrid and Barcelona to O_3 concentration and its dynamics. The results show that although the on-road transport is the major anthropogenic source emitter of O_3 precursors in the Madrid and Barcelona metropolitan areas accounting 65%/59% of NO_x, 40%/33% of NMVOC, and 67%/85% of CO, the daily maximum contribution of these emissions to the total O_3 concentration modelled under the most typical CTs affecting the IP is 23.5% for Madrid and 7.7% for Barcelona. For both Madrid and Barcelona areas of influence (~ 200 km) there is a background O_3 concentration of ~60 μg m^{-3} on average for all the CTs. The photochemical activity attributed to traffic emissions from local sources increases the ambient O_3 concentration in such a way that the maximum total O_3 concentration occurs when the $O_{3T\text{-}MAD}/O_{3T\text{-}BCN}$ is maximal. Therefore, the O_3 attributed to on-road transport emissions is relevant to explain the O_3 concentration peaks and exceedances of the regulatory target values.

Furthermore, the source apportionment method shows that the O_3 attributed to the long-range transport (accounted as boundary conditions in the present experiment) is the main contributor to the total O_3 concentration for all the CTs, especially in winter (BCON 70-96%), when the O_3 photochemical activity is hindered by low temperatures and low VOC emissions. This finding is in agreement with other source apportionment analysis in the IP which have used different modelling conditions (Pay *et al.* 2014b; Borrego *et al.,* 2015) and some observation-based studies (Gimeno *et al.*, 1999a; 1999b).

In general terms, in urban areas where NO_x concentrations are high, O_3 production is generally VOC-limited, whereas in suburban or rural areas where VOC emission is high due to biogenic sources and NO_x is scarce, O_3 formation is NO_x-limited. In addition O_3 titration occurs generally in urban areas with large NO_x concentrations. This different spatial behaviour in the O_3 formation regime is observed both in Madrid and Barcelona under CTs with high photochemical activity corresponding to warm CTs (NWadv, IBtl and ENEadv). Under these scenarios, the implementation of mitigation strategies focused on on-road transport NO_x emissions could be effective to reduce the O_3 concentration within an area of 200 km around Madrid and Barcelona.

The plume attributed to the on-road transport emission from the Madrid metropolitan area ($O_{3T\text{-}MAD}$) depends on the synoptic advection and it affects large areas of the IP channelled by the Tajo and the Henares valley. The plume of $O_{3T\text{-}MAD}$ affects up to 1400 km^2

depending on the CT and can affect areas up to 200 km. The 1-h maximum $O_{3T\text{-}MAD}$ is higher for CTs characterised by NW advection (80 μg m^{-3}), ENE advection (72 μg m^{-3}) than for the other CTs, and it is detected over the metropolitan area of Madrid just after the morning traffic rush hour. In rural background locations, the O_3 maxima that is associated to the traffic rush hour is delayed 2-4 hours. Note that under WSW advection, the $O_{3T\text{-}MAD}$ plume reaches the Barcelona metropolitan area with a concentration ranging 5-10 μg m^{-3}.

The dynamics of the O_3 plume from Barcelona metropolitan area ($O_{3T\text{-}BCN}$) depend more on mesoscale processes (sea-land and mountain-valley breezes) than on the synoptic conditions and it affects areas of land and the Mediterranean Sea in a radius of 200 km. The $O_{3T\text{-}BCN}$ concentration is also higher for the CTs with highest temperature when VOCs emissions and O_3 photochemistry are higher: NWadv (maximum in an hour up to 108 μg m^{-3}), ENEadv (110 μg m^{-3}) and the IBtl (85 μg m^{-3}). Under frequent NWadv, the $O_{3T\text{-}BCN}$ plume reaches the Madrid metropolitan area (< 5 μg m^{-3}).

It is noteworthy that ISAM is also a useful tool to establish the length of the spin-up period in CMAQ. In our study, we used an a priori 7-day period which resulted as a good choice except for the NWadv case. Under this CT, the ICON contribution after 7 days of spin-up ranges 1.3%-4.4% of the total O_3 with larger contributions in the Madrid area related to recirculations over the centre of the IP.

The obtained results are conditioned by the technical apportionment approach considered within the ISAM-CMAQ which is based on the $PH_2O_2/PHNO_3$ indicator ratio (Kwok *et al.*, 2015). Due to the ISAM novelty, further scientific and computational improvements are expected that will enable future in-depth studies on source attribution and pollution dynamics.

7.2 Perspectives for future research

This section is devoted to the discussion of possible future research regarding the CALIOPE-AQFS and the characterisation of pollution dynamics in Spain. Furthermore, it includes personal considerations of the Ph.D. candidate regarding the role of air quality research in the frame of sustainable development and the challenge of facing global environmental threats.

This Ph.D has been devoted to the analysis of air pollution dynamics in Spain under typical synoptic CTs. The Azores High and the Scandinavian Low have been identified as having a strong influence on the synoptic dynamics affecting the IP over the present climate (1983-2012). It is known that the North Atlantic Oscillation (NAO), which intimately depends on the relationship between the aforementioned actions centres, plays an important role in the

atmosphere dynamics at a hemispheric scale. It would be of particular interest to complete the air quality characterisation performed in this Ph.D. Thesis with an analysis of the influence of positive and negative phases of the NAO in line with recent works as Grundström *et al.* (2015). The analysis of the relationship between the NAO index and pollutant surface concentrations could be performed using the existing data from CALIOPE-AQFS and/or RedESP over a relative long period of years that cover changes in the NAO phase.

The synoptic classification performed in this Ph.D Thesis is of the type circulation-to-environment, in the terms of Yarnal (1993), which first establishes the typical CTs and then studies environmental phenomena associated to the identified types. As a complement to the air pollution dynamics characterisation performed in this Ph.D, it would be interesting to perform an environment-to-circulation classification to analyse the consistency of the results. This complimentary approach would objectively identify pollution patterns over the IP by means of the cost733software using the outputs of the operational CALIOPE-AQFS system of various year. It would then enable an identification of the atmospheric circulation dynamics responsible for these pollution patterns.

Still regarding classifications, Hu *et al.* (2010) indicate that an operational AQFS can benefit of being used in coordination with a synoptic classification. In general terms, the CT that will occur in 24-48 hours can be accurately forecasted and therefore, it is possible to foresee the associated pollution dynamics that will occur over a given territory. The AQFS can be adjusted prior the episode to produce a high resolution forecast (via nesting for example) focusing on given areas of interest that would lead to an improved prediction of the surface pollutant concentrations.

Concerning the emissions, this Ph.D. Thesis has focused on industrial/energy-generation and on-road transport sectors because they are the main sources of NO_x/SO_2 in Spain, and of O_3 precursors in big cities. Considering that Spain has a coastline length ~10 000 km and that the Strait of Gibraltar is the only entrance to the Mediterranean Sea, it would be of particular interest to analyse the contribution of shipping emission to SO_2/NO_2/O_3 dynamics in Spain. With the same spirit, it would be interesting to analyse other sources of emissions from the metropolitan areas of Madrid and Barcelona such as heating/cooling facilities, harbours/airports, etc. and assess their contribution to air pollution dynamics via source apportionment.

In fall 2015 it is a trending topic the "dieselgate" or car manufactureres industrial illegal modification of diesel exhaust for NO_x emissions. It would be interesting to know how much these extra emissions have contributed to exceed the target values of O_3 in Europe and Spain and which are the consequences in terms of health impacts for example. In Spain, where the dieselization of the vehicle fleet has been particularly large compared with

other European countries, the use of unreal emission factors could explain persisting high levels of NO_X in Spanish cities.

In summer daylight conditions, SO_2 is oxidized by hydroxyl radicals to form sulphuric acid which can nucleate/coagulate/condensate into sulphate aerosol. Considering that the main constituents of both PM_{10} and $PM_{2.5}$ in Europe are generally organic matter, sulphate and nitrate (Putaud *et al.*, 2010), it could be interesting to assess which is the contribution of sulphate and nitrate coming from power plants emissions and how the gas-to-particle conversion is affected by the atmospheric circulation at synoptic scale. Looking at the effects, Mangia *et al.* (2015) have studied how an individual coal-fired power plant affects human health in terms of PM2.5 exposure. Their study highlights that the exposure to secondary $PM_{2.5}$ increased significantly the estimated number of annual attributable non-accidental deaths at local scale < 50 km.

In Spain, PM concentration and chemical composition have significant variations across the country (Querol *et al.*, 2008; Basart et al., 2012b; Pay *et al.*, 2012a). However, PM needs to be viewed as an air quality problem year-round, especially in the Mediterranean Basin (Viana *et al.*, 2005). PM variations are linked to patterns of anthropogenic and natural PM emissions but also to circulation patterns (Salvador *et al.*, 2007). Furthermore, road transport is also a significant and increasing source of PM in urban environments (Colvile *et al.*, 2001) and has been proved to be the major contributor to PM concentration in Madrid (48% of PM10 concentration) (Salvador *et al.*, 2004). Transport from the Sahara to North Atlantic Ocean and the Mediterranean Sea has been closely related to synoptic conditions (Querol *et al.*, 2009; Gkikas *et al.*, 2012; Pey *et al.*, 2012). In particular, inter-annual variations in dust transport have been successfully related to climatic variability defined by NAO conditions through changes in precipitation and atmospheric circulation over the regions of dust mobilization and transport (Moulin *et al.*, 1997). Dust outbreaks in eastern Mediterranean Basin were analysed in relation to CT. High dust concentration episodes (PM10 concentration above 110 μg m^{-3}, at least during half an hour in 18 locations) were identified and related to CTs derived from a manual and a regression-computer assisted, classification techniques. Results showed that most of the dust episodes were linked to a cold low pressure system that created surface pressure advection with westerly winds (Dayan *et al.*, 2012). Another important source of PM is the sea-pray, which is important to be considered in Spain due to its large coast, both Mediterranean and Atlantic. Sea-salt particles contribute significantly to the global aerosol burden on a mass basis (Seinfeld and Pandis, 2006). Monger *et al.* (1989) have shown that the influence of sea-salt declines with increasing distance from the coast, whereas summer emissions in the Mediterranean area are higher as a consequence of the higher intensity of sea breeze dynamics (Querol *et al.*, 2004b). Therefore there is a need to understand the PM dynamics in relation to the typical CTs affecting the IP. It would be interesting to characterise the PM dynamics in Spain associated to the synoptic and mesoscale processes identified in this Ph.D. Thesis and to assess the contribution of different emission sources to the PM

concentrations. There is a specific ISAM version for CMAQ which is able to trace the origin of secondary PM (Kwok *et al.*, 2013) that has not yet been tested in Spain.

The CALIOPE-AQFS has proven to be mature over the last years to provide operational forecast over Europa and Spain as well to be used, as in this Ph.D research, for case studies. However, in order to keep the continuous improvement of the system several ideas identified during this research are discussed.

The use of the current CALIOPE-AQFS set up in combination with MOZART4-GEOS5 chemical boundary conditions lead to an overestimation of O_3 concentrations over Spain. The use of a larger number of vertical levels within CMAQ (it is possible to keep all the 36 vertical layers from WRF chosing not to collapse the layers in MCIP) has to be further analysed as it is a feasible set-up for all case studies. It is more complicated to do in the forecast because it is computationally costly. Furthermore, MACC global boundary conditions constitute a better source of information than MOZART4 because they have higher vertical, horizontal, and temporal resolution and the products assimilate gas and particle data from satellite products. The use of MACC chemical boundary conditions have to be properly tested within CALIOPE-AQFS to check if the overestimation in Spain can be reduced.

Regarding the skills of the meteorological model it is advisable to test the surface data assimilation option in WRF (observational nudging) in line with Li *et al.* (2015) who increased the performance of the WRF model over Texas, namely for the planetary boundary layer height, and the surface temperature and wind fields. This improvement in the local meteorology enabled a better simulation of O_3 concentrations with CMAQ in terms of bias reduction and more adjusted timing. With the same idea, Banks *et al.* (2015) studied how different PBL parametrization schemes within the WRF model affect the performance of PBLH – among other variables – comparing the model outputs from a variety of meteorological conditions against Lidar measurements in several Spanish locations. Results did not show a best overall PBL scheme for all the locations, all the meteorological conditions and all the PBL characteristics. Considering the contribution to local air pollution in terms of SO_2 and NO_2 associated to coal-fired power plants and that the plume dynamics is intimately associated to the PBLH at the emissions height, it would be interesting to test different PBL schemes in WRF as well as CMAQ diffusion schemes to assess the effects of varying PBL height on plume dynamics and local pollution.

In order to tackle the pollution in large Spanish cities where the NO_2 limit values are frequently exceeded there is a need to understand the dynamics of the emission-meteorology-topography interactions. The use of the high-resolution CALIOPE-AQFS with horizontal resolution of 1 km slightly improves the performance of the system for NO_2 when compared to the 4 km resolution (and it increases its computational cost) but the system remains unable to adequately simulate the subgrid air quality variability (Pay *et*

al., 2014). In order to appropriately simulate the NO_2 concentration in cities a complimentary simulation system, a computational fluid dynamics model (CFD), that takes into account the detailed geometry of the urban mesh, the subgrid emission heterogeneity, and the effects on the transfer of energy and momentum between the urban structures and the lower atmosphere has to be applied. Therefore, there is a need to explore the possibility of nesting a CFD model in CALIOPE-AQFS to adequately study pollution dynamics in very complex terrains.

Due to its relatively large lifetime in the atmosphere (~25 days) it is important to consider stratosphere-troposphere exchanges of O_3 to properly reproduce its concentrations at the surgace. It has been shown that the availability of an explicit tropospheric O_3 intrusion mechanism as in the global MOCAGE model (Watson *et al.*, 2015) favours the predictability of O_3 inter-annual variability. Considering that CMAQ does not include a stratospheric component or a cross-tropopause exchange mechanism future research should focus in finding an appropriate vertical profile and an accurate interpolation of the stratospheric O_3 of the global model providing the boundary conditions.

In order to evaluate the capabilities of CMAQ-ISAM to recreate the O_3 regime formation associated to the NO_x-VOC regimes, experimental campaigns are required. Xie *et al.* (2011) proved that simulated NO_x, VOCs and O_3 concentrations provided by CMAQ where in agreement with measurements from aircraft measurements, and that the O_3 regimes were close to those of the literature but this task is still necessary in the ISAM context. More complex apportionment approaches considering additional species and duplicative reactions that act as tracers of emissions sources of NO_x and individual VOCs exist. Alternative ways to the $PH_2O_2/PHNO_3$ indicator ratio for O_3 attribution have therefore to be tested within the CTM to increase the robustness of the conclusions presented here.

Finally, the use of ensemble air quality models has been proposed as a way to improve air quality forecasts (Menut and Bessagnet, 2010; Marécal *et al.*, 2015). In this sense, it is worth mentioning that several model intercomparison and ensemble exercises have already been performed/are currently being performed in Europe including the CALIOPE-AQFS or other WRF/CMAQ based modelling systems. For example, in the *ScaleDep* project, the comparison of five CTMs showed that there is a general increase in model performance when increasing the horizontal resolution up to 14 km for NO_2 and PM10 (Cuvelier *et al.*, 2013; Schaap *et al.*, 2015). Within the *Air Quality Model Evaluation International Initiative* (AQMEII) several approaches to the use of multi-model ensembles of CTMs have been studied such as the use of spectrally decomposed previsions (Galmarini *et al.*, 2013). Within AQMEII the evaluation of 16 CTMs has provided insight on a variety of topics for example, the bias in surface O_3 concentration has been associated to the influence of the boundary conditions (Im *et al.*, 2015). The *EURODELTA* model intercomparison has helped quantifying and understanding the sources of uncertainty when modelling pollutant concentrations. The evaluation and comparison of seven CTMs within the *EURODELTA*

phase III also related O_3 underestimations to a systematic bias produced by the boundary conditions. (Bessagnet *et al.*, 2014). The CALIOPE-AQFS could benefit to be run with several members (with changes in meteorological parametrizations, chemical boundary conditions, or emission sets) or as a member of multimodel runs in collaboration with other Spanish and European research centers.

In Europe, experimental O_3 studies carried out in Europe (Cristofanelli and Bonasoni, 2009), reported high background O_3 levels, especially during summer episodes with stagnant meteorological conditions, when high insolation and temperatures persist which is consistent with our findings in Spain. The use of high-resolution modelling proves to be an important asset to perform skilful O_3 simulations (Shrestha *et al.*, 2009). Considering that O_3 is considered as an air pollutant and a greenhouse gas, studies regarding O_3 concentration and dynamics in the context of climate change will be particularly useful. In this sense, some recent studies highlight the importance of understanding the origin of pollution to establish locally effective air pollution abatement strategies. For example, Heal *et al.* (2013) establish that in the United Kingdom, the reduction of NO_x emissions as a consequence of climate change mitigation policies does not necessary get reflected in the O_3 concentrations because of the large contribution of hemispheric background in the British Isles. Kinney (2008) focuses on changes in O_3 formation and deposition associated to changes in meteorology in a climate change scenario. The benefits of emission controls could be significantly counterbalanced by increasing background O_3 concentrations (Monks *et al.*, 2015). Air quality policies have to be developed beyond the state and national level thinking on the international implications and mechanisms of air pollution.

As well as air pollution is a threat for humans and the environment it is quite straightforward that climate change will have/is having consequences that poses new challenges to face. Considering the intimate air quality-climate change interactions (Manders et al., 2012; von Schneidemesser *et al.*, 2015) it would be interesting to use the CALIOPE-AQFS over several decades to study the trends in air pollution in Spain and changes in pollution dynamics that could be related to climate change in line with the excercices of the EMEP Task Force on Measurement and Modelling which is using a set of air quality models to study the effects of European policies in the air pollution trends in the 1990-2010 period.

Nowadays there is a general consensus in the fact that air pollution is a global challenging threat for the human kind that requires international agreements on emission cuts, and local and regional strategies for emission control. The provision of high-resolution and specific source-attributed pollution dynamics studies is a powerful tool to customize the air quality management at the airshed scale. In this context, the research conducted for this Ph.D. Thesis shows that air quality modelling enables the attribution and quantification of primary and secondary pollutant concentrations for point and area sources in a variety of locations, topographic contexts, and meteorological conditions. The analysis of the

dynamics of SO_2 and NO_2 demonstrates that the coal-fired power plants emissions contribute to the degradation of air quality close to the sources but also hundreds of kilometers from them, highlighting the necessity of substituting the current Spanish fossil fuel-based facilites for renwable sources of electricity. Additionally, the results of the Ph.D. Thesis prove that in urban areas, the emissions from on-road transport are essential to explain the daily maximum O_3 concentrations, which stresses the need of switching from gasoline/diesel fleets to hybrid/electrical vehicles, and promoting the bicycle/pedestrian mobility in Spanish cities. Furthermore, there is a need to overcome the current difficulties in shortening the path between the science behind air pollution control and the delivery of appropriate services to policy-makers and citizens.

Science can keep on providing more accurate and trustful evidences regarding the causes, mechanisms and consequences of environment degradation but if we want to succeed as a species, we need to go beyond the academia and the business of science research, and instigate a global awareness among stakeholders and public opinion that there is only one planet and that with the knowledge and tools we already have in the atmospheric sciences, we need to take coordinated and firm actions to protect it for the present and future generations. I am convinced that among the many serious challenges humans are currently facing, air pollution is one for which the causes are known and treatable.

8. References

Agrawal M, Singh B, Rajput M, Marshall F, Bell JNB., 2003. Effect of air pollution on peri-urban agriculture: a case study. *Environmental Pollution* **126**: 323-329. DOI: 10.1016/S0269-7491(03)00245-8.

Akritidis D, Zanis P, Katragkou E, Schultz M, Tegoulias I, Poupkou A, Markakis K, Pytharoulis I, Karacostas T., 2013. Evaluating the impact of chemical boundary conditions on near surface ozone in regional climate air quality simulations over Europe. *Atmospheric Research* **134**: 116-130. DOI: 10.1016/j.atmosres.2013.07.021.

Alonso-Pérez S, Cuevas E, Querol X., 2011. Objective identification of synoptic meteorological patterns favouring African dust intrusions into the marine boundary layer of the subtropical eastern north Atlantic region. *Meteorology and Atmospheric Physics* **113:** 109-124. DOI: 10.1007/s00703-011-0150-z.

Appel KW, Chemel C, Roselle SJ, Francis XV, Hu R-M, Sokhi RS, Rao ST, Galmarini S., 2012. Examination of the Community Multiscale Air Quality (CMAQ) model performance over the North American and European domains. *Atmospheric Environment* **53**: 142-152. DOI: 10.1016/j.atmosenv.2011.11.016.

Arévalo G, Baldasano JM, Pay MT., 2014. Evaluación del sistema de pronóstico de calidad del aire CALIOPE en España para el año 2013. 92 pp. Available at: <http://www.bsc.es/projects/earthscience/visor/bases_datos/image_viewer/docs/20140513_Informe_Evaluacion_Pronostico_CALIOPE_2013.pdf> [Accessed 20 December 2015].

Athanassiadis GA, Trivikrama-Rao S, Ku JY, Clark RD., 2002. Boundary Layer Evolution and its Influence on Ground-Level Ozone Concentrations. *Environmental Fluid Mechanics* **2**: 339-357. DOI: 10.1023/A:1020456018087.

Azorin-Molina C, Chen D, Tijm S, Baldi M., 2009. A multi-year study of sea breezes in a Mediterranean coastal site: Alicante (Spain). *International Journal of Climatology* **31**: 468-486. DOI: 10.1002/joc.2064.

Baker LH, Collins WJ, Olivié DJL, Cherian R, Hodnebrog Ø, Myhre G, Quaas J., 2015. Climate responses to anthropogenic emissions of short-lived climate pollutants. *Atmospheric Chemistry and Physics* **15**: 8201-8216. DOI: 10.5194/acp-15-8201-2015.

Baklanov A, Schlünzen K, Suppan P, Baldasano JM, Brunner D, Aksoyoglu S, Carmichael G, Douros J, Flemming J, Forkel R, Galmarini S, Gauss M, Grell G, Hirtl M, Joffre

S, Jorba O, Kaas E, Kaasik M, Kallos G, Kong X, Korsholm U, Kurganskiy A, Kushta J, Lohmann U, Mahura A, Manders-Groot A, Maurizi A, Moussiopoulos N, Rao ST, Savage N, Seigneur C, Sokhi RS, Solazzo E, Solomos S, Sørensen B, Tsegas G, Vignati E, Vogel B, Zhang Y., 2014. Online coupled regional meteorology chemistry models in Europe: current status and prospects. *Atmospheric Chemistry and Physics* **14**: 317-398. DOI: 10.5194/acp-14-317-2014.

Baldasano JM, Cremades L, Soriano C., 1994. Circulation of Air Pollutants over the Barcelona Geographical Area in summer. Proceedings of Sixth European Symposium Physico-Chemical Behaviour of Atmospheric Pollutants. Varese (Italy), 18-22 October. Report EUR 15609/1 EN: 474-479.

Baldasano JM, Millán MM., 2000. Guide for the application of Air Quality Models. IV Seminario sobre la Calidad del Aire en España. Sitges (Spain). 7-8 November. 38 pp.

Baldasano JM, Valera E, Jiménez P., 2003. Air quality data form large cities. *Science of The Total Environment* **307**: 141-165. DOI: 10.1016/S0048-9697(02)00537-5.

Baldasano JM, Güereca LP, López E, Gassó S, Jimenez-Guerrero P., 2008a. Development of a high-resolution (1 km x 1 km, 1 h) emission model for Spain: the high-elective resolution modelling emission system (HERMES). *Atmospheric Environment* **42**: 7215-7233. DOI: 10.1016/j.atmosenv.2008.07.026.

Baldasano JM, Jiménez-Guerrero P, Jorba O, Pérez C, López E, Güereca P, Martin F, García-Vivanco M, Palomino I, Querol X, Pandolfi M, Sanz MJ, Diéguez JJ., 2008b. CALIOPE: An operational air quality forecasting system for the Iberian Peninsula, Balearic Islands and Canary Islands. First annual evaluation and ongoing developments. *Advances in Science and Research* **2:** 89-98. DOI: 10.5194/asr-2-89-2008.

Baldasano JM, Piot M, Jorba O, Gonçalves M, Pay MT, Basart S, Jiménez P, Gassó S., 2010. CALIOPE: an Operational Air Quality Forecasting System for Europe and Spain. Mesoscale Modelling For Air Pollution Applications: Achievements And Challenges (COST 728 FinalWorkshop), Organisers: COST 728, WMO/GURME and MEGAPOLI, Geneva (Switzerland), 25-26 February.

Baldasano JM, Pay MT, Jorba O, Gassó S, Jiménez-Guerrero P., 2011. An annual assessment of air quality with the CALIOPE modeling system over Spain. *Science of the Total Environment* **409:** 2163-2178. DOI: 10.1016/j.scitotenv.2011.01.041.

Baldasano JM, Soret A, Guevara M, Martínez F, Gassó S., 2014. Integrated assessment of air pollution using observations and modelling in Santa Cruz de Tenerife (Canary Islands). *Science of the Total Environment* **473-474:** 576-588. DOI: 10.1016/j.scitotenv.2013.12.062.

Ballester F, Querol X, Medina S, Baldasano JM, Sunyer J., 2007. Current situation, priorities for intervention and research needs in air pollution and health in Spain: conclusions of the AIRNET. *Gaceta Sanitaria* **21**: 70-75. Available at: < http://www.gacetasanitaria.org/es/pdf/S0213911107719738/S300/> [Accessed 20 December 2015].

Baltacı H, Kındap T, Ünal A, Karaca M., 2015. The influence of atmospheric circulation types on regional patterns of precipitation in Marmara (NW Turkey). *Theoretical and Applied Climatology* 1-10. DOI: 10.1007/s00704-015-1653-1.

Banks RF, Tiana-Alsina J, Rocadenbosch F, Baldasano JM., 2015. Performance evaluation of the boundary-layer height from Lidar and the Weather Research and Forecasting model at an urban coastal site in the north-east Iberian Peninsula. *Boundary-Layer Meteorology* **157**: 265-292. DOI: 10.1007/s10546-015-0056-2.

Barros N, Toll I, Soriano C, Jiménez P, Borrego C, Baldasano JM., 2003. Urban Photochemical Pollution in the Iberian Peninsula: Lisbon and Barcelona Airsheds. *Journal of the Air & Waste Management Association* **53:** 347-359. DOI: 10.1080/10473289.2003.10466157.

Barry RG, Perry AH., 1974. Synoptic Climatology — Methods and Applications. *Weather* **29:** 195. DOI: 10.1002/j.1477-8696.1974.tb07430.x.

Basart S, Pérez C, Nickovic S, Cuevas E, Baldasano JM., 2012a. Development and evaluation of the BSC-DREAM8b dust regional model over Northern Africa, the Mediterranean and the Middle East. *Tellus Series B – Chemical and Physical Meteorology* **64:** 1-12. DOI: 10.3402/tellusb.v64i0.18539.

Basart S, Pay MT, Jorba O, Pérez C, Jiménez-Guerrero P, Schulz M, Baldasano JM., 2012b. Aerosols in the CALIOPE air quality modelling system: evaluation and analysis of PM levels, optical depths and chemical composition over Europe. *Atmospheric Chemistry and Physics* **12**: 3363-3392. DOI: 10.5194/acp-12-3363-2012.

Beck C, Philipp A., 2010. Evaluation and comparison of circulation type classifications for the European domain. *Physics and Chemistry of the Earth, Parts A/B/C* **35:** 374-387. DOI: 10.1016/j.pce.2010.01.001.

Beck C, Philipp A, Streicher F., 2013. The effect of domain size on the relationship between circulation type classifications and surface climate. *International Journal of Climatology*. DOI: 10.1002/joc.3688.

Beekmann M, Prévôt ASH, Drewnick F, Sciare J, Pandis SN, Denier van der Gon HAC, Crippa M, Freutel F, Poulain L, Ghersi V, Rodriguez E, Beirle S, Zotter P, Weiden-Reinmüller SL, von der Bressi M, Fountoukis C, Petetin H, Szidat S, Schneider J, Rosso A, El Haddad I, Megaritis A, Zhang QJ, Michoud V, Slowik JG, Moukhtar S,

Kolmonen P, Stohl A, Eckhardt S, Borbon A, Gros V, Marchand N, Jaffrezo JL, Schwarzenboeck A, Colomb A, Wiedensohler A, Borrmann S, Lawrence M, Baklanov A, Baltensperger U., 2015. In situ, satellite measurement and model evidence on the dominant regional contribution to fine particulate matter levels in the Paris megacity. *Atmospheric Chemistry and Physics* **15**: 9577-9591. DOI: 10.5194/acp-15-9577-2015.

Beelen R, and 75 other authors., 2014. Effects of long-term exposure to air pollution on natural-cause mortality: An analysis of 22 European cohorts within the multicentre ESCAPE project. *The Lancet* **383**: 785-795. DOI: 10.1016/S0140-6736(13)62158-3.

Bentayeb M, Wagner V, Stempfelet M, Zins M, Goldberg M, Pascal M, Larrieu S, Beaudeau P, Cassadou S, Eilstein D, Filleul L, Le Tertre A, Medina S, Pascal L, Prouvost H, Quénel P, Zeghnoun A, Lefranc A., 2015. Association between long-term exposure to air pollution and mortality in France: A 25-year follow-up study. *Environment International* **85**: 5-14. DOI: 10.1016/j.envint.2015.08.006.

Bessagnet B, Colette A, Meleux F, Rouïl L, Ung A, Favez O, Cuvelier C, Thunis P, Tsyro S, Stern R, Manders A, Kranenburg R, Aulinger A, Bieser J, Mircea M, Briganti G, Cappelletti A, Calori G, Finardi S, Silibello C, Ciarelli G, Aksoyoglu S, Prévot A, Pay MT, Baldasano JM, Vivanco M, Garrido JL, Palomino I, Martín F, Pirovano G, Roberts P, Gonzalez L, White L, Menut L, Dupont JC, Carnevale C, Pederzoli A., 2014. Model evaluation with observations issued from the 2009 EMEP intensive period and standard measurements in Feb/Mar 2009. TFMM&MSC–W Report 1/2014. 153 pp. Available at <http://emep.int/publ/reports/2014/MSCW_technical_1_2014.pdf> [Accessed 20 December 2015].

Bieser J, Aulinger A, Matthias V, Quante M, Builtjes PJH., 2011. SMOKE for Europe – adaptation, modification and evaluation of a comprehensive emission model for Europe. *Geoscientific Model Development* **4**: 47-68. DOI: 10.5194/gmd-4-47-2011.

Borken-Kleefeld J., 2014. Real World Emissions from Road Vehicles: Results from Remote Sensing, Emission Measurements and Models. Proceedings of the 20th International Transport and Air Pollution conference. Graz (Austria). 18-19 September. DOI: 10.13140/RG.2.1.2883.1203.

Borrego C, Monteiro A, Martins H, Ferreira J, Fernandes AP, Rafael S, Miranda AI, Guevara M, Baldasano JM., 2015. Air quality plan for ozone: an urgent need for North Portugal. *Air Quality, Atmospheric and Health* **8**: 352-366. DOI: 10.1007/s11869-015-0352-5.

Brunekreef B, Holgate ST., 2002. Air pollution and health. *Lancet*. **360**: 1233-1242. DOI: 10.1016/S0140-6736(02)11274-8.

Byun DW, Schere KL., 2006. Review of the governing equations, computational algorithms and other components of the Models-3 Community Multiscale Air Quality (CMAQ) Modeling System. *Applied Mechanics Reviews* **59:** 51-77. DOI: 10.1115/1.2128636.

Byun DW, Kim ST, Kim SB., 2007. Evaluation of air quality models for the simulation of a high ozone episode in the Houston metropolitan area. *Atmospheric Environment* **41**: 837-853. DOI: 10.1016/j.atmosenv.2006.08.038.

Cahynová M, Huth R., 2009. Enhanced lifetime of atmospheric circulation types over Europe: fact or fiction? *Tellus* **61A:** 407-416. DOI: 10.1111/j.1600-0870.2009.00393.x.

Casado MJ, Pastor MA, Doblas-Reyes FJ., 2010. Links between circulation types and precipitation over Spain. *Physics and Chemistry of the Earth* **35:** 437-447. DOI: 10.1016/j.pce.2009.12.007.

Casado MJ, Pastor MA., 2013. Circulation types and winter precipitation in Spain. *International Journal of Climatology*. DOI: 10.1002/joc.3860.

Cassou C, Terray L, Phillips A., 2005. Tropical Atlantic influence on European heat waves. *Journal of Climate* **18:** 2805-2811. DOI: 10.1175/JCLI3506.1.

Castell-Balaguer N, Téllez L, Mantilla E., 2012. Daily, seasonal and monthly variations in ozone levels recorded at the Turia river basin in Valencia (Eastern Spain). *Environmental Science and Pollution Research* **19:** 3461-3480. DOI: 10.1007/s11356-012-0881-5.

Cesaroni G, Badaloni C, Gariazzo C, Stafoggia M, Sozzi R, Davoli M, Forastiere F., 2013. Long-term exposure to urban air pollution and mortality in a cohort of more than a million adults in Rome. *Environmental Health Perspectives* **121**: 324-331. DOI: 10.1289/ehp.1205862.

Chaturvedi DK, Shashank S., 2015. An Experimental Study and Verification of the Facts Related to Factors Affecting the Performance of Solar PV Systems. Proceedings of Fifth International Conference on Communication Systems and Network Technologies. Gwalior (India), 4-6 April. pp 1185-1188. DOI: 10.1109/CSNT.2015.186.

Chen B, Xu YL, Qu WL., 2005. Evaluation of atmospheric corrosion damage to steel space structures in coastal areas. *International Journal of Solids and Structures* **42**: 4673-4694. DOI: 10.1016/j.ijsolstr.2005.02.004.

Chuwah C, van Noije T, van Vuuren DP, Stehfest E, Hazeleger W., 2015. Global impacts of surface ozone changes on crop yields and land use. *Atmospheric Environment* **106**: 11-23. DOI: 10.1016/j.atmosenv.2015.01.062.

Cohan DS, Hakami A, Hu Y, Russell AG., 2005. Nonlinear response of ozone to emissions: source apportionment and sensitivity analysis. *Environmental Science & Technology* **39**: 6739-6748. DOI: 10.1021/es048664m.

Cohan DS, Napelenok SL., 2011. Air Quality Response Modeling for Decision Support. *Atmosphere* **2**: 407-425. DOI: 10.3390/atmos2030407.

Colette A, Granier C, Hodnebrog O, Jakobs H, Maurizi A, Nyiri A, Bessagnet B, D'Angiola A, D'lsidoro M, Gauss M, Meleux F, Memmesheimer M, Mieville A, Rouil L, Russo F, Solberg S, Stordal F, Tampieri F., 2011. Air quality trends in Europe over the past decade: a first multi-model assessment, *Atmospheric Chemistry and Physics* **11**: 11657-11678. DOI: 10.5194/acp-11-11657-2011.

Colvile RN, Hutchinson EJ, Mindell JS, Warren RF., 2001. The transport sector as a source of air pollution. *Atmospheric Environment* **35**: 1537-1565. DOI: 10.1016/S1352-2310(00)00551-3.

Commission Directive (EU) 2015/1480 of 28 August 2015 amending several annexes to Directives 2004/107/EC and 2008/50/EC of the European Parliament and of the Council laying down the rules concerning reference methods, data validation and location of sampling points for the assessment of ambient air quality. *Official Journal of the European Union* L 226/4. Available at: < http://eur-lex.europa.eu/legal-content/EN/TXT/PDF/?uri=CELEX:32015L1480&from=EN> [Accessed 20 December 2015].

Cooper OR, Parrish DD, Ziemke J, Balashov NV, Cupeiro M, Galbally IE, Gilge S, Horowitz L, Jensen NR, Lamarque JF, Naik V, Oltmans SJ, Schwab J, Shindell DT, Thompson AM, Thouret V, Wang Y, Zbinden RM., 2014. Global distribution and trends of tropospheric ozone: An observation-based review. *Elementa Science of the Anthropocene* **2**: 000029 DOI: 10.12952/journal.elementa.000029.

Cooper OR, Langford AO, Parrish DD, Fahey DW., 2015. Challenges of a lowered U.S. ozone standard. *Science* **348**: 1096-1097. DOI: 10.1126/science.aaa5748.

Costa M, Baldasano JM., 1996. Development of a source emission model for atmospheric pollutants in the Barcelona area. *Atmospheric Environment* **30**: 309-318. DOI: 10.1016/1352-2310(95)00221-J.

Cristofanelli P, Bonasoni P., 2009. Background Ozone in the southern Europe and Mediterranean area: influence of the transport processes. *Environmental Pollution* **157**: 1399-1406. DOI: 10.1016/j.envpol.2008.09.017.

Cuvelier C, Thunis P, Karam D, Schaap M, Hendriks C, Kranenburg R, Fagerli H, Nyiri A, Simpson D, Wind P, Bessagnet B, Colette A, Terrenoire E, Rouil L, Stern R, Graff A, Baldasano JM, Pay MT., 2013. ScaleDep: Performance of European chemistry-

transport models as function of horizontal spatial resolution. EMEP - Technical Report 1/2013. 63 pp. Available at: < http://emep.int/publ/reports/2013/MSCW_technical_1_2013.pdf> [Accessed 20 December 2015].

Davis DL, Bell ML, Fletcher T., 2002. A Look Back at the London Smog of 1952 and the Half Century Since. *Environmental Health Perspectives* **110**: A374-A375. DOI: 10.1289/ehp.110-a734.

Dayan U, Levy I., 2005. The influence of meteorological conditions and atmospheric circulation types on PM10 and visibility in Tel Aviv. *Journal of Applied Meteorology* **44**: 606-619. DOI: /10.1175/JAM2232.1.

Dayan U, Tubi A, Levy I., 2012. On the importance of synoptic classification methods with respect to environmental phenomena. *International Journal of Climatology* **32**: 681-694. DOI: 10.1002/joc.2297.

De Pablo F, Tomás C, Rivas Soriano L, Diego L, 2008. Winter circulation weather types and hospital admissions for cardiovascular, respiratory and digestive diseases in Salamanca, Spain. *International Journal of Climatology* **29**: 1692-1703. DOI: 10.1002/joc.1802.

De Pablo F, Rivas Soriano L, Sánchez Llorente JM, Nájera López A., 2013. Effects of weather types on hospital admissions for respiratory diseases in Castilla-La Mancha, Spain. *Atmósfera* **26**: 95-107. DOI: 10.1016/S0187-6236(13)71064-6.

De Vries W, Dobbertin MH, Solberg S, van Dobben HF, Schaub M., 2014. Impacts of acid deposition, ozone exposure and weather conditions on forest ecosystems in Europe: an overview. *Plant and Soil* **380**: 1-45. DOI: 10.1007/s11104-014-2056-2.

Dee DP, Uppala SM, Simmons AJ, Berrisford P, Poli P, Kobayashi S, Andrae U, Balmaseda MA, Balsamo G, Bauer P, Bechtold P, Beljaars ACM, van de Berg L, Bidlot J, Bormann N, Delsol C, Dragani R, Fuentes M, Geer AJ, Haimberger L, Healy SB, Hersbach H, Hólm EV, Isaksen L, Kållberg P, Köhler M, Matricardi M, McNally AP, Monge-Sanz BM, Morcrette JJ, Park BK, Peubey C, de Rosnay P, Tavolato C, Thépaut JN, Vitart F., 2011. The ERA-Interim reanalysis: configuration and performance of the data assimilation system. *Quarterly Journal of the Royal Meteorological Society* **137:** 553-597. DOI: 10.1002/qj.828.

Demuzere M, Trigo RM, Vila-Guerau de Arellano J, van Lipzig NPM., 2009. The impact of weather and atmospheric circulation on O_3 and PM10 levels at a rural mid-latitude site. *Atmospheric Chemistry and Physics* **9:** 2695-2714. DOI: 10.5194/acp-9-2695-2009.

Demuzere M, Kassomenos P, Philipp A., 2011. The COST733 circulation type classification software: an example for surface ozone concentrations in Central Europe. *Theoretical and Applied Climatology* **105:** 143-166. DOI: 10.1007/s00704-010-0378-4.

Dennis R, Fox T, Fuentes M, Gilliland A, Hanna S, Hogrofe C, Irwin J, Trivikrama R, Scheffe R, Schere K, Steyn D, Venkatram A., 2010. A framework for evaluating regional-scale numerical photochemical modeling systems. *Environmental Fluid Mechanics* **10**: 417-489. DOI: 10.1007/s10652-009-9163-2.

DGT, Dirección General de Tráfico., 2015. Parque de vehículos por ccaa, provincias y tipos., 2012. Available at: <http://www.dgt.es/Galerias/seguridad-vial/estadisticas-e-indicadores/parque-vehiculos/prov-y-tipos-vehiculos/V.4-y-V.4.C.A_parque-x-prov.-y-CC.AA-2012.xls> [Accessed 20 December 2015].

Directive 2001/81/EC of the European Parliament and of the Council of 23 October 2001 on national emission ceilings for certain atmospheric pollutants. *Official Journal of the European Union* L 309/22. Available at: <http://eur-lex.europa.eu/LexUriServ/LexUriServ.do?uri=OJ:L:2001:309:0022:0030:EN:PDF > [Accessed 20 December 2015].

Directive 2008/50/EC of the European Parliament and of the Council of 21 May 2008 on ambient air quality and cleaner air for Europe. *Official Journal of the European Union* L 24/8. Available at: < http://eur-lex.europa.eu/legal-content/EN/TXT/PDF/?uri=CELEX:32008L0001&from=EN> [Accessed 20 December 2015].

Directive 2008/1/EC of the European Parliament and of the Council of 15 January 2008 concerning integrated pollution prevention and control. *Official Journal of the European Union* L 152/1. Available at: <http://eur-lex.europa.eu/LexUriServ/LexUriServ.do?uri=OJ:L:2008:152:0001:0044:EN:PDF > [Accessed 20 December 2015].

Downey N, Emery C, Jung J, Sakulyanontvittaya T, Hebert L, Blewitt D, Yarwood G., 2015. Emission reductions and urban ozone responses under more stringent US standards. *Atmospheric Environment* **101**: 209-216. DOI: 10.1016/j.atmosenv.2014.11.018.

Draxler RR, Rolph GD., 2013. HYSPLIT (HYbrid Single-Particle Lagrangian Integrated Trajectory) Model access via NOAA ARL READY Website (http://www.arl.noaa.gov/HYSPLIT.php). NOAA Air Resources Laboratory, College Park, MD.

ECMWF, European Centre for Medium-Range Weather Forecast. ERA-Interim reanalysis webserver: < http://apps.ecmwf.int/datasets/data/interim-full-daily > [Accessed 20 December 2015].

EEA, European Environmental Agency., 2009. EMEP/EEA emission inventory guidebook 2009. 1.a.3.b.v Gasoline evaporation. 30 pp. Available at: <http://www.eea.europa.eu/publications/emep-eea-emission-inventory-guidebook-2009/part-b-sectoral-guidance-chapters/1-energy/1-a-combustion/1.a.3.b-road-transport-gb2009-update.pdf>. [Accessed 1st December2015].

EEA, European Environmental Agency., 2011. The application of models under the European Union's Air Quality Directive: A technical reference guide. EEA Technical report 10/2011. EEA, Copenhagen, 72 pp. DOI: 10.2800/80600.

EEA, European Environmental Agency., 2012. Particulate matter from natural sources and related reporting under the EU Air Quality Directive in 2008 and 2009. Technical Report 10/2012. EEA, Copenhagen, 43 pp. DOI: 10.2800/55574.

EEA, European Environmental Agency., 2013. EEA Report No 3/2013. Air pollution by ozone across Europe during summer 2012. 48 pp. DOI: 10.2800/70933.

EEA, European Environmental Agency., 2014a. EEA Report No 5/2014. Air quality in Europe – 2014 report. 80 pp. DOI: 10.2800/22775.

EEA, European Environmental Agency., 2014b. Air pollution fact sheet 2014. Spain., 20 pp. Available at: <http://www.eea.europa.eu/themes/air/air-pollution-country-fact-sheets-2014/spain-air-pollutant-emissions-country-factsheet/at_download/file> [Accessed 20 December 2015].

Elminir HK., 2005. Dependence of urban air pollutants on meteorology. *Science of the Total Environment* **350:** 225-237. DOI: 10.1016/j.scitotenv.2005.01.043.

EMEP, 2015. Convention on Long-range Transboundary Air Pollution. Status Report 1/2015. Transboundary particulate matter, photo-oxidants, acidifying and eutrophying components. 228 pp. Available at: <http://emep.int/publ/reports/2015/EMEP_Status_Report_1_2015.pdf> [Accessed 20 December 2015].

Emery C, Jung J, Downey N, Johnson J, Jimenez M, Yarwood G, Morris R., 2012. Regional and global modeling estimates of policy relevant background ozone over the United States. *Atmospheric Environment* **47**: 206-217. DOI: 10.1016/j.atmosenv.2011.11.012.

Emmons LK, Walters S, Hess PG, Lamarque JF, Pfister GG, Fillmore D, Granier C, Guenther A, Kinnison D, Laepple T, Orlando J, Tie X, Tyndall G, Wiedinmyer C,

Baughcum SL, Kloster S., 2010. Description and evaluation of the Model for Ozone and Related chemical Tracers, version 4 (MOZART-4). *Geoscientific Model Development* **3**: 43-67. DOI :10.5194/gmd-3-43-2010, 2010.

EnAcc, Ecologistas en Acción en colaboración con la Fundación Biodiversidad., 2013. La calidad del aire en el estado español durante 2012. 77 pp. Available at: < http://www.ecologistasenaccion.org/IMG/pdf/informe_calidad_aire_2012.pdf> [Accessed 20 December 2015].

Enke W, Spekat A., 1997. Downscaling climate model outputs into local and regional weather elements by classification and regression. *Climate Research* **8**: 195-207. DOI: 10.3354/cr008195.

Erpicum M, Mabille G, Fettweis X., 2008. Automatic synoptic weather circulation types classification based on the 850 hPa geopotential height. In: Book of Abstracts COST 733 Mid-term Conference, Advances in Weather and Circulation Type Classifications & Applications, Krakow (Poland). 22-25 October. 33 pp.

Esteban P, Jones PD, Martín-Vide J, Moses M., 2005. Atmospheric circulation patterns related to heavy snowfall in Andorra, Pyrenees. *International Journal of Climatology* **25:** 319-329. DOI: 10.1002/joc.1103.

Esteban P, Martín-Vide P, Mases M., 2006. Daily atmospheric circulation catalogue for Western Europe using multivariate techniques. *International Journal of Climatology* **26**: 1501-1515. DOI: 10.1002/joc.1391.

Felzer BS, Cronin T, Reilly JM, Melillo JM, Wang X., 2007. Impacts of ozone on trees and crops. *Comptes Rendus Geosciences* **339**: 784-798. DOI: 10.1016/j.crte.2007.08.008.

Fereday D, Knight J, Scaife A, Folland C., 2008. Cluster analysis of North Atlantic-European circulation types and links with tropical Pacific Sea surface temperatures. *Journal of Climate* **21:** 3687-3703. DOI: 0.1175/2007JCLI1875.1.

Fernández-Montes S, Rodrigo FS, Seubert S, Sousa PM., 2012. Spring and summer extreme temperatures in Iberia during last century in relation to circulation types. In Press. *Atmospheric Research* **127**: 154-177. DOI: 10.1016/j.atmosres.2012.07.013.

Fettweis X, Mabille G, Erpicum M, Van den Broeke M, Nicolay S., 2010. The 1958–2008 Greenland ice sheet surface melt and the mid-tropospheric atmospheric circulation. *Climate Dynamics* **36**: 139-159. DOI: 10.1007/s00382-010-0772-8.

Fleig AK, Tallaksen LM, Hisdal H, Stahl K, Hannah DM., 2010. Inter-comparison of weather and circulation type classifications for hydrological drought development. *Physics and Chemistry of the Earth, Parts A/B/C* **35**: 507-515. DOI: 10.1016/j.pce.2009.11.005.

Flocas H, Kelessis A, Helmis C, Petrakakis M, Zoumakis M, Pappas K., 2009. Synoptic and local scale atmospheric circulation associated with air pollution episodes in an urban Mediterranean area. *Theoretical and Applied Climatology* **95:** 265-277. DOI: 10.1007/s00704-008-0005-9.

Franco V, Posada-Sánchez F, German J, Mock P., 2014. Real-world exhaust emissions from modern diesel cars. A meta-analysis of PEMS emissions data from EU (EURO 6) and US (Tier 2 Bin 5/ULEV II) diesel passenger cars. Part 1: Aggregated results. The International County on Clean Transportation White Paper. 53 pp. Available at: <http://www.theicct.org/sites/default/files/publications/ICCT_PEMS-study_diesel-cars_20141010.pdf>. [Accessed: 1st December2015].

Galmarini S, Kioutsioukis I, Solazzo E., 2013. E Pluribus Unum: ensemble air quality predictions. *Atmospheric Chemistry and Physics* **13:** 7153-7182. DOI: 10.5194/acp-13-7153-2013.

Gangoiti G, Millán MM, Salvador R, Mantilla E., 2001. Long-range transport and re-circulation of pollutants in the western Mediterranean during the project Regional Cycles of Air Pollution in the West-Central Mediterranean Area. *Atmospheric Environment* **35**: 6267-6276. DOI: 10.1016/S1352-2310(01)00440-X.

Ganor E, Osentinsky I, Stupp A, Alpert P., 2010. Increasing trend of African dust, over 49 years, in the eastern Mediterranean. *Journal of Geophysical Research* **115:** D07201. DOI: 10.1029/2009JD012500.

García-Bustamante E, González-Rouco J, Navarro J, Xoplaki E, Jiménez P, Montávez J., 2012. North Atlantic atmospheric circulation and surface wind in the northeast of the Iberian Peninsula: uncertainty and long term downscaled variability. *Climate Dynamics* **38:** 141-160. DOI: 10.1007/s00382-010-0969-x.

García-Valero JA, Montávez JP, Jérez S, Gómez-Navarro JJ, Lorente-Plazas R, Jiménez-Guerrero P., 2012. A seasonal study of the atmospheric dynamics over the Iberian Peninsula based on circulation types. *Theoretical and Applied Climatology* **110:** 219-310. DOI: 10.1007/s00704-012-0623-0.

Gimeno L, Hernández E, Rúa A, García R, Martín I., 1999a. On the origin of the elevated ozone concentration in Spain. *Physics and Chemistry of the Earth, Part C Solar Terrestrial & Planetary Science* **24**: 527-530. DOI: 10.1016/S1464-1917(99)00085-9.

Gimeno L, Hernández E, Rúa A, García R, Martín I., 1999b. Geographical Sources of Ozone Concentrations in Spain. *Physics and Chemistry of the Earth, Part C Solar Terrestrial & Planetary Science* **24**: 523-526. DOI: 10.1016/S1464-1917(99)00084-7.

Giorgi F, Meleux F., 2007. Modelling the regional effects of climate change on air quality. *Comptes Rendus Geoscience* **339:** 721-733. DOI: 10.1016/j.crte.2007.08.006.

Gkikas A, Houssos EE, Hatzianastassiou N, Papadimas CD, Barzokas A., 2012. Synoptic conditions favouring the occurrence of aerosol episodes over the broader Mediterranean basin. *Quarterly Journal of the Royal Meteorological Society* **138**: 932-949. DOI: 10.1002/qj.978.

Gonçalves M, Jiménez-Guerrero P, López E, Baldasano JM., 2008. Air quality models sensitivity to on-road traffic speed representations: Effects on air quality of 80 km h^{-1} speed limit in the Barcelona Metropolitan area. *Atmosferic Environment* **42**: 8389-8402. DOI: 10.1016/j.atmosenv.2008.08.022.

Gonçalves M, Jiménez-Guerrero P, Baldasano JM., 2009. Contribution of atmospheric processes affecting the dynamics of air pollution in South-Western Europe during a typical summertime photochemical episode. *Atmospheric Chemistry and Physics* **9**: 849-864. DOI: 10.5194/acp-9-849-2009.

Gonçalves M, Piot M, Jorba O, Pay MT, Gassó S, Baldasano JM., 2010. Near Real Time Evaluation System of the Spanish Air Quality Forecasting System CALIOPE. *Geophysical Research Abstracts* **12**: EGU2010-5266-2. Available at: <http://meetingorganizer.copernicus.org/EGU2010/EGU2010-5266-2.pdf> [Accessed 20 December 2015].

Gonçalves M, Dabdub D, Chang WL, Jorba O, Baldasano JM., 2012. Impact of HONO sources on the performance of mesoscale air quality models. *Atmospheric Environment* **54**: 168-178. DOI: 10.1016/j.atmosenv.2012.02.079.

González RM, Marrero G, Rodríguez-López J., 2014. Dieselization, emissions and rebound effect in cars: theory and applications to Europe. Barcelona (Spain), 8 May. Seminari de la Càtedra de Sostenibilitat Energètica. Institut d'Economia de Barcelona. Available at: <http://www.ieb.ub.edu/files/Marrero.pdf> [Accessed 1 December 2015].

Greene JS, Kalkstein LS, Ye H, Smoyer K., 1999. Relationships between synoptic climatology and atmospheric pollution at 4 US cities. *Theoretical and Applied Climatology* **62**: 163-174. DOI: 10.1007/s007040050081.

Grundström M, Tang L, Hallquist M, Nguyen H, Chen D, Pleijel H., 2015. Influence of atmospheric circulation patterns on urban air quality during the winter. *Atmospheric Pollution Research* **6**: 278-285. DOI: 10.5094/APR.2015.032.

Guenther A, Karl T, Harley P, Wiedinmyer C, Palmer P, Geron C., 2006. Estimates of global terrestrial isoprene emissions using MEGAN (Model of Emissions of Gases

and Aerosols from Nature). *Atmospheric Chemistry and Physics* **6**: 3181-3210. DOI: 10.5194/acp-6-3181-2006.

Guerreiro CBB, Foltescu V, de Leeuw F., 2014. Air quality status and trends in Europe. *Atmospheric Environment* **98**: 376-384. DOI: 10.1016/j.atmosenv.2014.09.017

Guevara M, Martínez F, Arévalo G, Gassó S, Baldasano JM., 2013. An improved system for modelling Spanish emissions: HERMESv2.0. *Atmospheric Environment* **81:** 209-221. DOI: 10.1016/j.atmosenv.2013.08.053.

Guevara M, Soret A, Martínez F, Baldasano JM., 2014a. Modelling and implementation of fugitive dust emissions caused by wind erosion and agricultural activities. 16th GEIA Conference: Bridging Emissions Science and Policy, Boulder, Colorado, (USA). 10-11 June.

Guevara M, Soret A, Arévalo G, Martínez F, Baldasano JM., 2014b. Implementation of plume rise and its impacts on emissions and air quality modelling. *Atmospheric Environment* **99:** 618-629. DOI: 10.1016/j.atmosenv.2014.10.029.

Guevara M, Pay MT, Martínez F, Soret A, van der Gon HD, Baldasano JM 2014c. Inter-comparison between HERMESv2.0 and TNO-MACC-II emission data using the CALIOPE air quality system (Spain). *Atmospheric Environment* **98**: 134-145. DOI: 10.1016/j.atmosenv.2014.08.067.

Gurjar BR, Jain A, Sharma A, Agarwal A, Gupta P, Nagpure AS, Lelieveld J., 2010. Human health risks in megacities due to air pollution. *Atmospheric Environment* **44**: 4606-4613. DOI: 10.1016/j.atmosenv.2010.08.011.

Haagen-Smit AJ., 1952. Chemistry and Physiology of Los Angeles Smog. *Industrial & Engineering Chemistry* **44**: 1342-1346. DOI: 10.1021/ie50510a045.

Hand E., 2014. China blamed for U.S. ozone. *Science* **345**: 1233. DOI: 10.1126/science.345.6202.1233.

Hauglustaine DA, Hourdin F, Jourdain L, Filiberti MA,Walters S, Lamarque JF, Holland EA., 2004. Interactive chemistry in the Laboratoire de Meteorologie Dynamique general circulation model: description and background tropospheric chemistry evaluation. *Journal of Geophysics Research* **109**: D04314. DOI: 10.1029/2003JD003957.

Heal MR, Heaviside C, Doherty RM, Vieno M, Stevenson DS, Vardoulakis S., 2013. Health burdens of surface ozone in the UK for a range of future scenarios. *Environment International* **61**: 36-44. DOI: 10.1016/j.envint.2013.09.010.

Hellmann G., 1908. The dawn of meteorology. *Quarterly Journal of the Royal Meteorological Society* **34**: 221-232. DOI: 10.1002/qj.49703414802.

Henschel S, Le Tertre A, Atkinson RW, Querol X, Pandolfi M, Zeka A, Haluza D, Analitis A, Katsouyanni K, Bouland C, Pascal M, Medina S, Goodman PG., 2015. Trends of nitrogen oxides in ambient air in nine European cities between 1999 and 2010. *Atmospheric Environment* **117**: 234-241. DOI: 10.1016/j.atmosenv.2015.07.013.

Hernández JF, Cremades L, Baldasano JM., 1995. Dispersion modelling of a tall stack plume in the Spanish Mediterranean Coast by a particle model. *Atmospheric Environment* **29**: 1331-1341. DOI: 10.1016/1352-2310(94)00346-M.

Hernández JF, Cremades L, Baldasano JM., 1997. Simulation of tracer dispersión from elevated and Surface releases in complex terrain. *Atmospheric Environment* **31**: 2337-2348. DOI: 10.1016/S1352-2310(97)00027-7.

Hess P, Brezowsky H., 1952. Katalog der Großwetterlagen Europas (Catalog of the European Large Scale Weather Types). Berichte des Deutschen Wetterdienstes in der US-Zone 33. Bad Kissingen (Germany). 40 pp.

Hu Y, Chang ME, Russell AG, Talat-Odman M., 2010. Using synoptic classification to evaluate an operational air quality forecasting system in Atlanta. *Atmospheric Pollution Research* **1**: 280-287. DOI: 10.5094/APR.2010.035

Huth R., 1996. An intercomparison of computer assisted circulation classification methods. *International Journal of Climatology* **16**: 893-922. DOI: 10.1002/(SICI)1097-0088(199608)16:8<893::AID-JOC51>3.0.CO;2-Q.

Huth R, Beck C, Philipp A, Demuzere M, Ustrnul Z, Cahynová M, Kyselý J, Tveito OE., 2008. Classifications of atmospheric circulation patterns: recent advances and applications. *Annals of the New York Academy of Science* **1146:** 105-152. DOI: 10.1196/annals.1446.019.

Huth R., 2010. Synoptic-climatological applicability of circulation classifications from the COST733 collection: First results. *Physics and Chemistry of the Earth, Parts A/B/C* **35**: 388-394. DOI: 10.1016/j.pce.2009.11.013.

Hyslop NP, White WH., 2008. An evaluation of interagency monitoring of protected visual environments (IMPROVE) collocated precision and uncertainty estimates. *Atmospheric Environment* **42**: 2691-2705. DOI: 10.1016/j.atmosenv.2007.06.053.

Im U and 41 other authors., 2014. Evaluation of operational on-line-coupled regional air quality models over Europe and North America in the context of AQMEII phase 2. Part I: Ozone. *Atmospheric Environment* **115** 404-420. DOI: 10.1016/j.atmosenv.2014.09.042.

Inness A, Baier F, Benedetti A, Bouarar I, Chabrillat S, Clark H, Clerbaux C, Coheur P, Engelen RJ, Errera Q, Flemming J, George M, Granier C, Hadji-Lazaro J, Huijnen V, Hurtmans D, Jones L, Kaiser JW, Kapsomenakis J, Lefever K, and Leitão J,

Razinger M, Richter A, Schultz MG, Simmons AJ, Suttie M, Stein O, Thépaut JN, Thouret V, Vrekoussis M, Zerefos C, the MACC team., 2013. The MACC reanalysis: an 8 yr data set of atmospheric composition. *Atmospheric Chemistry and Physics* **13**: 4073-4109. DOI: 10.5194/acp-13-4073-2013.

IPCC, Intergovernmental Panel on Climate Change., 2014: Climate Change 2014: Synthesis Report. Contribution of Working Groups I, II and III to the Fifth Assessment Report of the Intergovernmental Panel on Climate Change. IPCC, Geneva, Switzerland, 151 pp. Available at: <http://www.ipcc.ch/pdf/assessment-report/ar5/syr/SYR_AR5_FINAL_full.pdf>. [Accessed 20 December 2015].

Izquierdo R, Ávila A, Alarcón M., 2012. Trajectory statistical analysis of atmospheric transport patterns and trends in precipitation chemistry of a rural site in NE Spain in 1984-2009 *Atmospheric Environment* **51**: 400-408. DOI: 10.1016/j.atmosenv.2012.07.060.

Jacob D, Winner D., 2009. Effect of climate change on air quality. *Atmospheric Environment* **43**: 51-63. DOI: 10.1016/j.atmosenv.2008.09.051.

Jacobson MZ., 2005. Fundamentals of Atmospheric Modeling. 2nd Edition. Cambridge University Press. 828 pp.

Jamason PF, Kalkstein LS, Gergen PJ., 1997. A synoptic evaluation of asthma hospital admissions in New York City. *American Journal of Respiratory and Critical Care Medicine* **156**:1781-1788. DOI: 10.1164/ajrccm.156.6.96-05028.

James P., 2007. An objective classification method for Hess and Brezowsky Grosswetterlagen over Europe. *Theoretical and Applied Climatology* **88:** 17-42. DOI: 10.1007/s00704-006-0239-3.

Jenkinson AF, Collison BP., 1977. An Initial Climatology of Gales Over the North Sea. Synoptic Climatology Branch Memorandum No. 62. Meteorological Office, London (UK). 18 pp.

Jerrett M, Burnett RT, Pope III CA, Ito K, Thurston G, Krewski D, Shi Y, Calle E, Thun M., 2009. Long-Term Ozone Exposure and Mortality. *The New England Journal of Medicine* **360**: 1085-1095. DOI: 10.1056/NEJMoa0803894.

Jiménez P, Baldasano JM., 2004. Ozone response to precursor controls in very complex terrains: Use of photochemical indicators to assess O_3-NO_x-VOC sensitivity in the northeastern Iberian Peninsula. *Journal of Geophysical Research* **109**, D20309. DOI: 10.1029/2004JD004985.

Jiménez P, Jorba O, Parra R, Baldasano JM., 2005. Influence of high-model gird resolution on photochemical modelling in very complex terrains. *International Journal of Environment and Pollution* **24**: 180-200. DOI: 10.1504/IJEP.2005.007393.

Jiménez P, Jorba O, Parra R, Baldasano JM., 2006a. Evaluation of MM5-EMICAT2000-CMAQ performance and sensitivity in complex terrain: High-resolution application to thenortheastern Iberian Peninsula. *Atmospheric Environment* **40**: 5056-5072. DOI: 10.1016/j.atmosenv.2005.12.060.

Jiménez P, Lelieveld J, Baldasano JM., 2006b. Multiscale modelling of air pollutants dynamics in the northwestern Mediterranean basin during a typical summertime episode. *Journal of Geophysical Research* **111**: 1-21. DOI: 10.1029/2005JD006516

Jiménez PA, González-Rouco JF, Montávez JP, García-Bustamante E, Navarro J., 2009. Climatology of wind patterns in the northeast of the Iberian Peninsula. *International Journal of Climatology* **29:** 501-525. DOI: 10.1002/joc.1705.

Jiménez-Guerrero P, Jorba O, Baldasano JM, Gassó S., 2008. The use of a modelling system as a tool for air quality management: Annual high-resolution simulations and evaluation. *Science of the Total Environment* **390:** 323-340. DOI: 10.1016/j.scitotenv.2007.10.025.

Jorba O, Pérez C, Rocadenbosch F, Baldasano JM., 2004. Cluster Analysis of 4-Day Back Trajectories Arriving in the Barcelona Area, Spain, from 1997 to 2002. *Journal of Applied Meteorology* **43**: 887-901. DOI: 10.1175/1520-0450(2004)043<0887:CAODBT>2.0.CO;2.

Kadijk G, Ligterink NE, Spreen JS., 2015. On-road NO_x and CO_2 investigations of Euro 5 Light commercial vehicles. TNO Report 2015 R10192. 26 pp. Available at: <http://publications.tno.nl/publication/34618579/1enV8D/TNO-2015-R10192.pdf> [Accessed: 1st December2015].

Kannari A, Tonooka Y, Baba T, Murano K., 2007. Development of multiple-species resolution hourly basis emissions inventory for Japan. *Atmospheric Environment* **41**: 3428-3439. DOI: 10.1016/j.atmosenv.2006.12.015.

Kassomenos PA, Flocas HA, Lykoudis S, Skouloudis A., 1998. Spatial and temporal characteristics of the relationship between air quality status and mesoscale circulation over an urban Mediterranean basin. *Science of The Total Environment* **217**: 37-57. DOI: 10.1016/S0048-9697(98)00167-3.

Kassomenos P., 2010. Synoptic circulation control on wild fire occurrence. *Physics and Chemistry of the Earth, Parts A/B/C* **35**: 544-552. DOI: 10.1016/j.pce.2009.11.008.

Kirchhofer W., 1974. Classification of European 500 mb patterns. Working Reports of the Swiss Meteorological Institute. Zürich (Switzerland). 16 pp.

Kruizinga S., 1979. Objective classification of daily 500 mbar patterns. In: Preprints Sixth Conference on Probability and Statistics in Atmospheric Sciences, Banff, Alberta. American Meteorological Society, Boston, Massachussetts (USA). 126-129 pp.

Kucera V, Fitz S., 1995. Direct and indirect air pollution effects on materials including cultural monuments. *Water, Air and Soil Pollution* **85**: 153-165. DOI: 10.1007/BF00483697.

Kuebler J, Russell AG, Hakami A, Clappier A, van den Bergh H., 2002. Episode selection for ozone modelling and control strategies analysis on the Swiss Plateau. *Atmospheric Environment* **36**: 2817-2830. DOI: 10.1016/S1352-2310(02)00155-3.

Künzli N, Kaiser R, Medina S, Studnicka M, Chanel O, Filliger P, Herry M, Horak Jr F, Puybonnieux-Texier V, Quénel P, Schneider J, Seethaler R, Vergnaud JC, Sommer H., 2010. Public-health impact of outdoor and traffic-related air pollution: a European assessment. *The Lancet* **356**: 795-801. DOI: 10.1016/S0140-6736(00)02653-2.

Kwok RHF, Napelenok SL, Baker KR., 2013. Implementation and evaluation of PM2.5 source contribution analysis in a photochemical model. *Atmospheric Environment* **80**: 398-407. DOI: 10.1016/j.atmosenv.2013.08.017.

Kwok RHF, Baker KR, Napelenok SL, Tonnesen GS., 2015. Photochemical grid model implementation and application of VOC, NO_x, and O_3 source apportionment. *Geoscientific Model Development* **8**: 99-114. DOI: 10.5194/gmd-8-99-2015.

Lamb HH., 1972. Climate: Present, Past and Future. Volume 1: Fundamentals and climate now. Methuen, London (UK) 613 pp.

Lelieveld J, Evans JS, Fnais M, Giannadaki D, Pozzer A., 2014. The contribution of outdoor air pollution sources to premature mortality on a global scale. *Nature* **525**: 367-371. DOI: 10.1038/nature15371.

Ley 34/2007, de 15 de noviembre, de calidad del aire y protección de la atmósfera. Boletín Oficial del Estado **275**: 46962-46987 de 16/11/2007. Available at: <http://www.boe.es/buscar/act.php?id=BOE-A-2007-19744> [Accessed 20 December 2015].

Li GY, Koenig JL., 2005. A Review of Rubber Oxidation. *Rubber Chemistry and Technology* **78**: 355-390. DOI: 10.5254/1.3547889.

Li X, Choi Y, Czader B, Kim H, Lefer B, Pan S., 2015. The impact of observation nudging on simulated meteorology and ozone concentrations during DISCOVER-AQ 2013 Texas campaign. *Atmospheric Chemistry and Physics Discussions* **15**: 27357-27404. DOI: 10.5194/acpd-15-27357-2015.

Lin M, Fiore AM, Horowitz LW, Langford AO, Oltmans SJ, Tarasick D, Rieder HE., 2015. Climate variability modulates western US ozone air quality in spring via deep stratospheric intrusions. *Nature Communications* **6**: 7105. DOI: 10.1038/ncomms8105.

Liu B, Wang DW, Guo H, Ling ZH, Cheung K., 2014. Metallic corrosion in the polluted urban atmosphere of Hong Kong. *Environmental Monitoring and Assessment* **187**: 4111-4122. DOI: 10.1007/s10661-014-4112-z.

Lovett GM, Tear TH, Evers DC, Findlay SEG, Cosby BJ, Dunscomb JK, Driscoll CT, Weathers KC., 2009. Effects of Air Pollution on Ecosystems and Biological Diversity in the Eastern United States. *Annals of the New York Academy of Sciences* **1162**: 99-135. DOI: 10.1111/j.1749-6632.2009.04153.x.

Lund IA., 1963. Map-Pattern Classification by Statistical Methods. *Journal of Applied Meteorology* **2**: 56-65. DOI: 10.1175/1520-0450(1963)002<0056:MPCBSM>2.0.CO;2.

Luecken DJ, Phillips S, Sarwar G, Jang C., 2008. Effects of using the CB05 vs. SAPRC99 vs. CB4 chemical mechanism on model predictions: Ozone and gas-phase photochemical precursor concentrations. *Atmospheric Environment* **42**: 5805-5820. DOI: 10.1016/j.atmosenv.2007.08.056.

MAGRAMA, Ministerio de Agricultura, Alimentación y Medio Ambiente., 2013a. Plan Nacional de Calidad del Aire y Protección de la Atmósfera 2013-2016 – Plan Aire. 212 pp. Available at: < http://www.magrama.gob.es/es/calidad-y-evaluacion-ambiental/temas/atmosfera-y-calidad-del-aire/PLAN_AIRE_2013-2016_tcm7-271018.pdf> [Accessed 20 December 2015].

MAGRAMA, Ministerio de Agricultura, Alimentación y Medio Ambiente., 2013b. Análisis de la calidad del aire en España. Evolución 2001-2012. Available at: <http://www.magrama.gob.es/es/calidad-y-evaluacion-ambiental/temas/atmosfera-y-calidad-del-aire/Analisis_calidad_aire_Espa%C3%B1a_2001_2012_WEB_tcm7-311112.pdf> [Accessed 20 December 2015].

MAGRAMA, Ministerio de Agricultura, Alimentación y Medio Ambiente., 2014. Inventarios Nacionales de Emisiones a la Atmósfera 1990-2012. Volumen 2: Análisis por Actividades SNAP. 110 pp. Capítulo 1: combustión en la producción y transformación de energía. Available at: <http://www.magrama.gob.es/es/calidad-y-evaluacion-ambiental/temas/sistema-espanol-de-inventario-sei-/01_Combusti%C3%B3n_en_la_producci%C3%B3n_y_transformaci%C3%B3n_de_energ%C3%ADa_-_VNC_tcm7-219781.pdf> [Accessed 20 December 2015].

MAGRAMA, Ministerio de Agricultura, Alimentación y Medio Ambiente., 2015a Evaluación de la Calidad del Aire en España 2014. 50 pp. Available at: <http://www.magrama.gob.es/es/calidad-y-evaluacion-ambiental/temas/atmosfera-y-calidad-del-

aire/informeevaluacioncalidadaireespana2014_final_tcm7-398522.pdf> [Accessed 20 December 2015].

MAGRAMA, Ministerio de Agricultura, Alimentación y Medio Ambiente., 2015b. Inventario de emisiones de España. Emisiones de gases en el marco de la Directiva de Techos Nacionales de Emisión (serie 1990-2013). Sumario de resultados. Available at: <http://www.magrama.gob.es/es/calidad-y-evaluacion-ambiental/temas/sistema-espanol-de-inventario-sei-/3__Sumario_inventario_Techos_Espa%C3%B1a_-_Serie_1990-2013-Def_tcm7-362873.pdf> [Accessed 20 December 2015].

Manders AMM, van Meijgaard E, Mues AC, Kranenburg R, van Ulft LH, SchaapM., 2012. The impact of differences in large-scale circulation output from climate models on the regional modeling of ozone and PM. *Atmospheric Chemistry and Physics* **12**: 9441-9458. DOI: 10.5194/acp-12-9441-2012.

Mangia C, Cervino M, Gianicolo EAL., 2015. Secondary Particulate Matter Originating from an Industrial Source and Its Impact on Population Health. *International Journal of Environmental Research and Public Health* **12**: 7667-7681. DOI:10.3390/ijerph120707667.

Mani M, Pillai R., 2010. Impact of dust on solar photovoltaic (PV) performance: Research status, challenges and recommendations. *Renewable and Sustainable Energy Reviews* **14**: 3124-3131. DOI: 10.1016/j.rser.2010.07.065.

Marécal V and 58 other authors., 2015. A regional air quality forecasting system over Europe: the MACC-II daily ensemble production. *Geoscientific Model Development Discussion* **8**: 2739-2806. DOI: 10.5194/gmdd-8-2739-2015.

Martín F, Palacios M, Crespi S., 2001. Simulations of mesoscale circulations in the center of the Iberian Peninsula for thermal low pressure conditions. Part I: Evaluation of the topography vorticity-mode mesoscale model. *Journal of Applied Meteorology* **40**: 880–904. DOI: 10.1175/1520-0450(2001)040<0880:SOMCIT>2.0.CO;2.

Martín-Vide J., 1991. Mapas del tiempo: fundamentos, interpretación e imágenes de satélite. Oikos-Tau, Barcelona (Spain). 176 pp.

Martín-Vide J, Olcina J., 2001. *Climas y tiempos de España*. Alianza Editorial: Madrid (Spain). 264 pp.

Menut L, Flamant C, Pelon J., 1999. Evidence of interaction between synoptic and local scales in the surface layer over the Paris area. *Boundary-Layer Meteorology* **93** 269-286. DOI: 10.1023/A:1002013631786.

Menut L, Bessagnet B., 2010. Atmospheric composition forecasting in Europe. *Annales Geophysicae* **28**: 61-74. DOI; 10.5194/angeo-28-61-2010.

MFom, Ministerio de Fomento., 2013. Áreas urbanas +50. Información estadística de las Grandes Áreas Urbanas españolas 2012. 233 pp. Available at: <http://www.fomento.gob.es/MFOM.CP.Web/handlers/pdfhandler.ashx?idpub=BAW013> [Accessed 20 December 2015].

Michelangeli P, Vautard R, Legras B., 1995. Weather regimes: recurrence and quasi stationarity. *Journal of the Atmospheric Sciences* **52:** 1237-1256. DOI: 10.1175/1520-0469(1995)052<1237:WRRAQS>2.0.CO;2.

Millán M, Artíñano B, Alonso L, Navazo M, Castro M., 1991. The effect of the mesoscale flows on regional and long-range atmospheric transport in western Mediterranean area. *Atmospheric Environment* **25A:** 949-963. DOI: 10.1016/0960-1686(91)90137-V.

Millán M, Salvador R, Mantilla E, Artíñano B., 1996. Meteorology and photochemical air pollution in southern Europe: Experimental results from EC research projects. *Atmospheric Environment* **30**: 1906-1924. DOI: 10.1016/1352-2310(95)00220-0.

Millán M, Salvador R, Mantilla E, Kallos G., 1997. Photooxidant dynamics in the Mediterranean basin in summer: results from European research projects. *Journal of Geophysical Research* **102:** 8811-8823. DOI: 10.1029/96JD03610.

Monger JW, Collet J, Daube B, Hoffman MR., 1989. Chemical composition of coastal stratus clouds: dependence on droplet size and distance from the coast. *Atmospheric Environment* **23**: 2305-2320. DOI: 10.1016/0004-6981(89)90192-3.

Monks PS, Granier C, Fuzzi S, Stohl A, Williams ML, Akimoto H, Amann M, Baklanov A, Baltensperger U, Bey I, Blake N, Blake RS, Carslaw K, Cooper OR, Dentener F, Fowler D, Fragkou E, Frost GJ, Generoso S, Ginoux P, Grewe V, Guenther A, Hansson HC, Henne S, Hjorth J, Hofzumahous A, Huntrieser H, Isaksen ISA, Jenkin ME, Kaiser J, Kanakidou M, Klimont Z, Kulmala M, Laj P, Lawrence MG, Lee JD, Liousse C, Maione M, McFiggans G, Metzger A, Mieville A, Moussiopoulos N, Orlando JJ, O'Dowd CD, Palmer PI, Parrish DD, Petzold A, Platt U, Pöschl U, Prévôt ASH, Reeves CE, Reimann S, Rudich Y, Sellegri K, Steinbrecher R, Simpson D, ten Brink H, Theloke J, van der Werf GR, Vautard R, Vestreng V, Vlachokostas Ch, von Glasow R., 2009. Atmospheric composition change – global and regional air quality. *Atmospheric Environment* **43**: 5268-5350. DOI: 10.1016/j.atmosenv.2009.08.021.

Monks PS, Archibald AT, Colette A, Cooper O, Coyle M, Derwent R, Fowler D, Granier C, Law KS, Stevenson DS, Tarasova O, Thouret V, von Schneidemesser E, Sommariva R, Wild O, Williams ML., 2015. Tropospheric ozone and its precursors from the urban to the global scale from air quality to short-lived climate forcer. *Atmospheric Chemistry and Physics* **15**: 8889-8973. DOI: 10.5194/acp-15-8889-2015.

Monteiro A, Carvalho A, Ribeiro I, Scotto M, Barbosa S, Alonso A, Baldasano JM, Pay MT, Miranda AI, Borrego C., 2012. Trends in ozone concentrations in the Iberian Peninsula by quantile regression and clustering. *Atmospheric Environment* **56**: 184-193. DOI: 10.1016/j.atmosenv.2012.03.069.

Morabito M, Crisci A, Grifoni D, Orlandini S, Cecchi L, Bacci L, Modesti PA, Gensini GF, Maracchi G., 2006. Winter air-mass-based synoptic climatological approach and hospital admissions for myocardial infarction in Florence, Italy. *Environmental Research* **102**: 52-60. DOI: 10.1016/j.envres.2005.12.007.

Moulin C, Lambert CE, Dulac F, Dayan U., 1997. Control of atmospheric export of dust from North Africa by the North Atlantic Oscillation. *Nature* **387**: 691-694. DOI: 10.1038/42679.

Müller M, Kašpar M., 2010. Quantitative aspect in circulation type classifications – An example based on evaluation of moisture flux anomalies. *Physics and Chemistry of the Earth, Parts A/B/C* **35**: 484-490. DOI: 10.1016/j.pce.2009.09.004.

Myhre G, Shindell D, Bréon FM, Collins W, Fuglestvedt J, Huang J, Koch D, Lamarque JF, Lee D, Mendoza B, Nakajima T, Robock A, Stephens G, Takemura T, Zhang H., 2013. Anthropogenic and Natural Radiative Forcing. In: Climate Change 2013: The Physical Science Basis. Contribution of Working Group I to the Fifth Assessment Report of the Intergovernmental Panel on Climate Change [Stocker TF, Qin D, Plattner GK, Tignor M, Allen SK, Boschung J, Nauels A, Xia Y, Bex V, Midgley PM (eds.)]. Cambridge University Press, Cambridge, United Kingdom and New York, NY (USA). 659-740 pp. DOI: 10.1017/CBO9781107415324.018.

Nickovic S, Kallos G, Papadopoulos A, Kakaliagou O., 2001. A model for prediction of desert dust cycle in the atmosphere. *Journal of Geophysical Research* **106**: 18113-18130. DOI: 10.1029/2000JD900794.

Nord AG, Tronner K, Boyce A., 2001. Atmospheric bronze and copper corrosion as an environmental indicator. A Study Based on Chemical and Sulphur Isotope Data. *Water, Air and Soil Pollution* **127**: 193-204. DOI: 10.1023/A:1005254913598.

OCEM-CIEMAT: Oficina para el Control de las Emisiones de las Grandes Instalaciones de Combustión (OCEM), Centro de Investigaciones Energéticas, Medioambientales y Tecnológicas (CIEMAT). Spanish National Office of Emission Control for Large Combustion Facilities.

OECD, Organisation for Economic Co-operation and Development., 2012. Environmental Outlook to 2050: The Consequences of Inaction; OECD Publishing: Paris (France). 350 pp. DOI: 10.1787/9789264122246-en.

ORDEN PRE/77/2008, de 17 de enero, por la que se da publicidad al Acuerdo de Consejo de Ministros por el que se aprueba el Plan Nacional de Reducción de Emisiones de las Grandes Instalaciones de Combustión existentes. Available at: <http://www.boe.es/boe/dias/2008/01/28/pdfs/A05061-05090.pdf> [Accessed 20 December 2015].

Palau JL, Pérez-Landa G, Diéguez JJ, Monter C, Millán M.M., 2005. The importance of meteorological scales to forecast air pollution scenarios on coastal complex terrain. *Atmospheric Chemistry and Physics* **5**: 2771-2785. DOI: 10.5194/acp-5-2771-2005.

Palau JL, Pérez-Landa G, Millán M., 2009. Transitional dispersive scenarios driven by mesoscale flows on complex terrain under strong dry convective conditions *Atmospheric Chemistry and Physics* **9**: 119-131. DOI: 10.5194/acp-9-119-2009.

Papanastasious DK, Melas D, Kioutsioukis I., 2007. Development and Assessment of Neural Network and Multiple Regression Models in Order to Predict PM10 Levels in a Medium-sized Mediterranean City. *Water, Air, & Soil Pollution* **182**: 325-334. DOI: 10.1007/s11270-007-9341-0.

Parra R, Jiménez P, Baldasano JM., 2006. Development of the high-spatial resolution EMICAT2000 emission model for air pollutants from the north-eastern Iberian Peninsula (Catalonia, Spain). *Environmental Pollution* **140**: 200-219. DOI: 10.1016/j.envpol.2005.07.021.

Paschalidou AK, Kassomenos PA., 2016. What are the most fire-dangerous atmospheric circulations in the Eastern-Mediterranean? Analysis of the synoptic wildfire climatology. *Science of The Total Environment* **539**: 536-545. DOI: 10.1016/j.scitotenv.2015.09.039.

Pastor MA, Casado MJ., 2012. Evaluación de clasificaciones de tipos de circulación mediante los modos de variabilidad euro-atlánticos. In: Meteorología y Calidad del Aire. Proceedings of XXXII Jornadas Científicas de la Asociación Meteorológica Española. Madrid (Spain). 28-30 May.

Pay MT, Piot M, Jorba O, Gassó S, Gonçalves M, Basart S, Dabdubd D, Jiménez-Guerrero P, Baldasano JM., 2010. A full year evaluation of the CALIOPE-EU air quality system in Europe for 2004. *Atmospheric Environment* **44**: 3322-3342. DOI: 10.1016/j.atmosenv.2010.05.040.

Pay MT, Jiménez-Guerrero P, Jorba O, Basart S, Querol X, Pandolfi M, Baldasano JM., 2012a. Spatio-temporal variability of concentrations and speciation of particulate matter across Spain in the CALIOPE modelling system. *Atmospheric Environment* **46**: 376-396. DOI: 10.1016/j.atmosenv.2011.09.049.

Pay MT, Jiménez-Guerrero P, Baldasano JM., 2012b. Assessing sensitivity regimes of secondary inorganic aerosol formation in Europe with the CALIOPE-EU modelling system. *Atmospheric Environment* **51**: 146-164. DOI: 10.1016/j.atmosenv.2012.01.027.

Pay MT, Gassó S, Baldasano JM., 2012c. Evaluation of the CMAQ5.0 in the framework of the CALIOPE air quality forecasting system over Europe. 11th Annual CMAS Conference, Chapel Hill, NC (USA). 15-17 October. Available at < https://www.cmascenter.org/conference/2012/abstracts/pay_evaluation_cmaq5_2012.pdf>. [Accessed 1st December2015].

Pay MT, Baldasano JM., 2012. Evaluación del sistema de pronóstico de calidad del aire CALIOPE en España para el año 2011. 67 pp. Available at: <http://www.bsc.es/projects/earthscience/visor/bases_datos/image_viewer/docs/20120622_Informe_Evaluacion_CALIOPE_IP_2011.pdf> [Accessed 20 December 2015].

Pay MT, Martínez F, Guevara M, Baldasano JM., 2014a. Air quality at kilometre scale grid over Spanish complex terrains. *Geoscientific Model Development* **7**: 1979-1999. DOI: 10.5194/gmd-7-1979-2014.

Pay MT, Valverde V, Baldasano JM, Kwok R, Napelenok S, Baker K., 2014b. Photochemical modeling to attributing source and source regions to ozone exceedances in Spain. 13th Annual CMAS Conference, Chapel Hill, NC (USA). 27-29 October. Available at: <https://www.cmascenter.org/conference/2014/slides/maria_pay_photochemical_modeling_2014.pptx> [Accessed 20 December 2015].

Pay MT, Valverde V, Baldasano JM., 2015. Evaluating the global contribution from MACC when modelling an ozone episode over Spain. MACC-III Policy User Workshop. Vienna (Austria). 3-4 March. Available at: <https://www.gmes-atmosphere.eu/services/aqac/policy_interface/second_pol_workshop/Pay_03Mar2015.pdf>. [Accessed 1st December2015].

Pérez C, Sicard M, Jorba O, Comerón A, Baldasano JM., 2004. Summertime re-circulations of air pollutants over the north-eastern Iberian coast observed from systematic EARLINET lidar measurements in Barcelona. *Atmospheric Environment* **38:** 3983-4000. DOI: 10.1016/j.atmosenv.2004.04.010.

Pérez C, Nickovic S, Baldasano JM, Sicard M, Rocadenbosch F, Cachorro VE., 2006a. A long Saharan dust event over the western Mediterranean: Lidar, Sun photometer observations, and regional dust modeling. *Journal of Geophysical Research* **111:** D15214. DOI: 10.1029/2005JD006579.

Pérez C, Nickovic S, Pejanovic G, Baldasano JM, Ozsoy E., 2006b. Interactive dust-radiation modeling: A step to improve weather forecasts. *Journal of Geophysical Research* **111:** D16206. DOI: 10.1029/2005JD006717.

Petisco E., 2003. Metodología para una caracterización de la circulación atmosférica en el entorno de la Península Ibérica y Baleares. Nota técnica n 9 del Servicio de Variabilidad y Predicción del Clima. Instituto Nacional de Meteorología, Madrid (Spain). 39 pp.

Petisco SE, Martín JM, Gil D., 2005. Método de estima de precipitación mediante "downscaling". Nota técnica no. 11 del Servicio de Variabilidad y Predicción del Clima, Instituto Nacional de Meteorología, Madrid (Spain). 42 pp.

Pey J, Querol X, Alastuey A, Forastiere F, Stafoggia M., 2012. African dust outbreaks over the Mediterranean Basin during 2001–2011: PM10 concentrations, phenomenology and trends, and its relation with synoptic and mesoscale meteorology. *Atmospheric Chemistry and Physics Discussions*: **12**, 28195-28235. DOI: 10.5194/acpd-12-28195-2012, 2012.

Philipp A, Della-Marta PM, Jacobeit J, Fereday DR, Jones PD, Moberg A, Wanner H., 2007. Long-Term Variability of Daily North Atlantic–European Pressure Patterns since 1850 Classified by Simulated Annealing Clustering. *Journal of Climate* **20:** 4065-4095. DOI: 10.1175/JCLI4175.1.

Philipp A, Bartholy J, Beck C, Erpicum M, Esteban P, Fettweis X, Huth R, James P, Jourdain S, Kreienkamp F, Krennert T, Lykoudis S, Michalides S, Pianko K, Post P, Rasilla Álvarez D, Schiemann R, Spekat A, Tymvios FS., 2010. COST733CAT - a database of weather and circulation type classifications. *Physics and Chemistry of the Earth* **35:** 360-373. DOI: 10.1016/j.pce.2009.12.010.

Philipp A, Beck C, Huth, R, Jacobeit, J., 2014. Development and comparison of circulation type classifications using the COST 733 dataset and software. *International Journal of Climatology*. DOI: 10.1002/joc.3920.

Pineda N, Esteban P, Trapero L, Soler X, Beck C., 2010. Circulation types related to lightning activity over Catalonia and the Principality of Andorra. *Physics and Chemistry of the Earth* **35:** 469-476. DOI: 10.1016/j.pce.2009.12.009.

Pleim, J.E., 2007. A combined local and nonlocal closure model for the atmospheric boundary layer. Part II: Application and evaluation in a mesoscale meteorological model. *Journal of applied Meteorology and Climatology* **46**: 1396-1408. DOI: 10.1175/JAM2534.1.

Pope CA, Ezzati M, Dockery DW., 2009. Fine-Particulate Air Pollution and Life Expectancy in the United States. *The New England Journal of Medicine* **360**: 376-386. DOI: 10.1056/NEJMsa0805646.

Pope RJ, Savage NH, Chipperfield MP, Ordóñez C, Neal LS., 2015. The influence of synoptic weather regimes on UK air quality: regional model studies of tropospheric column NO_2. *Atmospheric Chemistry and Physics* **15**: 11201-11215. DOI: 10.5194/acp-15-11201-2015.

Pratt GC, Hendrickson RC, Chevone BI, Chritopherson DA, O'Brien MV, Krupa SV., 1983. Ozone and oxides of nitrogen in the rural upper-midwestern U.S.A. *Atmospheric Environment* **17**: 2013-2023. DOI: 10.1016/0004-6981(83)90358-X.

Prudhomme C, Genevier M., 2011. Can atmospheric circulation be linked to flooding in Europe? *Hydrological Processes* **25**: 1180-1190. DOI: 10.1002/hyp.7879.

Puig R, Àvila A, Soler A., 2008. Sulphur isotopes as tracers of the influence of a coal-fired power plant on a Scots pine forest in Catalonia (NE Spain). *Atmospheric Environment* **42**: 733-745. DOI: 10.1016/j.atmosenv.2007.09.059.

Putaud JP, Van Dingenen R, Alastuey A, Bauer H, BirmiliW, Cyrys J, Flentje H, Fuzzi S, Gehrig R, Hansson HC, Harrison RM, Herrmann H, Hitzenberger R, Hüglin C, Jones AM, Kasper-Giebl A, Kiss G, Kousa A, Kuhlbusch TAJ, Löschau G, Maenhaut W, Molnar A, Moreno T, Pekkanen J, Perrino C, Pitz M, Puxbaum H, Querol X, Rodríguez S, Salma I, Schwarz J, Smolik J, Schneider J, Spindler G, ten Brink H, Tursic J, Viana M, Wiedensohler A, Raes F., 2010. A European aerosol phenomenology – 3: Physical and chemical characteristics of particulate matter from 60 rural, urban, and kerbside sites across Europe. *Atmospheric Environment* **44**: 1308-1320. DOI: 10.1016/j.atmosenv.2009.12.011.

Putero D, Cristofanelli P, Laj P, Marinoni A, Villani P, Broquet A, Alborghetti M, Bonafè U,Calzolari F, Duchi R, Landi TC, Verza GP, Vuillermoz E, Bonasoni P., 2014. New atmospheric composition observations in the Karakorum region: Influence of local emissions and large-scale circulation during a summer field campaign. *Atmospheric Environment* **97**: 75-82. DOI: 10.1016/j.atmosenv.2014.07.063.

Querol X, Alastuey A, Rodríguez S, Viana MM, Artíñano B, Salvador P, Mantilla E, do Santos SG, Patier RF, de La Rosa J, Campa ASdl, Menendez M, Gil JJ., 2004a. Levels of particulate matter in rural, urban and industrial sites in Spain. *Science of The Total Environment* **334-335**: 359-376. DOI: 10.1016/j.scitotenv.2004.04.036.

Querol X, Alastuey A, Viana MM, Rodríguez S, Artíñano B, Salvador P, do Santos SG, Patier RF, Ruiz CR, de la Rosa J, Campa ASdl, Menendez M, Gil JJ., 2004b. Speciation and origin of PM10 and PM2.5 in Spain. *Journal of Aerosol Science* **35**: 1151-1172. DOI: 10.1016/j.jaerosci.2004.04.002.

Querol X, Alastuey A, Moreno T, Viana MM, Castillo S, Pey J, Rodríguez S, Artiñano B, Salvador P, Sánchez M, Garcia Dos Santos S, Herce Garraleta MD, Fernandez-Patier R, Moreno-Grau S, Negral L, Minguillón MC, Monforte E, Sanz MJ, Palomo-Marín R, Pinilla-Gil E, Cuevas E, de la Rosa J, Sánchez de la Campa A., 2008. Spatial and temporal variations in airborne particulate matter (PM10 and PM2.5) across Spain 1999–2005. *Atmospheric Environment* **42**: 3964-3979. DOI: 10.1016/j.atmosenv.2006.10.071.

Querol X, Alastuey A, Pey J, Cusack M, Pérez N, Mihalopoulos N, Theodosi C, Gerasopoulos E, Kubilay N, Koçak M., 2009. Variability in regional background aerosols within the Mediterranean. *Atmospheric Chemistry and Physics* **9**: 4575-4591. DOI: 10.5194/acp-9-4575-2009.

Querol X, Alastuey A, Pandolfi M, Reche C, Pérez N, Minguillón MC, Moreno T, Viana M, Escudero M, Orio A, Pallarés M, Reina F., 2014., 2001–2012 trends on air quality in Spain. *Science of the Total Environment* **490**: 957-969. DOI: 10.1016/j.scitotenv.2014.05.074.

Ramos AM, Ramos R, Sousa P, Trigo RM, Janeira M, Prior V., 2011. Cloud to ground lightning activity over Portugal and its association with circulation weather types. *Atmospheric Research* **101**: 84-101. DOI: 10.1016/j.atmosres.2011.01.014.

Rand WM., 1971. Objective criteria for the evaluation of clustering methods. *Journal of the American Statistical Association* **66:** 846-850. DOI: 10.1080/01621459.1971.10482356.

Rasilla D., 2003. Aplicación de un método de clasificación sinóptica a la Península Ibérica. *Investigaciones Geográficas* **30:** 27-45. Available at: <http://www.cervantesvirtual.com/descargaPdf/aplicacin-de-un-mtodo-de-clasificacin-sinptica-a-la-pennsula-ibrica-0/> [Accessed 20 December 2015].

Real Decreto 102/2011, de 28 de enero, relativo a la mejora de la calidad del aire. *BOE* **25**: 9574-9626. Available at: <http://www.boe.es/boe/dias/2011/01/29/pdfs/BOE-A-2011-1645.pdf> [Accessed 20 December 2015].

Real Decreto 989/2014, de 28 de noviembre, por el que se regula la concesión directa de ayudas del Plan de Impulso al Medio Ambiente «PIMA Aire 4» para la adquisición de vehículos comerciales, vehículos de gas y bicicletas de pedaleo asistido por motor eléctrico. *BOE* **289**: 97970-97980. Available at: <http://www.boe.es/boe/dias/2014/11/29/pdfs/BOE-A-2014-12413.pdf> [Accessed 20 December 2015].

REE, Red Eléctrica de España., 2013. Informe del Sistema Eléctrico Español. Año 2012. 140 pp. Available at: <http://ree.es/sites/default/files/downloadable/inf_sis_elec_ree_2012_v2.pdf> [Accessed 20 December 2015].

Ribas A, Peñuelas J., 2004. Temporal patterns of surface ozone levels in different habitats of the North Western Mediterranean basin. *Atmospheric Environment* **38**: 985-992. DOI: 10.1016/j.atmosenv.2003.10.045.

Richman MB., 1986. Rotation of principal components. *International Journal of Climatology* **6**: 293-335. DOI: 10.1002/joc.3370060305.

Romero R, Sumner G, Ramis C, Genovés A., 1999. A classification of the atmospheric circulation patterns producing significant daily rainfall in the Spanish Mediterranean area. *International Journal of Climatology* **19:** 765-785. DOI: 10.1002/(SICI)1097-0088(19990615)19:7<765::AID-JOC388>3.0.CO;2-T.

Royé D, Taboada JJ, Martí A, Lorenzo MN., 2015. Winter circulation weather types and hospital admissions for respiratory diseases in Galicia, Spain. *International Journal of Biometeorology*. DOI: 10.1007/s00484-015-1047-1.

Russo A, Trigo RM, Martins H, Mendes MT., 2014. NO_2, PM10 and O_3 urban concentrations and its association with circulation weather types in Portugal. *Atmospheric Environment* **89:** 768-785. DOI: 10.1016/j.atmosenv.2014.02.010.

Saavedra S, Rodríguez A, Souto JA, Casares JJ, Bermúdez JL, Soto B., 2012a. Trends of rural tropospheric ozone at the Northwest of the Iberian Peninsula. *The Scientific World Journal* **2012**: article ID 603034. DOI: 10.1100/2012/603034.

Saavedra S, Rodríguez A, Taboada JJ, Souto JA, Casares JJ., 2012b. Synoptic patterns and air mass transport during ozone episodes in northwestern Iberia. *Science of the Total Environment* **441:** 97-110. DOI: 10.1016/j.scitotenv.2012.09.014.

Salvador R, Artíñano B, Millán M., 1992. Aplicación de un modelo de dispersión de contaminantes para fuente puntual durante condiciones de brisa marina. *Energía* **2**: 133-138.

Salvador P, Artíñano B, Alonso DG, Querol X, Alastuey A., 2004. Identification and characterisation of sources of PM10 in Madrid (Spain) by statistical methods. *Atmospheric Environment* **38**: 435-447. DOI: 10.1016/j.atmosenv.2003.09.070.

Salvador P, Artíñano B, Querol X, Alastuey A, Costoya M., 2007. Characterisation of local and external contributions of atmospheric particulate matter at a background coastal site. *Atmospheric Environment* **41**: 1-17. DOI: 10.1016/j.atmosenv.2006.08.007.

Salvador P, Artíñano B, Querol X, Alastuey A., 2008. A combined analysis of backward trajectories and aerosol chemistry to characterise long-range transport episodes of particulate matter: The Madrid air basin, a case study. *Science of the Total Environment* **390:** 495-506. DOI: 10.1016/j.scitotenv.2007.10.052.

Salvador P, Artíñano B, Viana M, Alastuey A, Querol X., 2012. Evaluation of the changes in the Madrid metropolitan area influencing air quality: Analysis of 1999-2008

temporal trend of particulate matter. *Atmospheric Environment* **57**: 175-185. DOI: 10.1016/j.atmosenv.2012.04.026.

Salvador P, Artíñano B, Molero F, Viana M, Pey J, Alastuey A, Querol X., 2013. African dust contribution to ambient aerosol levels across central Spain: Characterization of long-range transport episodes of desert dust. *Atmospheric Research* **127:** 117-129. DOI: 10.1016/j.atmosres.2011.12.011.

Sánchez de la Campa AM, de la Rosa JD., 2014. Implications for air quality and the impact of financial and economic crisis in South Spain: Geochemical evolution of atmospheric aerosol in the ceramic region of Bailén. *Atmospheric Environment* **98**: 519-529. DOI: 10.1016/j.atmosenv.2014.09.023.

Santacatalina M, Yubero E, Mantilla E, Carratalá A., 2012. Relevance of the economic crisis in chemical PM10 changes in a semi-arid industrial environment. *Environmental Monitoring and Assessment* **184**: 6827-6844. DOI: 10.1007/s10661-011-2461-4.

Santurtún A, González-Hidalgo JC, Sánchez-Lorenzo A, Zarrabeitia MT., 2015. Surface ozone concentration trends and its relationship with weather types in Spain (2001-2010). *Atmospheric Environment* **101**: 10-22. DOI: 10.1016/j.atmosenv.2014.11.005.

Samoli E, Aga E, Touloumi G, Nisiotis K, Forsberg B, Lefranc A, Pekkanen J, Wojtyniak B, Schindler C, Niciu E, Brunstein R, Dodič Fikfak M, Schwartz J, Katsouyanni K., 2006. Short-term effects of nitrogen dioxide on mortality: an analysis within the APHEA project. *European Respiratory Journal* **27**: 1129-1139. DOI: 10.1183/09031936.06.00143905.

Schaap M, Cuvelier K, Hendriks C, Bessagnet B, Baldasano JM, Colette A, Thunis P, Karam D, Fagerli H, Graff A, Kranenburg R, Nyiri A, Pay MT, Rouïl L, Schulz M, Simpson D, Stern R, Terrenoire E, Wind P., 2015. Performance of European chemistry transport models as function of horizontal resolution. *Atmospheric Environment* **112**: 90-105. DOI: 10.1016/j.atmosenv.2015.04.003.

Segura S, Estellés V, Esteve AR, Utrillas MP, Martínez-Lozano JA., 2013. Analysis of a severe pollution episode in Valencia (Spain) and its effect on ground level particulate matter. *Journal of Aerosol Science* **56**: 41-52. DOI: 10.1016/j.jaerosci.2012.06.007.

Seinfeld JH, Pandis SN., 2006. Atmospheric Chemistry and Physics: From Air Pollution to Climate Change. 2nd Edition. John Wiley & Sons, Inc: New York (USA). 1232 pp.

Sepp M, Saue T., 2012. Correlations between the modelled potato crop yield and the general atmospheric circulation. *International Journal of Biometeorology* **56**: 591-603. DOI: 10.1007/s00484-011-0448-z.

Serra C, Fernández Mills G, Periago MC, Lana X., 1998. Surface Synoptic Circulation and Daily Precipitation in Catalonia. *Theoretical and Applied Climatology* **59**: 29-49. DOI: 10.1007/s007040050011.

Shah ASV, Langrish JP, Nair H, McAllister DA, Hunter AL, Donaldson K, Newby DE, Mills NL., 2013. Global association of air pollution and heart failure: a systematic review and meta-analysis. *The Lancet* **382**: 1039-1048. DOI: 10.1016/S0140-6736(13)60898-3.

Shahgedanova M, Burt T.P., Davies, T.D., 1998. Synoptic Climatology of Air Pollution in Moscow. *Theoretical and Applied Climatology* **61**, 85-102. DOI: 10.1007/s007040050054.

Shen L, Mickley LJ, Tai APK., 2015. Influence of synoptic patterns on surface ozone variability over the eastern United States from 1980 to 2012. *Atmospheric Chemistry and Physics* **15:** 10925-10938. DOI: 10.5194/acp-15-10925-2015.

Shrestha KL, Kondo A, Kaga A, Inoue Y., 2009. High-resolution modelling and evaluation of ozone air quality of Osaka using MM5-CMAQ system. *Journal of Environmental Science* **21:** 782-789. DOI: 10.1016/S1001-0742(08)62341-4.

Sicardi V, Ortiz J, Rincón A, Jorba O, Pay MT, Gassó S, Baldasano JM., 2012. Assessment of Kalman filter bias-adjustment technique to improve the simulation of ground-level ozone over Spain. *Science of The Total Environment* **416**: 329-342. DOI: 10.1016/j.scitotenv.2011.11.050.

Singh KP, Gupta S, Kumar A, Shukla SP., 2012. Linear and nonlinear modeling approaches for urban air quality prediction. *Science of the Total Environment* **426**: 244-255. DOI: 10.1016/j.scitotenv.2012.03.076.

Skamarock WC, Klemp JB., 2008. A time-split nonhydrostatic atmospheric model for weather research and forecasting applications. *Journal of Computational Physics* **227:** 3465-3485. DOI: 10.1016/j.jcp.2007.01.037.

Soret A, Jimenez-Guerrero P, Baldasano JM., 2011. Comprehensive air quality planning for Barcelona Metropolitan Area through traffic management. *Atmospheric Pollution Research* **2**: 255-266. DOI: 10.5094/APR.2011.032.

Soret A, Guevara M, Baldasano JM., 2014. The potential impacts of electric vehicles on air quality in the urban areas of Barcelona and Madrid (Spain). *Atmospheric Environment* **99**: 51-63. DOI: 10.1016/j.atmosenv.2014.09.048.

Soriano C, Baldasano JM, Buttler WT, Moore K., 2001. Circulatory patterns of air pollutants within the Barcelona air basin in a summertime situation: liar and numerical approaches. *Boundary Layer Meteorology* **98**: 33-55. DOI: 10.1023/A:1018726923826.

Stadlober E, Hörmann S, Pfeiler B., 2008. Quality and performance of a PM10 daily forecasting model. *Atmospheric Environment* **42**: 1098-1109. DOI: 10.1016/j.atmosenv.2007.10.073.

Stein AF, Mantilla E, Millán MM., 2005.Using measured and modeled indicators to assess ozone-NO_x-VOC sensitivity in a western Mediterranean coastal environment. *Atmospheric Environment* **39**: 7167-7180. DOI: 10.1016/j.atmosenv.2005.08.026.

Stull RB., 1988. An Introduction to Boundary Layer Meteorology. Kluwer Academic Publishers, Dortrecht (The Netherlands). 670 pp. DOI: 10.1007/978-94-009-3027-8.

Szopa S, Foret G, Menut L, Cozic A., 2009. Impact of large scale circulation on European summer surface ozone and consequences for modelling forecast. *Atmospheric Environment* **43**: 1189-1195. DOI: 10.1016/j.atmosenv.2008.10.039.

Tang MJ, Cox RA, Kalberer M., 2014. Compilation and evaluation of gas phase diffusion coefficients of reactive trace gases in the atmosphere: volume 1. Inorganic compounds. *Atmospheric Chemistry and Physics* **14**: 9233-9247. DOI: 10.5194/acp-14-9233-2014.

Tanner PA, Law PT., 2002. Effects of synoptic weather systems upon the air quality in an Asian megacity. *Water, Air, and Soil Pollution* **136**, 105-124. DOI: 10.1023/A:1015275404592.

Terrenoire E, Bessagnet B, Rouïl L, Tognet F, Pirovano G, Létinois L, Beauchamp M, Colette A, Thunis P, Amann N, Menut L., 2015. High-resolution air quality simulation over Europe with the chemistry transport model CHIMERE. *Geoscientific Model Development* **8**: 21-42. DOI: 10.5194/gmd-8-21-2015.

The Royal Society., 2008. Science Policy Report 15/08. Ground-level ozone in the 21st century: future trends, impacts and policy implications. 133 pp. Available at: <http://www.accent-network.org/accent_documents/ozone%20report%20web%20pdf%20final.pdf> [Accessed 20 December 2015].

Thunis P, Cuvelier C., 2015. DELTA Version 5.1. Concepts/User's Guide/Diagrams. Joint Research Center, Ispra. < http://aqm.jrc.ec.europa.eu/assessment/data/DELTA_UserGuide_V5_1.pdf> [Accessed 20 December 2015].

Timmermans RMA, Denier van der Gon HAC, Kuenen JJP, Segers AJ, Honoré C, Perrussel O, Builtjes PJH, Schaap M., 2013. Quantification of the urban air pollution increment and its dependency on the use of down-scaled and bottom-up

city emission inventories. *Urban Climate* **6**: 44-62. DOI: 10.1016/j.uclim.2013.10.004.

Toll I, Baldasano JM., 2000. Modeling of photochemical air pollution in the Barcelona area with highly disaggregated anthropogenic and biogenic emissions. *Atmospheric Environment* **34**: 3069-3084. DOI: 10.1016/S1352-2310(99)00498-7.

Tørseth K, Aas W, Breivik K, Fjæraa AM, Fiebig M, Hjellbrekke AG, Lund-Myhre C, Solberg S, Yttri KE., 2012. Introduction to the European Monitoring and Evaluation Programme (EMEP) and observed atmospheric composition change during 1972–2009. *Atmospheric Chemistry and Physics* **12**: 5447-5481. DOI: 10.5194/acp-12-5447-2012.

Tran HNQ, Tran TT, Mansfield ML, Lyman SN., 2014. Impacts of Oil and Gas Production on Winter Ozone Pollution in the Uintah Basin Using Model Source Apportionment. American Geophysical Union, Fall Meeting. San Francisco (USA). 15-19 December. Abstract #A14E-06.

Tveito OE., 2010. An assessment of circulation type classifications for precipitation distribution in Norway. *Physics and Chemistry of the Earth, Parts A/B/C* **35**: 395-402. DOI: 10.1016/j.pce.2010.03.044.

Van Dingenen R, Dentener FJ, Raes F, Krol MC, Emberson L, Cofala J., 2009. The global impact of ozone on agricultural yields under current and future air quality legislation. *Atmospheric Environment* **43**: 604-618. DOI: 10.1016/j.atmosenv.2008.10.033.

Valverde V, Pay MT, Baldasano JM., 2014. Circulation-type classification derived on a climatic basis to study air quality dynamics over the Iberian Peninsula. *International Journal of Climatology* **35**: 2877-2897. DOI: 10.1002/joc.4179.

Valverde V, Pay MT, Baldasano JM., 2015. A model-based analysis of SO_2 and NO_2 dynamics from coal-fired power plants under representative synoptic circulation types over the Iberian Peninsula. *Science of the Total Environment* **541**: 701-713. DOI: 10.1016/j.scitotenv.2015.09.111.

Vardoulakis S, Kassomenos P., 2008. Sources and factors affecting PM10 levels in two European cities: Implications for local air quality management. *Atmospheric Environment* **42**: 3949-3963. DOI: 10.1016/j.atmosenv.2006.12.021.

Vedrenne M, Borge R, Lumbreras J, Conlan B, Rodríguez ME, de Andrés JM, de la Paz D, Pérez J, Narros A., 2015. An integrated assessment of two decades of air pollution policymaking in Spain: Impacts, costs and improvements. *Science of the Total Environment* **527-528**: 351-361. DOI: 10.1016/j.scitotenv.2015.05.014.

Viana M, Pérez C, Querol X, Alastuey A, Nickovic S, Baldasano JM., 2005. Spatial and temporal variability of PM levels and composition in a complex summer atmospheric scenario in Barcelona (NE Spain). *Atmospheric environment* **39**: 5343-5361. DOI: 10.1016/j.atmosenv.2005.05.039.

Vivanco MG, Palomino I, Vautard R, Bessagnet B, Martín F, Menut L, Jiménez S., 2009. Multi-year assessment of photochemical air quality simulation over Spain. *Environmental Modelling & Software* **24**: 63-73. DOI: 10.1016/j.envsoft.2008.05.004.

Vivanco MG, Palomino I, Garrido JL, González MA, Alonso G, Martín F., 2012. Impact of the Transboundary Transport of Air Pollutants on Air Quality in Spain. *Journal of Environmental Protection* **3**: 1167-1175. DOI: 10.4236/jep.2012.329135.

von Schneidemesser E, Monks PS, Allan JD, Bruhwiler L, Forster P, Fowler D, Lauer A, Morgan WT, Paasonen P, Righi M, Sindelarova K, Sutton MA., 2015. Chemistry and the Linkages between Air Quality and Climate Change. *Chemical Reviews* **115**: 3856-3897. DOI: 10.1021/acs.chemrev.5b00089.

Watson JG., 2002. Visibility: Science and Regulation. *Journal of the Air & Waste Management Association* **52**: 628-713. DOI: 10.1080/10473289.2002.10470813.

Watson L, Lacressonnière G, Gauss M, Engardt M, Andersson C, Josse B, Marécal V, Nyiri A, Sobolowski S, Siour G, Vautard R., 2015. The impact of meteorological forcings on gas phase air pollutants over Europe. *Atmospheric Environment* **119**: 240-257. DOI: 10.1016/j.atmosenv.2015.07.037.

WHO, World Health Organization., 2006. Air Quality Guidelines. Global Update 2005. Particulate matter, ozone, nitrogen dioxide and sulfur dioxide 484 pp. Available at: <http://www.euro.who.int/__data/assets/pdf_file/0005/78638/E90038.pdf?ua=1> [Accessed 20 December 2015].

WHO, World Health Organization., 2013. Review of evidence on health aspects of air pollution – REVIHAAP project: final technical report. 309 pp. Available at: <http://www.euro.who.int/__data/assets/pdf_file/0004/193108/REVIHAAP-Final-technical-report-final-version.pdf?ua=1> [Accessed 20 December 2015].

Wild O, Akimoto H., 2001. Intercontinental transport of ozone and its precursors in a three-dimensional global CTM. *Journal of Geophysical Research: Atmospheres* **106**: 729-744. DOI: 10.1029/2000JD000123.

Wolff GT, Lioy PJ., 1978. An empirical model for forecasting maximum daily ozone levels in the Northeastern U.S. *Journal of the Air Pollution Control Association* **28**: 1034-1038. DOI: DOI:10.1080/00022470.1978.10470703.

Xie Y, Elleman R, Jobson T, Lamb B., 2011. Evaluation of O_3-NO_x-VOC sensitivities predicted with the CMAQ photochemical model using Pacific Northwest 2001 field

observations. *Journal of Geophysical Research* **116**: D20303. DOI: 10.1029/2011JD015801.

Yarnal B., 1993. Synoptic Climatology in Environmental Analysis: A Primer. Belhaven Press, London (UK)., 195 pp.

Yarnal B, Comrie AC, Frakes B, Brown DP., 2001. Developments and prospects in synoptic climatology. *International Journal of Climatology* **21**: 1923-1950. DOI: 10.1002/joc.675.

Yiou P, Nogaj M., 2004. Extreme climatic events and weather regimes over the North Atlantic: when and where? *Geophysical Research Letters* **31:** 1-4. DOI: 10.1029/2003GL019119.

Yiou P, Goubanova K, Nogaj M., 2008. Weather regime dependence of extreme value statistics for summer temperature and precipitation. *Nonlinear Processes in Geophysics* **15:** 365-378. DOI: 10.5194/npg-15-365-2008.

Yu K, Chen Z, Gao J, Zhang Y, Wang S, Chai F., 2015. Relationship between Objective and Subjective Atmospheric Visibility and Its Influence on Willingness to Accept or Pay in China. *PLoS ONE* **10**: e0139495. DOI:10.1371/journal.pone.0139495.

Zhang Y, Wen XY, Wang K, Vijayaraghavan K, Jacobson MZ., 2009. Probing into regional O_3 and particulate matter pollution in the United States: 2. An examination of formation mechanisms through a process analysis technique and sensitivity study. *Journal of Geophysical Research: Atmospheres* **114**: 2156-2202. DOI: 10.1029/2009JD011900.

Zhang JP, Zhu T, Zhang QH, Li CC, Shu HL, Ying Y, Dai ZP, Wang X, Liu XY, Liang AM, Shen HX, Yi BQ., 2012. The impact of circulation patterns on regional transport pathways and air quality over Beijing and its surroundings. *Atmospheric Chemistry and Physics* **12**: 5031-5053. DOI: 10.5194/acp-12-5031-2012.

Zhang Y, Mao H, Ding A, Zhou D, Fu C., 2013. Impact of synoptic weather patterns on spatio-temporal variation in surface O_3 levels in Hong Kong during 1999-2011. *Atmospheric Environment* **73:** 41-50. DOI: 10.1016/j.atmosenv.2013.02.047.

Annex I: Chapter's 2 Supplementary Material

1. Complementary evaluation metrics

Within-type Standard Deviation (WSD) and Fast Silhouette Index (FSIL) are other metrics that inform on classification quality. The metrics are included in the cost733class software and have been calculated for the classification techniques with higher EV (LND, KMN, DKM, CKM, and SAN) and for a growing number of patterns (2 to 15, 18, 27, and 50).

In this case, the use of complementary metrics does not help to the selection of the best configuration because the results of these metrics are convergent with those of the EV. The quality of the classification rises when the WSD is lower. The choice of nCT and classification technique is not made easier by using the WSD respect to EV (Figure AI-1).

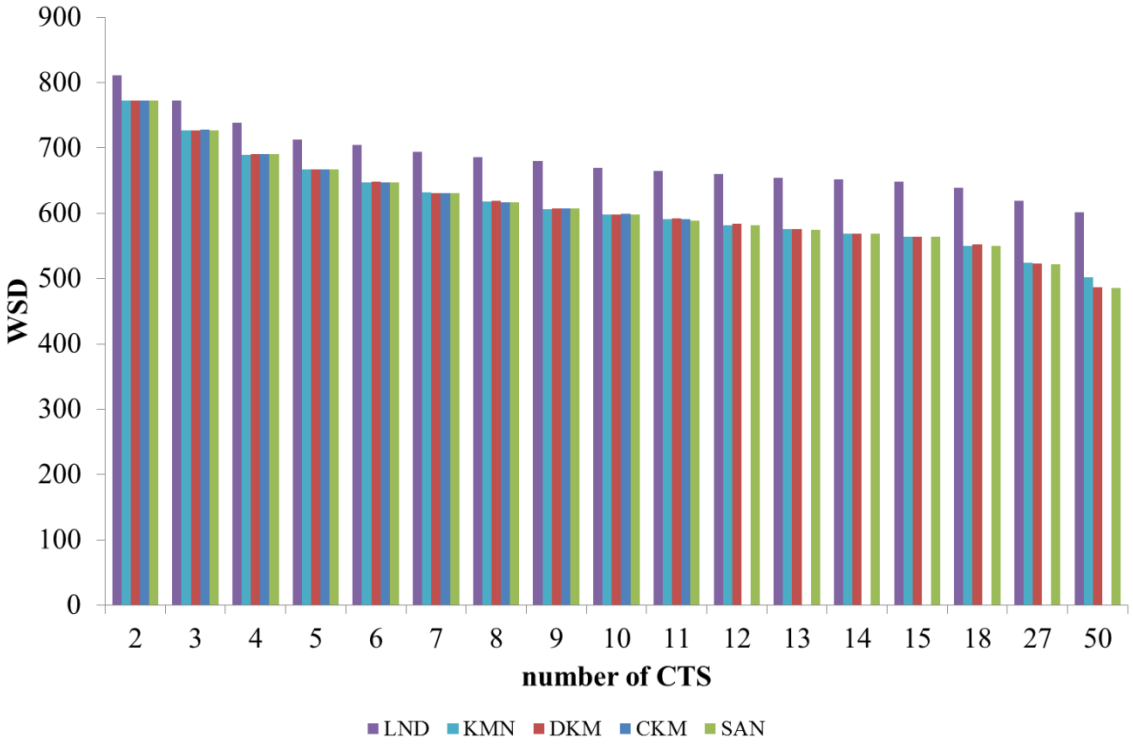

Figure A1-1. Classification quality for different classification techniques and number of CTs evaluated by means of the within-type standard deviation.

In relation to the FSIL, the classification quality is maximum when FSIL~1 but when PF~0 the identified patterns have a large within-type diversity and therefore the identified CTs are not trustable. The information obtained from FSIL in order to select the most reliable classification technique and number of CTs is equivalent to the one obtained with EV (Figure AI-2).

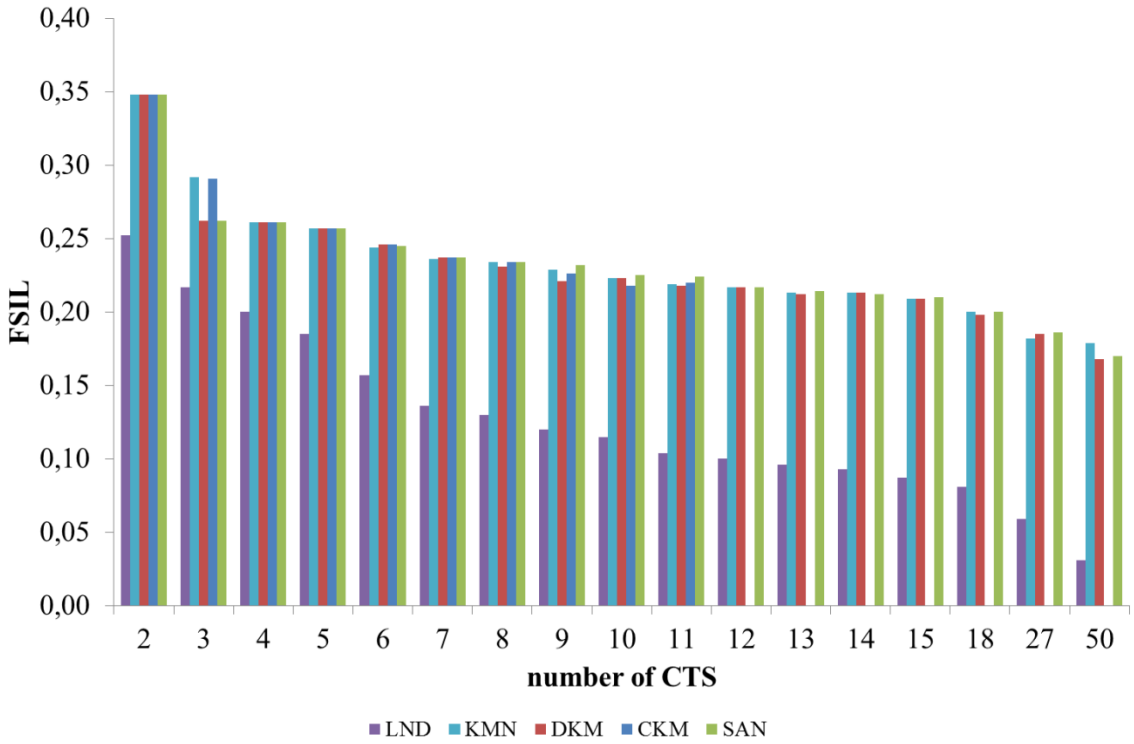

Figure AI-2. Classification quality for different classification techniques and number of CTs evaluated by means of the within-type standard deviation.

2. Explained variation for different number of CT

The complete explained variation (EV) for growing number of CTs for CKM is provided (Table AI-1).

Table AI-1. EV for the complete range of number of CTs evaluated with the reference set-up.

nCT	EV	EV increase (%)
2	0.250	30.8
3	0.327	22.0
4	0.399	11.8
5	0.446	6.5
6	0.475	5.9
7	0.503	4.4
8	0.525	2.9
9	0.540	2.8
10	0.555	2.3
11	0.568	-

Note that considering the limitation of CKM (the method does not allow to create CT with less than 5% of the total data in order to avoid extreme infrequent patterns) it is not possible to create a larger number of CTs for the climatic database of mslp.

For a larger number of cluster-based techniques, the average EV is shown in Figure 2-3b.

3. Evaluation of input meteorological variables used as proxy for different classification techniques

According to the EV index, the mslp is the best non-seasonalised input meteorological variable to be used to obtain a CTC. In order to increase the robustness of the choice of the mslp as the proxy variable, the sensitivity analysis has been performed for other cluster-based techniques. The results of KMN, DKM, CKM and SAN are convergent showing that T2m has the highest EV followed by mslp (Figure AI-3).

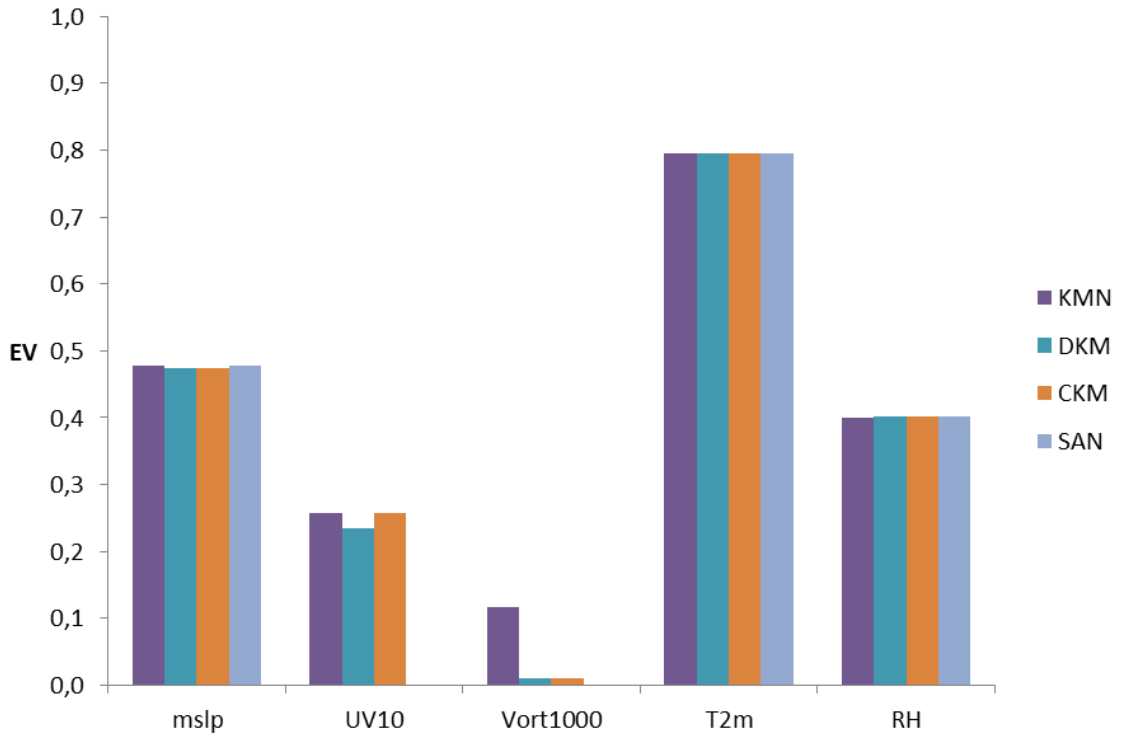

Figure AI-3. Evaluation of input meteorological variables used as proxy for different classification techniques by means of the Explained Variation index.

4. Characteristics of 2nd and 3rd most representative years

The year 2012 is chosen as the representative year because it has the highest value (68%) of temporal stability compared to the 1983-2012 classification. In order to evaluate the robustness of the choice of the representative year, the 2nd and 3rd most temporal stable years (1995 and 1990, respectively with 66% and 64% temporal stability) have been analysed in terms of the location of the action centres (Figure AI-4) and the CT characteristics (Table AI-2). The results are coherent with those obtained for 2012 with little variations respect to the 1983-2012 classification.

Table AI-2: Characteristics of the CTs derived with the reference set-up for the 2nd and 3rd most temporally stable years, 1990 and 1995.

	NWadv CT1	IBtl CT2	ENEadv CT3	AtlHi CT4	WSWadv CT5	ZonWadv CT6
Description	NW advection	Summer low surface pressure gradient	E/NE advection	Atlantic high with polar maritime advection	W/SW advection	Western Atlantic zonal advection
Criteria						
			1990			
Frequency (%) during 1990	22.5	15.6	14.0	19.2	18.6	10.1
Most frequent month	MAY	OCT	MAR	DEC	APR	FEB
Seasonal frequency (%): DJF/ MAM/ JJA/ SON	6.1/ 34.1/ 35.4/ 24.4	10.5/ 7.0/ 36.8/ 45.6	58.8/ 37.3/ 0.0/ 3.9	17.1/ 38.6/ 24.3/ 20.0	5.9/ 20.6/ 36.8/ 36.8	89.2/ 0.0/ 0.0/ 10.8
Mean / Max persistence (days)	2.5 / 8	2.7 / 6	6.4 / 18	4.1 / 9	3.0 / 9	6.2 / 13
Transitions	IBtl / AtlHi	NWadv / WSWadv	ZonWadv	NWadv	NWadv	ENEadv / WSWadv
			1995			
Frequency (%) during 1995	29.0	19.7	6.3	16.4	15.9	12.6
Most frequent month	AUG	JUL	DEC	JAN/MAR	MAR/SEP	FEB
Seasonal frequency (%): DJF/ MAM/ JJA/ SON	2.8/ 24.5/ 50.0/ 22.6	16.7/ 26.4/ 27.8/ 29.2	39.1/ 21.7/ 26.1/ 13.0	33.3/ 31.7/ 8.3/ 26.7	27.6/ 27.6/ 13.8/ 31.0	62.2/ 15.2/ 0.0/ 19.6
Mean / Max persistence (days)	3.9 / 17	3.3 / 7	2.9 / 6	2.3 / 7	2.4 / 8	4.2 / 13
Transitions	IBtl / AtlHi	AtlHi	NWadv	NWadv	NWadv	WSWadv

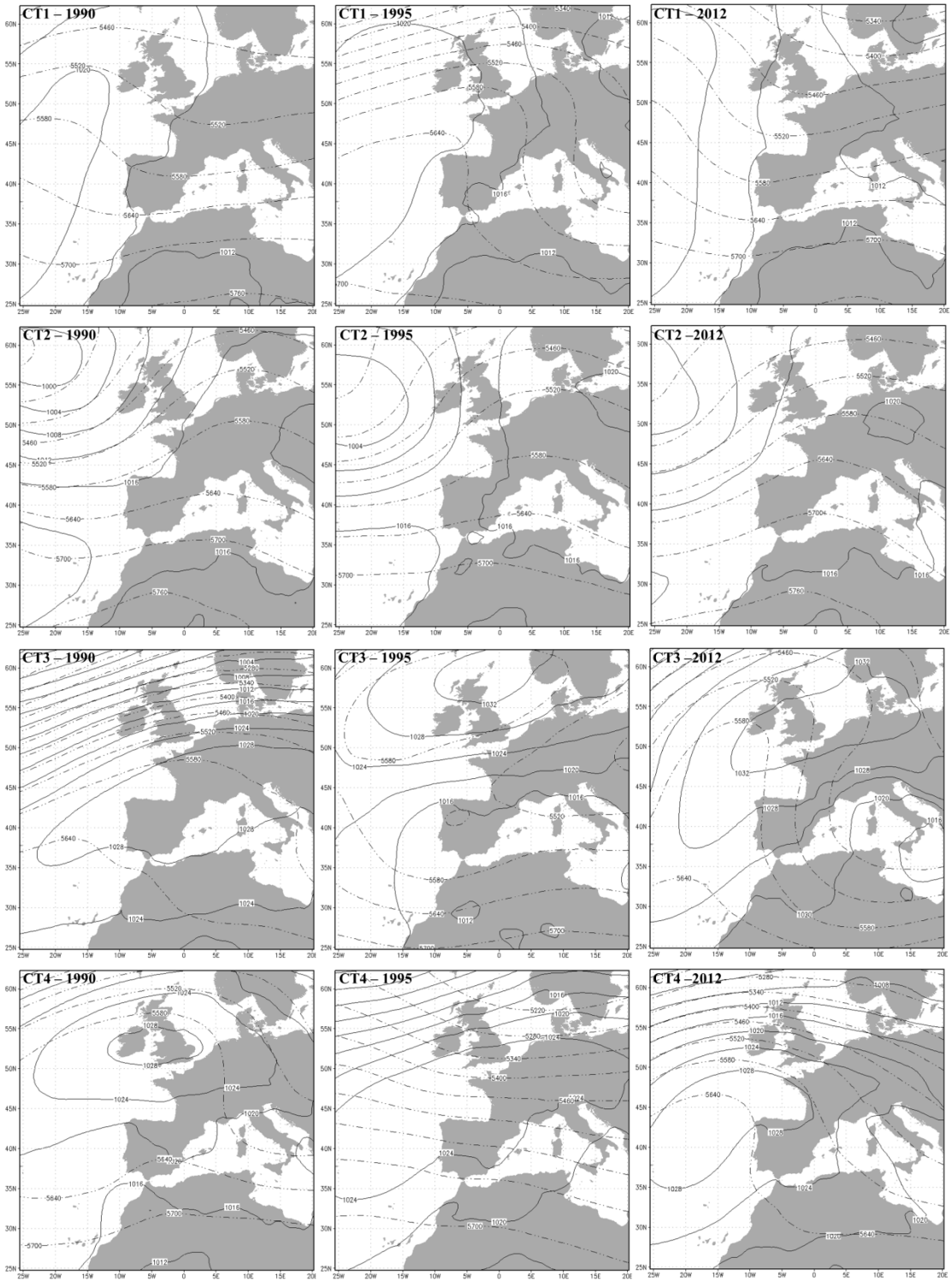

Figure AI-4. 1990 (left), 1995 (centre) and 2012 (right) CTs identified with the reference configuration.

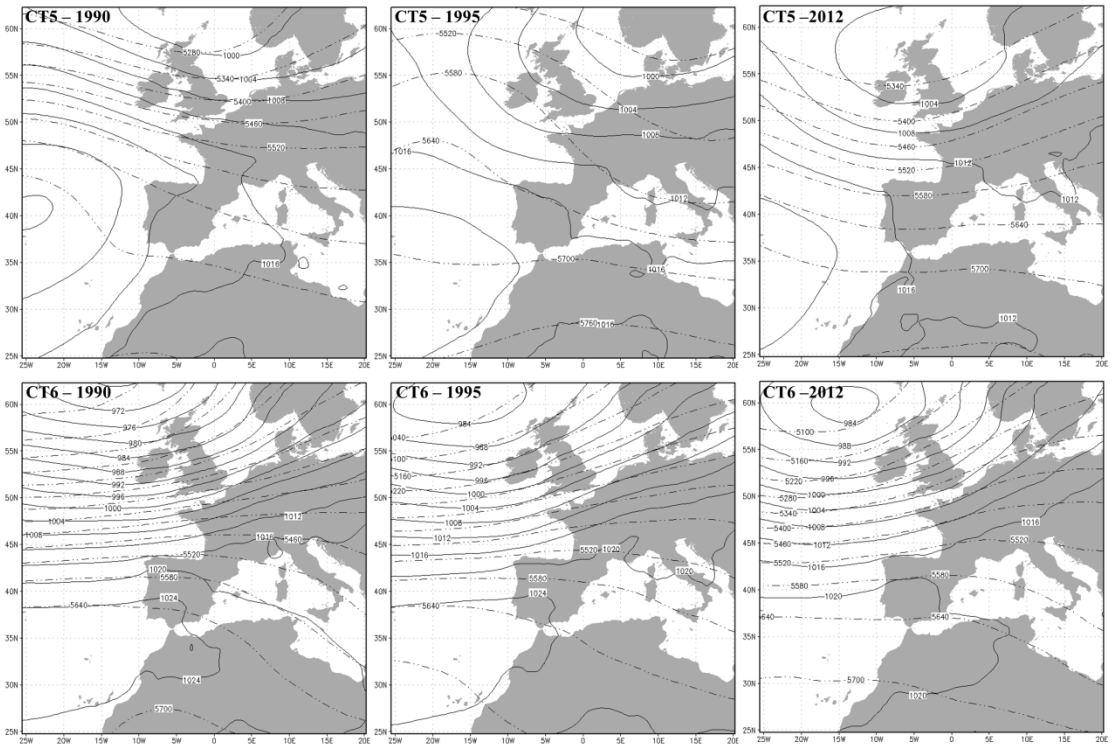

Figure AI-4. Continue.

5. Ensemble back-trajectories

Sixty hour back-trajectories have been obtained by means of the HYSPLIT model using an ensemble approach for each location cited in Figure 2-2a (Madrid, Barcelona, Seville, Bilbao, Zaragoza, Santiago de Compostela, and Palma de Mallorca) and for each of the six CTs in order to sample the history of air masses.

For each location a composite figure (Figures AI-5 to AI-11) has been produced combining the results of the 1500 magl and the 5500 magl level. The ensemble is composed by 27 back-trajectories that are calculated by offsetting the meteorological data by a fixed grid factor (one meteorological grid point in the horizontal and 0.01 sigma units in the vertical). The results have been obtained from the NOAA ARL READY Website: http://www.arl.noaa.gov/HYSPLIT.php. Results are convergent with the single trajectory back-trajectories presented in the manuscript.

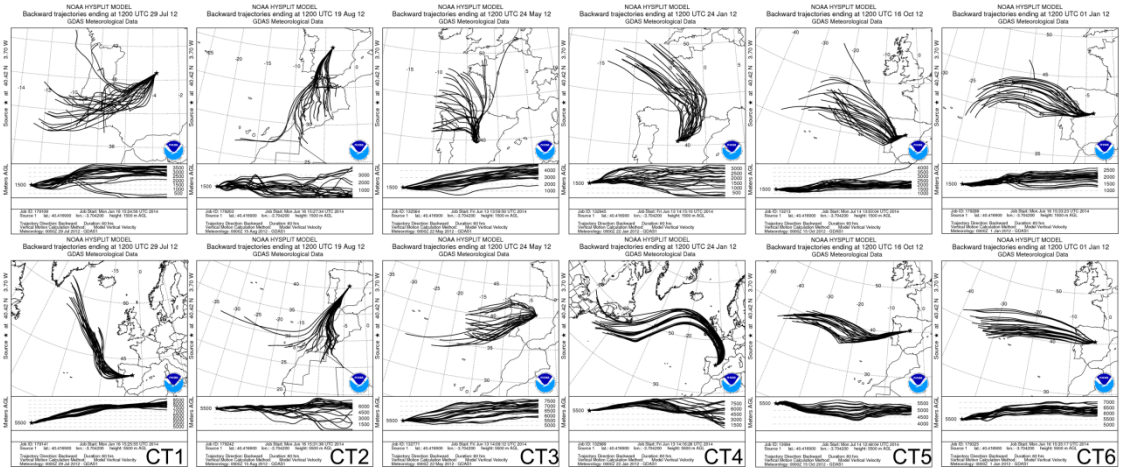

Figure AI-5. Sixty hour ensemble back-trajectories at 1500 magl (top) and 5500 magl (bottom) arriving at Madrid for the representative day of each CT in 2012.

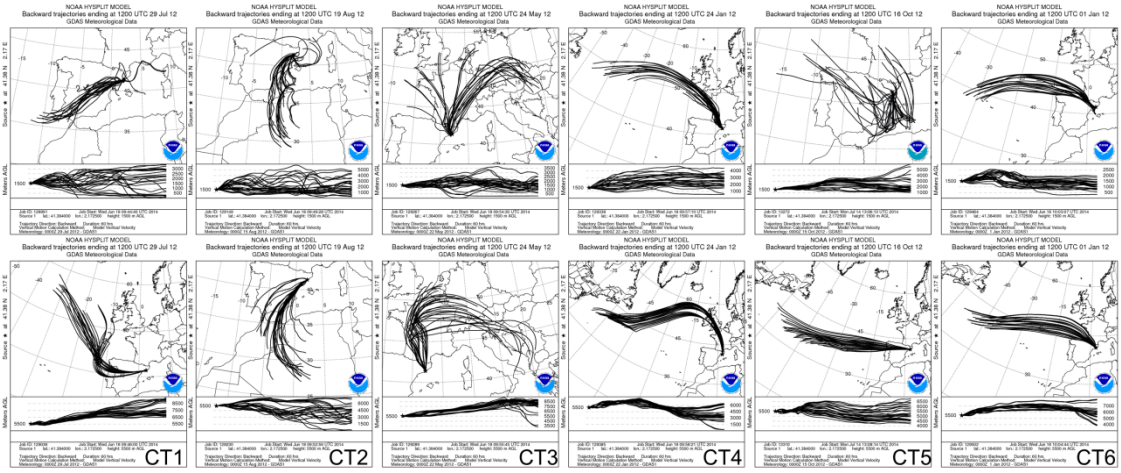

Figure AI-6. Sixty hour ensemble back-trajectories at 1500 magl (top) and 5500 magl (bottom) arriving at Barcelona for the representative day of each CT in 2012.

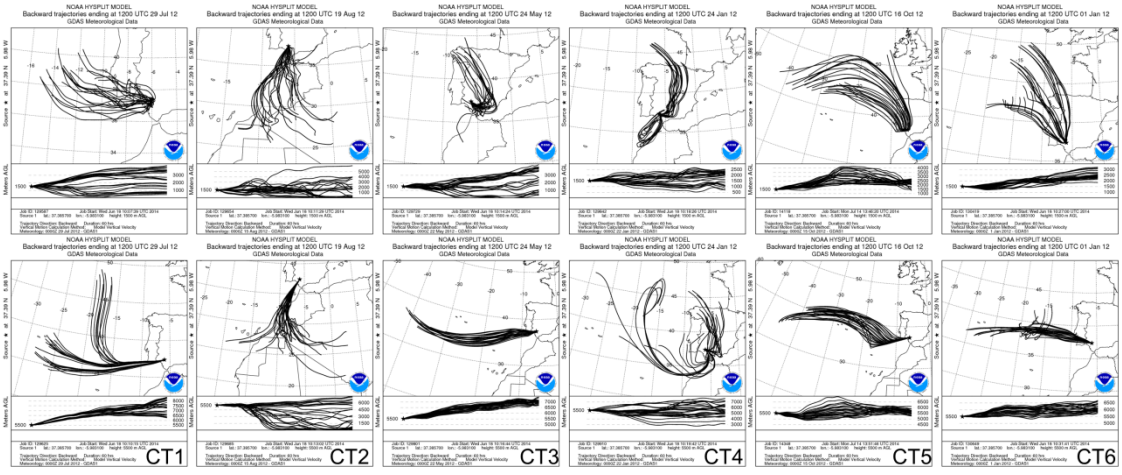

Figure AI-7. Sixty hour ensemble back-trajectories at 1500 magl (top) and 5500 magl (bottom) arriving at Seville for the representative day of each CT in 2012.

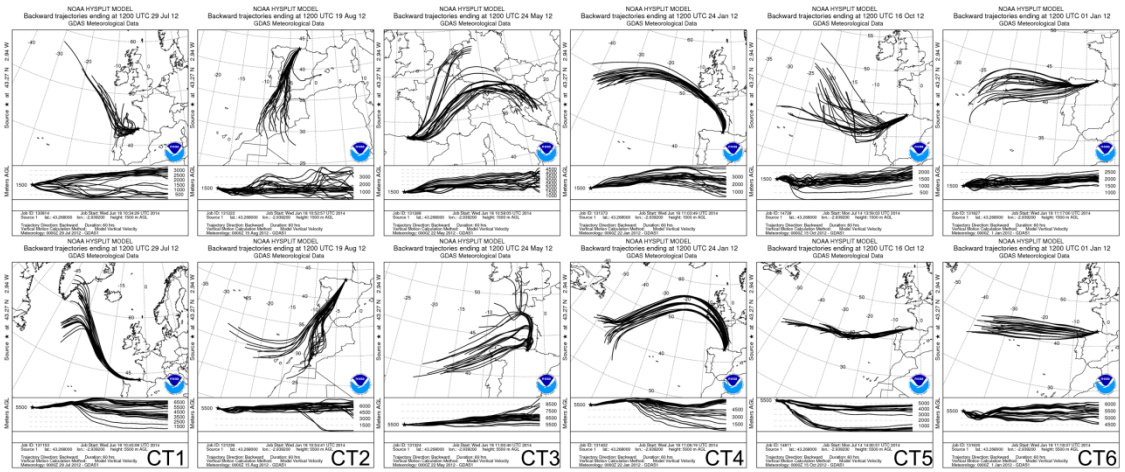

Figure AI-8. Sixty hour ensemble back-trajectories at 1500 magl (top) and 5500 magl (bottom) arriving at Bilbao for the representative day of each CT in 2012.

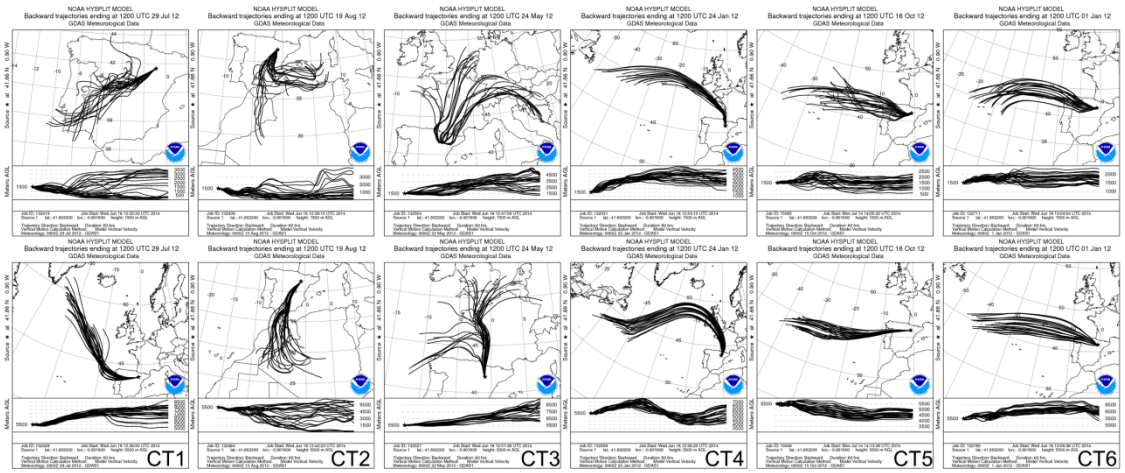

Figure AI-9. Sixty hour ensemble back-trajectories at 1500 magl (top) and 5500 magl (bottom) arriving at Zaragoza for the representative day of each CT in 2012.

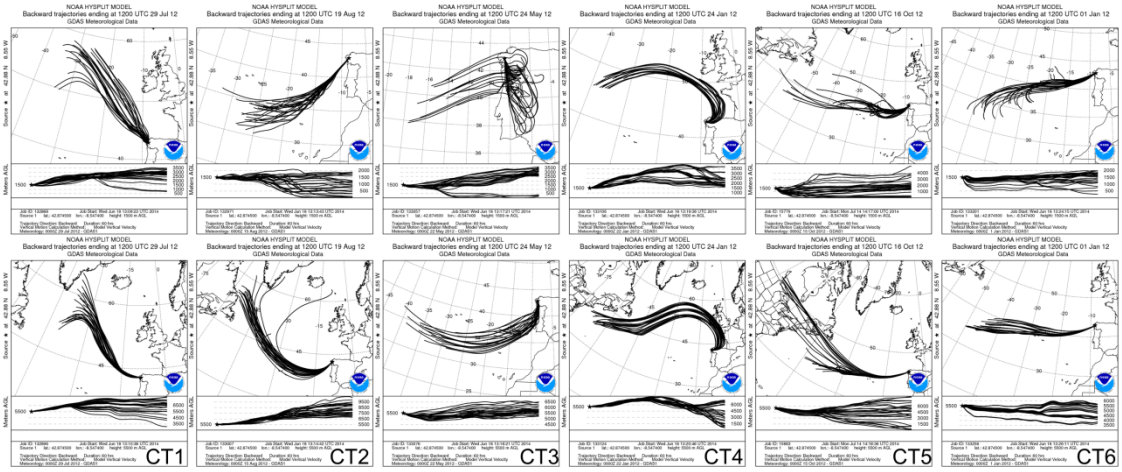

Figure AI-10. Sixty hour ensemble back-trajectories at 1500 magl (top) and 5500 magl (bottom) arriving at Santiago de Compostela for the representative day of each CT in 2012.

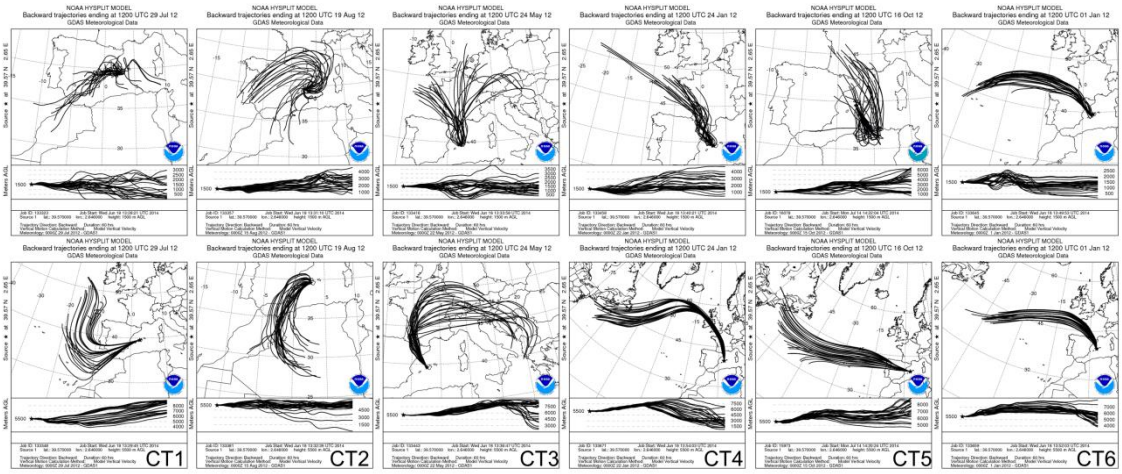

Figure AI-11. Sixty hour ensemble back-trajectories at 1500 magl (top) and 5500 magl (bottom) arriving at Palma de Mallorca for the representative day of each CT in 2012.

Annex II: Chapter's 5 Supplementary Material

SO_2 and NO_2 surface concentration, planetary boundary layer height (PBLH), wind speed and direction, and vertical vorticity daily cycle at As Pontes (ASP), Aboño (ABO), Compostilla (COM), Guardo (GUA), Andorra (AND), Carboneras (CAR) and Los Barrios (LBB) power plants, on the representative day of each CT.

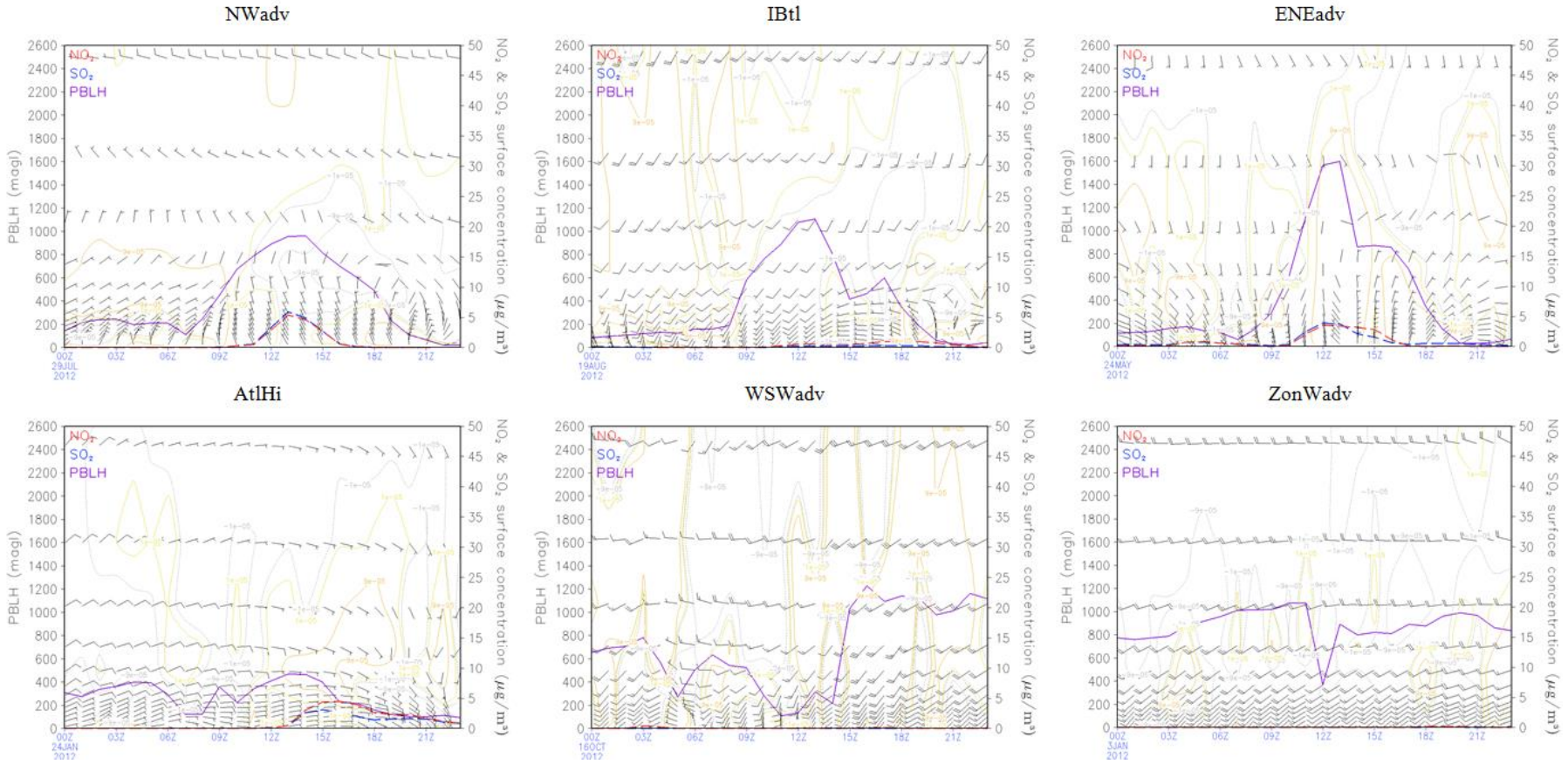

Figure AII-1. Hourly SO_2 (blue dashed line) and NO_2 (red dashed line) surface concentration (µg m^{-3}), PBLH (magl, purple line), wind barbs, and vertical vorticity (m s^{-1}) at the 4 km x 4 km cell where ASP is located on the representative day of each CT.

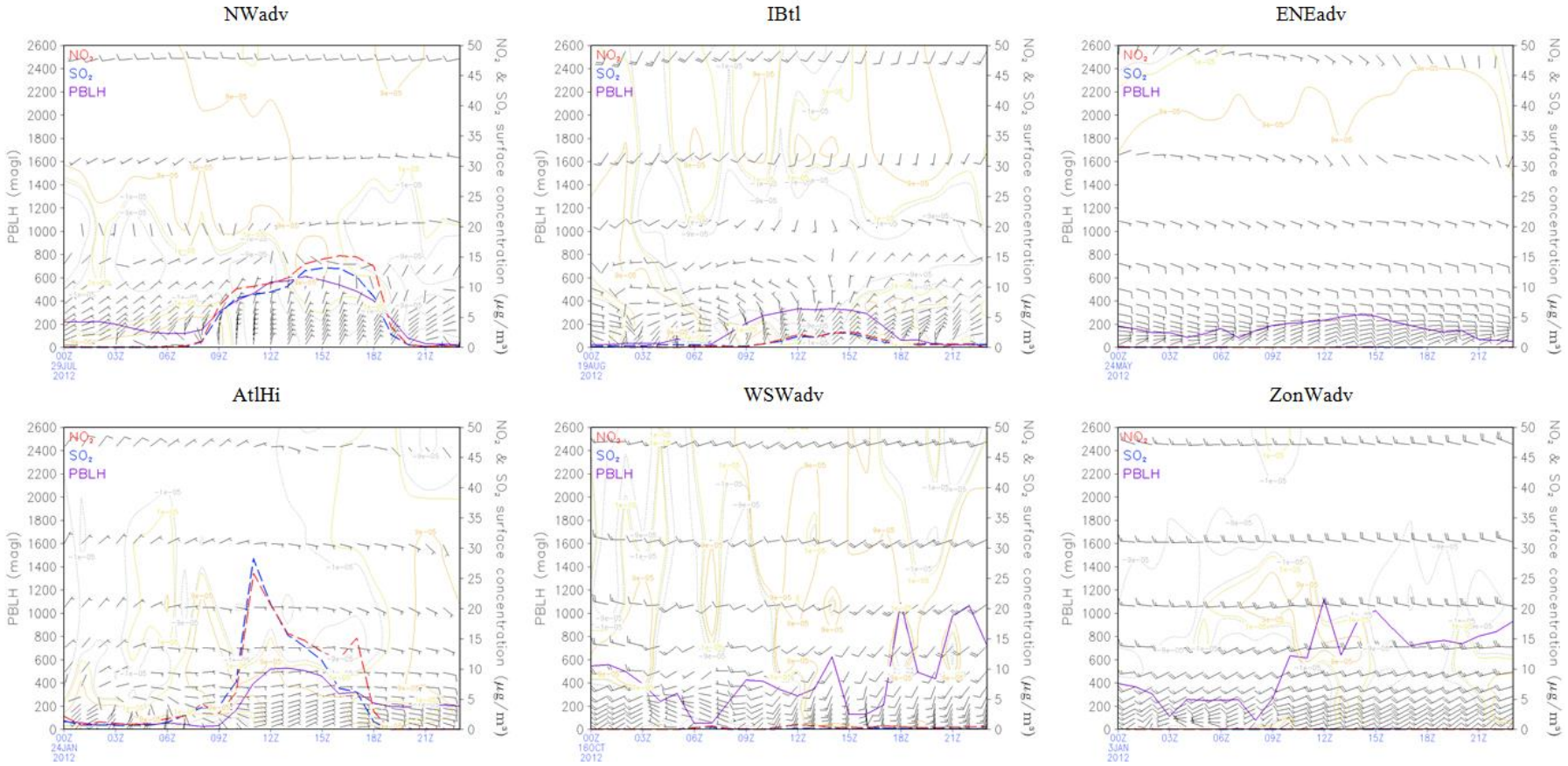

Figure AII-2. Hourly SO_2 (blue dashed line) and NO_2 (red dashed line) surface concentration (µg m^{-3}), PBLH (magl, purple line), wind barbs, and vertical vorticity (m s^{-1}) at the 4 km x 4 km cell where ABO is located on the representative day of each CT.

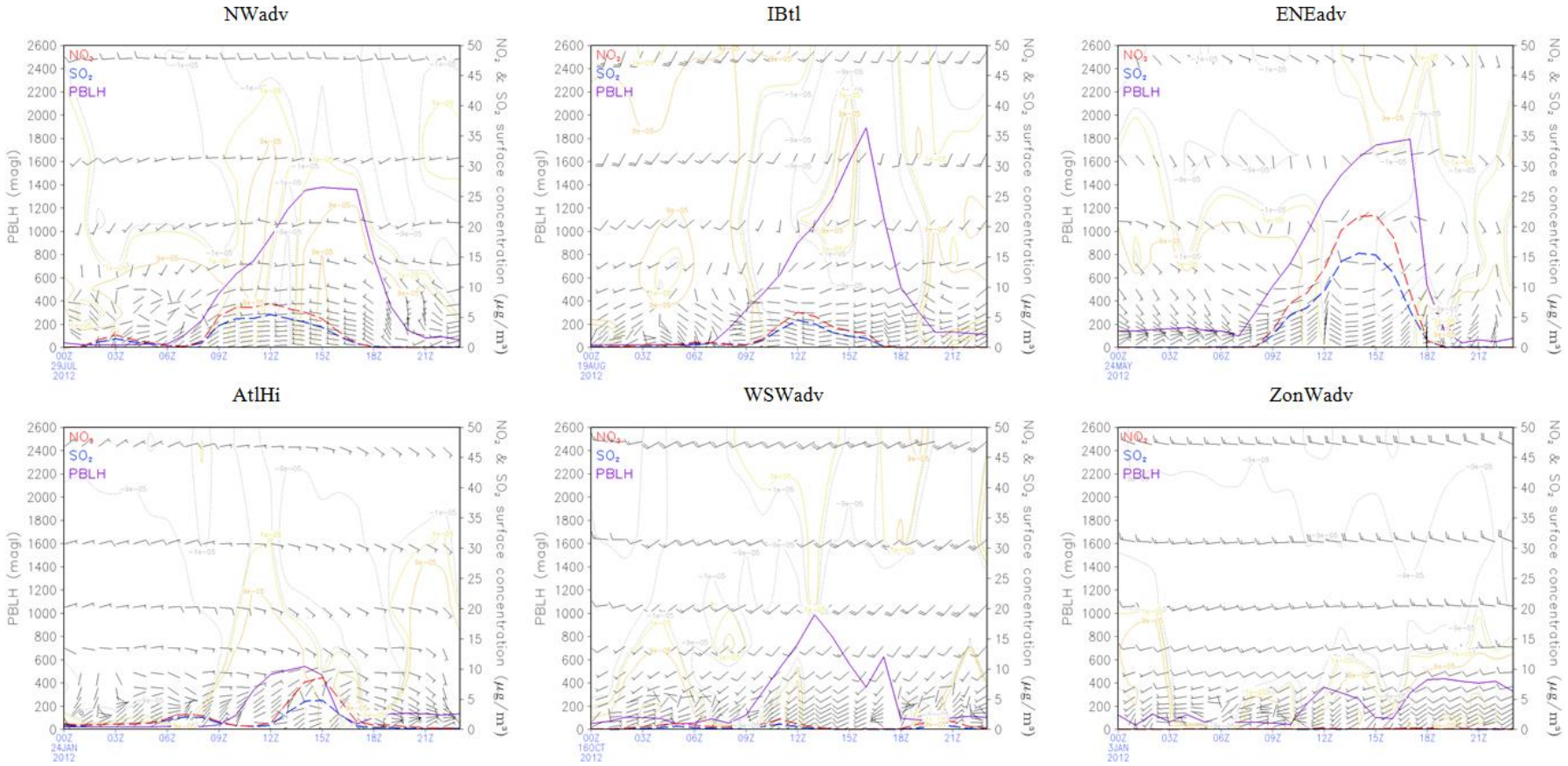

Figure AII-3. Hourly SO_2 (blue dashed line) and NO_2 (red dashed line) surface concentration (µg m^{-3}), PBLH (magl, purple line), wind barbs, and vertical vorticity (m s^{-1}) at the 4 km x 4 km cell where COM is located on the representative day of each CT.

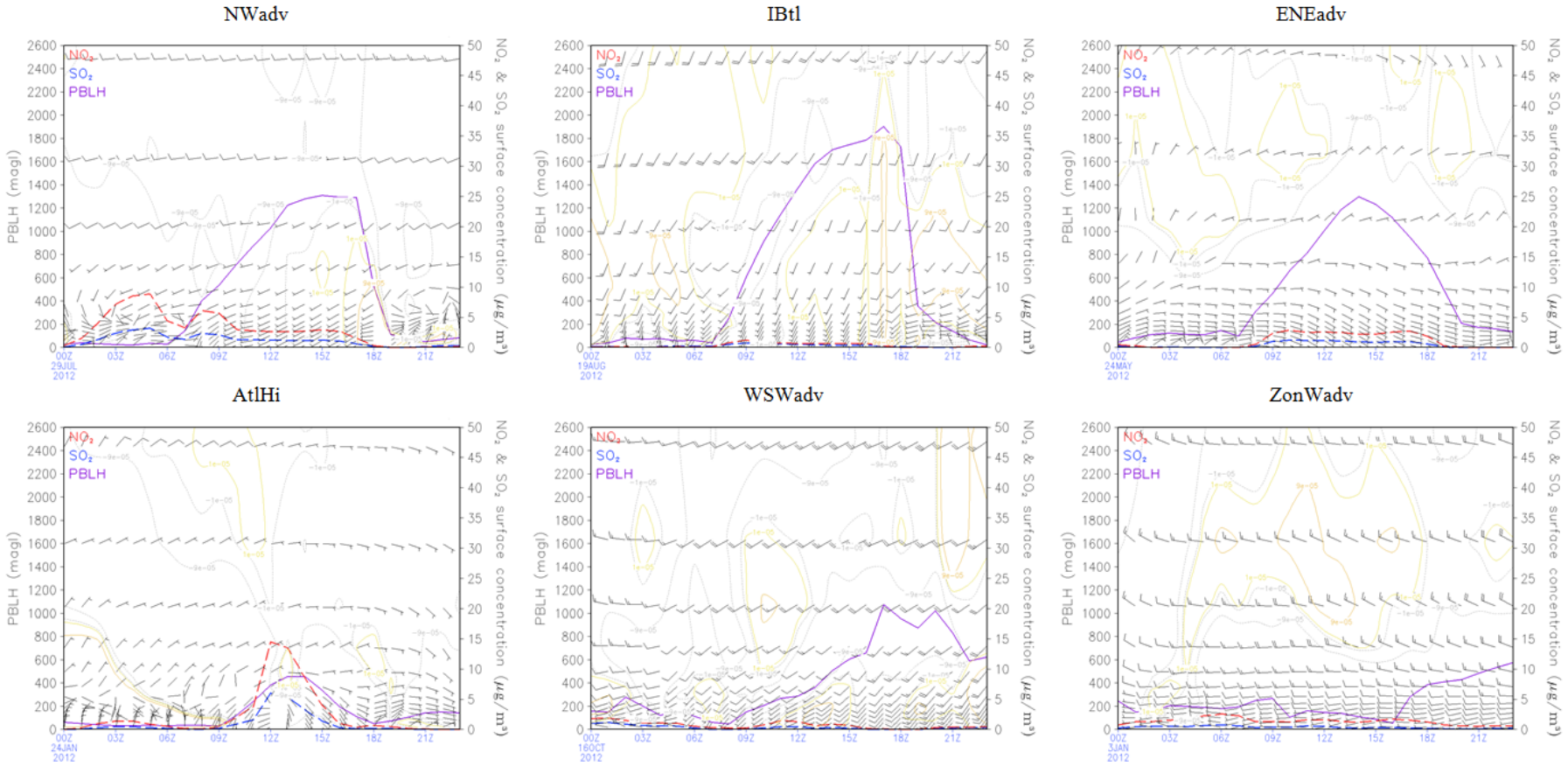

Figure AII-4. Hourly SO_2 (blue dashed line) and NO_2 (red dashed line) surface concentration (µg m^{-3}), PBLH (magl, purple line), wind barbs, and vertical vorticity (m s^{-1}) at the 4 km x 4 km cell where GUA is located on the representative day of each CT.

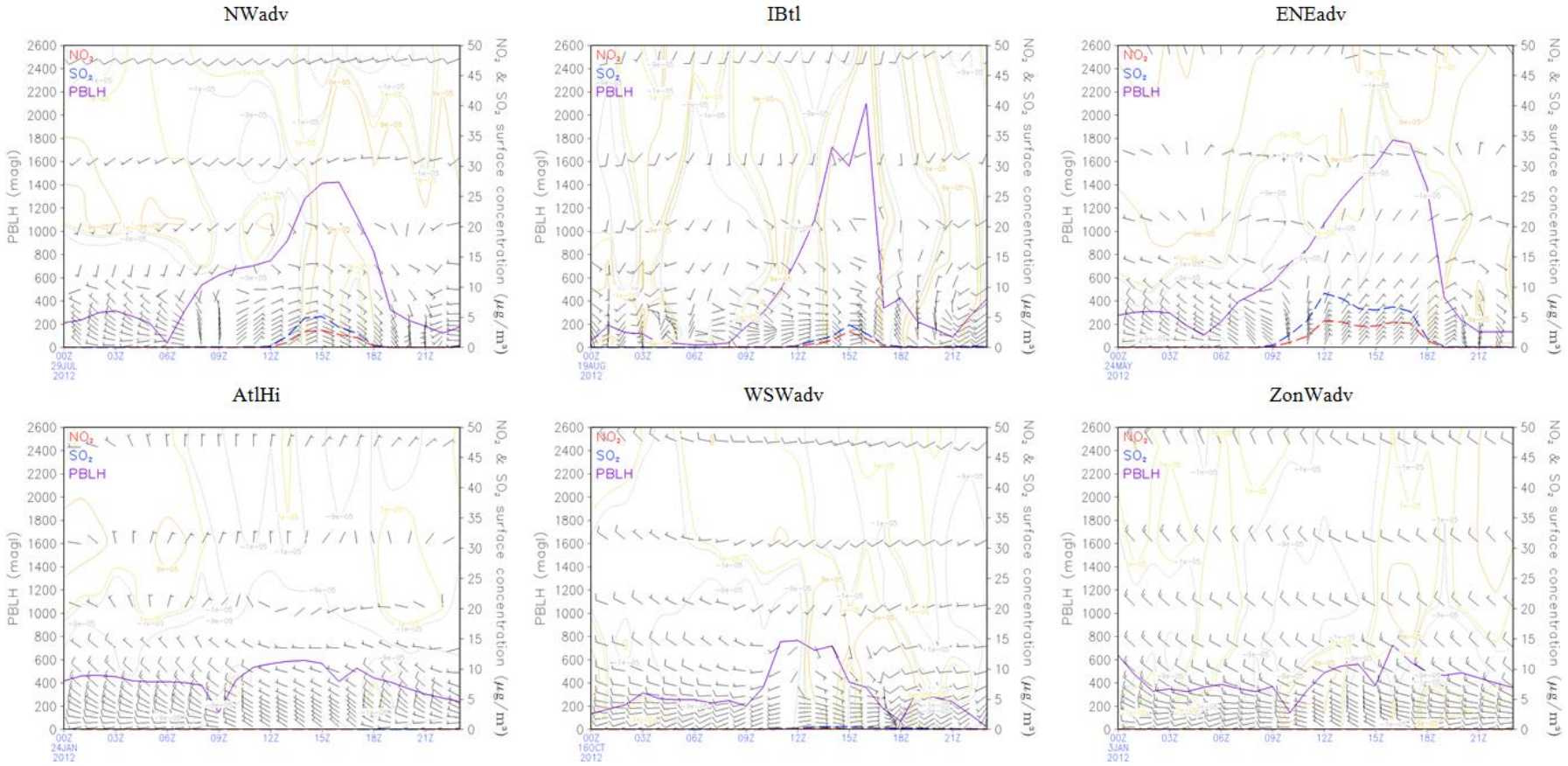

Figure AII-5. Hourly SO_2 (blue dashed line) and NO_2 (red dashed line) surface concentration (μg m^{-3}), PBLH (magl, purple line), wind barbs, and vertical vorticity (m s^{-1}) at the 4 km x 4 km cell where AND is located on the representative day of each CT.

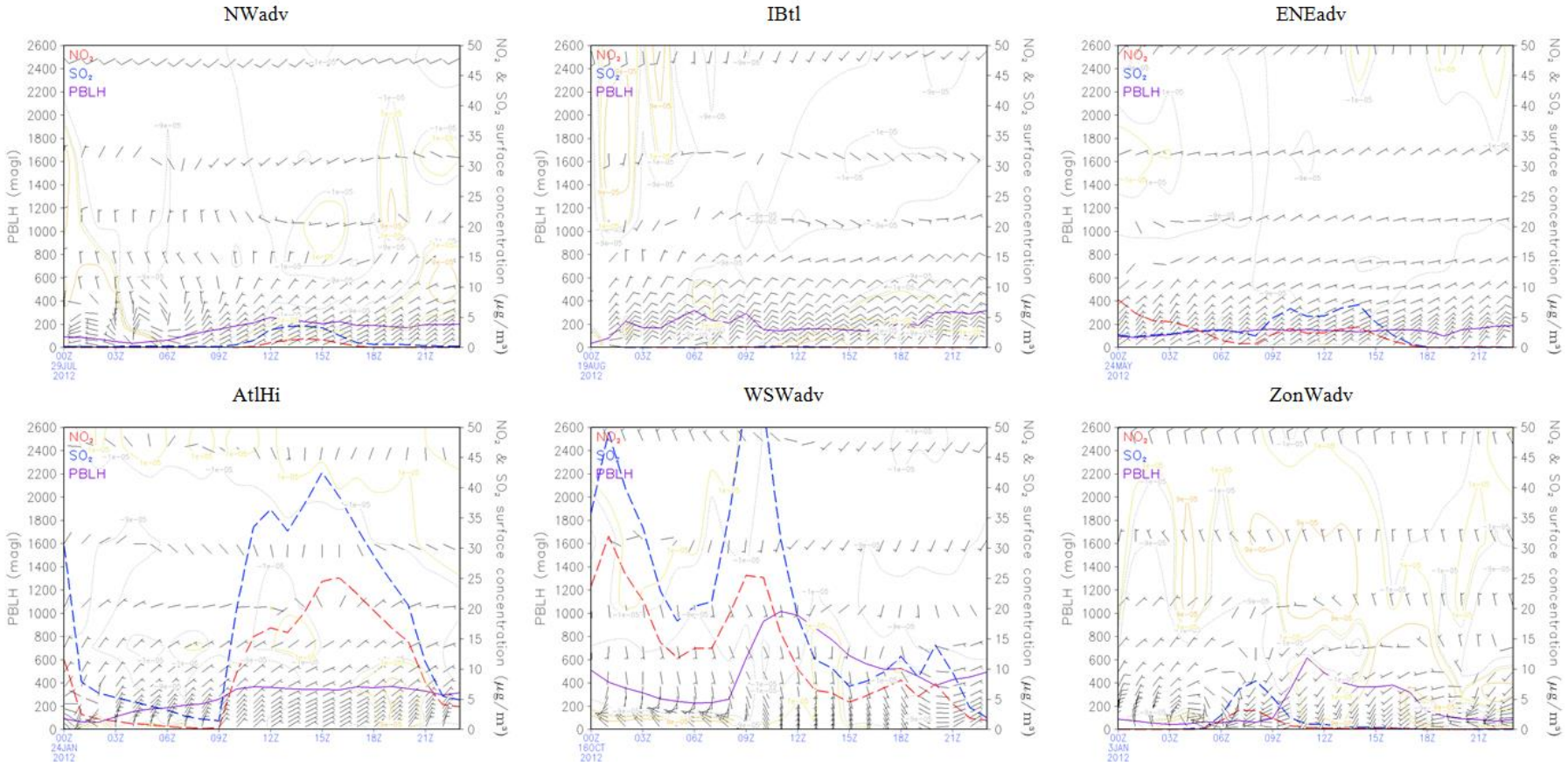

Figure AII-6. Hourly SO_2 (blue dashed line) and NO_2 (red dashed line) surface concentration (μg m^{-3}), PBLH (magl, purple line), wind barbs, and vertical vorticity (m s^{-1}) at the 4 km x 4 km cell where CAR is located on the representative day of each CT.

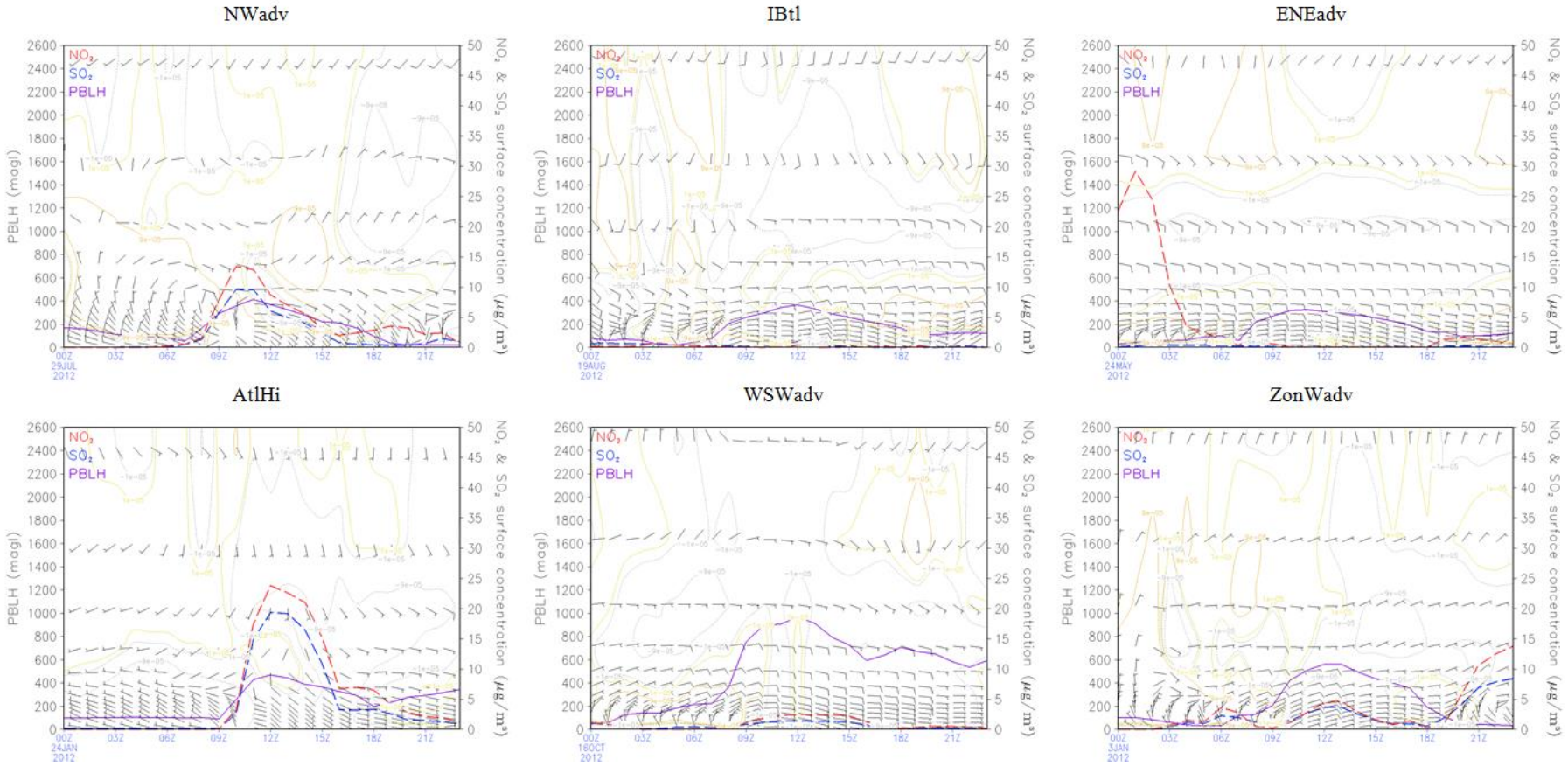

Figure AII-7. Hourly SO_2 (blue dashed line) and NO_2 (red dashed line) surface concentration (µg m^{-3}), PBLH (magl, purple line), wind barbs, and vertical vorticity (m s^{-1}) at the 4 km x 4 km cell where LBB is located on the representative day of each CT.

Annex III: Chapter's 6 Supplementary Material

Table AIII-1a. Characteristics of the monitoring stations from the Spanish air quality network (Figure 6-3 and Figure 6-4).

Station code	Latitude (ºN)	Longitude (ºE)	Altitude (masl)	Autonomous region	Station name	Station type	Station area
ES0009R	41.2742	-3.1425	1360	Castilla-La Mancha	Campisábalos	Background	Rural
ES0118A	40.4217	-3.6822	672	Madrid	Escuelas Aguirre (Madrid)	Traffic	Urban
ES1348A	42.3703	1.7781	1043	Catalonia	Bellver de Cerdanya	Background	Rural
ES1480A	41.4003	2.1544	57	Catalonia	Gràcia-Sant Gervasi (Barcelona)	Traffic	Urban
ES1616A	39.8492	-5.9397	376	Extremadura	Monfragüe (Toril)	Background	Rural
ES1778A	41.7793	2.3580	693	Catalonia	Montseny La Castanya	Background	Rural
ES1802A	40.9103	-3.4667	995	Madrid	El Atazar	Background	Rural
ES1806A	40.2869	-3.2222	800	Madrid	Orusco de Tajuña	Background	Rural
ES1991A	41.7236	-2.8569	1005	Castilla y León	Muriel de la Fuente	Background	Rural

Table AIII-1b. O_3 surface contribution (µg m^{-3}) by source, CT and air quality monitoring station averaged for sunlight hours for stations in Figure 6-3 and Figure 6-4. T-MAD: Madrid metropolitan road transport emissions; T-BCN: Barcelona metropolitan road transport emissions; OTHER: other source of emissions within the Iberian Peninsula domain and road transport emissions from outside MAD and BCN; ICON: initial conditions contribution; BCON: boundary conditions contribution; TOT: total modelled O_3 concentration; OBS: validated observation at the monitoring station.

	NWadv							IBtl							ENEadv						
Station code	T-MAD	T-BCN	OTHER	ICON	BCON	TOT	OBS	T-MAD	T-BCN	OTHER	ICON	BCON	TOT	OBS	T-MAD	T-BCN	OTHER	ICON	BCON	TOT	OBS
ES0009R	1.3	0.1	41.8	3.6	34.5	81.2	-	7.0	0.0	34.9	0.1	53.8	95.8	-	0.0	0.0	6.4	0.0	74.8	81.2	99.5
ES0118A	14.4	0.1	40.6	3.3	29.7	88.0	81.2	3.1	0.0	28.1	0.0	42.0	73.3	53.8	24.6	0.0	18.0	0.0	49.5	92.1	65.3
ES1348A	1.7	0.4	43.5	2.8	35.1	83.5	112.9	0.0	7.5	20.7	0.1	69.3	97.7	101.7	0.0	0.4	6.9	0.0	75.4	82.7	102.8
ES1480A	0.2	4.1	25.1	1.0	38.3	68.7	86.3	0.0	1.5	12.3	0.0	70.5	84.4	46.9	0.0	2.5	20.2	0.0	33.8	56.4	49.7
ES1616A	0.2	0.1	44.3	4.1	41.7	90.3	102.1	0.0	0.0	26.2	0.0	47.5	73.7	74.9	4.4	0.0	21.1	0.0	54.0	79.6	99.9
ES1778A	0.6	18.9	50.4	1.2	45.6	116.8	113.2	0.1	8.1	21.0	0.1	71.7	101.0	100.1	0.0	8.4	22.4	0.0	75.8	106.6	111.7
ES1802A	5.9	0.1	39.1	3.6	36.5	85.2	137.2	10.9	0.0	37.4	0.1	49.8	98.1	109.1	0.1	0.0	5.3	0.0	69.0	74.5	-
ES1806A	1.7	0.1	56.7	4.6	32.4	95.4	125.1	0.1	0.0	33.1	0.1	54.9	88.1	90.1	5.4	0.0	21.9	0.0	59.5	86.9	144.8
ES1991A	0.6	0.1	41.8	2.9	35.0	80.4	84.2	2.4	0.0	32.6	0.1	52.1	87.1	68.6	0.0	0.0	11.1	0.0	67.5	78.7	90.6

	AtlHi							WSWadv							ZonWadv						
Station code	T-MAD	T-BCN	OTHER	ICON	BCON	TOT	OBS	T-MAD	T-BCN	OTHER	ICON	BCON	TOT	OBS	T-MAD	T-BCN	OTHER	ICON	BCON	TOT	OBS
ES0009R	0.0	0.0	2.8	0.0	69.9	72.7	59.6	8.1	0.0	14.4	0.0	54.8	77.3	63.0	0.0	0.0	3.7	0.0	65.4	69.0	65.4
ES0118A	0.1	0.0	1.6	0.0	43.5	45.2	22.4	0.9	0.0	8.8	0.0	31.7	41.4	19.2	1.9	0.0	2.8	0.0	20.8	25.5	10.2
ES1348A	0.0	0.1	1.0	0.0	70.8	71.9	51.2	0.1	0.0	7.0	0.0	60.2	67.3	61.9	0.0	0.0	1.7	0.0	65.4	67.0	44.3
ES1480A	0.0	1.1	2.3	0.0	14.7	18.1	13.8	1.3	0.3	11.4	0.0	43.4	56.4	43.3	0.0	0.5	1.8	0.0	28.0	30.3	16.5
ES1616A	5.8	0.0	4.9	0.0	47.1	57.7	41.9	0.0	0.0	23.5	0.0	47.8	71.3	69.6	0.0	0.0	7.5	0.0	48.3	55.9	49.4
ES1778A	0.0	3.6	12.0	0.0	52.7	68.2	36.2	1.5	0.2	15.7	0.0	57.8	75.3	73.9	0.0	0.0	3.7	0.0	60.3	64.0	47.5
ES1802A	0.0	0.0	2.6	0.0	67.5	70.0	68.5	9.5	0.0	15.5	0.0	48.7	73.7	-	3.6	0.0	5.6	0.0	51.8	61.1	64.9
ES1806A	0.0	0.0	2.4	0.0	67.3	69.7	-	0.0	0.0	12.7	0.0	51.8	64.5	73.5	0.4	0.0	7.7	0.0	43.7	51.7	44.0
ES1991A	0.0	0.0	3.4	0.0	56.1	59.5	33.5	4.4	0.0	14.5	0.0	53.3	72.3	46.3	0.0	0.0	5.8	0.0	57.1	62.8	54.1

Table AIII-2. Correlation coefficient for 2-meter temperature (T2m, ºC) and downward longwave flux at ground surface (GLW, W m^{-2} $hour^{-1}$) with O_3 concentration attributed to on-road transport emissions from Madrid ($O_{3T\text{-}MAD}$) and Barcelona ($O_{3T\text{-}MAD}$) metropolitan areas calculated considering the median value at the monitoring stations as in Figure 6-2.

		NWadv	IBtl	ENEadv	AtlHi	WSWadv	ZonWadv
T2m $O_{3T\text{-}BCN}$/ $O_{3T\text{-}MAD}$	MAD Urban traffic	0.46	0.80	0.84	0.86	0.45	0.43
	MAD Rural background	-0.13	0.10	0.71	0.54	0.01	-0.01
	BCN Urban traffic	-0.11	-0.17	0.39	0.53	0.45	0.60
	BAR Rural background	0.49	0.76	0.76	0.68	-0.14	-0.07
GLW $O_{3T\text{-}BCN}$/ $O_{3T\text{-}MAD}$	MAD Urban traffic	0.31	0.23	0.79	0.58	0.60	-0.01
	MAD Rural background	-0.41	0.12	0.79	0.64	0.14	-0.30
	BAR Urban traffic	-0.41	0.35	-0.01	0.51	0.37	0.55
	BCN Rural background	0.21	0.65	0.56	0.13	-0.31	-0.18

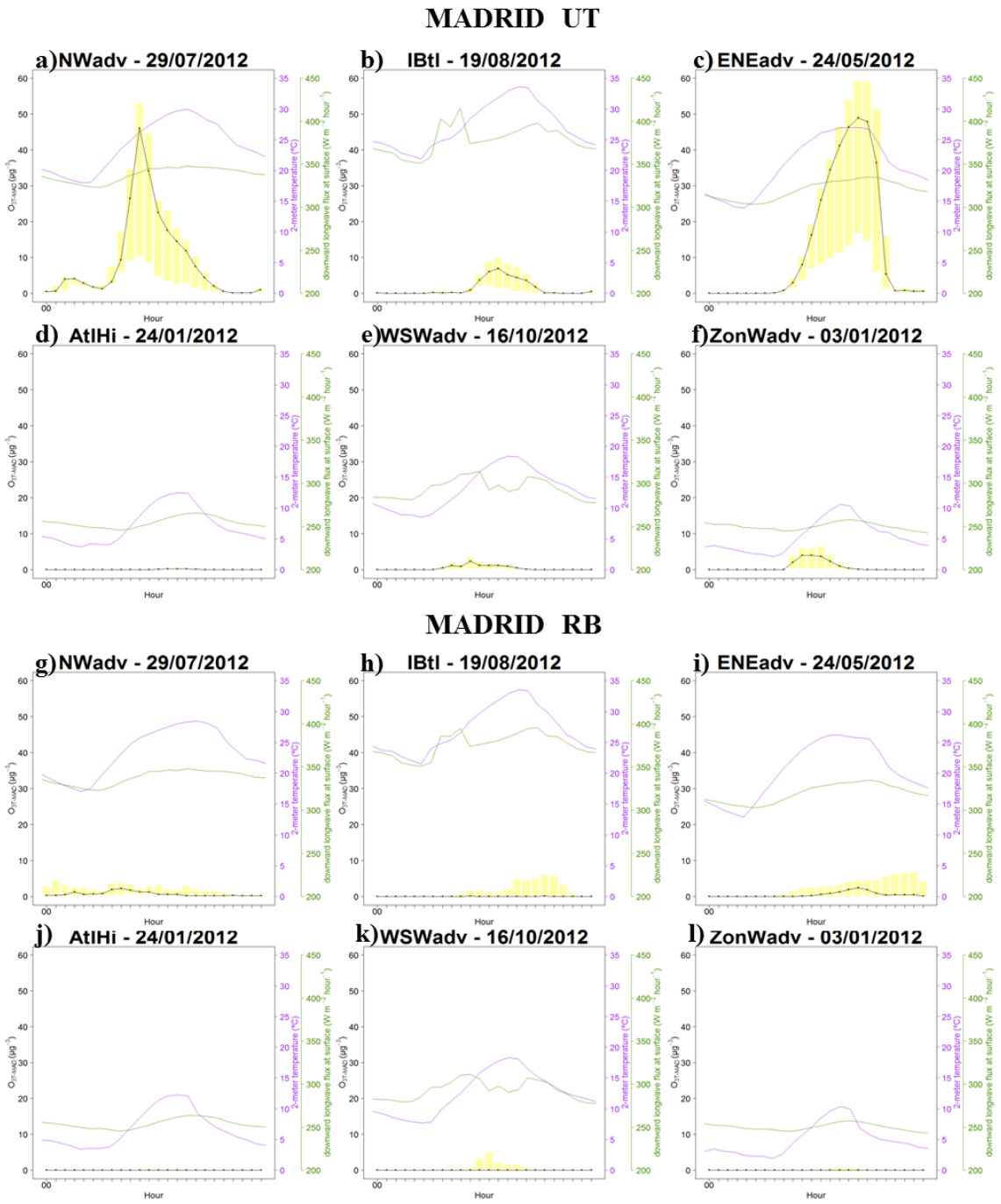

Figure AIII-1. Daily cycle (hours in GMT) of 2-meter temperature (ºC, purple line), downward longwave flux at ground surface (W m^{-2} $hour^{-1}$, green line) and modelled O_3 concentration (µg m^{-3}) attributed to on-road transport emissions from Madrid metropolitan areas in urban traffic (UT, a) and rural background (RB, b) monitoring stations on the representative day of each CT. Median 2-meter temperature and downward longwave flux at ground surface, 1st quartile, median and 3rd quartile of O_3 concentration calculated considering the number of monitoring stations as in Figure 6-2.

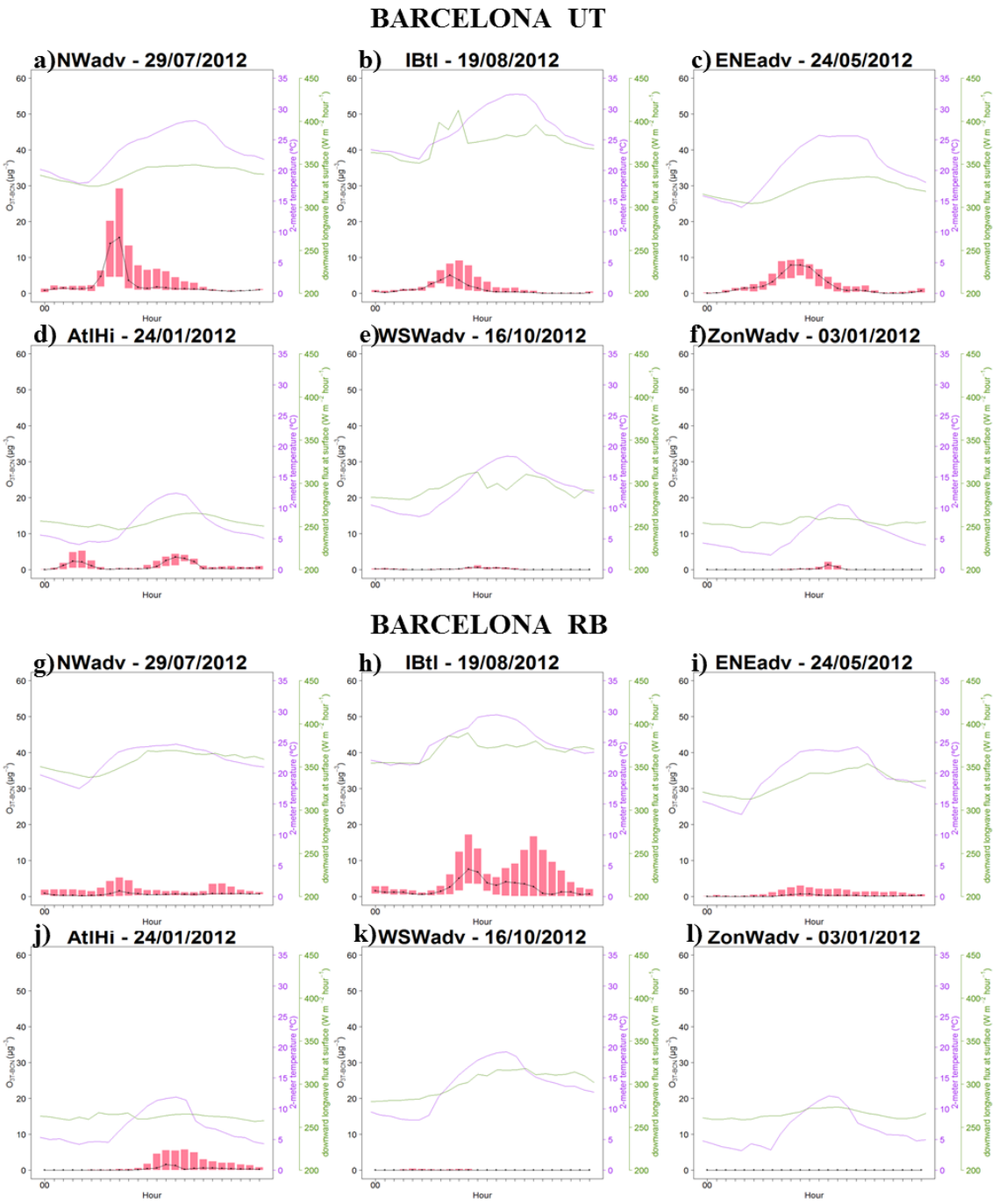

Figure AIII-2. Daily cycle (hours in GMT) of 2-meter temperature (ºC, purple line), downward longwave flux at ground surface (W m^{-2} $hour^{-1}$, green line) and modelled O_3 concentration (µg m^{-3}) attributed to on-road transport emissions from Barcelona metropolitan areas in urban traffic (UT, a) and rural background (RB, b) monitoring stations on the representative day of each CT. Median 2-meter temperature and downward longwave flux at ground surface, 1st quartile, median and 3rd quartile of O_3 concentration calculated considering the number of monitoring stations as in Figure 6-2.

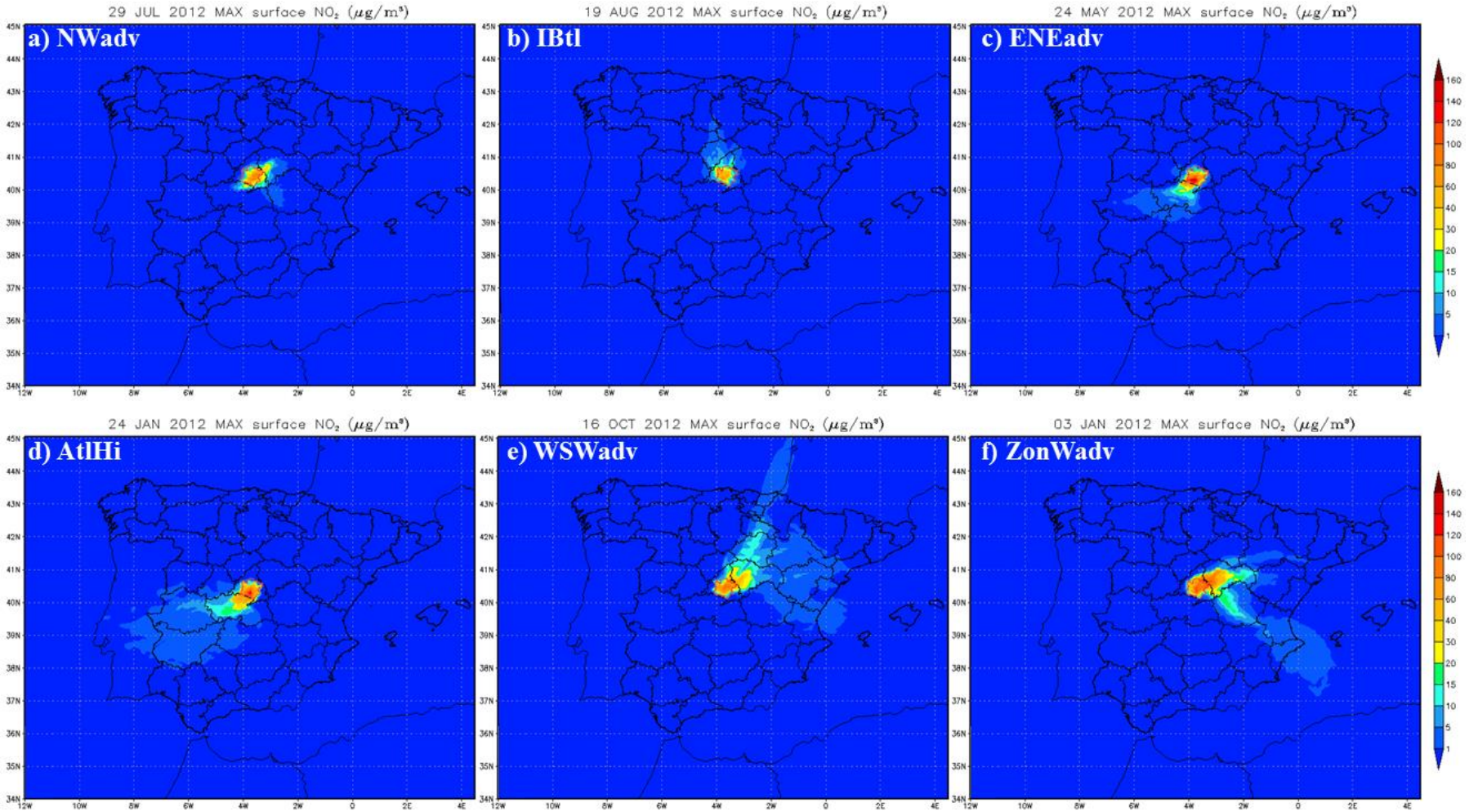

Figure AIII-3. Daily maximum NO_2 surface concentration (μg m^{-3}) attributed to on-road transport emissions from Madrid metropolitan area on the representative day of each CT: a) NWadv, b) IBtl, c) ENEadv, d) AtlHi, e) WSWadv; and f) ZonWadv.

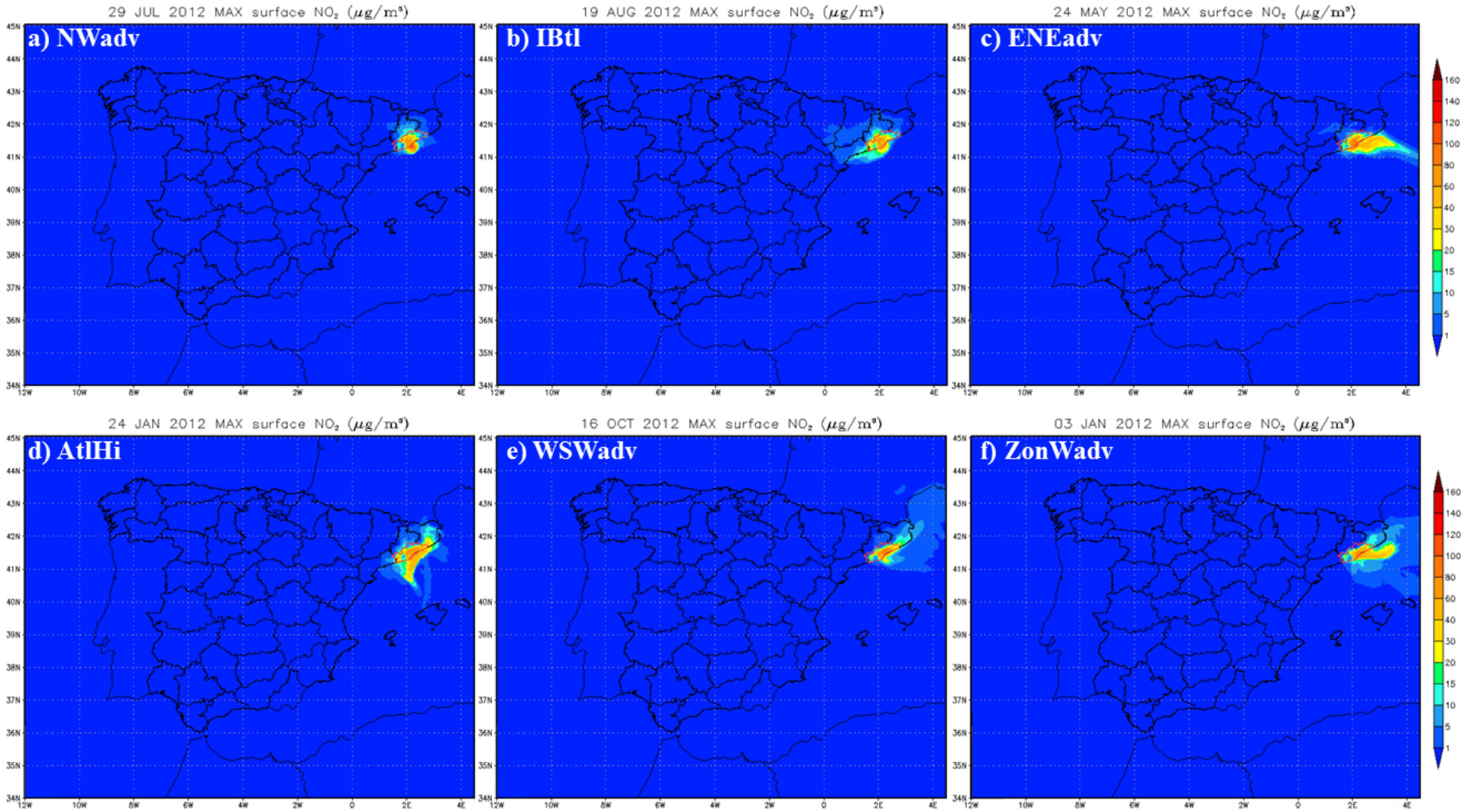

Figure AIII-4. Daily maximum NO_2 surface concentration (µg m^{-3}) attributed to on-road transport emissions from Barcelona metropolitan area on the representative day of each CT: a) NWadv, b) IBtl, c) ENEadv, d) AtlHi, e) WSWadv; and f) ZonWadv.

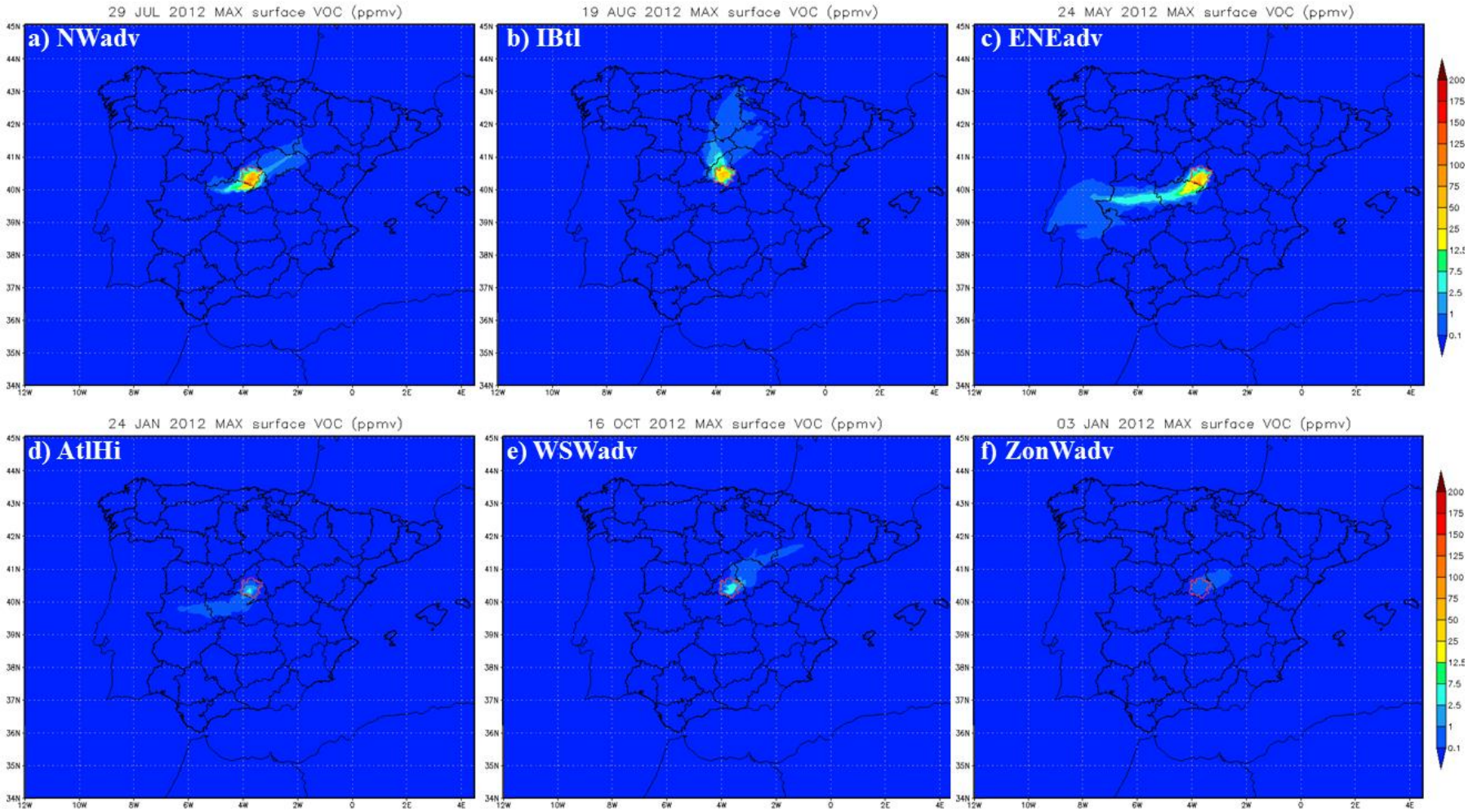

Figure AIII-5. Daily maximum VOCs surface concentration (ppmv) attributed to on-road transport emissions from Madrid metropolitan area on the representative day of each CT: a) NWadv, b) IBtl, c) ENEadv, d) AtlHi, e) WSWadv; and f) ZonWadv.

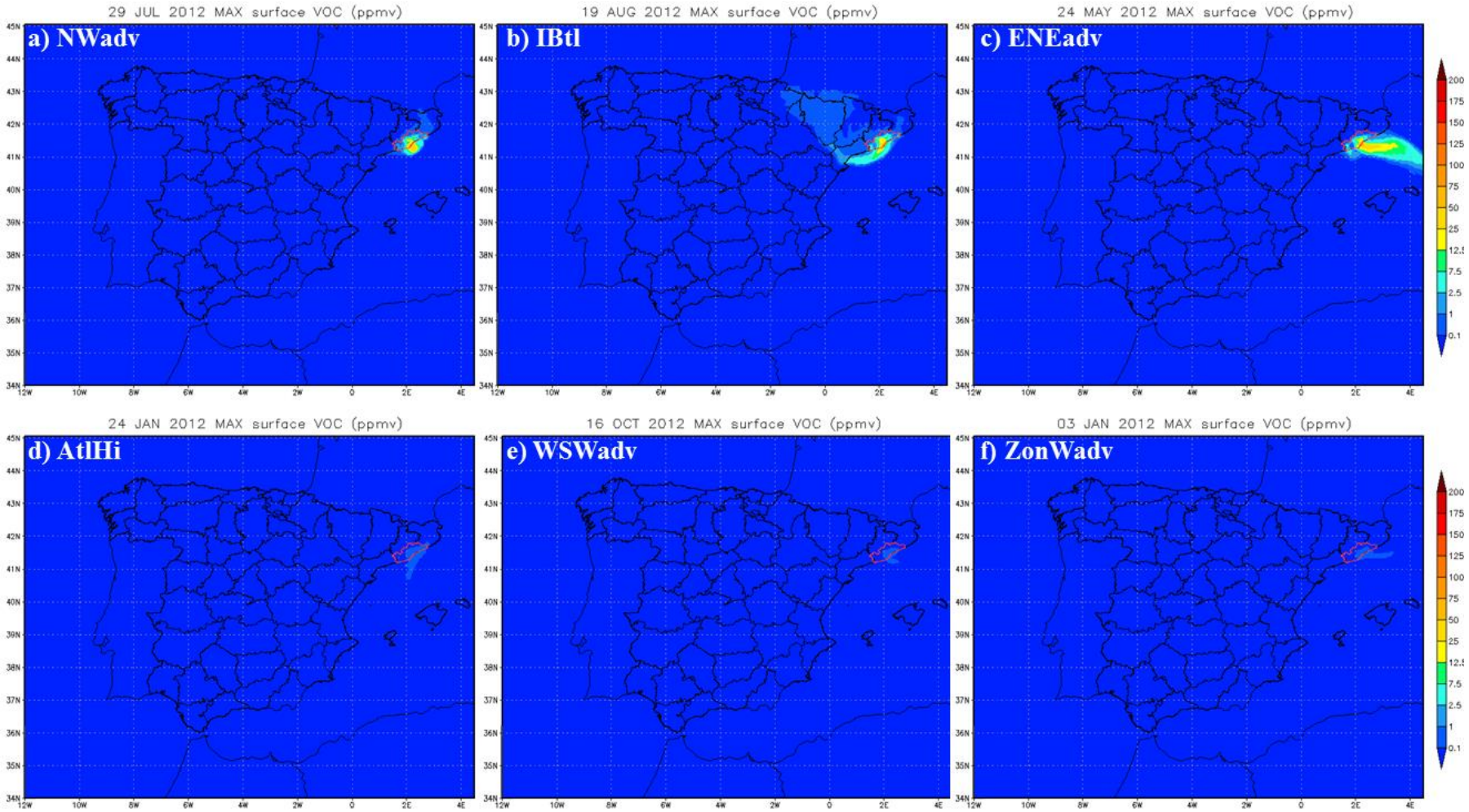

Figure AIII-6. Daily maximum VOCs surface concentration (ppmv) attributed to on-road transport emissions from Barcelona metropolitan area on the representative day of each CT: a) NWadv, b) IBtl, c) ENEadv, d) AtlHi, e) WSWadv; and f) ZonWadv